The role of the class III phosphoinositide 3-kinase VPS34 in regulatory T cells and activated CD8$^+$ T cells

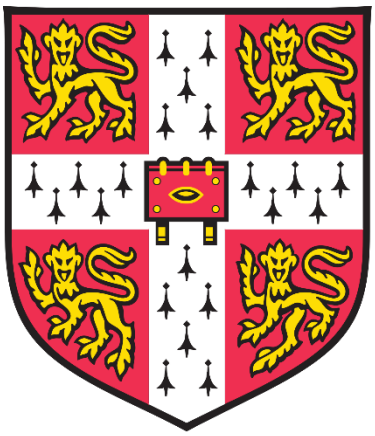

Christina Johanna Felicia COURREGES

Darwin College

Babraham Institute & Department of Pathology

This thesis is submitted to the University of Cambridge

for the degree of *Doctor of Philosophy*

January 2020

Declaration

This dissertation is the result of my own work and includes nothing which is the outcome of work done in collaboration except as declared in the Preface and specified in the text.

It is not substantially the same as any that I have submitted, or, is being concurrently submitted for a degree or diploma or other qualification at the University of Cambridge or any other University or similar institution except as declared in the Preface and specified in the text. I further state that no substantial part of my dissertation has already been submitted, or, is being concurrently submitted for any such degree, diploma or other qualification at the University of Cambridge or any other University of similar institution except as declared in the Preface and specified in the text.

This dissertation does not exceed the word limit set by the Faculty of Biology of 60,000 words.

The role of the class III phosphoinositide 3-kinase VPS34 in regulatory T cells and activated CD8$^+$ T cells

submitted by Christina Johanna Felicia COURREGES

Summary

The class III PI3-kinase VPS34 is a mediator of endocytosis, trafficking of intracellular membranes and vesicles, and autophagy in various cell types. Given its central role in key cell-biological processes, we explored whether VPS34 is critical for immune cells by generating conditional knockout mice where exon 21 of *Pik3*c3 (the VPS34 gene) is deleted specifically in regulatory T (Treg) cells or activated CD8$^+$ T cells, respectively.

We found that mice with VPS34-deficient Treg cells died within 6 weeks of birth from an autoimmune lymphoproliferative disease, similar to mice lacking Treg cells. However, VPS34-deficient Treg cells developed normally and populated the peripheral lymphoid organs, demonstrating a critical role for VPS34 in Treg cell suppressive functions rather than survival. However, none of the known Treg cell suppressive mechanisms were impaired by the loss of VPS34. Nonetheless, VPS34-deficient Treg cells had a competitive disadvantage and impaired activation compared to VPS34-sufficient Treg cells, suggesting that VPS34 is required for Treg cells maturation or the survival of mature Treg cells. In an attempt to determine which cellular processes are affected by the loss of VPS34, we performed proteomic profiling, and while the results could not provide a definite clue about the mechanism leading to the observed phenotype in mice with VPS34-deficient Treg cells, they suggested that loss of VPS34 induces a state of heightened metabolic activity in Treg cells.

Autophagy is critical for the formation of memory CD8$^+$ T cells, while it is dispensable during the effector phase. Since VPS34 is required for the induction of autophagy, it was striking to observe that deletion of VPS34 in activated CD8$^+$ T cells did not result in a phenotype similar to mice with autophagy (ATG7)-deficient CD8$^+$ T cells. Rather, mice with VPS34-deficient, activated CD8$^+$ T cells displayed reduced proportions of antigen-specific CD8$^+$ T cells and reduced effector functions at the peak of expansion after infection with *Listeria monocytogenes*, while memory formation seemed intact. Results from *in vitro* data suggested that while proliferation was intact, the transition through the cell cycle was impaired in VPS34-deficient, activated CD8$^+$ T cells.

Acknowledgements

Three years and four months have just passed - I must admit, this time has been incredibly enriching, immensely instructive and is for the least full of good memories. Now has come the time to thank everyone (*or lets say try not to forget anyone*) that has shared the walk, reached out to get me up again, pushed me to run faster, asked me to sit down and take a rest.

The first one to thank must surely be Klaus, the Captain of the OkkenVikings. Thank you for steadily sailing this ship through rough seas and calm waters, and be such an inspirational, helpful, and cool boss.

Elisabeth and Priya – your work has immensely contributed to understanding the role of VPS34 in Treg cells and led to the work presented in the first chapter of this thesis. Thank you for your dedication and hard work!

To Benoit, for your input and your time, for being there even though you didn't have the time; thanks to Bart for your support and invaluable feedbacks.

Thanks to the other OkkenVikings for being part of this intensive and educative journey. Working and learning alongside you has been a great pleasure! Thanks to James E (*part-time Viking*), fantastically competent – thank you for your support and encouragements; Kris – CRISPR/Kris – brilliant and always helpful – *Muchas gracias muchacho*! To Anne, you are such an inspiring scientist – thank you for always knowing everything and your unshakable calmness – I have so much more to learn from you. Thanks to Anita for just being yourself – always up for a chat or a drink at *The Lab*. To Leandra, for being part of our OkkenViking group. To Rafeah, many thanks for all your help with the (*not so*) nasty infections and the entertaining conversations in TC and CAT2.

To Fiore, thank you for being both a lab mate and a loyal friend. You helped me through the toughest time of my life. I am sorry things went as they went… I wish you the best for you and your little family.

A special thanks to James T – Summer 2015 at the CIMR made me the PhD scientist I am today. Thank you for believing in me and introducing me to the Cambridge Immunology network.

To all the technicians in the BSU of the Babraham Institute, MIRA and Gurdon – Carly, Lewis, Michael, Jon, Emma, Jenny, Tegan, Katie, and Andrew – thanks for keeping an ever-attentive

eye on my mice, for always rising to the occasion with my last-minute requests, and for your invaluable help with all kind of experiments.
To Rachael and Joana, for running the Flow facility at an unimpeachable level, and for doing my sorts at irregular hours. To Laura and Christina for walking an obvious novice through the daunting procedure of proteome profiling, and for helping me make sense of what came out the other end.

Marie Curie ITN people – thank you guys for being an amazing support group – for the common meetings in various European cities, the struggles through the presentations and the paper work – but above all for being such a fun group. I have made friends for life!

Elenita (*aka* Greta) – simply put, I couldn't have gotten here without you. Thank you for your irreplaceable sisterhood, the late-nights chats, sharing (*reluctantly*) your lab bench with me, your constant support and just being the most unexpected but truly best friend I could have ever imagined to have. And for the best data you ever created being for my thesis – I am really grateful ;)
To Jon, who was unconditionally there during the hardest time of my life – thank you for listening, sharing, for the deep and silly conversations, the Saturday Squash Sessions, the Wine and Cheese events, and many more. No words can express my gratitude.
To Adria – Cambridge wouldn't have been the same without sharing this with you from the first day. You made this experience just incredible.
Thanks to all my friends here in Cambridge and around the world – you are too many to name each of you – but from the bottom of my heard – thank you for being in my life!

To my family – Mum&Dad, Jojo, Clarisse, and Myriam - for always believing in me, for your love and support. This thesis is for you Ma&Dad, because even though things are going up and down, you are the true heart of this treasure I call our family.
To Willy, who recently appeared in my life, and makes me shine. Thank you for humouring me, keeping pace with my disastrous mood swings, pushing me on my feet until I smile again. Thank you for never letting me go. With all my heart, I love you.

This project has received funding from the European Union's Horizon 2020 Research and Innovation programme under the Marie Skłodowska-Curie grant agreement No 675392.

Table of acknowledgement of assistance received during the course of this thesis

1) Initial training in techniques and laboratory practice and subsequent mentoring:

- Priya Schoenfelder – CHOs-Treg cells co-cultures
- Anne-Katrien Stark – *in vitro* Treg cell differentiation
- Rafeah Alam – Stock preparation, infection with Lm-OVA, and bacterial load determination
- Leandra Jackson – Western Blotting
- Rachael Walker and Joana Cerveira – Flow cytometry
- James Edgar and Kristoffer Johansen – Cloning, transformation and transfection
- Kristoffer Johansen – gRNA design
- Benoit Bilanges – SeaHorse assays
- Elena Lopez Guadamillas - qPCR

2) Data obtained from a technical service provider (e.g. DNA sequencing, illustrations, simple bioinformatics information etc.):

- Arthur Davis, George Morrow, and Joana Cerveira – Cell sorting
- Babraham Biological Services Import Unit – Animal husbandry, intravenous injections
- MIRA University of Cambridge Biomedical Services – Animal husbandry
- Gurdon Institute University of Cambridge Biomedical Services – Animal husbandry, subcutaneous injections of tumour cells

3) Data produced jointly (e.g. where it was necessary or desirable to have two pairs of hands):

- Rafeah Alam, Joana Guedes, Kristoffer Johansen – processing of tissues
- Kristoffer Johansen – tumour cell injections and recording of flow cytometry data

4) Data/materials provided by someone else (e.g. one-off analysis, bioinformatics analysis, where parallel data or technical provision in a very different area is needed to provide a connected account in the thesis)

- Elisabeth Slack and Priya Schoenfelder – experiments and conclusions leading to the hypotheses and work presented in the first chapter of my PhD thesis (mentioned in more detail in the corresponding chapters)
- Elena Rebollo Gomez – cloning, *in vitro* pull down assays, Western blotting and kinase assay of a tagged version of the truncated and wild-type allele of *Pik3c3* in transiently transfected HEK293 cells
- Laura Spinelli and Christina Rollings – Mass spectrometry, sample processing and analysis (and methods)

List of abbreviations

4E-BP1	eukaryotic translation initiation factor 4E-binding protein 1
7-AAD	7-aminoactinomycin D
ActA	actin assembly-inducing protein
AICD	activation induced cell death
Ala	alanine
AMARC	alpha-methylacyl-CoA racemase
AMBRA	autophagy and Beclin 1 Regulator
AMP	adenosine monophosphate
AMPK	AMP-activated protein kinase
AP-1	activator protein 1
APC	antigen-presenting cell
ATG	autophagy
ATP	adenosine trisphosphate
aTreg cell	activated Treg cell
Bcl	B-cell lymphoma
BclxL	B-cell lymphoma-extra large
Bid	BH3 (Bcl-2 homology) Interacting Domain Death Agonist
Bif-1	Bax-Interacting Factor-1
Blimp-1	B lymphocyte-induced maturation protein-1
BrdU	bromodeoxyuridine / 5-bromo-2'-deoxyuridine
CAD	activated deoxyribonuclease
cAMP	cyclic AMP
CCL	CC chemokine ligand
CCR7	CC-chemokine receptor 7
CD	cluster of differentiation
CFU	colony-forming units
COX	cyclooxygenase
CPT1a	carnitine palmitoyltransferase 1a
CTL	cytotoxic T lymphocyte
CTLA-4	cytotoxic T lymphocyte antigen-4

CXCR	CXC-chemokine receptor
CYBB	cytochrome b-245, beta polypeptide
DAVID	Database for Annotation, Visualization and Integrated Discovery
DC	dendritic cell
DFCP1	zinc-finger FYVE domain-containing protein 1
DN	double negative
DNA	deoxyribonucleic acid
DP	Double positive
ECAR	extracellular acidification rate
EDTA	ethylenediaminetetraacetic acid
EEA1	early endosome antigen 1
EOMES	Eomesodermin
ER	endoplasmatic reticulum
FACS	fluorescence-activated cell sorting
FAO	fatty acid oxidation
FasL	Fas ligand
FBS	foetal bovine serum
FCS	foetal calf serum
FOXO	forkhead box O transcription factor
FoxP3	forkhead box P3
FSC	forward scatter
FYVE	Fab 1, YOTB, *Vac* 1 (vesicle transport protein), and *early endosome antigen 1E* (EA1)
FYVE-CENT	FYVE domain-containing centrosomal protein
GABARAPL2	gamma-aminobutyric acid receptor-associated protein-like 2
GalNAc	N-acetylgalactosamine
GALNT	N-acetylgalactosaminyltransferase
GBP-1	interferon-induced guanylate-binding protein 1
GDP	guanosine diphosphate
GFP	green fluorescent protein
GITR	glucocorticoid-induced tumour necrosis factor-related receptor
Glut1	glucose transporter 1

GO	gene ontology
GORASP	Golgi reassembly stacking protein
GPR68	ovarian cancer G-protein couples receptor 1
GRASP	Golgi reassembly-stacking protein
GTP	guanosine triphosphate
GzmB	Granzyme B
HDAC	Histone deacetylases
HET	heterozygous
HEV	high endothelial venules
HMGCR	3-hydroxy-3-methylglutaryl-CoA reductase
hrIL-2	human recombinant IL-2
HRS	hepatocyte growth factor-regulated tyrosine kinase substrate
ICAM1	intercellular Adhesion Molecule 1
ICB	intercellular bridge
ICOS	Inducible T cell co-stimulator
IDI1	isopentyl-diphosphate δ isomerase 1
IFN	interferon
IL	interleukin
IL-10Rα	interleukin-10 receptor α
IN1	inhibitor 1
IPEX	immune dysregulation, polyendocrinopathy, enteropathy, X-linked syndrome
IS	immunological synapse
iTreg cell	induced Treg cell
KEGG	Kyoto Encyclopedia of Genes and Genomes
KLRG1	killer-cell lectin-like receptor G1
KO	knock-out
LAG3	lymphocyte-activation gene 3
LAMP	lysosome-associated membrane glycoprotein
LC3	L chain 3
Lck	lymphocyte-specific protein tyrosine kinase
LFA-1	leukocyte functional antigen-1

LKB1	Liver-Kinase B1
Lm	*Listeria monocytogenes*
MACS	magnetic-activated cell sorting
Mbd2	methyl-CpG-binding domain protein 2
Mdr-1	multidrug resistance protein A1
MHC	major histocompatibility complex
miRNA	microRNA
MPEC	memory precursor effector cell
mRNA	messenger RNA
MS	mass spectrometry
MTMR3	myotubularin-related protein 3
MTOC	microtubule organising centre
mTOR	mammalian target of rapamycin
MVB	multivesicular body
NDUFV	NADH dehydrogenase [ubiquinone] flavoprotein
NFAT	nuclear factor of activated T cell
NK	natural killer
NK-κB	nuclear factor κB
NOX2	NADPH oxidase 2
OCR	oxygen consumption rate
OVA	ovalbumin
OXPHOS	oxidative phosphorylation
PBS	phosphate-buffered saline
PCR	polymerase chain reaction
PD-1	programmed death-1
PD-L	programmed death-ligand
PH	Peckstrin homology
PI	phosphoinositide
PIP_2	phosphatidylinositol-(4,5)-diphosphate
PI3K	phosphoinositide 3-kinase
PI3P	phosphatidylinositol (3,4,5)-trisphosphate
PTEN	phosphatase and tensin homolog

PX	phox (phagocytic oxidase)
RAPTOR	regulatory-associated protein of mTOR
RICTOR	rapamycin-insensitive companion of mTOR
RILP	Rab-interacting lysosomal protein
RNA	ribonucleic acid
rTreg cell	resting Treg cell
Runx1	runt-related transcription factor 1
ROS	reactive oxygen species
SLEC	short lived effector cell
SLO	secondary lymphoid organ
SQLE	squalene epoxidase
SREBP	sterol regulatory element-binding protein
SSC	side scatter
STAT	signal transducer and activator of transcription
T-bet	T-box factor expressed in T cells
TCM	T central memory
Tcon	conventional T cell
TCR	T cell receptor
TEM	T effector memory
Tet	tetramer
TGN	trans-Golgi network
TLR	Toll-like receptor
TMEM-38	trimeric intracellular cation channel type B
TGF	transforming growth factor
Th cell	T helper cell
Thr	threonine
TLR	Toll-like receptor
TNF	tumour necrosis factor
TRAF6	TNFR-associated factor 6
Treg cell	regulatory T cell
TSLP	thymic stromal lymphopoietin
TTC19	tetratricopeptide Repeat Domain 19)

tTreg cell	thymic Treg cell
UDP	uridine phosphorylase
VPS34	vacuolar protein sorting 34
ULK1	Unc-51-like kinase 1
UQCRB	ubiquinol-Cytochrome C Reductase Binding Protein
UVRAG	ultra-violet radiation resistance-associated gene
WIPI	WD-repeat protein interacting with phosphoinositides
WT	wild-type
XBP-1	X-box binding protein 1
YFP	yellow fluorescent protein

Table of Content

List of Figures

List of Tables

Chapter 1

Introduction

1.1 The immune system

The immune system represents a complex network of cells, tissues, molecules, and organs working together to protect the host from foreign pathogens and malignant cells. This protection is accomplished by the inherent ability of the immune system to distinguish 'self' from 'non-self' and to eliminate potentially harmful molecules and non-self cells. The immune system has also the capacity to recognize and eliminate cells that display an 'altered self', e.g. virally infected and transformed cells that are derived from the host's tissue, or self-reactive cells, such as auto-reactive T cells.

Cells of the immune system originate in the bone marrow and arise from hematopoietic stem cells which further differentiate to either common myeloid progenitor cells or common lymphoid progenitor cells [1]. The former give rise to granulocytes, macrophages, dendritic cells and mast cells, while the latter are the precursors of lymphocytes, i.e. *Natural Killer* (NK) cells, B cells, and T cells. Based on antigen specificity and timing of activation, the immune system can be, broadly speaking, divided into two distinct immune compartments - the innate and the adaptive immune system. The innate immune system is an evolutionary ancient defence mechanism that serves as an early mechanism of host-defence against tumour cells and invading pathogens [2]. Innate immune cells play a crucial role in the initiation and the subsequent direction of the adaptive immune response and participate in the removal of pathogens targeted by cells of the adaptive immune system. The adaptive immunity represents the second phase of an immune response. It is defined by a high degree of specificity in recognising foreign antigens and the ability to form an immunological memory, which is faster, stronger and generally more effective at neutralising pathogens in the event of renewed exposure to the same antigen [1]. In contrast to the innate immune response, the initial adaptive immune response does not act immediately and only reaches the peak of cell expansion and functional activity by four to seven days, a period during which the innate immune response is critical for controlling the infection. Both arms of the immune system regulate each other in many different ways and act in concert to eliminate foreign antigen and malignant cells [3]. The interplay between the innate and the adaptive immune system is an important basis for the effective protection of the host.

In the following chapters, I will concentrate on two cell subsets belonging to the adaptive immunity, $CD8^+$ T cells and regulatory T cells, as those cell types are the focus of this thesis. Since both arise from the T cell compartment, the next sub-chapter will describe in general the development of T cells, before subsequently focusing on either $CD8^+$ T cells or regulatory T cells.

1.1.1 T cell development – from being born to being educated

T cells derive from haematopoietic stem cells found in the bone marrow. T cell progenitors migrate to the thymus where they undergo a series of maturation steps that can be discern from each other based on the expression of different cell surface markers. The majority of the T cells gives rise to αβ T cells, with only ~ 5% bearing the γδ *T cell receptor* (TCR). When entering the thymus, T cells lack the expression of both co-receptors CD4 and CD8 and are therefore termed *double negative* (DN) cells. This DN population can be further sub-divided by the expression of the adhesion molecule CD44 and the *interleukin-2 receptor α* chain (IL-2Rα, also referred to as CD25). Cells expressing CD25 but lacking CD44 undergo beta-selection – a process selecting for cells that have successfully rearranged their TCR-β chain locus. The β chain pairs with the surrogate pre-TCR-α chain to produce a pre-TCR. Successful pre-TCRs form a complex with CD3 molecules, leading to the survival, proliferation, arrest of further β chain loci rearrangement, and the up-regulation of CD4 and CD8. This stage is called the *double positive* (DP) stage. In the DP stage, T cells rearrange their TCR-α chain loci to produce an αβ-TCR.

Next, T cells undergo positive selection in the cortex. DP cells are tested for the ability to interact with self-antigens in the context of major *histocompatibility complex* (MHC) class I or class II molecules. Depending on the affinity of the engagement between the antigen and the MHC, i.e. appropriate affinity versus weak affinity, T cells may survive or die by apoptosis, respectively. In the medulla, T cells undergo negative selection, i.e. they are presented to self-antigens on *antigen presenting cells* (APCs), such as dendritic cells and macrophages. T cells that interact too strongly with an antigen undergo apoptosis, which is the case for the majority of the T cells. Surviving T cells down-regulation either co-receptor to produce either CD4 or CD8 single positive cells and exit the thymus to carry out their distinct roles.

1.2 Regulatory T cells

1.2.1 The Ying and the Yang of the immune system

The adaptive immune system is a powerful and immensely versatile defence mechanism against both external and internal threats, including harmful microorganisms and malignant cells, respectively. However, inappropriate, overwhelming, and prolonged immune answers represent a potential risk to the host. The immune system is therefore endowed with a control mechanism to maintain tolerance against commensal microorganisms, harmless and self-antigens, and to control desirable immune response to limit tissue damage.

Two types of control mechanisms have been described, i.e. 'recessive' and 'dominant' control mechanisms. Recessive mechanisms are cell intrinsic and include death by apoptosis or cell anergy of overly self-reactive T cells that are exposed to their cognate antigen in the thymus during negative selection [4]–[7]. In the periphery, anergy is being induced by prolonged exposure to a self-antigen. The requirement of CD28 to interact with the co-stimulatory receptor CD80/86 expressed on APCs, in addition to TCR engagement, provides a further level of control in the periphery [8]. However, these mechanisms are not sufficient on their own to maintain immune homeostasis. A subset of T cells, characterised by the expression of CD4, IL-2Rα (CD25), and the transcription factor *forkhead-box transcription factor* (FoxP3) is critical for the maintenance of peripheral tolerance. This cell subset was first identified in experiments conducted on neo-nataly thymectomized mice that displayed autoimmunity until restored with adult thymocytes or splenocytes [9]–[12] and was therefore named *regulatory T cells* (Treg cells). Treg cells are essential for the control and the termination of ongoing immune responses, maintain peripheral tolerance to self-antigens, and prevent autoimmunity by suppressing or downregulating the activation and proliferation of effector T cells [13]. Lack of Treg cells or impairment in their suppressive functions results in autoimmune diseases and lymphoproliferative disorders.

1.2.2 Treg cell development and activation

Treg cells comprise between 5 to 10% of all peripheral $CD4^+$ T cells [14] and arise from two distinct sources; *thymic Treg* (tTreg) cells develop in the thymus from $CD4^+$ T precursor cells and have a diverse TCR repertoire which confers specificity for self and non-self antigens [15]–

[17]. *Induced Treg* (iTreg) cells arise from naïve peripheral $CD4^+$ T cells following activation in the presence of *transforming growth factor beta* (TGF-β) [18]. Both Treg cell subsets can be distinguished by their expression of neuropilin-1, which is expressed on tTreg cells but not iTreg cells [19], [20]. In mice, FoxP3 is unique to and required for the identity of Treg cells [21], [22], and depletion of the FoxP3 gene leads to the so-called *Scurfy* phenotype, a fatal lymphoproliferative disease associated with the massive activation and proliferation of effector $CD4^+$ T cells and the production of pro-inflammatory cytokines [23]. Similarly, in human, dysfunction of the transcription factor FoxP3 results in a disease termed *immunodysregulation polyendocrinopathy enteropathy X-linked* (IPEX) syndrome [24], [25], resulting in autoimmunity with a lethal outcome for the patient.

FoxP3 controls the differentiation and the function of Treg cells by controlling their transcriptional signature, i.e. by repressing the expression of genes that promote immune responses while reinforcing the expression of genes that intrinsically limit the activation of effector T cells, i.e. CTLA-4, IL-10, and IL-10Rα [26]. Around 700 genes are thought to be regulated by FoxP3, and 20-30% are directly bound by FoxP3 [27], [28], such as genes encoding transduction molecules, transcription factors, cytokines, cell-surface molecules, and metabolic enzymes [14]. FoxP3 also interact with chromatin remodelling factors, such as the acetyl transferase TIP60, histone deacetylases, and the transcription factors *nuclear factor of activated T* cells (NFAT) and Runx1 [26]. TIP60 and HDAC7 regulate the activity of FoxP3 [29], [30] and its interaction with Runx1 suppresses the transcription of IL-2, a key cytokine for the survival and proliferation of effector T cells.

NFAT binding to the *activator protein 1* (AP-1) and NFκB induce the expression of IL-2, IL-4, and CTLA-4 in conventional T cells, and their differentiation into effector T cells. The replacement of AP-1 by FoxP3 represses the expression of IL-2 while increasing the expression of CD25 and CTLA-4 [31].

FoxP3 also regulates the expression of micro-RNAs (miRNAs) [14], [26] that are critical for the fitness of Treg cells: miR-155 is required for Treg cell development [32] and to increase the response to IL-2 [33], while miR-146a expression prevents the differentiation of Treg cells into a Th1-phenotype [34]. Hence, mice deficient for Dicer or Drosha, two components of the miRNA maturation machinery, fail to generate Treg cells and display a Scurfy phenotype [35]–[37]. In summary, the continuous expression of FoxP3 is required to maintain the

transcriptional programme in mature Treg cells, making FoxP3 the master regulator of Treg cell differentiation, survival and suppressive functions [38].

1.2.3 Mechanisms of Treg cell suppression

Treg cells employ diverse mechanisms to maintain a balanced response to exogenous and self-antigens, involving the production of secreted immunosuppressive cytokines, directly suppressing effector T cells or indirectly by suppressing dendritic cells [39]. The relative contribution of each mechanism is still a matter of investigation, and so far no mechanism has been identified as being absolutely indispensable for the function of Treg cells.

Treg cells secrete immuno-suppressive cytokines such as IL-10, IL-35, and TGFβ-1 and can directly kill target cells. In mice, Treg cells express mainly granzyme B, and target cells are killed in a perforin-dependent manner [40].

Besides directly inhibiting effector T cells, Treg cells regulate the immune response by modulating the ability of APCs to prime naïve T cells. *Cytotoxic T lymphocyte-associated protein 4* (CTLA-4), a member of the immunoglobulin superfamily, plays an important role in regulating the expression of co-stimulatory molecules required for the activation of naïve T cells on *dendritic cells* (DCs) by Treg cells. Similar to CD28, CTLA-4 binds CD80 and CD86, but with a much higher affinity and is intrinsically inhibitory rather than activating [41]. Treg cells sequester CD80/CD86 from the cell surface of DCs through a process called transendocytosis [42], thereby indirectly preventing naïve T cell activation. Furthermore, the binding of CTLA-4 to CD80/CD86 induces the production of indolamine-2,3-dioxygenase (IDO), an enzyme which catabolises tryptophan [41], [43]. Tryptophan is an amino acid required for the proliferation of T cells [44], and its breakdown results in kynurenines that have a pro-apoptotic influence on T cells [45]. Hence, CTLA-4 deficiency or blockade has detrimental effects: CTLA-4 – deficient mice develop multi-organ inflammation leading to death at three to four weeks of age [46], [47], Treg cell-specific depletion of CTLA-4 results in lymphadenopathy, splenomegaly, myocarditis, gastritis, and death at seven weeks of age [48], while antibody blockade of CTLA-4 abrogates Treg cell suppressive functions [49]. In the absence of CTLA-4, CD80/CD86 levels are heightened on DCs, leading to an increased activation of naïve T cell through the interaction with CD28.

Treg cells also mediate indirect inhibition of naïve T cells through their expression of the *lymphocyte-activation gene 3* (LAG3), a CD4 homologue highly specific for MHC class II molecules. LAG3 binding to MHC class II on immature DCs inhibits the maturation and the immune-stimulatory capacity of DCs [50].

Expression of the IL-2 receptor on the cell surface is critical for Treg cell homeostasis and their suppressive functions [51]. Upon IL-2 binding, the IL-2R – IL-2 complex is rapidly endocytosed, IL-2 is degraded through the lysosomal pathways and the IL-2 receptor recycled to the cell surface [52]. This mechanism allows the consumption of extracellular IL-2, thereby depriving effector T cells of a key growth factor and leading to Bim-mediated apoptosis [53].

Treg cells can also suppress the survival, the proliferation, and effector functions of target cells through the disruption of their metabolism. One of this mechanism involves the release of *cyclic adenosine monophosphate* (cAMP), which potently inhibits the proliferation of T cells and their production of IL-2 [54]. A further mechanism by which Treg cells disrupt the metabolism of target cells is through the expression of the ectoenzymes CD39 and CD73 on their cell surface, which synergize to elevate the level of pericellular adenosine. Adenosine binds to the adenosine receptor A2 on target cells and thereby supresses T cell effector functions [55]. This mechanism also promotes the secretion of TGFβ-1 and supresses IL-6 production, contributing to the generation of iTreg cells in the periphery [56].

1.3 CD8$^+$ T cells

CD8$^+$ T cells are critical for the elimination of intracellular bacteria- or virus-infected cells, and of transformed cells [57], [58]. Upon activation, naïve CD8$^+$ T cells undergo many rounds of proliferation and differentiate into mature effector cells termed as *cytotoxic T lymphocytes* (CTLs). CTLs are specialized in the direct, contact-dependent cytolysis of target cells [59].

1.3.1 CD8$^+$ T cell development and activation

Naïve single positive CD8$^+$ T cells circulate throughout the body, migrating through the blood system and *secondary lymphoid organs* (SLOs) (spleen and lymph nodes) via *high endothelial venules* (HEVs). HEVs are specialized post-capillary venous swellings which express ICAM1, CD34 as well as the CCR7 ligands CCL19 and CCL2 [60]–[62]. Their role is the constant search of pathogen-derived peptides presented in the context of the class I *major histocompatibility complex* (MHC) which is expressed on all nucleated cells [63] and recognised through their TCR and the CD8 co-receptor (consisting of a CD8α and a CD8β chain). The encounter of a naïve CD8$^+$ T cell with its cognate antigen results into numerous molecular changes within the T cell, leading to cell activation and differentiation into distinct subpopulations. The activation of CD8$^+$ T cells depends on three signals: 1) stimulation by the antigen through the TCR; 2) co-stimulation through molecules such as CD28, CD40, 4-1BB, CD27, ICOS, and/or OX40; and 3) stimulation by inflammatory cytokines, especially IL-12 and *type I interferon* (IFN) [64]–[66]. Upon activation, antigen-specific CD8$^+$ T cells undergo three distinct phases: 1) clonal expansion, during which effector functions are acquired; 2) contraction of the effector population through *activation induced cell death* (AICD), where only a small percentage of cells remaining to generate memory cells; and 3) maturation of memory cells. Memory formation is independent of the contraction phase, and is believed to be already programmed during the early stages of the priming phase [67].

Once activated, CD8$^+$ T cells loose the expression of the lymph node homing receptors L-selectin (CD62L) and the *CC-chemokine receptor 7* (CCR7) [68]. Activated cells increase the expression of tissue-specific integrins and chemokines allowing them to transmigrate into the tissues following their expression [68]. The expression of the cell surface glycoprotein CD44 mediates the primary adhesion of activated CD8$^+$ T cells to endothelial cells through binding

to the ligand HA [69] and the integrin α4β1 (VLA-4) [70]. CTLs also express CD11a/CD18 (*leukocyte functional antigen-1*, LFA-1), which binds ICAMs on the endothelium and is expressed only during inflammation, CD49d, and chemokine receptors including *CXC-chemokine receptor 3* (CXCR3).

At the peak of the primary $CD8^+$ T cell response, two distinct subsets of $CD8^+$ T cells can be distinguished from each other based on the expression of two receptors, i.e. *IL-7 receptor alpha chain* (IL-7Rα, also referred to as CD127) and *killer-cell lectin-like receptor G1* (KLRG1). Kaech et *al*. described how the expression of CD127 inversely correlates with effector $CD8^+$ T cell survival [71]. They adoptively transferred $CD127^{high}$ or $CD127^{low}$ effector $CD8^+$ T cells into naive mice, and found that $CD8^+$ T cells expressing high levels of CD127 preferentially survived and differentiated into long-lived memory cells [71]. Therefore, *memory precursor effector cells* (MPECs) can be defined by their high expression of CD127 [71], and *short lived effector cells* (SLECs) by their low CD127 expression [71]–[73]. Voehringer et *al*. suggested KLRG1 as an early and unique marker for replicative senescence of $CD8^+$ T cells [74]. Together with CD127, KLRG1 can therefore be used to distinguish effector $CD8^+$ T cells (i.e. SLECs) from memory precursor cells (i.e. MPECs) [75], [76] - $KLRG1^{high}$ $CD127^{low}$ defining SLECs and $KLRG1^{low}$ $CD127^{high}$ defining MPECs. The ratio between these two populations is often taken as a measure to assess the ability of cells to react to an infection as well as to form a pool of memory cells.

A multitude of mechanisms control the differentiation into either MPECs or SLECs, including the strength of antigen stimulation and the exposure to cytokines such as IL-2 and IL-12 [76]. SLEC differentiation is favoured by enhanced signal 1 (prolonged antigen exposure, TCR affinity/avidity/peptide concentration) and signal 3 (high levels of IFN-γ, IL-12), while brief TCR stimulation, defects in inflammatory cytokine signalling, enhanced anti-inflammatory cytokine availability (TGF-β, IL-10) or the presence of regulatory T cells promotes the formation of MPECs [77]. The differentiation into SLECs is favoured by the expression of *T-box transcription factor* (T-bet), Blimp-1, XBP-1, ID2, whereas increase levels of *Eomesodermin* (Eomes), Bcl-6, ID3 and Mbd2 promotes MPEC differentiation [76], [78].

Joshi et *al.* proposed T-bet as a master regulator of cell-mediated immunity, able to control the expression of genes encoding a wide range of effector molecules [76]. For example, inhibition of T-bet favours the formation of memory T cells and the expression of CXCR3 (also known as CD183). The expression of CD183 affects the balance between the

generation of effector and memory $CD8^+$ T cell [79]. Consequently, fewer SLECs and more MPECs developed when $CD8^+$ T cells lacked CD183 expression due to reduced co-localisation of effector $CD8^+$ T cells with antigen in the spleen. Eomes has also been shown to be key for the function of $CD8^+$ T cells, and it has been established that Eomes and T-bet have both overlapping and separate functions in the regulation of $CD8^+$ T cell effector functions. One example is that the abrogation of IFN-γ production requires both T-bet and Eomes to be knocked-out [80].

1.3.2 Effector mechanisms of activated $CD8^+$ T cells

Activated effector $CD8^+$ T cells differentiate into *cytotoxic T lymphocytes* (CTLs), in reference to their specialisation in the direct, contact-dependent lysis of target cells [81]. CTLs display several effector functions with both direct and indirect effects on target cells.

Through the release of pro-inflammatory cytokines such as *tumour necrosis factor-α* (TNF-α) and *interferon-γ* (IFN-γ), CTLs shape the ongoing immune response by indirectly inhibiting intracellular pathogens [82], [83], upregulating antigen presentation on MHCs [84] and shaping the immune response of several immune cell subsets, including $CD8^+$ T cells themselves [85]–[87]. IFN-γ directly interferes with viral replication, leads to the recruitment of macrophages to the site of infection, and activate those to kill pathogens and present antigens. Furthermore, IFN-γ stimulates the expression of MHC class I, rendering it more likely for any infected cells to be recognised and killed, as most cells express the IFN-γ receptor.

$CD8^+$ T cells rapidly and directly kill target cells, either by the release of cytotoxic granules, or ligation of receptors that initiate apoptosis [88]–[90]. Both mechanisms of targeted cell lysis require direct contact between the effector and the target cell [91], an interaction termed as the *immunological synapse* (IS) [92]–[94]. Binding of the Fas ligand (FasL) on the surface of the $CD8^+$ T cells to death receptor Fas (CD95) on the target cell induces classical caspase-dependent apoptosis [95].

CTLs also contain special granules, or modified lysosomes, containing perforin, granzymes and granulysin [96]–[98], which are released in a regulated manner when the CTL is in direct contact with the target cell. When a T cell is activated through its TCR, microtubule-associated granules migrate towards the plasma membrane along microtubules that direct the release of these granules [91]. The microtubules emerge from the *microtubule organising*

centre (MTOC) located at the IS upon cellular activation [99]. The amplitude of the degranulation is controlled by the avidity of the TCR and peptide ligands interactions within the IS [100].

Perforin forms transmembrane pores in the target cells, allowing water and salts to enter the cell and cause osmotic lysis. Perforin is absolutely required for granule-mediated killing [101], as shown by genetic knock-out studies. Perforin knock-out mice are susceptible to viruses and intracellular pathogens, such as *Listeria* [102].

Granzymes are serine proteases and to date, five granzymes (A, B, G, H and K) have been described in humans, while ten in mice [103]. Granzyme B is the most studied granzyme and is expressed both in mice and humans. It cleaves and activates caspase-3, leading to the activation of *caspase-activated deoxyribonuclease* (CAD), resulting in the degradation of DNA and the induction of apoptosis [104], [105]. Granzyme B can also initiate apoptosis independently of caspase through the activation of the Bcl-2-family, pro-apoptotic protein Bid [106]–[108]. While it is widely believed that Granzyme B enters the target cell via perforin pores [109], it has also been suggested that Granzyme B enters the cell in the absence of perforin [110].

1.3.3 $CD8^+$ T cell memory formation

Memory T cells are present in relatively large numbers and located at multiple sites in the body [111]; in the case of re-infection, they are at the front line of potential pathogen entry sites. Once a pathogen has breached the first line of defence, memory cells are able to rapidly re-express effector molecules, such as cytokines and lytic proteins [112]. The ability to quickly respond is a result of the hyper-responsive state of memory T cells compared to naïve T cells [113], [114]. Antigen-specific naïve $CD8^+$ T cells represent an operational army of effector cells that can protect the host from the present infection, as well as a pool of memory cells poised to quickly and efficiently react to future infections with the same pathogens.

After the rapid expansion, the population of $CD8^+$ effector cells undergoes a rapid contraction phase whereby approximately 95% of the cells die by apoptosis. This contraction phase is mediated mainly by the ratio between the expression of survival versus apoptotic factors, including Bcl-2, Bclx, and components of the Bim and Fas pathways [115]–[117]. The remaining antigen-specific $CD8^+$ T cells eventually form a population of long-lived memory T

cells that survive for a long time in the host in an antigen- and TCR-independent manner [118]. However, the long-term maintenance of the memory $CD8^+$ T cell population depends on cytokines, especially from the γc-cytokine family. IL-7 and probably *thymic stromal lymphopoietin* (TSLP) enhance memory cell survival [73], [119], [120] while IL-15 is essential for the slow homeostatic turnover of memory cells [118], [121].

Memory cells are a heterogeneous pool of cells, including *T central memory* (TCM) cells and *T effector memory* (TEM) cells. Both subsets express CD44 but can be distinguished based on the expression of cell surface markers determining their ability to migrate to peripheral tissues [122]. TCM cells express high levels of the lymph node homing receptors CD62L and CCR7, allowing them to circulate between bloodstream and secondary lymphoid organs [123]. They secrete IL-2, but not IFN-γ [124]–[126]. TEM cells, on the other hand, lack the expression of CD62L and CCR7, and circulate through the bloodstream, permissive non-lymphoid tissues and secondary lymphoid organs. They quickly respond to reinfection with their specific pathogen, migrate to the site of infection and produce effector molecules such as IFN-γ.

1.4 Metabolic regulation of immune cells

Recent findings have increase our understanding on how intracellular metabolism can shape the development, trafficking, and function of Treg cells [127]–[129]. Indeed, the integration of multiples extrinsic and intrinsic signals are directly influencing cellular transcriptional programs and signalling pathways involved in cell proliferation, cytokine production, and energy metabolism [130].

Glycolysis and *fatty acid oxidation* (FAO) are differentially used by *conventional T cells* (Tcons) and Treg cells. *In vitro*, mouse Treg cells display a low glycolytic rate and oxidize lipids at a higher rate than Tcons, doing so through activation of the *AMP-activated protein kinase* (AMPK) (5). *In vivo*, mouse Treg cells display a high glycolytic rate associated with hyperactivation of the "environmental" sensor *mechanistic target of rapamycin* (mTOR) [131]–[133]. In the last decade, a special emphasis has been placed on the mTOR complex as it can sense environmental nutrients and growth factors and thereby modulate Treg cell

differentiation and functions [131], [132], [134], [135]. mTOR is an evolutionary conserved, 289 kDa serine/threonine protein kinase found in two multi-protein complexes: mTOR complex 1 (mTORC1), which contains the *regulatory-associated protein of mTOR* (RAPTOR), and mTOR complex 2 (mTORC2), which contains the *rapamycin-insensitive companion of mTOR* (RICTOR) [136]. mTORC1 is an important regulator of cell growth and differentiation [137], [138], and plays bidirectional roles in Treg cell induction and functions. mTORC1 can act as a negative regulator of *de novo* differentiation of Treg cells, but is critical for Treg cell suppressive activity [131], [132], [139]. Mechanistically, mTORC1/Raptor couples TCR and IL-2 signalling to Treg cell suppressive functions [132] and, metabolically, drives cholesterol and lipid biosynthesis through the induction of genes including *3-hydroxy-3-methylglutaryl-CoA reductase* (HMGCR), *squalene epoxidase* (SQLE) and *isopentyl-diphosphate δ isomerase 1* (IDI1). Furthermore, it drives the induction of the mevalonate pathway which is required for the expression of suppressive Treg cell markers such as *cytotoxic T-lymphocyte-associated protein 4* (CTLA-4) and *inducible co-stimulator* (ICOS) [132], [140]. Hence, Treg cell-specific deletion of mTORC1 impairs Treg cell suppressive function and homeostasis, resulting in the spontaneous activation of effector T cells and in the development of inflammation in barrier tissues [141]. In contrast, Toll-like receptor (TLR) signals enhance Treg cell proliferation through mTORC1 signalling pathway, *glucose transporter 1* (Glut1) upregulation, and glycolysis. However, these signals decrease the suppressive ability of Treg cells [142]. It is likely that the TLR signal results in high levels of pro-inflammatory cytokines that decrease Treg cell functionality even as Treg cells maintain mTORC1 expression [136].

While Treg cells are highly dependent on mitochondrial metabolism with the flexibility to also oxidize lipid or glucose, Tcons mainly convert glucose to lactate [143]–[145]. Treg cells appear to have a stronger respiratory capacity and preferentially oxidize glucose-derived pyruvate as compared to Tcons [146]. The high expression of *carnitine palmitoyltransferase 1a* (CPT1a) - the rate-limiting enzyme of FAO that allows the entry of acyl groups into the mitochondria - supports the possibility that Treg cells can use multiple fuel sources [143], [144].

By increasing the expression of glucose transporters, such as Glut1, on activated T cells, mTORC1 activation augments the intracellular concentration of glucose to support glycolysis [147]. mTORC1 signalling also induces glycolysis via the oncogene c-MYC, a crucial regulator of metabolic reprogramming in T cells [145]. The role of mTORC1 in lipogenesis is also

supported by the findings that rapamycin blocks the expression of genes involved in lipid synthesis and alters nuclear localization of the master regulators of lipid homeostasis, *sterol regulatory element-binding proteins* (SREBPs) [148].

Freshly isolated Treg cells express high levels of mTORC1 and ATP due to their high proliferation rate *in vivo* [133], making them refractory to TCR stimulation *in vitro* and renders them therefore anergic. The over-activation of mTORC1 in Treg cells also depends on the capacity of Treg cells to secrete leptin, a cytokine that activates mTORC1 via its class I cytokine receptor [149]. Hence, leptin neutralisation or transient rapamycin treatment reverses Treg cell anergy, hence re-inducing Treg cell proliferation upon TCR stimulation [149]. Recent findings suggested that Treg cells need to reduce transiently their metabolic rate to enter the cell cycle and proliferate [131]. This implicates that although high mTORC1 activity renders Treg cells refractory to TCR stimulation, it is also necessary for Treg cells to proliferate over time once the cell cycle is engaged [143].

Modulation of PI3K signalling can also alter cellular metabolism and FoxP3 expression. Genetic ablation of phosphatase and *tensin homolog on chromosome 10* (PTEN), the primary negative regulator of PI3K, results in an increase in glycolysis, loss of FoxP3 expression, and the induction of effector T cells [150], [151]. The observations by Wei et *al.*, who showed that deletion of Atg7 or Atg5 leads to Treg cells loss, is due to the upregulation of the metabolic regulators mTORC1 and glycolysis in autophagy-deficient Treg cells, contributing to defective Treg function [152].

1.5 The world of phosphoinositide 3-kinases

Based on their structure, substrate specificity and function, *phosphoinositide 3-kinases* (PI3-kinases) comprise eight members that are divided into three classes (class I, class II and class III), all of which phosphorylate the 3' hydroxy position of the inositol ring of phosphatidylinositol. PI3-kinase class I family members (that can be further divided into Class IA and Class IB based on their associated regulatory subunits) phosphorylate *phosphatidylinositol-(4,5)-diphosphate* (PIP_2) to generate the lipid second messenger *PI(3,4,5)P3* (PIP_3). Class II (i.e. PI3KC2α, PI3KC2β, and PI3KC2γ) phosphorylate phosphatidylinositol-(4)-phosphate and Class III PI3K (VPS34) phosphorylate PI on the third position to generate $PI(3,4)P_2$ and PI3P, respectively.

PI3-kinases are intracellular signal transducer lipid kinases and regulate multiple intracellular pathways by integrating signals from growth factors, cytokines, and other environmental cues. Therefore, PI3-kinases regulate diverse physiological functions and cellular processes including cell growth, survival and proliferation, cellular motility and differentiation, as well as intracellular trafficking and nutrient metabolism [153], [154]. Given the importance of PI3-kinases in controlling versatile intracellular pathways, alterations in PI3-kinases are frequently found in various cancer types as well as pathological immune deficiencies, and an increase interest is emerging towards delineating the molecular mechanisms influenced by PI3-kinases [155].

This work has solely been investigating the role of the class III PI3-kinase, with VPS34 being its sole member. Hence, the following chapters will focus on the Class III PI3-kinase VPS34.

1.5.1 The class III PI3-kinase VPS34

VPS34 (vacuolar protein sorting 34) is encoded by *Pik3c3* and is highly conserved from yeast to mammals. In yeast, where it was first identified, it is required for vacuole protein sorting [154], [156]–[159]. It is the catalytic subunit of the class III PI3-kinase family and it phosphorylates PI on the 3’ position of the inositol ring to generate the second messenger *phosphatidylinositol 3-phosphate* (PI3P) [156]. VPS34 is the main source of PI3P, and provides a platform for the recruitment of effector proteins containing phox homolog (PX) or FYVE

domains (FYVE zinc finger domain is named after the four cysteine-rich proteins: Fab 1 (yeast orthologue of PIKfyve), YOTB, *Vac* 1 (vesicle transport protein), and *early endosome antigen 1E* (EA1)) [160]–[162].

VPS34 is closely associated with the serine threonine kinase VPS15, which is required for the activation of VPS34 [163]. In yeast and specific mammalian cell types, VPS34 plays an important role in autophagy and endocytosis, with two different protein complexes mediating these distinct processes (autophagy complex vs. endocytosis complex). Both complexes contain VPS34 and VPS15 as well as the functional adapter Beclin-1 (Atg6 in yeast) [164]. The forth unit of complex I (autophagy complex) is Atg14L (Atg14 in yeast) while UVRAG (UV radiation resistance-associated gene, Vps38 in yeast) is part of complex II (endocytosis complex) [156], [164]. Further distinct proteins interact with both complexes, such as Bcl-2 [165] and Ambra [166] in the case of the autophagy complex, and Rubicon in the case of the endocytosis complex [167]. Meanwhile, Bif-1 is thought to interact with both complexes [166]–[168].

1.5.2 VPS34 in autophagy

Autophagy is an evolutionary conserved and fundamental catabolic process required for cellular homeostasis. It plays an important role in the degradation of protein aggregates, damaged organelles, and the recycling of nutrients. Autophagy is upregulated by nutrient deprivation (starvation-induced autophagy) and various forms of stress, such as oxidative stress, accumulation of misfolded proteins, bacterial and viral infection, in order to adapt to energy demand.

There are three forms of autophagy, referred to as macroautophagy, microautophagy and chaperone mediated autophagy (CMA). During microautophagy, autophagic substrates are directly engulfed by the lysosome; CMA consists in the degradation of tagged proteins with a specific sequence motif that binds to chaperone HSP70 which are then transported and internalised in the lysosome [169]. Macroautophagy is the most widely studied form of autophagy and will hereafter simply be referred to as autophagy. Autophagy is generally divided into three different steps: a) initiation, formation and closure of the autophagosome; b) maturation of the autophagosome and fusion with the lysosome, leading to lysosomal degradation; and c) autophagosome-lysosome reformation. The initiation of autophagy

involves the formation of doubled membraned vesicles, so-called autophagosomes, from the phagophore (also referred to as isolation membrane) [170]. During the elongation step, the pagophore enlarges and closes around cytoplasmic proteins, damaged or excess organelles, or invading intracellular pathogens [171]. This process is mediated by two ubiquitin-like conjugation systems, Atg7-Atg10 and Atg7-Atg3. Analogous to ubiquitination, Atg12 is conjugated to Atg5 by Atg7—an E1-like protein—and Atg10—an E2-like protein [172]. The Atg7-Atg3 conjugation system catalyses the conjugation of the microtubule-associated protein *L chain 3-I* (LC3-I) to phosphatidylethanolamine to generate the membrane-bound lipid form, LC3-phosphatidylethanolamine, also called LC3-II [173]. This ultimately leads to membrane closure and fusion of the mature autophagosome with the lysosome, where the cargo is degraded by lysosomal hydrolases. A simplified scheme of the autophagy process is shown in **Figure 1.1**.

Depending on the context and the cytoplasmic material engulfed, two form of autophagy can be distinguished - selective autophagy and non-selective autophagy. Selective autophagy described the degradation of particular organelles or content such as mitochondria, ER, aggregates, Golgi, etc. These processes have been named according to the organelle engulfed (mitophagy, ER-phagy, aggrephagy, Golgi-phagy etc).

In budding yeast, flies and some mammalian cell lines, VPS34 is critical for autophagic processes by providing the main source of PI3P [174]. The level of PI3P is tightly controlled by VPS34 as well as Jumpy and MTMR3, two PI3P phosphatases, and determines the size and the production rate of autophagosomes, and inhibition of PI3P phosphatases enhances autophagy [175], [176]. During vesicle nucleation and autophagosome biogenesis, PI3P synthesis allows the recruitment of effector proteins harbouring PI3P-binding domains, such as DFCP1 (*double FYVE-containing protein 1*) or WIPI1-2 (*WD-repeat protein interacting with phosphoinositide*) [177], [178]. These proteins promote autophagosome maturation and serve as a scaffold for the recruitment of Atg proteins required for the downstream steps. PI3P is also continuously required during the maturation step, where it regulates the trafficking of autophagosomes and their fusion with the lysosome [179]. However, alternative pathways mediate this process as it has been reported that other lipids, in particular PtdInsI4P and PtdInsI5P, are also involved in autophagosome formation [180]–[183].

While the role of VPS34 is well documented for budding yeast, it is less straight forward to assess the role of VPS34 in mammalian cell types due to the redundancy of PI3P

sources (PI3K class II has also been shown to contribute to PI3P production, however at a very low level); and the possible role(s) of VPS34 beyond autophagy and endocytosis. Genetic mouse models have brought insights into the *in vivo* role and function of mammalian VPS34: VPS34 null mutants are prenatally lethal (between E7.5 and E8.5) [184]; Tissue-specific deletions have shown that in heart and liver, VPS34 is essential for autophagy and the functioning of these organs [185]; VPS34 deletion in sensory neurons leads to neuron degeneration, due to a drastic defect in the endo-lysosomal pathways. However, sensory neurons lacking VPS34 were still able to form LC3-positive autophagosomes, due to an alternative pathway that requires Atg7 and the conventional conjugation system [186].

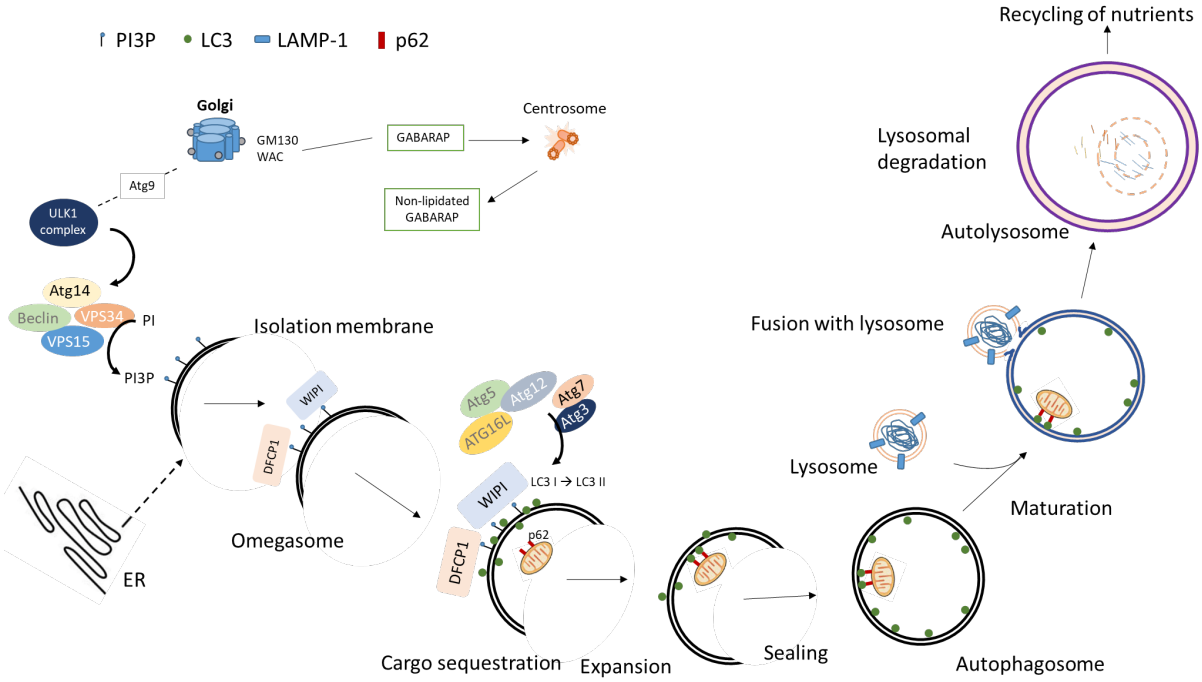

Figure 1.1: Overview of the autophagy process.
Autophagy is initiated by various conditions of stress, including starvation, hypoxia, oxidative stress, protein aggregation, and *endoplasmic reticulum* (ER) stress. Recruitment of the *Unc-51-like kinase 1* (ULK1) complex (consisting of ULK1, *autophagy- related protein 13* (ATG13), *RB1-inducible coiled- coil protein 1* (FIP200) and ATG101, not displayed in the scheme), and Atg9 to the omegasome triggers the nucleation of the phagophore by phosphorylating components of VPS34 complex I (consisting of *vacuolar protein sorting* 34 (VPS34), VPS15, Beclin 1, and ATG14). Together with the *activating molecule in Beclin 1-regulated autophagy protein 1* (AMBRA1)), VPS34 complex I activates the production of PI3P at the omegasome. PI3P then recruits the PI3P effector proteins *WD repeat domain phosphoinositide- interacting proteins* (WIPIs) and *zinc-finger FYVE domain-containing protein 1* (DFCP1) to the omegasome via interaction with their PI3P- binding domains. WIPI binds ATG16L1, which subsequently recruits the ATG12~ATG5–ATG16L1 complex that induces the conjugation of the microtubule- associated protein *light chain 3* (LC3-I) protein to membrane- resident

phosphatidylethanolamine (PE), thus forming the membrane-bound, lipidated form of LC3 (LC3-II). The cargo to be degraded is sequestered (e.g. malfunctioning mitochondria), and sealing of the autophagosomal membrane gives rise to a double-layered vesicle called the autophagosome, which matures and finally fuses with the lysosome, giving rise to the autolysosome were acidic hydrolases degrade the autophagic content, and nutrients are released back to the cytoplasm to be used again by the cell. *Scheme based on Dikic and Elazar* [187].

Autophagy is a tightly controlled process induced upon stress signals. The master regulators that integrate these signals to modulate autophagy activation are mTORC1 and AMPK. mTORC1 is critical to direct the balance of catabolic and anaerobic activities. In nutrient rich conditions, mTORC1 is activated and phosphorylates S6K1 and 4E-BP1, which in turn trigger the synthesis of proteins, lipids, and nucleotides. mTORC1 represses autophagy by phosphorylating UNC51-like Ser/Thr kinase (ULK1), responsible for autophagy initiation [188], and the *transcription factor EB* (TFEB), which triggers transcription of genes involved in lysosome biogenesis [189]. On the other side, AMPK positively regulates autophagy. AMPK is activated by cellular stress and an imbalance in the cell energy status, such as a low ATP/AMP ratio, and the depletion of glucose (which drops the ATP/AMP ratio) by phosphorylation via LKB1 (*liver kinase B1*) [190]. Once activated, AMPK phosphorylates and activates the TSC2 complex, which inhibits mTORC1. Moreover, AMPK can directly phosphorylate Raptor, the regulatory subunit of mTORC1 complex, at S863, which has an inhibitory effect on the mTORC1 complex [191].In addition, it can directly activate ULK1 by phosphorylation [192], [193].

After induction of autophagy, ULK1 complex (formed of ULK1, FIP200, Atg13 and Atg101) is activated and translocates from the cytoplasm to the omegasome until completion of the phagophore. ULK1 act as a platform for the recruitment of the machinery necessary for autophagosome formation. It recruits and positively regulates VPS34 activity by phosphorylating Beclin1 at S14 [194] and S30 [195], ATG14L at S29 [196], and by directly binding to VPS34 complex I [197]. ULK1 also phosphorylates Raptor at multiple sites, preventing the binding of Raptor to mTORC1 substrates [198].ULK1 also regulates Atg9 trafficking, a transmembrane protein that travels from the Golgi, endosomes or Atg9 positive membranes to autophagic structures (omegasome, phagophores and autophagosomes). Atg9 function is still unclear but has been suggested to deliver components to the recruited locations and to participate in membrane scaffolding [199].

ULK1 is indirectly recruited to the omegasome by the Golgi apparatus. WAC and GM130, two proteins located at the Golgi apparatus, regulate a pool of GABARAP (a member of the Atg8 family) that traffics to the centrosome. The non-lipidated centrosomal GABARAP binds then the omegasome, where it recruits ULK1 by its LIR (*LC3 interacting region*) domain [177]. Upon recruitment and activation by ULK1 at the omegasome, VPS34 produces PtdIns3P that serves as a platform for FYVE and PROPPIN domain – containing proteins, such as DFCP1 or WIPI2. WIPI2 directly binds Atg16L1 [200], a critical step for the induction of the autophagic flux [201].

The elongation of the phagophore relies on two ubiquitin-like conjugation systems. Cytosolic precursor Atg8 proteins (LC3/GABARAP) are cleaved by Atg4, a cysteine protease, exposing a Gly residue at the C-terminal region of Atg8. Cleaved Atg8 binds to Atg7 (an E1-like enzyme), is then transferred to Atg3 (an E2-like enzyme) and conjugated to the membrane-bound form of *phosphatidylethanolamine* (PE) through the activity of Atg12-Atg5-Atg16L1 system (which acts as an E3-like enzyme). The formation of the ATG16L1 complex start with the linking of Atg12 and Atg7 through a thioester bond, giving rise to an Atg12-Atg7 intermediate complex. Atg12 is then transferred to Atg10 (an E2-like enzyme). Atg5 has an acceptor Lys, where Atg12 is finally conjugated via an isopeptide bond, and two sets of the Atg12-Atg5 complex bind to Atg16L1 for form one Atg16L1 complex [202], [203].

The initiation, nucleation and expansion steps of autophagy are followed by the maturation of the autophagosome and fusion with the lysosome, critical for degradation of the engulfed materials. Lipidated members of the LC3 family are crucial for the expansion and the closure of the phagophore. They associate with protein membranes where they act as an anchor for cargo receptors (SARs) such as p62 as well as other proteins like ULK1, VPS34, ATG14L, Beclin-1, Atg4 or Atg12-Atg5 to autophagic membranes.

The recruitment to and the fusion of the autophagosome with the lysosome requires changes in lysosomal pH, tethering factors such as the HOPS complex and RAB7, cytoskeleton motor proteins such as dynein, phospholipids including PtdIns3,5P2, the SNARE complex, and LC3 [177], [204], [205]. When the autophagosomal membrane fuses with the lysosome, giving rise to a so-called autolysosome, lysosomal hydrolyses degrade the engulfed material/organelles [177], [206] and export the obtained amino acid, nucleic acids, etc. to the cytoplasm [189].

To maintain their structure and identity, lysosomes undergo *autophagosome-lysosome reformation* (ALR). PtdIns4P and PtdIns(4,5)P2 orchestrate the induction of the autolysosome tubulation [207], [208], and PtdIns4P provides the substrate for the PIP5K1A kinase, which drives tubule scission together with the VPS34 complex II. Microtubules are necessary for ALR [209], and Dynamin2, a GTPase that mediates scission of cellular membranes and that can be activated by PtdIns3P, PtdIns4P, or PtdIns(3,4)P2, is involved in the process of tubule scission [210].

1.5.3 The role of autophagy in T cell activation

The first evidence that autophagy is taking place in T cells was provided by Li and colleagues who observed the formation of autophagosomes in Th1 and Th2 cells upon *in vitro* activation with αCD3/αCD28, leading to the conclusion that TCR signalling induces autophagy in effector $CD4^+$ T cells [211]. These observations were confirmed subsequently by several studies, as well as shown to hold true for human primary $CD4^+$ T cells as well. Together with Pua et *al*., who demonstrated the presence of lipidated LC3 in primary mouse $CD4^+$ T cells cultured in the presence of αCD3 [212], Li et *al*. reported that the key autophagy genes Atg5, Atg7, Beclin-1, and LC3 are expressed in $CD4^+$ T cells [211], [212]. Downregulation of these genes and inhibition of Jun amino-terminal kinase (JNK)/mitogen-activated protein (MAP) kinase pathways or PI3-kinase could inhibit autophagy in $CD4^+$ T cells, while inhibition of mTOR led to autophagy induction [211]. TCR-activation induces the expression of Beclin-1 [213] and LC3 protein levels and promotes TCR-driven proliferation of $CD4^+$ T cells. Indeed, Atg5-deficient $CD4^+$ T cells display impaired proliferation following in vitro TCR activation with αCD3/αCD28 and IL-2. However, autophagy inhibition did not alter TCR-driven activation of $CD4^+$ T cells, as cell surface expression of the activation markers CD25 and CD69 were not altered [212]. These observations were confirmed in other mouse models of Atg3, Atg5, Atg7 and VPS34 deletion in $CD4^+$ T cells [171], [214]–[217]. Published finding about how autophagy regulates effector and regulatory $CD4^+$ T cell activation, differentiation and effector functions are summarized in **Table 1. 1**.

Table 1.1: Summary of autophagy-related knock-out mouse models in T cells.

Deletion strategy	Phenotype	Authors & Reference
ATG3 *Lck-Cre Atg$^{f/f}$* *or ER-Cre Atg3$^{f/f}$*	- Reduced survival of naive CD4$^+$ and CD8$^+$ T cells - Expanded mitochondria and ER - *In vitro*: temporal accumulation of mitochondria and ER beginning 10 d after the deletion - cell death does not begin to increase until >3 week after deletion - proliferation defect	Jia et *al*. [171]
ATG5 Reconstitution with *Atg5$^{-/-}$* hematopoietic precursors.	- Enhanced CD8$^+$ T cell apoptosis in the periphery - Inability of CD4$^+$ and CD8$^+$ T cells to undergo TCR-induced proliferation	Pua et *al*. [212]
Lck-Cre Atg5$^{f/f}$	- Reduced survival of CD8$^+$ T cells but no influence on CD4$^+$ T cell numbers and short-term activation - Autophagy in CD4$^+$ T cells is required to transfer humoral memory - Mitochondrial and lipid load defects in in vitro differentiated memory CD4$^+$ T cells, compromised survival, without any collapse of energy production	Murera et *al*. [218]
GzmB-Cre Atg5$^{f/f}$	- Intact proliferation and function of effector cells - Reduced memory T cells	Xu et *al*. [219]
Lck-Cre Atg5$^{f/f}$	- Decreased thymocyte and peripheral T cell numbers, and decrease in cell survival - Increased mitochondrial mass in peripheral T cells	Stephenson et *al*. [216]
Cre-ERT2 Atg5$^{f/f}$	- Decreased peak effector response - Reduced cell viability during effector phase - Impaired effector-to-memory cell survival - Upregulation of p53, resulting in high ROS levels and ROS-dependent apoptotic cell death	Schlie et *al*. [220]
Foxp3-Cre Atg5$^{f/f}$	- Same observations as for FoxP3-Cre Atg7$^{f/f}$ (published by the same authors)	Wei et *al*. [152]

ATG7		
Lck-Cre Atg7$^{f/f}$	- Enhanced apoptotic death in mature CD4+ and CD8+ T cells - Increased mitochondrial content in autophagy-deficient CD4+ and CD8+ T cells, resulting in increased ROS accumulation and cell death	Pua et *al*. [221]
Lck-Cre Atg7$^{f/f}$	- Increased ER content in mature T lymphocytes - Deregulated stimulation-induced calcium influx and efflux - Autophagy regulates calcium mobilization in T lymphocytes through controlling ER homeostasis - Failure of T cell proliferation *in vitro* - Failure of CD8$^+$ T cells to enter into S-phase after TCR stimulation - Accumulation of the cell-cycle inhibitor CDKN1B (Cyclin-dependent kinase inhibitor 1B)	Jia et *al*. [222] and [214]
Lck-Cre Atg7$^{f/f}$	- Reduced thymocytes and peripheral T cell numbers - Decreased IL-2 and IFN-γ production and defective activation-induced cell proliferation *in vivo* and *in vitro* - Macroautophagy activation is required to ensure sufficient energy production during T cell activation - Decreased proliferation in response to TCR stimulation	Hubbard et *al*. [215]
Lck-Cre Atg7$^{f/f}$	- Similar observations to *Lck-Cre Atg5$^{f/f}$* (published by the same authors)	Stephenson et *al*. [216]
GzmB-Cre Atg7$^{f/f}$	- Similar to GzmB-Cre Atg5$^{f/f}$ mice: intact proliferation and function of effector cells but reduced memory T cells - Dysregulated lipid metabolism, mitochondrial FAO, glucosamine 6-phosphate, and glycan-biosynthesis pathways	Xu et *al*. [219]
CD4-Cre Atg7$^{f/f}$	- Peripheral T cell lymphopenia, leading to proliferation and an activated phenotype - Failure to establish CD8$^+$T cell memory to influenza and MCMV infection - Autophagy is highest in antigen-specific CD8$^+$ T cells	Puleston et *al*. [223]

Foxp3-Cre Atg7$^{f/f}$	- Increased cell death at the time of memory formation, - Compromised mitochondrial health - Increased expression of GLUT1 - Increased apoptosis of Treg cells - Lymphoid hyperplasia, increased cellularity of the spleen and peripheral lymph nodes, and increased effector/memory $CD4^+$ and $CD8^+$ T cells - Loss of Foxp3, Foxo, and Bach2 expression, especially after activation - Upregulation of the metabolic regulators mTORC1 and c-Myc and glycolysis, contributing to defective T_{reg} function - Enhanced glycolytic metabolism results in lineage destabilization and loss of effector function - Normal proliferate upon *in vitro* TCR stimulation with αCD3/CD28 + IL-2 and after adoptive transfer into Rag1$^{-/-}$ mice, suggesting that Atg7 may be dispensable for TCR-induced proliferation of Treg cells	Wei et *al*. [152]
ATG16L1 *Atg16l1*$^{\Delta CD4}$ *Atg16l1*$^{\Delta Foxp3}$	- Chronic intestinal inflammation accompanied by aberrant type 2 responses toward commensal and dietary antigens - Loss of $Foxp3^+$ Treg cells - Aberrant mucosal T_H2 cell expansion - Reduced survival and impaired metabolic adaptation to the intestine - Enhanced glycolytic metabolism results in lineage destabilization and loss of effector function	Kabat et *al*. [224]
Beclin-1 Rag1$^{-/-}$ blastocysts injected in Beclin-1$^{-/-}$ ESCs and implanted into foster mothers. *CD4-Cre BECN1$^{fl/fl}$*	- Reduction in thymic cellularity: impaired maintenance of lymphoid progenitors *in vivo* and *in vitro* - Normal *in vitro* proliferation of peripheral T cells - Reduced autophagic activity (reduced LC3 staining) - No differences in thymic development, but decrease in $CD4^+$ and $CD8^+$ T cells in the spleen and lymph nodes	Arsov et *al*. [225] Kovacs et *al*. [226]

	- Increased apoptosis upon TCR stimulation due to increased cell death-related proteins (procaspase-3, caspase-8, capsase-9, and Bim) - Th1 more susceptible to cell death than Th17	
VPS34 *Lck-Cre Pik3c3* $^{\Delta 17/18}$	- Increased T cell death and reduced proliferation - Impaired IL-7Rα trafficking, signalling, ad recycling - Mislocalized intracellular EEA1, HGF-regulated tyrosine kinase substrate, and Vps36 - Intact autophagy (TCR stimulated autophagy, starvation-induced, basal autophagy)	McLeod et *al*. [227]
CD4-Cre Pik3c3 $^{\Delta 4}$	- Reduced stability of Vps15 and Beclin-1 - Dispensable for T cell development but important for the survival of naïve T cells - Impaired autophagy in T cells - increased mitochondrial mass and accumulation of ROS	Willinger and Flavell [228]
CD4-Cre Pik3c3 $^{\Delta 4}$	- inflammatory wasting syndrome characterized by weight loss, intestinal inflammation, and anemia - severe defects in autophagic flux and accumulation of cellular organelles - normal intrathymic development of $CD4^+$ and $CD8^+$ T cells but impaired development of iNKT cells - Impaired peripheral homeostasis and function of Treg cells	Parekh et *al*. [217]
CD4-Cre Pik3c3 $^{\Delta 4}$	- Impaired cellular metabolism - $CD4^+$ T cells failed to differentiate into T helper 1 cells - reduced levels of active mitochondria upon T cell activation	Yang et *al*. [229]

1.5.4 VPS34 in endocytosis

Endocytosis is a process by which eukaryotic cells take up macromolecules and particles from the surrounding medium [230]. During endocytosis, extracellular material is internalized by plasma membrane which buds off inside the cell and the cargo might be recycled to the cell surface, trafficked to the *trans-Golgi network* (TGN) through the retrograde system, or sorted to *multivesicular bodies* (MVBs)/late endosomes for lysosomal degradation [231]. Different lipid phosphatases and kinases contribute to the endocytic trafficking. For instance, PtdIns(4,5)P2 is enriched at the plasma membrane where it recruits proteins of the clathrin-mediated endocytosis (CME) pathway; PtdIns3P is present at early endosomes and intraluminal vesicles (ILVs) and recruits proteins containing FYVE or PX domain (such as EEA1 or HRS).

The endosomal VPS34 complex (complex II) comprising VPS34, VPS15, Beclin-1 and UVRAG assembles at the early endosome by associating with Rab5-GTP to generate PI3P [154]. Rab5 interacts with VPS15 of the endocytosis complex, thereby increasing the synthesis of PI3P at this site. Endosomal PI3P recruits various downstream effector molecules such as EEA1, HRS, endosomal SNXs, and ESCRT proteins. These proteins directly bind to PI3P via their FYVE or PX domains, and regulate endosomal fusion, intralumenal vesicle formation, tubulation, and maturation [232], [233].

Endosomal maturation from early to late endosome depends on PI3P and is accompanied by the conversion from the early endosomal Rab5 to the late endosomal Rab7 [234], and cargo sorting into intraluminal vesicles mediated by the ESCRT complex. This process is partially regulated by VPS34. As small GTPases, Rab5 and Rab7 need GAP and GEFs to modulate their activity [235]. VPS15 binds to the activated form of Rab5 [236], [237], which consequently recruits the VPS34 complex. VPS34 is also able to interact with Rab7 through VPS15 [238], and recruits Armus to repress Rab7 activation in mammals [239].

Rab7 recruits RILP (Rab-interacting lysosomal protein) to mediate the fusion with the lysosome. PI3P also promotes translocation of late endosomes/lysosomes to the cell periphery by promoting the contact between late endosome and lysosomes to the *endoplasmatic reticulum* (ER) via the kinesin adaptors protrudin and FYCO1 [240]. Fusion of the late endosomes with lysosomes is depending on the conversion of PI3P to PI(3,5)P2 on

the late endosome, a process dependent on the PI(3)P 5-kinase PIKFYVE. A simplified scheme of the endocytic process is shown in **Figure 1.2**.

Lack of VPS34 protein or its kinase activity in yeast and flies results in defective endosomal sorting [241]. In mammalian cells, VPS34 inhibition results in impaired endolysosomal trafficking and recycling [238], [242] while VPS34 deletion in sensory neurons disrupts the endolysosomal pathway [186]. In the immune system, VPS34 is important for phagocytosis by generating PI3P at the phagosomal membrane [243]. While the initial step in phagosome formation is dependent in PI3K class Ia, maturation requires VPS34-generated PI3P [244]. PI3P is also important for the activation of the NOX2 NADPH oxidase, which generates *reactive oxygen species* (ROS) required for the destruction of the content of phagosomes [245]. More specifically, the PX-domain containing p40 subunit of NOX2 requires PI3P for its recruitment, and mutation in the PX domain leads to reduced ROS production [246].

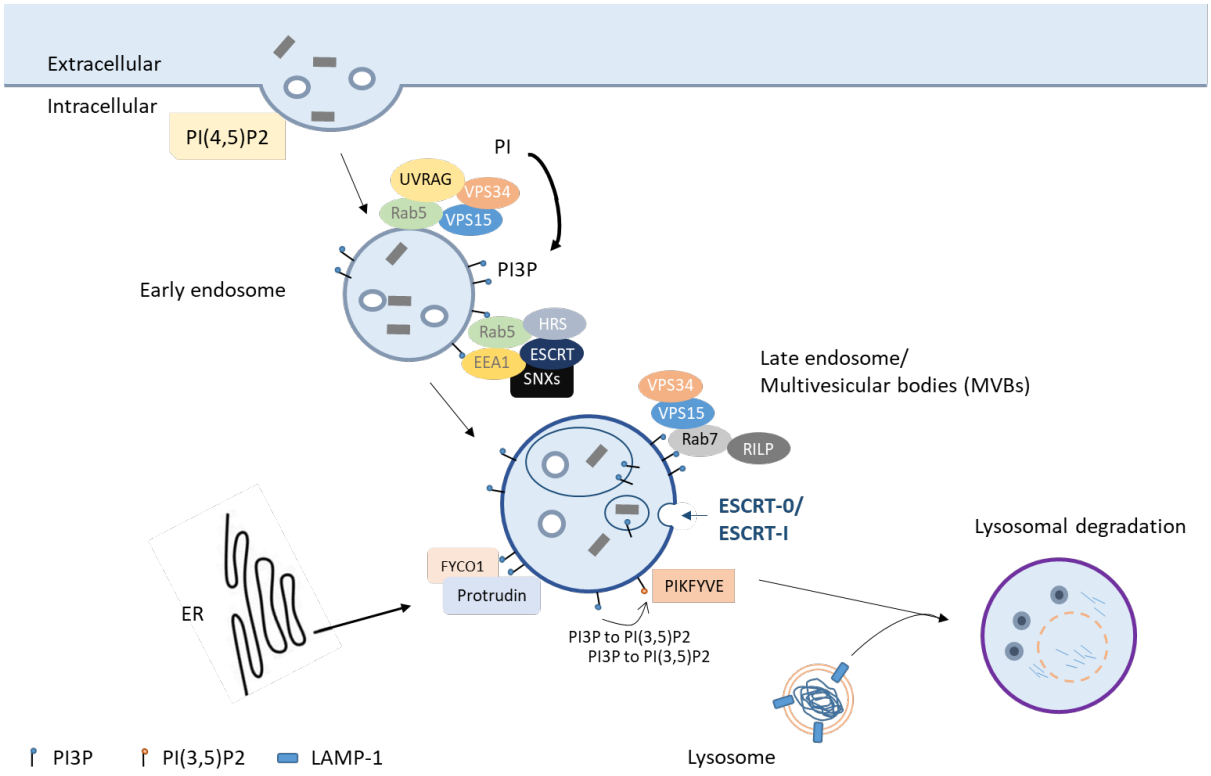

Figure 1.2: Overview of the endocytosis process.
Extracellular material is trafficked into the cell by clathrin-mediated endocytosis (relying on plasma membrane PI(4,5)P2 and PI(3,4)P2 generated by the class II PI3K), and sorted into PI3P-enriched early endosomes. The majority of PI3P is generated by the class III PI3K VPS34 complex II (including VPS34, VPS15, Beclin-1, and UVRAG), which assembles at the early endosomes via association of VPS15 with

Rab5-GTP. Endosomal PI3P recruits various downstream effectors, including *early endosome autoantigen 1* (EEA1), the ESCRT component *hepatocyte growth factor-regulated tyrosine kinase substrate* (Hrs), endosomal SNXs, and ESCRT proteins. Endosomal maturation is accompanied by the conversion of the early endosomal Rab5 to late endosomal Rab7, and cargo sorting into intraluminal vesicles is mediated by the ESCRT complex, two processes critically depending on PI3P. ESCRT proteins mediate the inward vesicle budding to generate *multivesicular bodies* (MVBs) and PI3P promotes the contact between late endosomes/lysosomes and the endoplasmatic reticulum (ER) via the kinesin adaptors protrudin and FYCO1, enabling the microtubule-dependent translocation of late endosomes and lysosomes to the cell periphery. Rab7 recruits RILP (Rab-interacting lysosomal protein) to mediate the fusion with the lysosome. Fusion of the late endosome with lysosomes is depending on the conversion of PI3P to PI(3,5)P2 on the late endosome, a process mediated by the PI(3)P 5-kinase PIKFYVE. Fusion with the lysosome gives rise to the autolysosome, were acidic hydrolases degrade the endosomal content. *Scheme based on Wallroth and Haucke* [231].

1.5.5 VPS34 in cytokinesis

Cell division by mitosis ends in a very complex physical separation of the two daughter cells, a process referred to as cytokinesis. Cytokinesis starts in the anaphase, with the assembly and the activation of the actomyosin contractile ring, that leads to the formation and the cleavage of the furrow ingression. Furrow-associated membrane trafficking and phosphoinositides have been shown to be an essential feature of cytokinesis. PI3P was suggested to regulate cytokinesis based on the observations that PI3P-positive endosomes are present at the *intercellular bridge* (ICB) [247]. Although still not fully understood, PI3P might be required for the recruitment and assembly of the ESCRT-III complex during abscission [248]. PI3P also recruits several effector proteins to endosomes, such as FYVE-CENT, ensuring their delivery to the ICB [249]. In return, FYVE-CENT binds and recruits several other effector proteins, i.e. TTC19, Beclin-1, VPS15, and UVRAG, which are known to regulate protein degradation and the recruitment of the ESCRT-III complex [250]. Interestingly, FYVE-CENT also can bind and directly recruit VPS34. Thus, the FYVE-CENT/VPS34 complex is probably involved in a positive-feedback loop that is critical to maintain high concentrations of PI3P within the cleavage furrow.

1.5.6 VPS34 in T cells

In the immune system, autophagy is a process essential for the development and function of T lymphocytes. It is a mechanism required for the clearance of intracellular pathogens, presentation of exogenous antigens [251], and cross-presentation of endogenous antigens by MHC class II molecules [252], [253]. It regulates the calcium mobilization and energy metabolism in T cells, is critical for effector $CD8^+$ T cell survival and memory formation, promotes the proliferation and survival of NKT cells, and downregulates *T cell receptor* (TCR) signalling through degradation of Bcl10.

The role of VPS34 in T cell immunity has been investigated using mouse models with T cell specific deletion of VPS34 [227], [228], [254]. McLeod et *al*. used a mouse model where exons 17 and 18 of *Pik3c3* was deleted in T cells through the activity of the Cre-recombinase expressed under the Lck promoter [227]. This led to a severely reduced numbers of $CD4^+$ and $CD8^+$ T cells in spleen and lymph nodes. Analysis of freshly-isolated T cells showed an increase

in apoptosis, a phenotype already observed in autophagy-deficient T cells (Atg5- or Atg7-null mutants), along with impaired proliferation, increased apoptosis, and failure to clear defective mitochondria [255], [256].

TCR stimulation and starvation induced comparable levels of LC3 puncta in VPS34$^{\Delta 17,18}$ and wild-type T cells, suggesting that these forms of autophagy are intact in the absence of VPS34 activity [227]. Similarly, basal autophagy, determined by the presence of autophagosomes by electron microscopy, seemed to be intact in VPS34$^{\Delta 17,18}$ T cells. The authors suggested that reduced T cell survival arises from a defect in endocytosis, as they observed a reduction in cell surface expression of IL-7Rα due to impaired receptor trafficking and recycling to the cell surface [227]. However, two other studies challenged these observations: Willinger and Flavell [228] and Parekh et *al*. [254] deleted VPS34 in T cells by using a system where the Cre-recombinase is expressed under the CD4 promoter and exon 4 of *Pik3c3* is flanked of *LoxP* sites. In VPS34$^{\Delta 4}$ T cells, the authors observed a reduction in the autophagic flux [228], challenging the observed 'normal' formation of LC3 punctae in VPS34$^{\Delta 17,18}$ T cells. The suggested role of VPS34 in IL-7Rα trafficking and recycling was challenged by a study showing that VPS34-deficient T cells from mixed bone marrow chimera expressed normal cell surface levels of IL-7Rα [228]. This implies that the observed reduction of IL-7Rα is caused by the lymphopenic environment rather a cell-intrinsic role for VPS34. Meanwhile, both studies reported a role of VPS34 in autophagy, as the autophagic flux was reduced in VPS34-deficient T cells [228], [254]. Intact autophagic flux is required for autophagosome production and removal of damaged or excessive mitochondria. When impaired, it results in increased ROS production eventually leading to cell death.

Figure 1.3 displays the domain organization of VPS34, highlighting in red the exons floxed in the different mouse models used to investigate the role of VPS34. The differences in targeting strategies might explain the observed discrepancies between the different studies described above: impaired autophagy was reported in studies using a mouse model with Cre-mediated deletion of exon 4 (VPS34$^{\Delta 4}$) while defective endocytosis was observed in VPS34$^{\Delta 17,18}$ T cells. Deletion of exon 4 could lead to a truncated protein unable to bind its protein partners. It has been show that the binding to VPS34 is necessary for the stability of Beclin-1, and lack of VPS34 lead to a reduction in Beclin-1 levels [257]. Beclin-1 is independently involved in autophagy, and Beclin-1 reduction might be a possible explanation

for the observed defect. Meanwhile, deletion of exon 17 and 18 could lead to a mutated version of VPS34 that can still bind and stabilize Beclin-1.

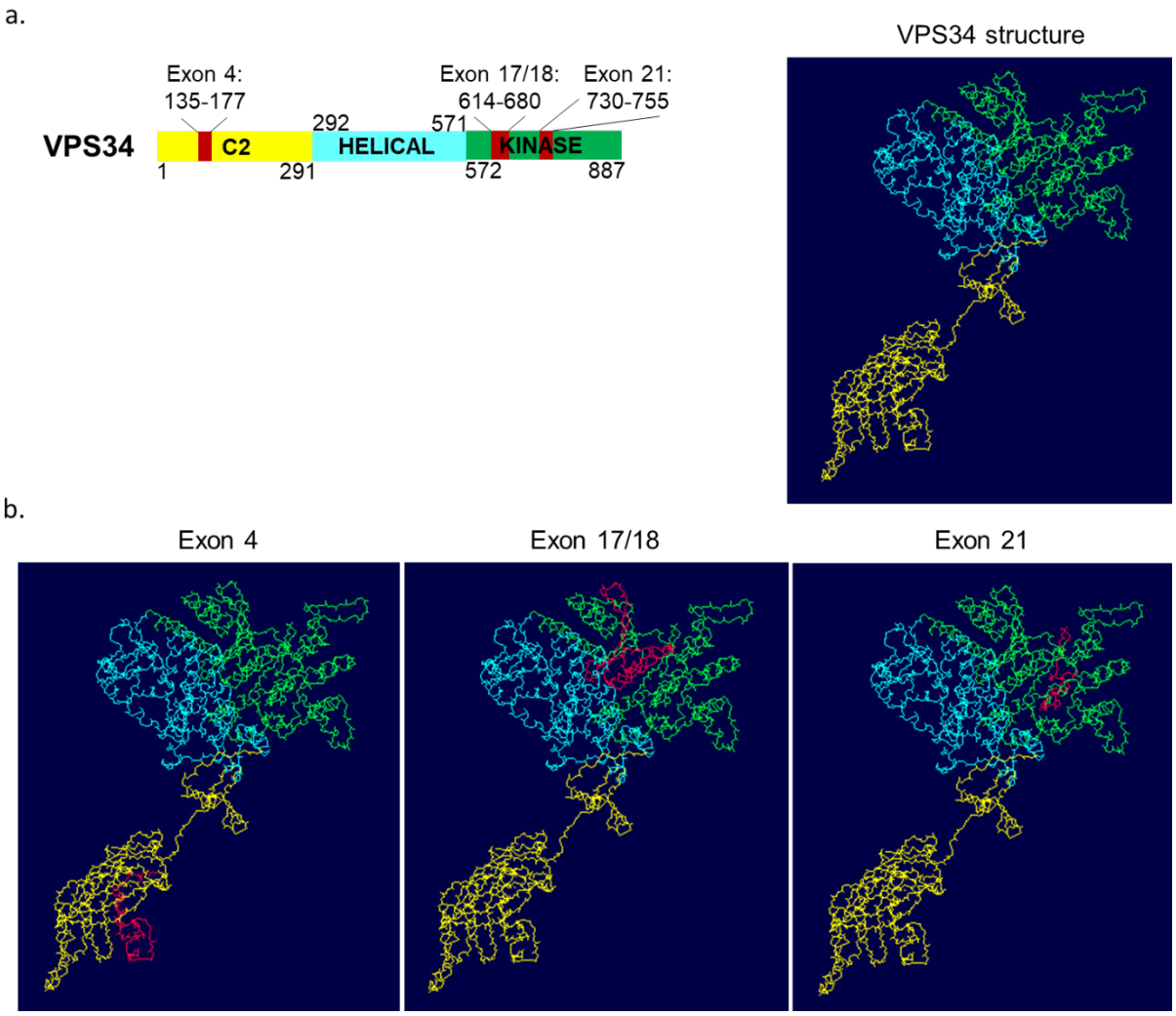

Figure 1.3: VPS34 structure and targeting strategies.

a) Domain organization and 3D structure of VPS34. **b**) 3D structure of VPS34 highlighting in red the exons floxed in the different mouse models used to investigate the role of VPS34. DeepView /SwissPdbViewer (v4.1.0) was used to create the 3D models [258].

1.6 Questions, Hypotheses and Objectives

1.6.1 Role of VPS34 in Treg cells: What are the molecular mechanisms underlying the fatal lympho-proliferative disease observed in mice with VPS34-deficient Treg cells?

While the biology and the functions of the class I PI3-kinases have been extensively studied and are well understood, less is known about class II and class III PI3-kinases, and even less in the context of the immune system.

A previous study conducted in aged $CD4^{Cre}$ *Pik3c*$3^{fl/fl}$ mice suggested that VPS34 controls T cell homeostasis, probably by regulating canonical autophagy, and has an effect on the number and effector functions of Treg cells, as these mice developed a wasting phenotype [254]. However, so far, no definite role for VPS34 in Treg cells has been proposed.

The cell-intrinsic role of VPS34 in Treg cells was investigated by Elisabeth Slack, a previous PhD student in the laboratory of Klaus Okkenhaug. She used a mouse model in which exon 21 of *Pik3c3* is conditionally excised under the action of *FoxP3*-induced Cre recombinase. These mice suffered from an autoimmune lymphoproliferative disease and died within 6 weeks, similar to mice lacking Treg cells. However, VPS34-deficient Treg cells developed normally, populated the peripheral lymphoid organs. This suggested that VPS34 is intrinsically required for effective suppressive functions of Treg cells.

My aim was to continue the work that Elisabeth Slack and Dr. Priya Schoenfelder (a postdoc that continued Elisabeth's work) had started and further dissect the role of VPS34 in Treg cells, concentrating on the following questions:

1) Which (novel) suppressive mechanism(s) of Treg cells is/are impaired by the deletion of VPS34?
2) Which further proteins are involved in processes relying on VPS34?

The approaches used to study these questions and the results obtained are presented in ***Chapter 3*** and ***4***.

1.6.2 Role of VPS34 in activated CD8⁺ T cells: Is VPS34 required for CD8⁺ T cell function and/or memory formation?

Upon clearance of pathogens or malignant cells, most effector $CD8^+$ T cells undergo apoptosis and only a small pool of cells remains that survive and differentiate into memory cells [71], [76], [259]. During this naïve-to-effector-to-memory – differentiation process, $CD8^+$ T cells undergo a cellular and metabolic reprogramming, i.e. a shift from anabolic processes and proliferation, to catabolic processes and contraction of the population size [219]. Using a mouse model where *Atg5* or *Atg7* is specifically depleted in antigen-specific $CD8^+$ T cells, Xu et *al*. [219] reported that autophagy is required for the formation of memory $CD8^+$ T cells, while it is dispensable for effector functions of *cytotoxic T lymphocytes* (CTLs). Therefore, I aimed to investigate the role of VPS34 in activated $CD8^+$ T cells using a *Granzyme B*-Cre recombinase system, in which naïve T cells develop normally and exon 21 of *Pik3c3* is deleted only after activation of $CD8^+$ T cells. In order to explore the role of VPS34 during the recruitment, the expansion and the activation of $CD8^+$ T cells *in vivo*, I used two different experimental strategies to analyse the numbers and phenotype of CTLs responding to an antigenic stimulus *in vivo*. First, I analysed antigen-specific $CD8^+$ T cells that have undergone clonal expansion in response to infection with *Listeria monocytogenes* expressing Ovalbumin (*Lm-OVA*) using antigen-specific MHC-II tetramers. I investigated the primary and, upon re-challenge, development of the secondary immune answer and immune memory formation. Secondly, I implanted $GzmB^{YFP\text{-}Cre}$ $Pik3c3^{fl/fl}$ mice subcutaneously with a syngeneic tumour cell line expressing the model antigen ovalbumin. CTLs infiltrate the tumour and become activated by cognate antigens expressed by the cancer cells. I used both models to assess whether VPS34-deficiency affects the activation, effector functions and/or memory formation of $CD8^+$ T cells. Finally, I supplemented *in vivo* experiments with *in vitro* analyses of activated $CD8^+$ T cells.

Since, to the best of my knowledge, the role of VPS34 in activated $CD8^+$ T cells has not been investigated yet, I had only one, but for the furthest broad, question: '*What is the role of VPS34 in activated CD8⁺ T cells?* '. The results I have obtained are presented in ***Chapter 5***.

Chapter 2

Material and Methods

2.1 Mice

2.1.1 Deletion of VPS34

Mice with a floxed version of the exon 21 of the *Pik3c3* gene (*Pik3c3*$^{fl/fl}$ mice) were crossed to mouse strains expressing the Cre-recombinase under the promoter of a cell type-defining protein to achieve cell type-specific deletion of VPS34. Exon 21 encodes a critical stretch (Ala730 to Thr754) of the VPS34 kinase domain. The floxed region comprised 75 base pairs, resulting in the in-frame deletion of 25 amino acids. This strategy was designed to create a kinase-dead truncated mutant VPS34 protein that retains its scaffolding properties and thus its ability to bind to Beclin-1 and VPS15. These mice were kindly provided by Bart Vanhaesebroeck.

2.1.2 Conditional depletion of VPS34 in regulatory T cells

Pik3c3$^{fl/fl}$ mice were crossed to *FoxP3*$^{Cre\text{-}YFP}$ transgenic mice to generate *FoxP3*$^{YFP\text{-}Cre}$ *Pik3c3*$^{fl/fl}$ mice where VPS34 is deleted specifically in Treg cells. In *FoxP3*$^{Cre\text{-}YFP}$ transgenic mice, the 3' UTR of the *FoxP3* locus harbours a viral IRES followed by a *yellow fluorescent protein* (YFP)-Cre recombinase fusion protein. The location of *FoxP3* on the X chromosome enabled the breeding of heterozygous *FoxP3*$^{YFP\text{-}Cre/wt}$ female offspring with VPS34-deficient and VPS34-sufficient Treg cells arising from a common environment.

2.1.3 Conditional depletion of VPS34 in activated CD8$^+$ T cells

To generate mice with a conditional depletion of VPS34 in activated CD8$^+$ T cells, *Pik3c3*$^{fl/fl}$ mice were crossed to a mouse strain expressing the transgene encoding the Cre recombinase under the *Granzyme B* promoter and a ROSA26-loxP-STOP cassette followed by the transgene for enhanced YFP (eYFP) to generate *GzmB*$^{YFP\text{-}Cre}$ *Pik3c3*$^{fl/fl}$ mice.

2.1.4 Housing and husbandry

FoxP3$^{Cre\text{-}YFP}$ *Pik3c3*$^{fl/fl}$ mice were used at 3.5–5.5 weeks old unless otherwise noted, with the age- and gender-matched wild-type mice containing the *FoxP3*$^{Cre\text{-}YFP}$ allele as control. Other mice were used at 8–12 weeks old unless otherwise noted. Breeding and *in vivo* procedures were carried out in accordance with the United Kingdom Home Office Regulation Office. Mice

were maintained in pathogen-free conditions at the Biological Service Unit of the Babraham Institute, the Veterinary School (MIRA) facility, and the Gurdon Institute of the University of Cambridge. Mice were euthanized by exposure to carbon dioxide, followed by cervical dislocation, or cervical dislocation followed by destruction of the brain.

2.1.5 Genotyping

Genotyping was performed by Transnetyx (www.transnetyx.com) using real-time PCR.

2.2. Isolation of cells

Mice were euthanized according to a Schedule 1 method and spleen, thymus, lymph nodes (axillary, cervical, brachial, and inguinal) and were applicable tumours were harvested in PBS or RMPI-1640. Distinct population of cells were enriched for by *magnetic-activated cell sorting* (MACS) using cell-type specific kits from Miltenyi or StemCell. In both cases, manufacturers' protocol was followed. To increase the purity of the isolated cell population, cell enrichment was followed by fluorescence-activated cell sorting (FACS) when required.

2.2.1 Magnetic-activated cell sorting (MACS) using Miltenyi kits

Following preparation of single cell suspensions, cells were resuspended at $1x10^8$ cells/ml in MACS buffer and incubated with 1 µg/ml biotin-conjugated αCD8 or αCD4, αB220, αDX5 and αMHC-class II (Ia/b) (all from BioLegend) for 30 minutes at 4 ^oC. Samples were washed, centrifuged for 5 minutes at 500 g and incubated with anti-Biotin MicroBeads (Miltenyi Biotech) for 30 mins at 4 ^oC. Cells of interest were negatively selected using LS separation columns and MidiMACS^{TM} Separator (Miltenyi Biotech) in accordance to the manufacturer's instructions.

2.2.2 Magnetic-activated cell sorting (MACS) using EasySep® (StemCell) kits

Briefly, cells in single cell suspensions were resuspended at $1x10^8$ cells/ml in FACS buffer, transferred to FACS tubes and 50µl/ml Rat Serum was added. 25µl/ml of the Isolation Cocktail was added and cells were incubated for 10mins at room temperature. RapidSheresTM were

vortexed for 30 seconds, 37.50µl/ml added to the cells and incubated at room temperature for 2.5 minutes. Samples were topped-up with up to 2.5ml FACS buffer, tubes were placed in the magnet and incubated for 2.5 minutes at room temperature to allow separation. In a continuous motion, the magnet was inverted and the enriched cell suspension was transferred to a fresh tube.

2.2.3 Fluorescence activated cell sorting (FACS)

Following single cell preparation and immune-magnetic enrichment (where applicable), cells were stained with the appropriate surface antibodies for FACS sorting depending on the experiment. Cells were incubated for 45 minutes at 4°C, washed twice with FACS buffer, and passed through 30µm filters (Partec CellTrics) to remove cell clumps. Cells were resuspended in 500ul of FACS buffer containing 5% FCS and cell sorting was carried out on a BD Aria IIu (BD Biosciences) or MoFlo Astrios (Beckman Counter) cell sorter.

For experiments using *GzmB*$^{YFP\text{-}Cre}$ *Pik3c3*$^{fl/fl}$ mice, viable CD8^{+} CD62L^{high} CD44^{low} were FACS sorted for subsequent in vitro stimulation with αCD3/CD28. For Western blot analysis or DNA isolation, viable CD8^{+} CD44^{high} YFP^{+} cells were FACS sorted.

For *in vitro* Treg cell differentiation assays, viable CD4^{+} CD62L^{high} CD44^{low} were FACs sorted. For proteomic profiling of Treg cells from mosaic *FoxP3*$^{YFP\text{-}Cre/wt}$ *Pik3c3*$^{fl/fl}$ mice, DNA isolation for PCR, metabolic analysis by SeaHorse or protein analysis by Western blot, viable CD4^{+} CD25^{+} YFP^{+} cells were FACs sorted. Cells were collected in Falcon tubes contained 1ml RPMI with 5% FCS.

2.3 Staining and analysis by flow cytometry

2.3.1 Staining for cell surface markers

Single cell suspensions from spleen, thymus and lymph nodes was prepared by passing the organs through a 40µm cell strainer (BD Falcon) using the plunger from 2.5 ml syringes into FACS buffer (2% v/v foetal calf serum (FCS, heat inactivated, LabTech) in PBS). Red blood cells were lysed with 1 ml/spleen ACK buffer (Sigma-Aldrich) and stopped after 5 minutes by adding FACS buffer. Staining for flow cytometry was performed in 96 well plates (round

bottom, Greiner). Samples were centrifuged for 3 minutes at 540 x g and supernatant discarded. The cell pellet was resuspended in 50 µl staining FACS buffer containing the appropriate fluorochrome-conjugated antibodies, αCD16/CD32 to block unspecific Fc receptor binding and a fixable viability dye. A complete list of fluorochrome-conjugated antibodies used in flow cytometric assays is given in **Table 2.1**. Samples were incubated for 30 to 45 minutes at 4^{o}C and then washed twice with FACS buffer. If required, samples were subsequently stained for intracellular antigens, cytokines, or Annexin V (as specified) (**2.3.2 – 2.3.3**).

The CD8^{+} T cells response to Lm-OVA infections was detected by staining with PE or APC labelled H-2D^{b} MHC class I tetramer loaded with the OVA 257-264 (SIINFEKL) peptide (NIH tetramer core facility USA) at a dilution of 1 in 100.

Table 2.1: List of fluorochrome-conjugated antibodies used for extracellular staining for flow cytometric analysis

Specificity	Clone	Conjugation	Concentration (µg/ml)	Supplier
CD4	RM4-5	BV510	0.5	BioLegend
CD4	GK1.5	BUV805	0.5	BioLegend
CD8α	N418	BV785	0.5	BioLegend
CD11c	N418	Pacific Blue	1	BioLegend
CD19	6D5	PE Dazzle594	0.5	BioLegend
CD19	1D3	BUV395	0.5	BD Bioscience
CD25	PC61	BV605	0.5	BioLegend
CD25	PC61	BV785	0.5	BioLegend
CD38	90	PE Dazzle594	1	BioLegend
CD44	IM7	PerCP Cy5.5	0.5	eBiosciences
CD44	IM7	AF700	0.5	BioLegend
CD62L	MEL-14	PE	1	BioLegend
CD62L	MEL-14	BV711	1	BioLegend
CD69	H1.2F3	PE-Cy7	1	eBiosciences
CD80	16-10A1	PerCP Cy5.5	1	BioLegend

CD86	GL-1	PE-Cy7	1	BioLegend
CD98	4F2	PE	1	BioLegend
CD103	2E7	PE	1	eBiosciences
CD107 (Lamp-1)	1D4B	BV421	1	BioLegend
CD127	A7R34	PE-Cy7	1	BioLegend
CD183 (CXCR3)	CXCR3-173	BV605	1	BioLegend
CD223 (LAG-3)	C9B7W	APC	1	BioLegend
CD278 (ICOS)	15F9	PE	1	BioLegend
CD278 (ICOS)	7E.17G9	BV421	1	BD Bioscience
CD279 (PD-1)	29F.1A12	PE-Cy7	1	BioLegend
F4/80	BM8	PE	1	BioLegend
GITR	YGITR 765	PE-Cy7	1	BioLegend
I-A/I-E (MHC-II)	M5/114.15.2	PE-Cy7	1	BioLegend
KLRG1	2F1/KLRG1	BV605	0.5	BioLegend
NK1.1	PK136	BV650	0.5	BioLegend
TCRβ	H57-597	BUV737	0.5	BD Bioscience
Tetramer	SIINFEKL	PE	2	NIH

2.3.2 Staining for transcription factors and cytokines

To assess cytokine production, 0.2 – 1 x10^6 cells per sample were incubated in 200µl T cell culture medium (TCM) (RPMI-1640 (Gibco) with 10% v/v FCS, 0.005% v/v β-mercaptoethanol (Sigma), 1% v/v Penicillin/Streptomycin (Gibco)) containing 50ng/ml PdBU (Tocris) and 1µM ionomycin (Sigma) for a total of 5-6 hours at 37 ^oC, 5% CO_2. Alternatively, 5x10^6 splenocytes were stimulated in the presence of 10nM OVA257-264 peptide (SIINFEKL) (ProImmune, UK) for to measure antigen specific cytokine release from mice infected with either Lm-OVA. To assess levels of LAMP-1 (CD107a), α-CD107a-BV421 (BioLegend) was added during the re-stimulation phase.

One hour after the start of the re-stimulation, 1x Brefeldin A (eBioscience) was added to each well. At the end of the re-stimulation, cells were washed once with FACS buffer and stained for cell surface antigens. For intracellular staining, samples were resuspended in 100µl/well

Fixation Buffer (eBiosciences, FoxP3 Fix-Perm kit) and incubated for 15 minutes at room temperature. Subsequently, cells were washed with Permeabilization Buffer (eBiosciences) and resuspended in 50µl Permeabilization Buffer containing the appropriate fluorochrome-conjugated antibodies. **Table 2.2** provides a list of antibodies used for intracellular staining. Samples were incubated for 20 minutes at room temperature and washed twice with Permeabilization Buffer and resuspended in 50µl FACS buffer for FACS analysis.

Table 2.2: List of fluorochrome-conjugated antibodies used for intracellular staining for flow cytometric analysis

Specificity	Clone	Conjugation	Concentration (µg/ml)	Supplier
CD152 (CTLA-4)	UC10-4B9	BV421	1	BioLegend
FoxP3	MF-14	AF488	1	BioLegend
FoxP3	FJK-16s	PE-Cy5.5	1	eBiosciences
FoxP3	FJK-16s	eFluor450	1	eBiosciences
Granzyme B	GB11	AF647	1	BioLegend
IL-10	JES5-16E3	PE	1	eBiosciences
IL-17A	eBio17B7	APC	1	eBiosciences
IFN-γ	4S.B3	PE-Cy7	1	BioLegend
Ki-67	SolA15	eF405	1	eBiosciences
TNF-α	MP6-XT22	AF700	1	BioLegend

2.3.3 Detection of apoptotic cells by Annexin V staining

The Annexin V/Dead Cell Apoptosis Kit with PerCP-Cy7 Annexin V (BioLegend, Cat #640950) was used alongside Fixable Viability Dye eFluor 780 (eBioscience) to detect apoptotic cells. Following staining for cell surface markers, cells were washed twice with FACS and centrifuged at 540 x g for 3 minutes, and subsequently washed twice with Annexin-binding buffer. Cells were stained with Annexin V in 50µl Annexin-binding buffer for 20 minutes at room temperature in the dark. After the incubation period, 200µl Annexin-binding buffer were added and cells were analysed by flow cytometric analysis within 1 hour of staining.

2.3.4 Staining for mitochondria

Cells were stained with 0.25µM MitoTracker Orange Orange CM-H_2-TMRos, staining for mitochondrial potential/active oxidative phosphorylation, or MitoTracker Orange CM-TMRos, staining for mitochondrial potential in RPMI-1640 medium containing 10% FCS and 1% Pen/Strep for 15 minutes at 37 ^{o}C. Samples were washed twice with TCM and staining for flow cytometry was performed as described above.

2.3.5 Flow cytometry and data analysis

Flow cytometry analyses were performed on either a Becton Dickinson LSR Fortessa 5 equipped with BD FACSDiva™software (BD Biosciences), an Attune NxT (Thermo Fisher Scientific), or a Cytek Aurora (Cytek Biosciences). Data were analysed using FlowJo software (Version vx.10.2 and 10.5.3, Tree Star Inc.) and results were plotted in and statistical analysis calculated using Prism version 7 and 8 (GraphPad, LaJolla, CA).

2.4 Functional assays

2.4.1 In vitro stimulation with anti-CD3 and anti-CD28

For *in vitro* T cell stimulation assays, flat bottomed 96 well Nunclon delta surface plates (#167008, Thermo Scientific) were coated overnight at 37°C with plate bound anti-CD3 (1-2µg/ml) (BioLegend, #100314) and anti-CD28 (2µg/ml) (#102112). On the following day, the preparation of cells (either total splenocytes, lymph nodes or sorted naïve $CD4^+$ or $CD8^+$ T cells) was carried out as described earlier in section 2.2.

In order to assess *in vitro* proliferation, equal numbers of cells from each sample was resuspended in 1ml PBS and mixed with an equal volume of 10µM Cell Proliferation Dye eFluor 450 (eBioscience, #65-0842-85) in PBS and incubated for 10 minutes at 37°C. Cells were then washed twice in PBS by centrifuging at 500 x g for 5 minutes, before resuspending at 2 x 10^6 cells/ml in RPMI complete medium (RPMI 1640 (Life Technologies #21875-034) + 5% heat-inactivated FCS (Labtech) + 1% Pen/Strep (Invitrogen #15070-063) + 50 µM β-Mercapto-ethanol (Sigma-Aldrich #M3701)). 2x10^5 cells/100µl were plated and 100µl of RPMI complete medium containing 1µM VPS34-IN1 or DMSO were added (these were made up at 2x final

concentration in order to take in account the dilution within the wells). Plates were incubated for 3 days at 37°C (5% CO_2).

2.4.2 In vitro BrdU cell cycle analysis

The BrdU phase flow kit (BioLegend# 3707040) was used to carry out *in vitro* cell cycle analysis. $CD8^+$ T cells stimulated with anti-CD3/CD28 for 48h and expanded in IL-2 for five days were were pulsed with 1mM BrdU made up in complete RPMI medium and incubated at 37°C for 2 hours. Cells were centrifuged at 540g for 3 minutes at 4°C and washed twice with PBS. Cells were stained with appropriate surface antibodies in 50µl of FACS buffer and incubated for 45 minutes at 4°C. Cells were washed twice with FACS buffer, fixed by adding 100µl of Buffer A (provided in the kit) and incubated at 4°C for 20 minutes. Cells were washed twice in FACS buffer and left in FACS buffer overnight in the fridge. Following day, cells was washed with Buffer B (Buffer B was diluted 1:10 with MilliQ water). Cells were incubated with 100µl Buffer C and incubated at room temperature for 10 minutes. Cells were washed once with Buffer B and the fixation step was repeating by incubating the cells with 100µl Buffer at room temperature for 5 minutes, following by washes using Buffer B. Cells were centrifuged and treated with 30µl DNAse (Reconstituted DNAse by adding 1 ml of PBS (Ca/Mg_2^+) per vial, allowing for the DNAse to dissolve for 2-3 minutes). Cells were incubated for 1 hour at 37°C. Following this, cells were washed in 200µl of Buffer B and stained with anti-BrdU antibody for 20 minutes at room temperature in the dark. Cells were washed first in Buffer B, then in FACS buffer. Cells were resuspended in 50µl FACS buffer containing 1:10 dilution of 7-AAD, incubated for 10 minutes in the dark at room temperature before acquisition.

2.4.3 CD80 trans-endocytosis and degradation assay

To test the capacity to deplete and digest CD80 from antigen presenting cells (APCs) through CTLA-4 – mediated trans-endocytosis, Treg cells were co-cultured with Chinese Hamster Ovary (CHO) cells expressing GFP-tagged CD80 (a kind gift from Professor David Sansom) in CHO cell medium (DMEM containing 25mM D-glucose (Sigma), 1mM sodium pyruvate (PAA), 10% v/v FBS, 2mM glutamine, 1% v/v Pen/Strep, 5mM β-mercaptoethanol and 500ug/ml G418 sulphate (Invitrogen)). CHO cells were co-cultured in a 1:10 ratio with $CD4^+$ T cells obtained by MACS purification in αCD3-coated (1 µg/ml) 48-well plates in CHO cell medium

supplemented with rhIL-2 (20 ng/ml) and αCD28 (1 µg/ml). After 24h co-culture at 37°C, 5% CO_2, Treg cells were separated from the CHO cells by FACS sorting, transferred to a new 48-well plate and treated with the selective inhibitor VPS34 IN1 (1mM). The percentage and the MFI of GFP^+ Treg cells was assessed by flow cytometry at the indicated time points.

2.4.4 In vitro Treg cell differentiation

Naïve $CD4^+$ T cells were FACS sorted from *FoxP3*$^{YFP\text{-}Cre}$ *Pik3c3*$^{fl/fl}$, mosaic *FoxP3*$^{YFP\text{-}Cre/wt}$ *Pik3c3*$^{fl/fl}$ and corresponding control mice were obtained by FACS sorting as previously described (). Following FACS, cells were resuspended at $2x10^6$ cell/ml in complete IMDM media (IMDM with GlutaMAX supplement (GIBCO) containing 5% FCS (LabTech), 100 U/ml penicillin/streptomycin (GIBCO)), and 50 µM β-mercaptoethanol (Sigma-Aldrich) and transferred to a 96 U-bottom well plate previously coated with aCD3 and aCD28 (2µg/ml and 2.5µg/ml, respectively) over night at 4°C. The following cytokines were added: 10ng/ml TGF-β (Peprotech), 20ng/ml recombinant human IL-2 (Peprotech). The following antibodies were added: 5µg/ml anti-IL-4 (11B11, BioLegend) and 10µg/ml anti-IFNγ (XMG1.2, BioLegend). After 3 days of culture, half of the media was carefully removed and replaced with fresh media containing cytokines and cultured for a further 2 days. At day 5, the cells were used for further analyses.

2.5 Biochemical assays

2.5.1 Polymerase chain reaction (PCR)

Deletion of exon 21 of the *Pik3c3* gene was confirmed by using the polymerase chain reaction (PCR). Treg cells were isolated from spleen and lymph nodes, enriched by enriched by immunomagnetic separation (EasySep™ Mouse $CD4^+$ $CD25^+$ Regulatory T Cell Isolation Kit II from StemCell) according to manufacturer's protocol. Fluorescence-activated cell sorting (FACS) was performed to obtain a Treg cell purity of 98%. Cells were lysed in 75µl Cell Lysis Buffer for 30 mins at 95^{o}C, placed on ice for 10 mins, 75µl Neutralisation Buffer added and snap-frozen.

The PCR reaction was performed in 50µL, comprising 2µl sample DNA and 48µl reaction mixture containing per reaction 5µl PCR buffer 10x (Invitrogen), 2µl MgCl2 (50mM), 1µldNTPs (10mM), 1µl of each primer (1450_33: GCTGGTAGTACTGATGTTGC; 1450_34: GCATGGTCCTACTTTCTTCC; 1451_38: AGTCGAAGGTTGACTGTACC; Sigma), 0.4µl Taq Polymerase (5U/µl, Invitrogen), 37.6µl H2O. Samples were run at the following programme:

Step	**Details**	**Cycles**
1	95°C for 5’	1
2	95°C for 30’’	35
	60°C for 30’’	
	70°C for 1’	
3	72°C for 10’	1
4	4°C hold	1

Expected fragments: 357bp (wt), 521bp (*Pik3c3*$^{\Delta 21}$). PCR products were resolved on a 1% agarose gel at 100V for 60 mins.

2.5.2 Western blot analysis

For Western blot analysed, cells were lysed in 25µl/10^6 cells in lysis buffer (50mM HEPES, 150mM NaCl, 10mM NaF, 10mM Indoacetamide, 1% IGEPAL and proteinase inhibitors (Complete Ultra tablets, Roche)) for 30mins. Following centrifugation at maximum speed for 30 min at 4°C, the supernatants were mixed with 1xNuPage LDS sample buffer (Life Technologies) supplemented with 0.5% β-mercaptoethanol and boiled at 95°C for 5mins. Samples were either kept at -80°C or loaded straight away on a 4-12% NuPage Bis-Tris gel (Invitrogen) and run at 150V for 75mins. Proteins were transferred to a PVDF membrane for 1h at 40V on ice. Proper transfer was assessed by Coomassie Red staining. The membrane was blocked for 1h at room temperature in Intercept ® Blocking buffer (Licor), shaking. For the detection of proteins of interest, membranes were incubated over night at 4°C, shaking, with the following antibodies: pAKT (T308, Cell Signaling, 1 in 1000 dilution); pS6 (S235/236, Cell Signaling, 1 in 500 dilution); VPS34 (Cell Signaling, 1 in 500 dilution); VPS15 (Cell Signaling, 1 in 500 dilution); Atg14L (Cell Signaling, 1 in 500 dilution); β-actin (Sc47778, Santa Cruz Biotechnology, 1 in 2000 dilution). Membranes were washed trice with T-BST and incubated

with either anti-mouse or anti-rat secondary antibodies coupled to IRDye800CW or IRDye 680RD, respectively (1:5000), for 1.5h at room temperature, shaking. A CLx Licor system was used for the detection of the proteins bands. ImageStudio (LiCor) was used for the analysis of the band density, Excel was subsequently used to perform normalization and data were plotted in GraphPad.

2.6 Metabolic assays

2.6.1 CellTiterGlo® Luminescent Cell Viability Assay

20.000 cells/well in 100µl PBS were seeded in opaque-walled multiwell plates adequate for cell culture and treated with either the pharmacological inhibitor VPS34-IN1 (1µM) or the vehicle control DMSO for 4 or 24h. The plate and its contents was equilibrated at room temperature for 30 minutes, and 100µl CellTiter-Glo® Reagent was added to each well. The content was mixed for 2 minutes on an orbital shaker to induce cell lysis. Subsequently, the plate was incubated at room temperature for 10 minutes to stabilize luminescent signal. Luminescence was detected on a microplate reader using the software SkanIt (Thermo Scientific™).

2.6.2 Seahorse XF Cell Energy Phenotype Test Assay (with the help of Dr. Benoit Bilanges)

Prior to the assay, Agilent Seahorse XF96 Cell Culture Microplate were coated with Cell-Tak solution for 20 minutes at room temperature. On the day of the assay, Cell-Tak coated XF96 Cell Culture Microplates Cell Culture Microplates were allowed to warm to room temperature for 1h. $0.5x10^5$ cells per well in 50uL of assay medium (Seahorse XF Base Medium supplemented with 1mM pyruvate, 2mM glutamine, and 10mM glucose, pH 7.4) were transferred to the XF96 Cell and centrifuged at 200 × g (zero braking) for 1 minute. The plate was transferred to a 37 °C incubator not supplemented with CO_2 for 30 minutes, subsequently 130 µL warm assay medium were gently added to each well, and the plate was returned to the incubator for 15–25 minutes. The sensor cartridge was loaded with the appropriate volumes described in the manufacturer's protocol. The Seahorse XF Cell Energy Phenotype Test Assay was performed using 0.5uM FCCP and 10µM oligomycin.

At the end of the assay, protein levels were quantified to allow normalization. Supernatant was removed, cells washed once with PBS and lysed with 20µl 0.2M NaOH for 10 mins. Subsequently, a BCA assay was performed according to the manufacturer's protocol using 5µl of the samples. After 30mins incubation at 37°C in a non-supplemented CO_2 incubator, samples were read at 560nm.

2.7 Bacterial strains and infection

2.7.1 Listeria monocytogenes *strains*

The recombinant strain of *Listeria monocytogenes*-OVA was a kindly obtained from Dr Hao Shen [260]. *Lm*-OVA is derived from the wild-type strain 10403s (WT-*Lm*) and was modified to secrete the recombinant chicken ovalbumin protein (aa 134-387), and to include an erythromycin resistance gene. An attenuated version of this strain with the gene encoding ActA being deleted (ΔActA- Lm-OVA) was purchased from DMXbio [261]. All of these strains were obtained from Verity Pearce and were subsequently expanded by Hicham Bouabe, Rafeah Alam and myself. The attenuated Lm-OVA and Lm expressing the yellow fluorescent protein (attenuated Lm-YFP) was used in experiments to detect $CD8^+$ T cell responses. The Lm-YFP was used as a control to gate on antigen specific $CD8^+$ T cells. The virulent strain was used to measure colony-forming units (CFU) to assess bacterial load.

2.7.2 Listeria monocytogenes *culture and stocks*

All *Listeria* strains were grown in BBL™ Brain Heart Infusion (BD) liquid medium supplemented with 5ug/mL erythromycin (Sigma-Aldrich) or 7µg/mL Chloramphenicol at 37°C with shaking. *In vivo* passage of all strains was performed as detailed in Current Protocols in Immunology [262]. Briefly, log phase bacteria (OD_{500}=0.8-1.2) were washed and resupsended in PBS, then intravenously injected into a mouse. After 48 hours, a single cell suspension of the spleen was prepared, diluted and grown on BHI agar plates. A single colony was picked and grown to mid-log phase, washed in PBS, and then stocks were stored in aliquots at -80°C in 20% glycerol (Sigma-Aldrich). For all *in vivo* infections with attenuated Lm-OVA, 5 x 10^6 CFU was intravenously injected into the lateral tail vein. For bacterial load

experiments 5 x 10^4 CFU virulent Lm-OVA was used. For each experiment, a new aliquot was used. Frozen stocks were thawed at room temperature, washed and diluted in PBS to the appropriate concentration and injected within 2hrs.

2.7.3 Assessing bacterial load in Listeria monocytogenes *-infected tissues*

To determine colony-forming units (CFU) in spleens and liver, mice were injected intravenously with the virulent strain of Lm-OVA and culled 48 hours post infection. Livers were perfused by cutting the hepatic vein and injecting 5 ml of phosphate-buffered saline (PBS) into the hepatic artery. Livers were weighed, following which spleens and livers were passed through 40µM nylon strainers (BD Falcon) to generate single cell suspensions. Ten-fold serial dilutions of homogenates in PBS were plated (100µL/plate) on BHI agar plates supplemented with 5µg/ml erythromycin (Sigma-Aldrich). Bacterial colonies were counted after incubation for approximately 48 hours and enumeration of CFUs were calculated according to the formula CFU/mL= colony count on plate x dilution factor x 10.

2.7.4 Infection with attenuated Listeria monocytogenes*-OVA*

Listeria monocytogenes strain expressing OVA (*Lm*-OVA) have been previously described [260]. Infections were performed i.v. with 10^6 CFU *Lm*-OVA per mouse. Mice were bled on day 0, 8, 14, 21 and 30. To assess the secondary response, mice were re-injected with 10^6 CFU *Lm*-OVA per mouse on day post 36 and spleen and lymph nodes (inguinal) were analysed five days post re-infection.

2.8 Cancer cell lines and inoculation

2.8.1 Cell culture

The murine metastatic melanoma cell line B78ChOva-mCherry was obtained as a generous gift from Prof. Matthew F. Krummel (UCSF). This transgenic line expresses the specific antigen chicken ovalbumin (OVA) peptide tagged to a mCherry reporter that can be recognised by antigen-specific OT-I^+ T-cells. The line was generated via the transfection of B78 parental cells with a MMTV-PyMT vector containing a mCherry reporter gene and a chicken ovalbumin gene

intercalated with two porcine teschovirus-1 2A (P2A) sequences [263]. Cells were mycoplasma-tested and cultured in RPMI-1640 media containing L-glutamine (Gibco, Thermo Fisher Scientific) with 10% heat-inactivated fetal bovine serum (LabTech, UK) and 100 U/mL penicillin-streptomycin (Invitrogen) in a humidified atmosphere of 5% CO_2 at 37°C. Cells were split using 10 mM EDTA in PBS when reaching >70% confluency.

2.8.2 Inoculation with the melanoma cell line B78Ch-OVA mCherry

B78ChOva-mCherry cell line (1.5 – 5 x 10^5 cells in 100 µl PBS) were injected subcutaneously in the right flanks of mice. Tumours were palpable from day 1- to 12 and measured every second until day 18 where mice were culled by Schedule 1 and tumour, draining and resting lymph nodes and spleen were harvested for analysis.

2.9 Liquid chromatography mass spectrometry proteomics (LC-MS/MS)

2.9.1 Sorting of YFP$^+$ Treg cells

Single cell suspension from lymph nodes and spleen from mosaic *FoxP3*$^{YFP\text{-}Cre/wt}$ *Pik3c3*$^{fl/fl}$ and wild-type mice were prepared and stained in 500µl FACS buffer containing fixable live dead dye, anti-CD25, anti-CD4, and anti-CD8 antibodies for 45 minutes at 4°C. Cells were washed twice in FACS buffer and resuspended in PBS containing 0.5% FCS. Cells were sorted by FACS on viable CD8$^-$, CD4$^+$, CD25$^+$ YFP$^+$ cells. Sorted cells were washed twice in HBSS at maximum speed for 10 seconds, tubes were rotated by 180 degrees and cells were spun again at maximum speed for 10 seconds. Supernatant was removed, the cells snap frozen in liquid nitrogen and couriered to the laboratory of Doreen Cantrell at the School of Life Sciences, University of Dundee for subsequent sample processing and protein analysis by mass spectrometry.

2.9.2 Sample processing (performed by Dr. Christina Rollings)

An SP3 approach was used to process samples for proteomic analysis [264]. Cell pellets were resuspended in 400 µL lysis buffer (4% SDS, 10 mM TCEP, 50 mM TEAB), boiled for 5 mins then allowed to cool for 5 mins while being shaken at 500rpm on a thermomixer. Samples

were sonicated and incubated with 1 µL benzonase for 15 mins at 37°C. Protein concentration was determined using an EZQ assay. Cysteine residues were carbaminomethylated by incubation with 20 mM iodoacetemide for 1hr at room temperature in the dark. Magnetic beads (200µg per sample of a 50:50 mix of hydrophobic and hydrophilic Sera-Mag Speedbead carboxylate-modified magnetic particles, GE Life Sciences) and 550µL of a 10:1 acetonitrile: 10% formic acid solution was added to each sample. Samples were incubated for 8mins while mixing at 500rpm, centrifuged briefly and the supernatant removed following 2mins incubation on a magnetic rack. Beads were washed twice with 1mL 70% ethanol and once with 1mL acetonitrile. Beads were air-dried briefly, resuspended in 65 µL digestion buffer (0.1% SDS, 50mM TEAB, 1mM $CaCl_2$) and LysC added at a ratio of 1µg LysC per 100µg protein. Samples were incubated overnight at 37°C with mixing at 500rpm. Following digestion with LysC, 1µg trypsin/100µg protein was added and samples were incubated overnight at 37°C with mixing at 500rpm. Beads were washed with 1.425 mL acetonitrile, then 500 µL acetonitrile. Peptides were eluted following incubation with 189µL 2% DMSO for 2mins and peptide concentration determined using a CBQCA assay. Samples were adjusted to 5% formic acid, then dried down in a SpeedVac.

2.9.3 Fractionation (performed by Dr. Christina Rollings)

Samples were resuspended with 210µL 5% formic acid. For each sample, 200µL was fractionated into 16 fractions using high pH reversed phase chromatography using an UltiMate 3000 HPLC with an XBridge Peptide BEH C18 column. The buffers used for separation were buffer A (10mM ammonium formate/2% acetonitrile, pH 9.0) and buffer B (10mM ammonium formate/80% acetonitrile, pH 9.0). A flow rate of 0.3mL/min was used throughout fractionation. An elution gradient increasing the percentage of acetonitrile was used for fractionation, beginning with 90% buffer A and 10% buffer B, then moving to 50% buffer A and buffer B at 11mins and to 0% buffer A and 100% buffer B at 12mins. Following fractionation, fractions were combined to form 8 fractions per sample, dried down in a SpeedVac and resuspended in 5% formic acid for submission to the University of Dundee FingerPrints Proteomics and Mass Spectrometry facility.

2.9.4 Mass spectrometry

Mass spectrometry analysis was performed by the Proteomics Facility at the University of Dundee. A maximum of 1µg per fraction was analysed. Before introduction to the mass spectrometer, samples were separated using an Ultimate 3000 HPLC (Thermo Scientific). Peptides were trapped and washed on an Acclaim PepMap 100 (C18, 100µM x 2 cm) column with a 0.1% formic acid buffer, then separated on an Easy-Spray Pep-Map RSLC C18 column (75 µM x 50 cm). The buffers used for separation were 0.1% formic acid (buffer A) and 0.08% formic acid in 80% acetonitrile (buffer B), and a flow rate of 0.3µL/min was used throughout fractionation. Samples were separated using an elution gradient, beginning with 2% buffer B, switching to 5% buffer B at 6mins, 35% buffer B at 130mins and reaching 98% buffer B at 132mins, which was held until 152mins, at which point the buffers were reset to the starting concentration of 2% buffer B with a total run time of 170mins. Samples were then introduced to an LTQ OrbiTrap Velos Pro (Thermo Scientific) using an Easy-Spray Source (Thermo Scientific) at 50°C and source voltage of 1.9 kV. The mass spectrometer was run in a data-dependent acquisition mode, using a top 15 method for selection of ions for fragmentation. MS spectra were collected over a range of 355 – 1800 m/z with a resolution of 60,000 using a full scan and in a positive ion mode. The top 15 most intense peptide ions were selected for fragmentation via CID (collision-induced dissociation) after the accumulation of 5000 ions, with normalised collision energy of 35%, activation Q of 0.25, and activation time of 10ms.

2.9.5 Data analysis

The raw data files generated during mass spectrometry were analysed using MaxQuant version 1.6.1.0 and searched against the reviewed mouse Uniprot database, the contaminants database supplied with MaxQuant and a reversed database used for FDR (false discovery rate) determination. Cysteine carbamidolyation was set as a fixed modification and methionine oxidation, protein N-terminal acetylation, deamidation of asparagine and glutamine and pyroglutamic acid formationfrom glutamine were set as variable modifications. Minimum peptide length was set to 6, digestion was set to trypsin/P and LysC with a maximum of two missed cleavages. Match between runs was enabled. Quantification used unique and razor peptides. PSM (peptide to spectrum match) FDR and protein FDR were set to 1%.

Following protein identification and quantification, proteins identified in the reverse database, proteins listed as contaminants and proteins only identified by a modified peptide were filtered from the database. Copy numbers were then calculated using the proteome ruler plugin in the Perseus analysis software version 1.6.0.2 [265]. Copy numbers were log2 transformed and an unpaired T-test with unequal variance performed. Proteins with a 1.5-fold change in different conditions and a p value ≤ 0.05 were considered differentially abundant.

The generated protein list was filtered for potential contaminants, reverse hits, and ‘‘only identified by site’’. The label-free quantification (LFQ) values were transformed in log2 scale, the three technical replicates per experimental condition grouped and averaged based on the median. To identify the proteins with the most prominent differences in expression profiles within the different T cell subsets statistical significance ($p \leq 0.05$).

Pathway analyses were performed using the Database for Annotation, Visualisation and Integrated Discovery (DAVID) bioinformatics tools based on Kyoto Encyclopedia of Genes and Genomes (KEGG).

2.10 Statistical Analysis

Statistical analyses were carried out using GraphPad Prism (version 8.3.0). Where data were normally distributed, parametric tests were performed: unpaired students t-test with Welch’s correction was used when two groups were compared, or one-way ANOVA with Tukey post-test when three or more groups were compared. A two-tailed Student’s *t*-test was used for the statistical analysis of differences between two groups with Sidak’s correction when comparing two groups at multiple time points. Comparison of multiple groups was done using one-way ANOVA followed by Tukey’s post-hoc test. Significance is shown as * $p < 0.05$, ** $p < 0.01$, and *** $p < 0.001$.

Chapter 3

VPS34 is critical for regulatory T cell functions

3.1 Introduction

The cell-intrinsic role of VPS34 in Treg cells was investigated by Elisabeth Slack, a previous PhD student in the laboratory of Klaus Okkenhaug. She used a mouse model in which exon 21 of *Pik3c3* is conditionally excised under the action of *FoxP3*-induced Cre-recombinase. Selective deletion of VPS34 in Treg cells led to a *Scurfy*-like phenotype, but since the number of Treg cells was near-normal in VPS34-deficient mice, this implied that VPS34 is critical for Treg cell functions rather than for survival. In line with that, the proportion of activated $CD4^+$ and $CD8^+$ T cells was greatly increased in the spleen and lymph nodes, suggesting that VPS34 is required for effective suppressive functions of Treg cells. However, VPS34-deficient Treg cells supressed the proliferation of *conventional T cells* (Tcons) equally well in an *in vitro* suppression assay.

Based on the knowledge that VPS34 is a kinase involved in autophagy and endocytosis in various cell types, Elisabeth tested the hypothesis that depletion of VPS34 impairs the consumption of IL-2 and/or the transendocytosis of CD80, two key effector mechanisms by which Treg cells suppress naïve T cell survival and activation. Although the cell surface level of CD25 was increased in VPS34-deficient Treg cells, resulting in increased IL-2 endocytosis, downstream IL-2 receptor signalling was intact, as assessed by STAT5 phosphorylation. Similarly, cell surface expression of CTLA-4 and CD80 on Treg cells and DCs, respectively, was increased in mice with VPS34-deficient Treg cells; concomitantly, the level of transendocytosed CD80 was increased in VPS34-deficient compared to wild-type Treg cells. She therefore concluded that VPS34 is not required for known Treg cell suppressive mechanisms relying on endocytosis (*see Elisabeth's thesis* [266]).

Together with Priya, she investigated whether VPS34-deficiency impairs autophagy. Autophagic flux, as assessed by monitoring LC3b lipidation, was unchanged in VPS34-deficient Treg cells and results obtained so far could not provide evidences that mitophagy, a selective form of autophagy required for the removal of excessive and/or damaged mitochondria, is affected by VPS34 depletion. Furthermore, when *Atg7*, a protein essential for the induction of autophagy, was specifically deleted in Treg cells, mice survived for a median time of 9 months, suggesting that impaired autophagy cannot fully explain the observed phenotype in $FoxP3^{YFP\text{-}Cre}$ $Pik3c3^{fl/fl}$ mice. Taken together, Elisabeth and Priya established that VPS34 is

essential for Treg cells homeostasis and/or function, as depletion leads to a striking lymphoproliferative disease but so far, its physiological role is still not completely understood. Therefore, I aimed to repeat some of the experiment to produce publication-ready figures (*by including sufficient n numbers, for instance*), and to continue the work of Elisabeth and Priya in order to understand which effector mechanism(s) is/are affected by the deletion of VPS34 in Treg cells.

For the sake of the comprehension of the here presented data and conclusions, I will, where needed, mention whether the results have been obtained by Elisabeth and/or Priya, however without showing data (i.e. I will notify as follow: *data not shown*). Where I have repeated experiments already performed by Elisabeth and/or Priya, with the aim to repeat and consolidate data, I will only show results obtained from my own experiments.

3.2 Results

3.2.1 Treg cell-specific deletion of VPS34 causes a Scurfy-like phenotype

To study the function of VPS34 *in vivo,* two loxP sites flanking exon 21 of the VPS34 gene were introduced by homologous recombination (**Fig. 3.1.1 a**) [267]. *Pik3c3*$^{flox/flox}$ (*Pik3c3*$^{fl/fl}$) mice were viable and fertile and did not present any overt phenotype, indicating that the insertion of the loxP sites does not alter *Pik3c3* gene function (*data not shown*). To generate Treg cell-specific deletion of exon 21 of *Pik3c*3, these mice were crossed to a transgenic mouce strain expressing the Cre-recombinase under the *FoxP3* promoter (*FoxP3*$^{YFP\text{-}Cre}$) (**Fig. 3.1.1 b**). *FoxP3* is a transcription factor unique and required for Treg cell identity [9]–[12]. Genomic excision was verified by the absence of the amplicon spanning exon 21-22 boundary in FACS-sorted Treg cells (purity > 98%, data not shown) from *FoxP3*$^{YFP\text{-}Cre}$ *Pik3c3*$^{fl/fl}$ mice but not in Treg cells from control *FoxP3*$^{YFP\text{-}Cre}$ *Pik3c3*$^{+/+}$ mice (**Fig. 3.1.1 c**). Exon 21 of *Pik3c3* encodes a critical stretch (Ala730 to Thr754) of the VPS34 kinase domain and its deletion renders the truncated VPS34 protein catalytically inactive, as assessed by a kinase assay performed by Elena Rebollo Gomez (**Fig. 3.1.1 d**).

Elisabeth previously showed that loss of VPS34 kinase activity in Treg cells causes an early systemic lymphoproliferative disease from approximately 4 weeks of age (median survival time = 37 days) (*data not shown*). *FoxP3*$^{YFP\text{-}Cre}$ *Pikc3c3*$^{fl/fl}$ mice exhibited smaller body size, hunched posture, and crusting and scaling of the ears and abdomen (*data not shown*). Moreover, mutant mice developed splenomegaly and lymphadenopathy (*data not shown*), while the thymus was reduced in size, which is likely secondary to the observed inflammation relating to the autoimmune phenotype. We assessed cell numbers by flow cytometry and found that they were increased in the spleen and lymph nodes while reduced in the thymus (**Fig. 3.1.2 a**). Analyses by flow cytometry showed that these infiltrating cells were of macrophage-like origin (*data not shown*). Furthermore, histopathological analysis revealed a massive infiltration of lymphocytes into multiple organs such as the liver, the lung and the bone marrow (*data not shown*), suggesting an autoimmune lymphoproliferative disease. In support of this, *FoxP3*$^{YFP\text{-}Cre}$ *Pikc3c3*$^{fl/fl}$ mice had substantial expansion of CD4^{+} CD25^{-} conventional T cells (Tcons) and CD8^{+} T cells in the spleen and the lymph nodes (**Fig. 3.1.2 b and c**), among which an increase proportion displayed an effector phenotype (CD44^{high}

CD62L^{low}) (**Fig. 3.1.2 d**). Additionally, a large amount of Tcons produced the immuno-regulatory T cell cytokine *interferon- γ* (IFN-γ) (**Fig. 3.1.2 e**).

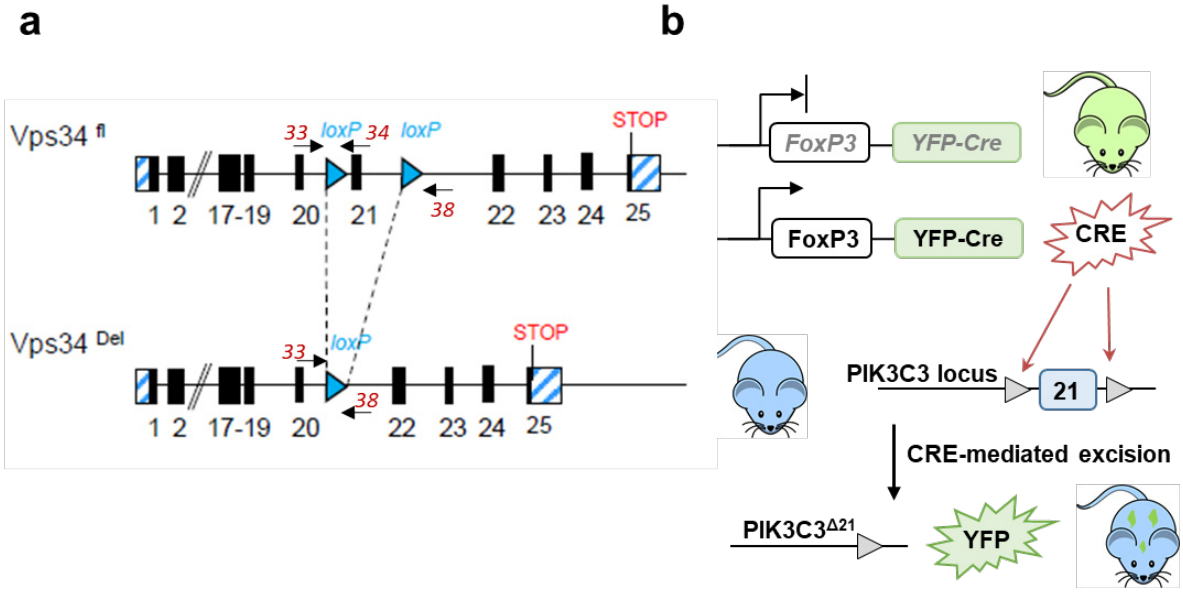

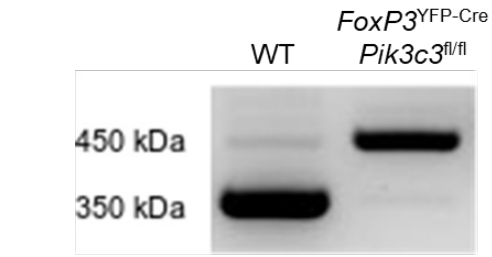

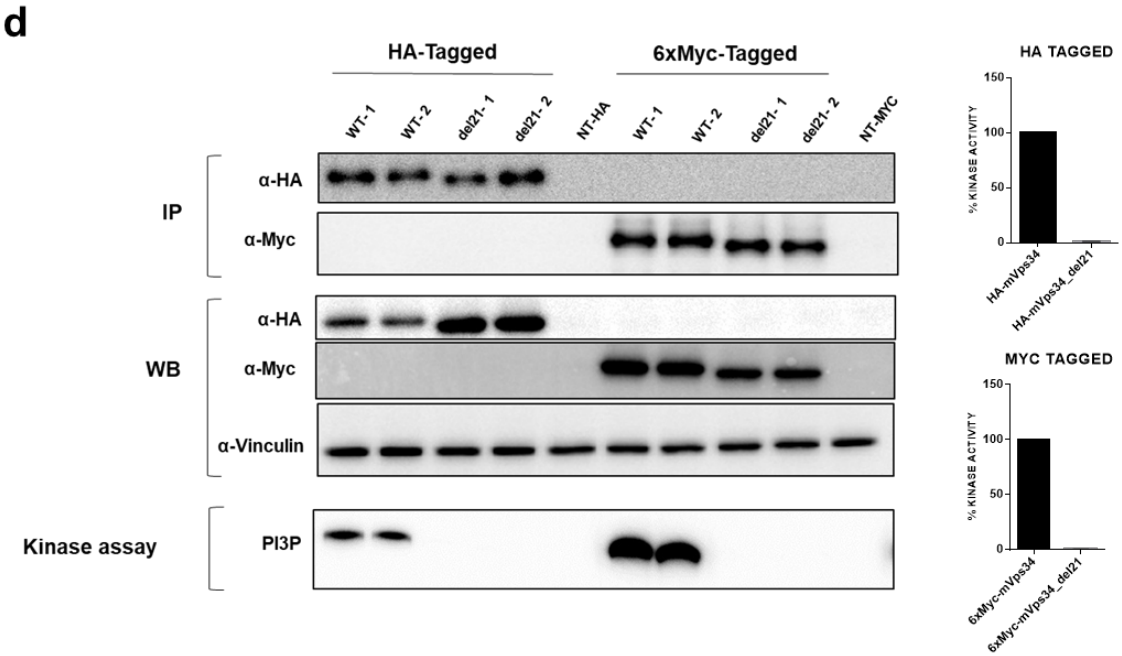

Figure 3.1.1: Generation of Treg cell-specific VPS34-kinase dead mice.
a) Targeting strategy to generate Treg cell-specific VPS34-kinase dead mice: exon 21 (located in the kinase domain) of the *Pik3c3* gene encoding VPS34 was flanked with LoxP sites. The enframed region is 75 nucleotides long, and Cre-mediated excision does not change the open reading frame, thereby giving rise to a predicted truncated VSP34 protein that is 25 amino acids shorter than the wild-type version.
b) For Treg cell-specific deletion, *Pik3c3*$^{fl/fl}$ mice were crossed with a transgenic mice strain expressing the Cre-recombinase under the *FoxP3* promoter (*FoxP3*$^{YFP\text{-}Cre}$ mice), with all Treg cells expressing the Cre-recombinase also expressing the fluorescent tag YFP.
c) A representative image of agarose electrophoresis showing PCR products generated from DNA isolated from FACS-sorted Treg cells using the primer trio #33/34/38 (marked in (**a**) for detection of heterozygous/homozygous or wild-type and loxP alleles. In wild-type cells, only the PCR product between the primers 33 and 34 will be generated (the distance between 33 and 38 being too long to generate a PCR product), leading to a PCR product of 350 kDa. Deletion of the floxed DNA stretch will remove the binding site for primer 34, but also decrease the length between the primers 33 and 38, leading the a PCR product of 450 kDa.
d) Immunoprecipitation (IP), expression (WB) and *in vitro* Kinase assay of tagged version of the truncated (del21) and wild-type (WT) allele in transiently transfected HEK293 cells. IPs were performed using anti-HA (left part of the panel) or anti-Myc (right part of the panel) antibodies. Bar graphs showing the percentage of Kinase activity in both WT and del21 VPS34 proteins (HA tagged on the top graph panel and 6xMyc-tagged on the bottom graph). HEK293 were transiently transfected in duplicates (1, 2). NT corresponds to the non-transfected controls. *In vitro* lipid kinase assay was performed using PI as a substrate on either HA-tagged-VPS34 or 6xMyc-tagged VPS34 IPs. Representative data of 3 independent experiments is shown with 2 replicates per experiments (labelled as WT-1, WT-2, del21-1, del21-2). This experiment was performed by Elena Rebollo.

The phenotype of mice with VPS34-deficent Treg cells is similar in severity to those observed in *Scurfy* mice. The *Scurfy* phenotype arises from a frame shift mutation in the fork head domain of *FoxP3*, resulting in the absence of thymus-derived Treg cells and leading to a fatal lymphoproliferative disease with multi-organ inflammation [23]. However, in contrast to *Scurfy* mice and other models that recapitulate the *Scurfy* phenotype, VPS34-deficient Treg cells developed and populated the peripheral lymphoid organs of *FoxP3*$^{YFP\text{-}Cre}$ *Pik3c3*$^{fl/fl}$ mice, albeit with reduced numbers in the spleen compensated by increased numbers in the lymph nodes (**Fig. 3.1.3 a**). Meanwhile, Treg cells were reduced in term of percentage in the lymph nodes and the spleen of *FoxP3*$^{YFP\text{-}Cre}$ *Pik3c3*$^{fl/fl}$ mice (**Fig. 3.1.3 b and c**), suggesting that VPS34-deficient Treg cells fail to accumulate proportionally with effector T cells. In contrast, the thymus showed an increase percentage of Treg cells (**Fig. 3.1.3 d**); which is constituent with the reduced size of the thymus and near-normal number of Treg cells.

As firstly observed by Elisabeth and confirmed by myself during the first year of my PhD, the expansion of activated T cells in presence of Treg cells, even if reduced in numbers, suggests that the loss of VPS34 interferes with Treg cell suppressive functions rather than simply by preventing their development.

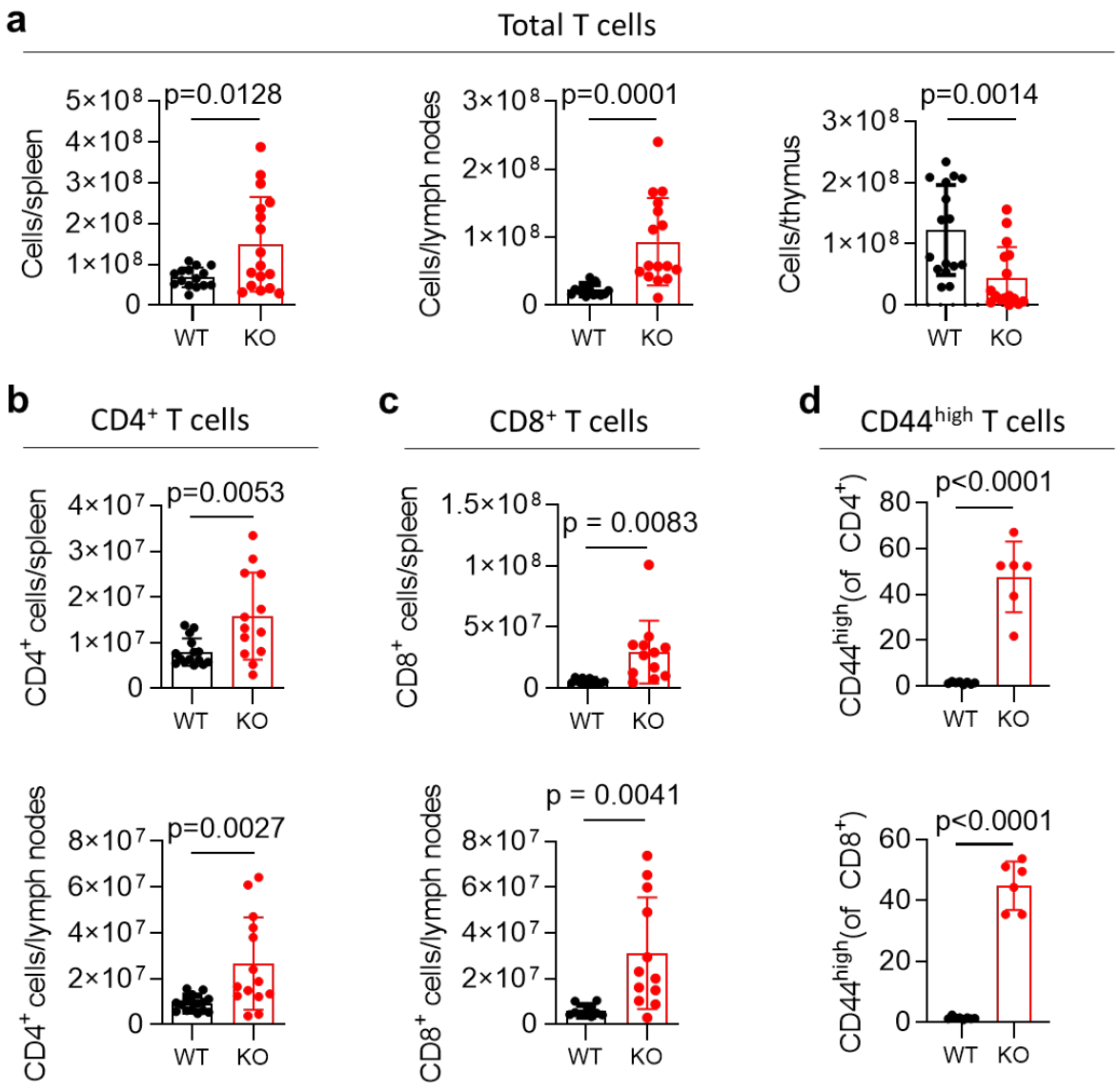

Figure 3.1.2: *FoxP3*$^{YFP\text{-}Cre}$ *Pik3c3*$^{fl/fl}$ mice have a substantial expansion of CD4$^+$ and CD8$^+$ T cells, among which an increase proportion displayed an effector phenotype.

a) Absolute numbers of cells in spleen, lymph nodes (inguinal, brachial, and axiliary), and thymus. Absolute numbers of CD4$^+$ CD25$^-$ (**b**) and CD8$^+$ T cells (**c**) in spleen and the lymph nodes (inguinal, brachial, and axiliary). **d**) Percentage of CD44^{high} CD62^{low} CD4$^+$ CD25$^-$ and CD8$^+$ T cells in the spleen. **e**) Percentage of IFN-γ$^+$ CD4$^+$ CD25$^-$ T cells in the spleen.
Mice were between 4 and 5.5 weeks old. n = 6 – 15 mice per group. Statistical significance was determined using a two-tailed Student's t-test. Results are pooled from three independent experiments. Similar data was produced by Elisabeth.

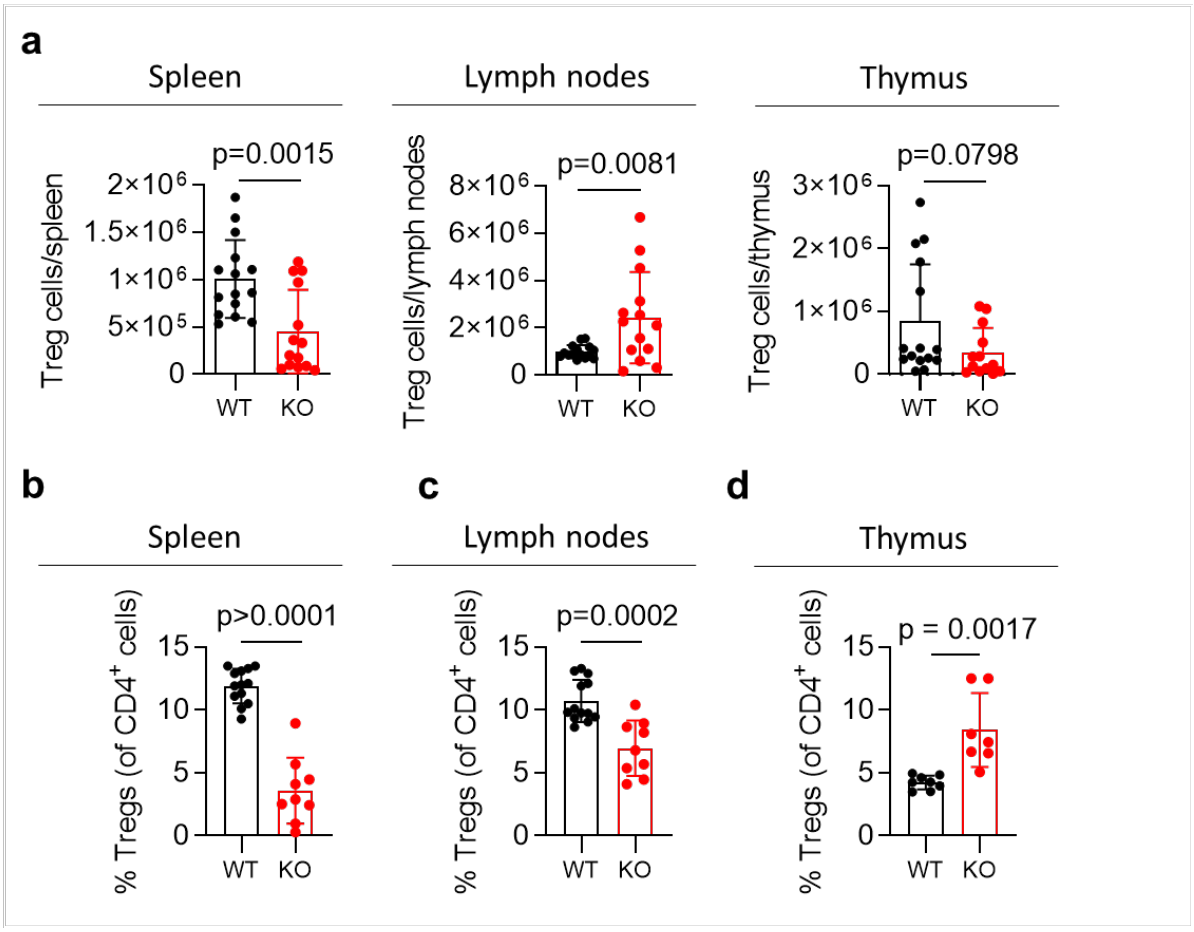

Figure 3.1.3: VPS34-deficient Treg cells developed and populated the peripheral lymphoid organs of *FoxP3*$^{YFP\text{-}Cre}$ *Pik3c3*$^{fl/fl}$ mice.

a) Absolute numbers of Treg cells in spleen, lymph nodes (inguinal, brachial, and axiliary), and thymus of *FoxP3*$^{YFP\text{-}Cre}$ *Pik3c3*$^{fl/fl}$ mice (KO) and wild-type control mice (WT).

b – d) Percentage of Treg cells in the spleen (**b**), lymph nodes (inguinal, brachial, and axiliary) (**c**), and thymus (**d**) of *FoxP3*$^{YFP\text{-}Cre}$ *Pik3c3*$^{fl/fl}$ mice (KO) and wild-type control mice (WT).

Mice were between 4 and 5.5 weeks old. n = 6 – 15 mice per group. Statistical significance was determined using a two-tailed Student's t-test. Results are pooled from three independent experiments. Similar data was produced by Elisabeth.

3.2.2 Autophagy is important, but not critical, for the maintenance of Treg cells homeostasis

Autophagy is a highly conserved degradation process that is critical for the maintenance of cellular homeostasis, required for the establishment of Treg cell-mediated immune tolerance, and supports Treg cell lineage stability and survival [152]. Autophagy is increased after the initial activation of T cells, presumably as a mechanism to degrade the increasing cytoplasmic content that is generated as the T cells become more metabolically active [211].

To assess the involvement of VPS34 in autophagy, I monitored mitophagy, a selective form of autophagy that is required for the removal of defective and excessive mitochondria. *Atg7*-deficient Treg cells displayed increased staining for MitoTracker Orange dye, showing damaged mitochondria with altered membrane potential and *oxidative phosphorylation* (OXPHOS) (**Fig. 3.2 a**). Atg7 is a protein essential for the induction of autophagy [268]. Similarly, I observed an increase in mitochondrial potential and OXPHOS in VPS34-deficient Treg cells from *FoxP3*$^{YFP\text{-}Cre}$ *Pik3c3*$^{fl/fl}$ mice and mosaic *FoxP3*$^{YFP\text{-}Cre/WT}$ *Pik3c3*$^{fl/fl}$ mice (**Fig. 3.2 b and c**, respectively). Since the incorporation of the MitoTracker Orange dye is not only dependent on mitochondrial potential, but also on mitochondrial mass, I assessed the level of mitochondrial DNA in Treg cells from *FoxP3*$^{YFP\text{-}Cre}$ *Pik3c3*$^{fl/fl}$ mice by quantitative PCR analysis. Results showed elevated mitochondrial DNA (**Fig. 3.2 d**), suggesting an increase in mitochondria number and impaired intracellular mitochondria clearance rather than increased mitochondrial potential.

Priya considered whether defective autophagy may prevent VPS34-deficient Treg cells from functioning normally. To explore the implication of autophagy in the context of the phenotype observed in *FoxP3*$^{YFP\text{-}Cre}$ *Pik3c3*$^{fl/fl}$ mice, she analysed the phenotype of mice with Treg cell-specific deletion of Atg7. Remarkably, *FoxP3*$^{YFP\text{-}Cre}$ *Atg7*$^{fl/fl}$ mice were healthy at a younger age but developed systemic inflammation leading to death at around 36 weeks (*data not shown*). Interestingly, asymptomatic/moribund *FoxP3*$^{YFP\text{-}Cre}$ *Atg7*$^{fl/fl}$ mice displayed a reduced percentage of Treg cells in the spleen but not the lymph nodes already at two months of age (**Fig. 3.2 e**). Together, these results imply that defective autophagy may contribute to, but is not the primary cause of the profound autoimmune disease observed upon inactivation of VPS34 in Treg cells.

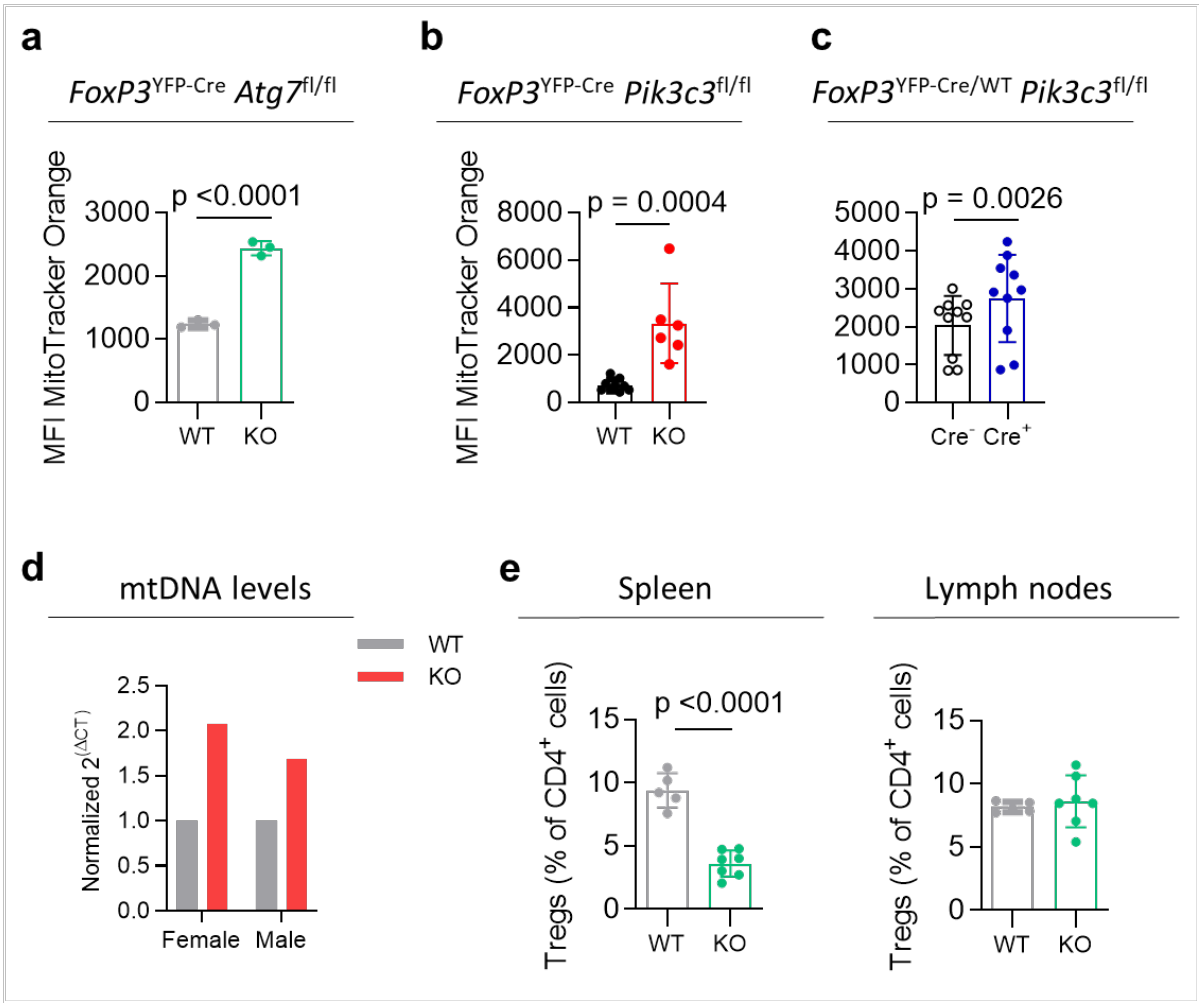

Figure 3.2: Assessing autophagy in ATG7- and VPS34-deficient Treg cells.

Mean fluorescence intensity (MFI) of the MitoTracker Orange in splenic Treg cells from *FoxP3*$^{YFP\text{-}Cre}$ *Atg7*$^{fl/fl}$ mice (KO) and the respective wild-type control mice (WT) (**a**); *FoxP3*$^{YFP\text{-}Cre}$ *Pik3c3*$^{fl/fl}$ mice (KO) and the respective wild-type control mice (WT) (**b**); VPS34-deficient (Cre^+) and VPS34-sufficient (Cre^-) Treg cells from mosaic *FoxP3*$^{YFP\text{-}Cre/WT}$ *Pik3c3*$^{fl/fl}$ mice (KO) (**c**).

d) Quantitative PCR analysis of the mitonchodria DNA (mtDNA) levels of FACS-sorted Treg cells from *FoxP3*$^{YFP\text{-}Cre}$ *Pik3c3*$^{fl/fl}$ mice (KO) and wild-type control mice (WT). Normalised 2(ΔCT) are displayed for Treg cells from female and male mice.

e) Percentage of Treg cells from the spleen and the lymph nodes of *FoxP3*$^{YFP\text{-}Cre}$ *Atg7*$^{fl/fl}$ mice (KO) and wild-type control mice (WT).

FoxP3$^{YFP\text{-}Cre}$ *Atg7*$^{fl/fl}$ mice and the respective wild-type controls were between 8 and 20 weeks of age. *FoxP3*$^{YFP\text{-}Cre}$ *Pik3c3*$^{fl/fl}$ mice and the respective control mice were between 4 and 5.5 weeks of age. *FoxP3*$^{YFP\text{-}Cre/WT}$ *Pik3c3*$^{fl/fl}$ mice and the respective control mice were between 8 and 12 weeks of age. n = 3 – 10 mice per group. Statistical significance was determined using an unpaired two-tailed Student's t-test (a, b, d, e) or paired two-tailed Student's t-test (c). Results are representative of three independent experiments (a – c), representative of two independent experiments (d and e).

3.2.3 VPS34 deficient Treg cells are not intrinsically pathological but have a competitive disadvantage compared to VPS34-sufficient Treg cells

The severe inflammatory disease of *FoxP3*$^{YFP\text{-}Cre}$ *Pik3c3*$^{fl/fl}$ mice made it challenging to investigate the intrinsic role of VPS34 in Treg cells as we could not be certain whether the observed differences between VPS34-sufficient and -deficient Treg cells are due to an intrinsic role of VPS34 in Treg cells or whether the altered Treg cell phenotype is secondary to the inflammatory milieu. We therefore generated mosaic knockout mice by taking advantage of the localisation of the *FoxP3* gene on the X chromosome (**Fig. 3.3.1**). Hence, random X chromosome inactivation should lead to the depletion of VPS34 in approximately 50% of Treg cells [269] in female mice heterozygous for the *FoxP3*$^{YFP\text{-}Cre}$ transgene (*FoxP3*$^{YFP\text{-}Cre/WT}$). Accordingly, such mosaic female mice harbour two populations of Treg cells: a YFP^{-} VPS34-sufficient and a YFP^{+} VPS34-deficient Treg cell population. *FoxP3*$^{YFP\text{-}Cre/WT}$ *Pik3c3*$^{WT/WT}$ mice were used as control mice. Such mosaic female mice did not show any signs of inflammatory disease (*data not shown*), demonstrating that even when VPS34 is kinase-dead in about half of the Treg cells, the presence of wild-type, VPS34-sufficient Treg cells prevents autoimmunity. This system therefore allows to explore the cell-intrinsic role of VPS34 in Treg cells, independently of the *Scurfy* phenotype, i.e. external inflammation caused by Treg cell deficiency.

In line with the lack of lymphoproliferative disease, *FoxP3*$^{YFP\text{-}Cre/WT}$ *Pik3c3*$^{fl/fl}$ mosaic mice had normal numbers of CD4^{+} and CD8^{+} T cells in the spleen and the lymph nodes (**Fig. 3.3.2 a** and **b**, respectively) which displayed a normal activation status (**Fig 3.3.2 c**). Similarly, Treg cell cellularity (**Fig. 3.3.2 d**) and proportions (**Fig. 3.3.2 e**) in the spleen, lymph nodes and thymus of *FoxP3*$^{YFP\text{-}Cre/WT}$ *Pik3c3*$^{fl/fl}$ mosaic mice were comparable to control mice. However, a substantially lower proportions of YFP^{+} VPS34-deficient Treg cells were present in *FoxP3*$^{YFP\text{-}Cre/WT}$ *Pik3c3*$^{fl/fl}$ mosaic mice compared to YFP^{+} VPS34-sufficient Treg cells from control mice (**Fig. 3.3.3**). Furthermore, even in wild-type control mice, the percentage of YFP^{+} Treg cells did not reach 50% (as one might have expected based on the random inactivation of the X chromosome), but rather 30%.

Together, these data suggest that even though Treg cells with kinase-dead VPS34 are not intrinsically pathological, they suffer from a competitive disadvantage compared to VPS34-sufficient Treg cells.

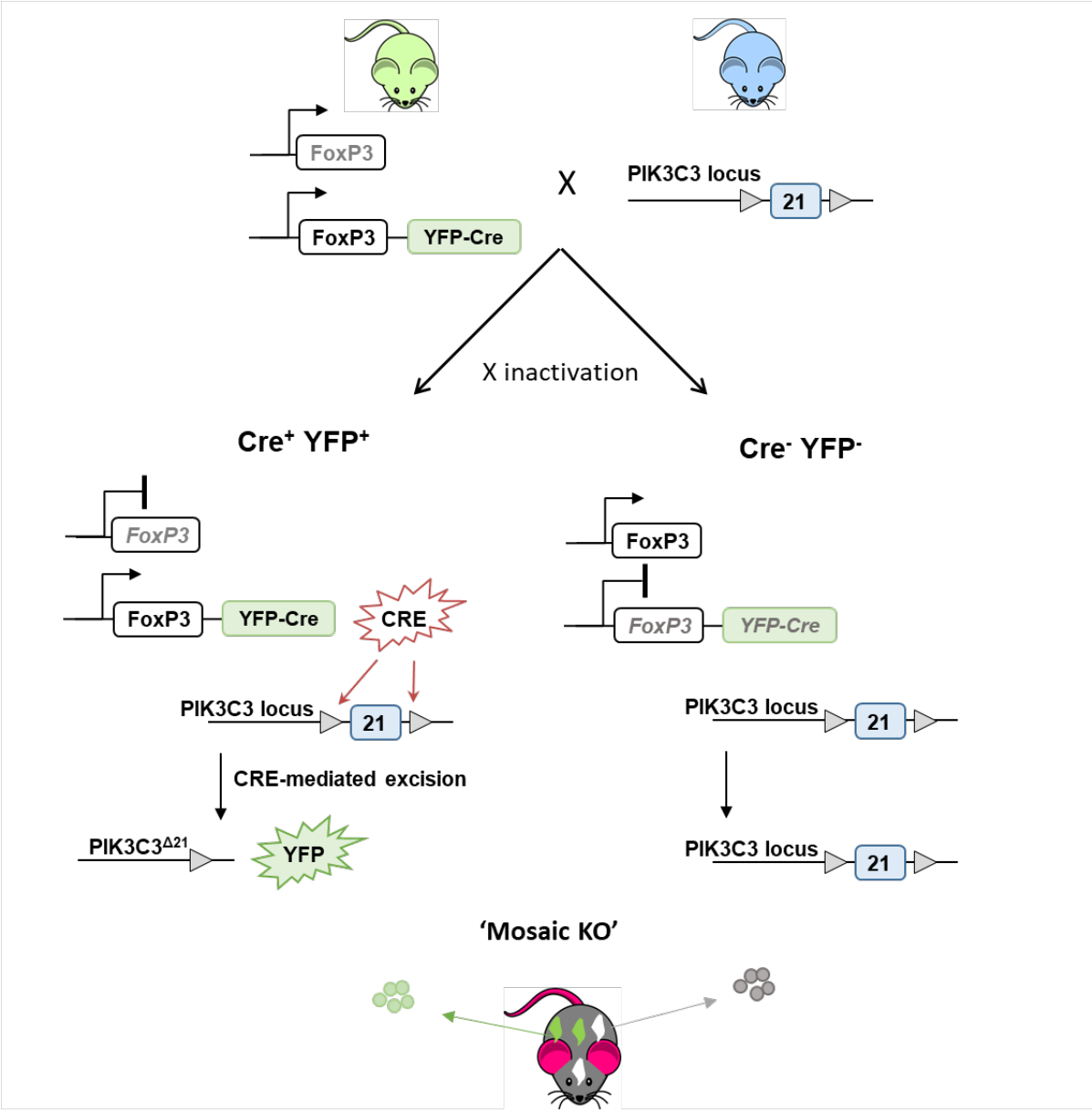

Figure 3.3.1: Generation of *FoxP3*$^{YFP\text{-}Cre/WT}$ *Pik3c3*$^{fl/fl}$ mosaic mice.
Mosaic knockout mice were generated by taking advantage of the localisation of the *FoxP3* gene on the X chromosome. Random X chromosome inactivation leads to the depletion of VPS34 in approximately 50% of Treg cells in female mice heterozygous for the *FoxP3*$^{YFP\text{-}Cre}$ transgene (*FoxP3*$^{YFP\text{-}Cre/WT}$). Accordingly, such mosaic female mice harbour two populations of Treg cells: a YFP^{-} VPS34-sufficient and a YFP^{+} VPS34-deficient Treg cell population.

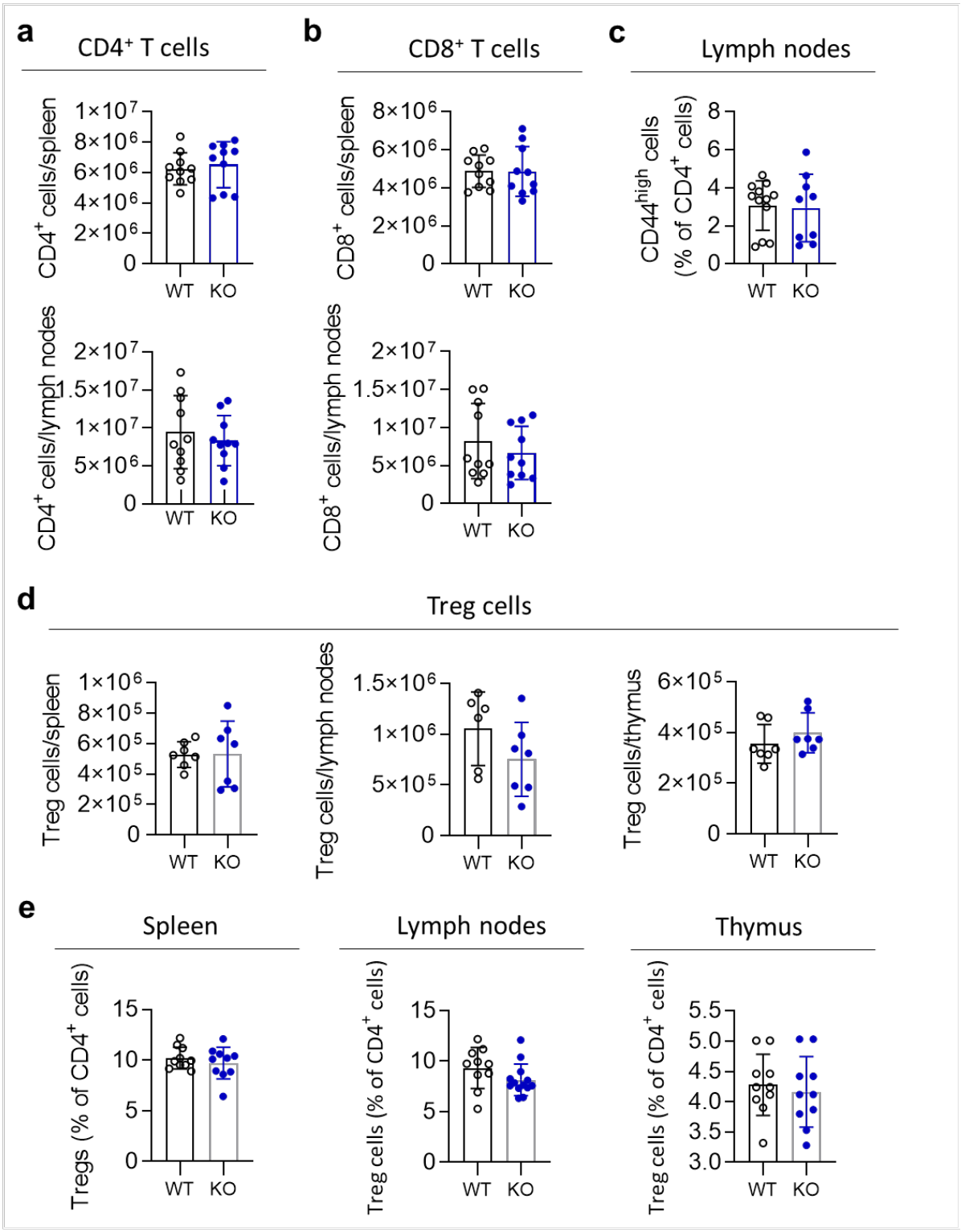

Figure 3.3.2: *FoxP3*$^{YFP\text{-}Cre/WT}$ *Pik3c3*$^{fl/fl}$ mosaic mice are phenotypically healthy.

Absolute numbers of CD4$^+$ (**a**) and CD8$^+$ T cells (**b**) in spleen and the lymph nodes (inguinal, brachial, and axiliary) of *FoxP3*$^{YFP\text{-}Cre/WT}$ *Pik3c3*$^{fl/fl}$ mosaic mice (KO) and wild-type control mice (WT).

c) Percentage of CD44^{high} CD62^{low} CD4$^+$ T cells in the lymph nodes of *FoxP3*$^{YFP\text{-}Cre/WT}$ *Pik3c3*$^{fl/fl}$ mosaic mice.

d) Absolute numbers of Treg cells in spleen, lymph nodes (inguinal, brachial, and axiliary), and thymus of *FoxP3*$^{YFP\text{-}Cre}$ *Pik3c3*$^{fl/fl}$ mice (KO) and wild-type control mice (WT).
e) Percentage of Treg cells in the spleen, lymph nodes (inguinal, brachial, and axiliary), and thymus of *FoxP3*$^{YFP\text{-}Cre}$ *Pik3c3*$^{fl/fl}$ mice (KO) and wild-type control mice (WT).
Mice were between 8 and 12 weeks old. n = 6 – 13 mice per group. Statistical significance was determined using a two-tailed Student's t-test. Results are pooled from three independent experiments. Similar data was produced by Elisabeth.

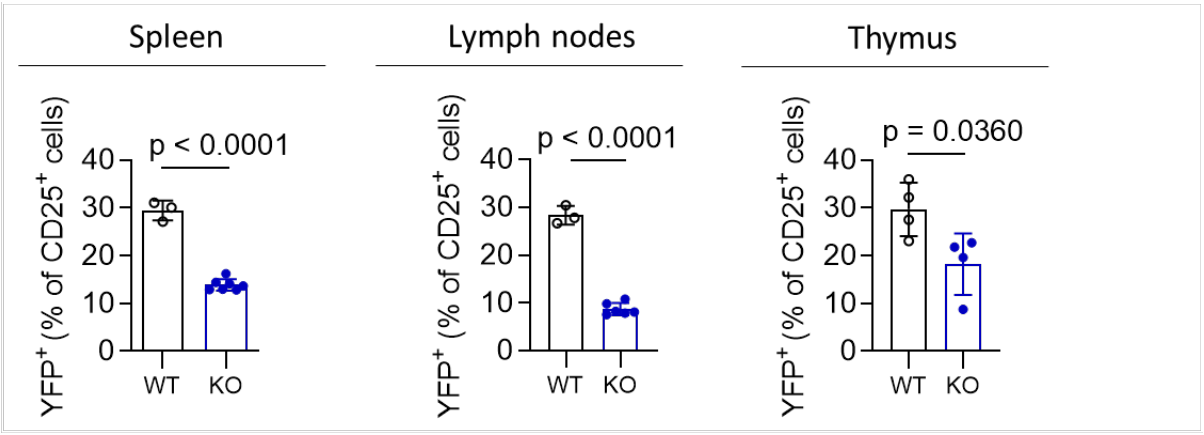

Figure 3.3.3: YFP^{+} Treg cells are reduced in *FoxP3*$^{YFP\text{-}Cre/WT}$ *Pik3c3*$^{fl/fl}$ mosaic mice.
Percentage of YFP^{+} Treg cells in in spleen, the lymph nodes (inguinal, brachial, and axiliary), and the thymus of *FoxP3*$^{YFP\text{-}Cre/WT}$ *Pik3c3*$^{fl/fl}$ mosaic mice (KO) and wild-type control mice (WT).
Mice were between 8 and 12 weeks old. n = 3 – 7 mice per group. Statistical significance was determined using a two-tailed Student's t-test. Results are representative from three independent experiments.

3.2.4 Increased effector molecules levels on Treg cells is second to VPS34-deficiency

The regulatory functions of Treg cells are closely associated with the expression of effector molecules. Therefore, we performed a detailed phenotypic analysis of Treg cells from *FoxP3*$^{YFP\text{-}Cre}$ *Pik3c3*$^{fl/fl}$ mice (lacking VPS34 kinase activity in all Treg cells) and VPS34-sufficient (Cre^-) and VPS34-deficient (Cre^+) Treg cells arising from female *FoxP3*$^{YFP\text{-}Cre/WT}$ *Pik3c3*$^{fl/fl}$ mosaic mice. The expression levels of ICOS, a member of the CD28-superfamily that enhances stability and suppressive functions of Treg cells [270], and CD38, a marker for highly suppressive Treg cells [271] were assessed by flow cytometry. VPS34-deficient Treg cells from *FoxP3*$^{YFP\text{-}Cre}$ *Pik3c3*$^{fl/fl}$ mice expressed elevated level of ICOS (**Fig. 3.4.1 a**) while CD38 expression was decreased by half (**Fig. 3.4.1 b**) compared to control mice. Interestingly, there was no difference in the expression of both markers on VPS34-sufficient (Cre^-) compared to VPS34-deficient (Cre^+) Treg cells from *FoxP3*$^{YFP\text{-}Cre/WT}$ *Pik3c3*$^{fl/fl}$ mosaic mice (**Fig. 3.4.1 c and d**, respectively). These results indicate that the differential expression of ICOS and CD38 observed on Treg cells from *FoxP3*$^{YFP\text{-}Cre}$ *Pik3c3*$^{fl/fl}$ mice is due to a cell-extrinsic effect, probably such as the inflammatory milieu, and is not primarily due to the lack of VPS34.

Treg cells are characterised by the constitutive expression of the *interleukin-2* (IL-2) receptor and CTLA-4. CTLA-4 on Treg cells captures CD80 and CD86 from antigen-presenting cells through a process termed transendocytosis, thus depriving *conventional T cells* (Tcons) of these costimulatory ligands [42], [49]. Similarly, the IL-2 receptor on Treg cells internalises and degrades IL-2, thus depriving Tcons of this essential cytokine [53] . CTLA-4 expression was increased on Treg cells from *FoxP3*$^{YFP\text{-}Cre}$ *Pik3c3*$^{fl/fl}$ mice (**Fig. 3.4.2 a**). Concomitantly, the co-stimulatory molecule CD80 was increased on splenocytes from *FoxP3*$^{YFP\text{-}Cre}$ *Pik3c3*$^{fl/fl}$ mice (**Fig. 3.4.2 b)** while CD86 levels were unchanged (**Fig. 3.4.2 c)**. Next, we tested whether the increased expression of CTLA-4 on Treg cells from *FoxP3*$^{YFP\text{-}Cre}$ *Pik3c3*$^{fl/fl}$ mice is a secondary effect due to the inflammatory environment rather than a direct effect of VPS34-deficiency. The expression CTLA-4 on VPS34-deficient (Cre^+) Treg cells was unchanged compared to VPS34-sufficient Treg cells (Cre^-) (**Fig. 3.4.2 d**), and we detected normal levels of CD80 and CD86 on splenocytes from *FoxP3*$^{YFP\text{-}Cre/WT}$ *Pik3c3*$^{fl/fl}$ mosaic mice (**Fig. 3.4.2 e and f,** respectively).

The expression of the IL-2Rα-chain (also referred to as CD25) was markedly increased on Treg cells from *FoxP3*$^{YFP\text{-}Cre}$ *Pik3c3*$^{fl/fl}$ mice (**Fig. 3.4.2 g**), while it was unchanged on VPS34-deficient (Cre^{+}) Treg cells compared to VPS34-sufficient Treg cells (Cre^{-}) on splenocytes from *FoxP3*$^{YFP\text{-}Cre/WT}$ *Pik3c3*$^{fl/fl}$ mosaic mice (**Fig. 3.4.2 h**).

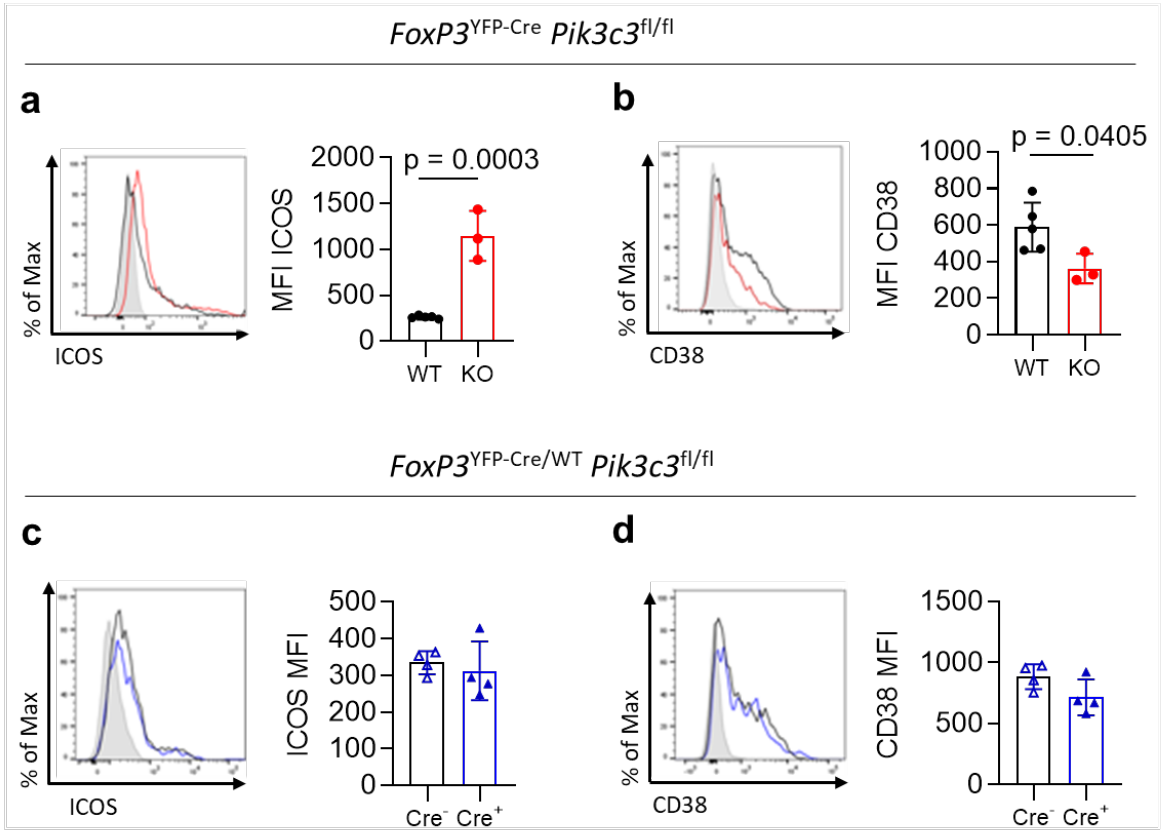

Figure 3.4.1: Increased expression of ICOS and CD38 is a secondary effect of the inflammatory environment rather than a direct effect of VPS34-deficiency.
Mean fluorescence intensity (MFI) of ICOS and CD38 in splenic Treg cells from *FoxP3*$^{YFP\text{-}Cre}$ *Pik3c3*$^{fl/fl}$ mice (KO) and the respective wild-type control mice (WT) (**a** and **b**) and VPS34-deficient (Cre^{+}) and VPS34-sufficient (Cre^{-}) Treg cells from mosaic *FoxP3*$^{YFP\text{-}Cre/WT}$ *Pik3c3*$^{fl/fl}$ mice (**c** and **d**).
FoxP3$^{YFP\text{-}Cre}$ *Pik3c3*$^{fl/fl}$ mice and the respective control mice were between 4 and 5.5 weeks of age. *FoxP3*$^{YFP\text{-}Cre/WT}$ *Pik3c3*$^{fl/fl}$ mosaic mice and the respective control mice were between 8 and 12 weeks of age. n = 3 – 4 mice per group. Statistical significance was determined using an unpaired two-tailed Student's t-test (a, b, d, e) or paired two-tailed Student's t-test (c). Results are representative of three independent experiments. Similar data was produced by Elisabeth.

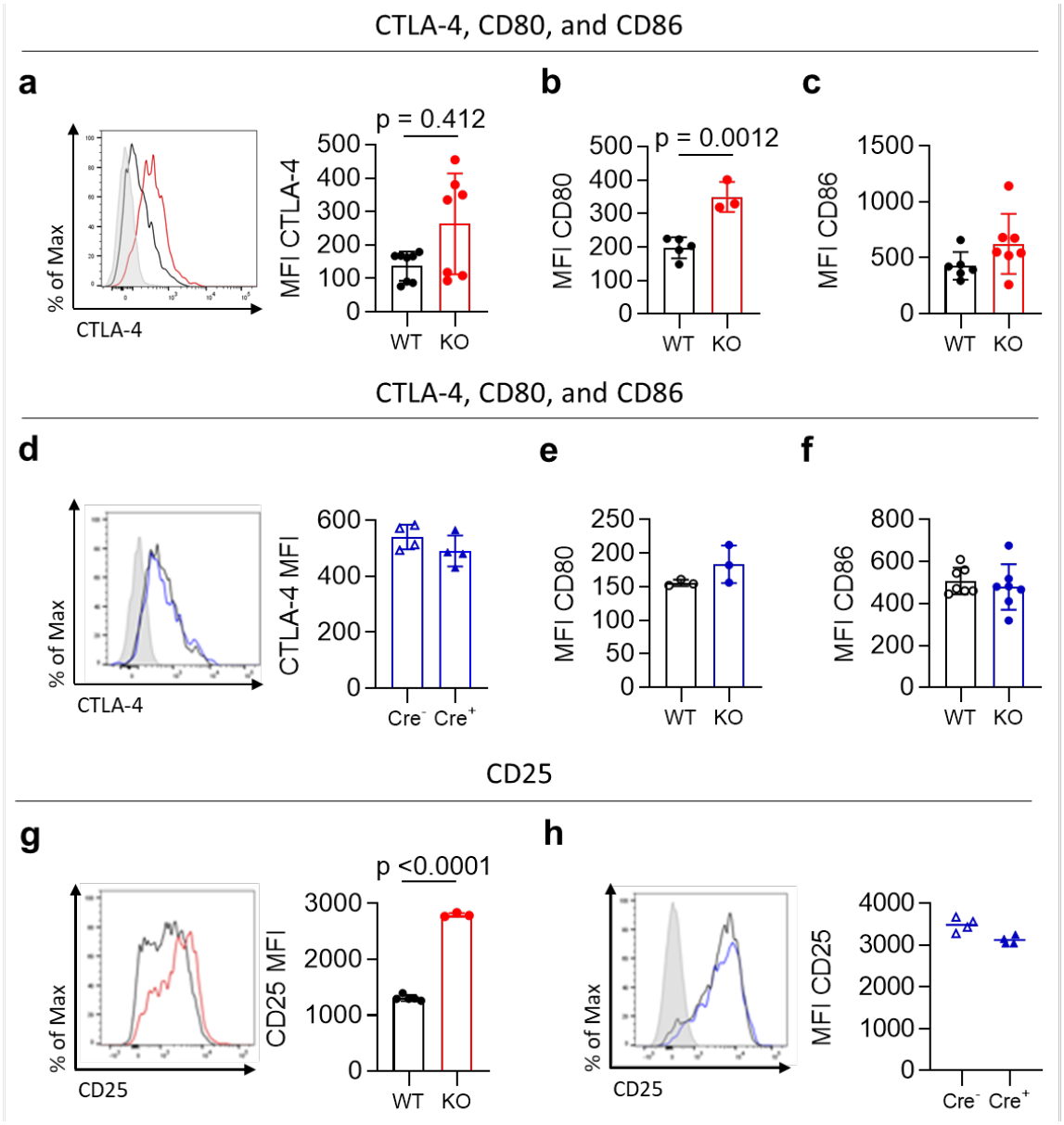

Figure 3.4.2: Increased expression of CTLA-4 on Treg cells and CD80/CD86 on splenic APC is a secondary effect of the inflammatory environment rather than a direct effect of VPS34-deficiency.
(**a – c**) Mean fluorescence intensity (MFI) of CTLA-4 on splenic Treg cells and MFI of CD80 and CD86 on antigen-presenting cells (APCs) from *FoxP3*$^{YFP\text{-}Cre}$ *Pik3c3*$^{fl/fl}$ mice (KO) and the respective wild-type control mice (WT). (**d – f**) Mean fluorescence intensity (MFI) of CTLA-4 on VPS34-deficient (Cre^{+}) and VPS34-sufficient (Cre^{-}) splenic Treg cells and MFI of CD80 and CD86 on antigen-presenting cells (APCs) from *FoxP3*$^{YFP\text{-}Cre/WT}$ *Pik3c3*$^{fl/fl}$ mosaic mice (KO) and the respective wild-type control mice (WT).
(**g**) Mean fluorescence intensity (MFI) of CD25 on splenic Treg cells from *FoxP3*$^{YFP\text{-}Cre}$ *Pik3c3*$^{fl/fl}$ mice (KO) and the respective wild-type control mice (WT). (**h**) Mean fluorescence intensity (MFI) of CD25 on VPS34-deficient (Cre^{+}) and VPS34-sufficient (Cre^{-}) splenic Treg cells from *FoxP3*$^{YFP\text{-}Cre/WT}$ *Pik3c3*$^{fl/fl}$ mosaic mice.
FoxP3$^{YFP\text{-}Cre}$ *Pik3c3*$^{fl/fl}$ mice and the respective control mice were between 4 and 5.5 weeks of age. *FoxP3*$^{YFP\text{-}Cre/WT}$ *Pik3c3*$^{fl/fl}$ mosaic mice and the respective control mice were between 8 and 12 weeks of age. n = 3 – 7 mice per group. Statistical significance was determined using an unpaired two-tailed

Student's t-test (a, b, c, e, f, g) or paired two-tailed Student's t-test (d and h). Results are representative of three independent experiments. Similar data was produced by Elisabeth.

3.2.5 Expression of CD69 and LAG-3 are reduced while GITR is increased on VPS34-deficient Treg cells from mosaic mice

Next, I performed a more detailed phenotypical analysis of activation markers that have been shown to regulate the suppressive capacity of Treg cells. To ascertain that observed differences in the expression profile of these markers is only based on cell-intrinsic effects, I performed this analysis using Treg cells from *FoxP3*$^{YFP\text{-}Cre/WT}$ *Pik3c3*$^{fl/fl}$ mosaic mice. I noted that KLRG1, CD69 and LAG3 were significantly downregulated in Cre^{+} VPS34-deficient Treg cells compared to Cre^{-} VPS34-sufficient Treg cells (**Fig. 3.5 a, b,** and **c**, respectively). CD69 is an early activation marker that modulates the balance between Th1/Th17 and Treg cells and has been proposed as a metabolic gatekeeper [272]. Meanwhile, LAG3 is expressed after activation and has been shown to be required for maximal regulatory activity of Treg cells [273]. Interestingly, GITR expression was upregulated on VPS34-deficient Treg cells (**Fig. 3.5 d**). GITR is involved in Treg cells differentiation and expansion and it has been suggested that triggering of GITR decreases the suppressive activity of Treg cells [274].

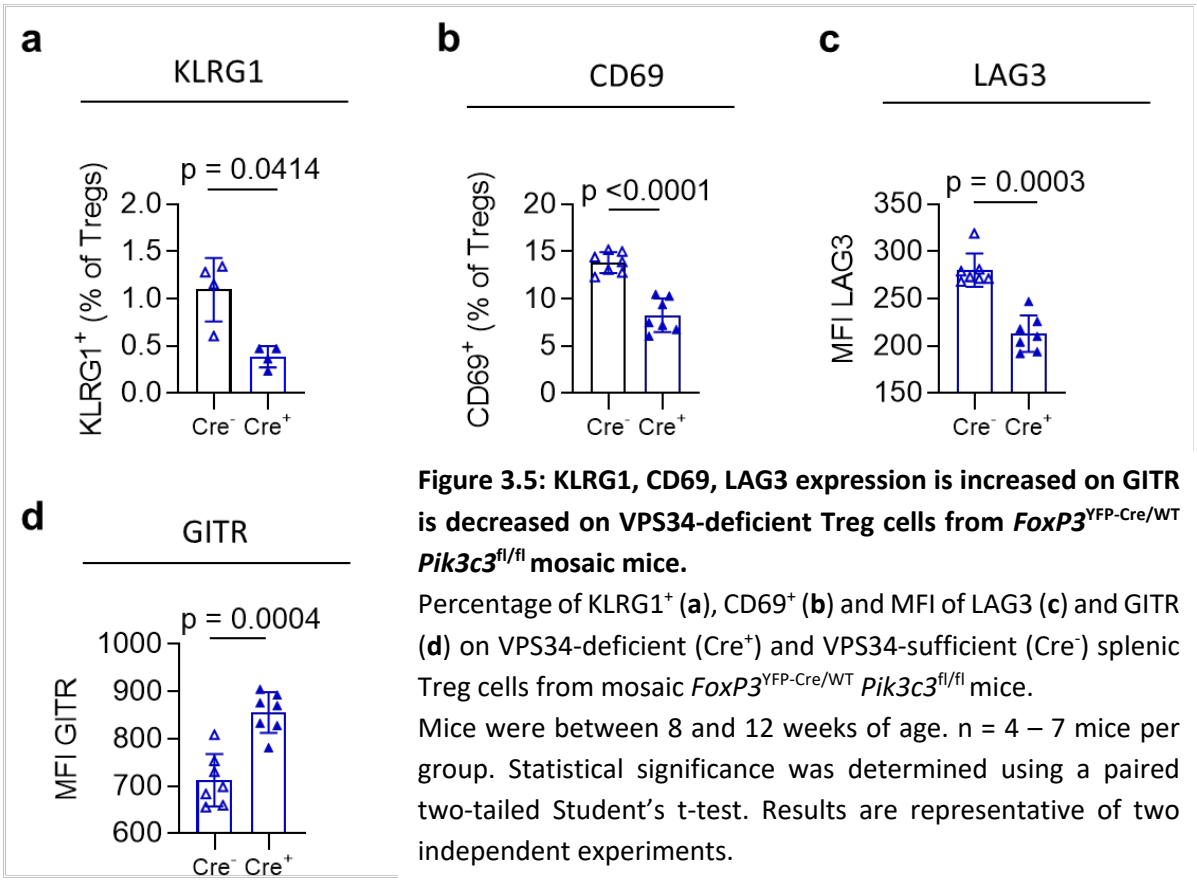

Figure 3.5: KLRG1, CD69, LAG3 expression is increased on GITR is decreased on VPS34-deficient Treg cells from *FoxP3*$^{YFP\text{-}Cre/WT}$ *Pik3c3*$^{fl/fl}$ mosaic mice.

Percentage of KLRG1$^+$ (**a**), CD69$^+$ (**b**) and MFI of LAG3 (**c**) and GITR (**d**) on VPS34-deficient (Cre$^+$) and VPS34-sufficient (Cre$^-$) splenic Treg cells from mosaic *FoxP3*$^{YFP\text{-}Cre/WT}$ *Pik3c3*$^{fl/fl}$ mice.
Mice were between 8 and 12 weeks of age. n = 4 – 7 mice per group. Statistical significance was determined using a paired two-tailed Student's t-test. Results are representative of two independent experiments.

3.2.6 VPS34 is required for the maturation of Treg cells into CD44-expressing cells

I also assess the expression of the activation cell surface marker CD44. In support of the hypothesis that the lack of VPS34-kinase activity impairs Treg cell function rather than survival, we observed that fewer VPS34-deficient Treg cells expressed high levels of CD44 in *FoxP3*$^{YFP\text{-}Cre}$ *Pik3c3*$^{fl/fl}$ mice (**Fig. 3.6.1 a**). However, CD44-expression was reduced on VPS34-deficient (Cre$^+$) compared to VPS34-sufficient (Cre$^-$) Treg cells arising from *FoxP3*$^{YFP\text{-}Cre/WT}$ *Pik3c3*$^{fl/fl}$ mosaic mice (**Fig. 3.6.1 c**). These data suggest that VPS34 is required for Treg cells to differentiate into a CD44^{high} phenotype or that CD44^{high} Treg cells depend on VPS34 for their survival and/or proliferation, especially under inflammatory conditions.

In line with this hypothesis, VPS34-deficient Treg cells from the lymph nodes of *FoxP3*$^{YFP\text{-}Cre/WT}$ *Pik3c3*$^{fl/fl}$ mosaic mice were less proliferative than VPS34-sufficient Treg cells from the same mice (**Fig. 3.6.2 a**). However, in the spleen, VPS34-deficient Treg cells had a proliferation potential similar to their wild-type Treg cells (**Fig. 3.6.2 b**).

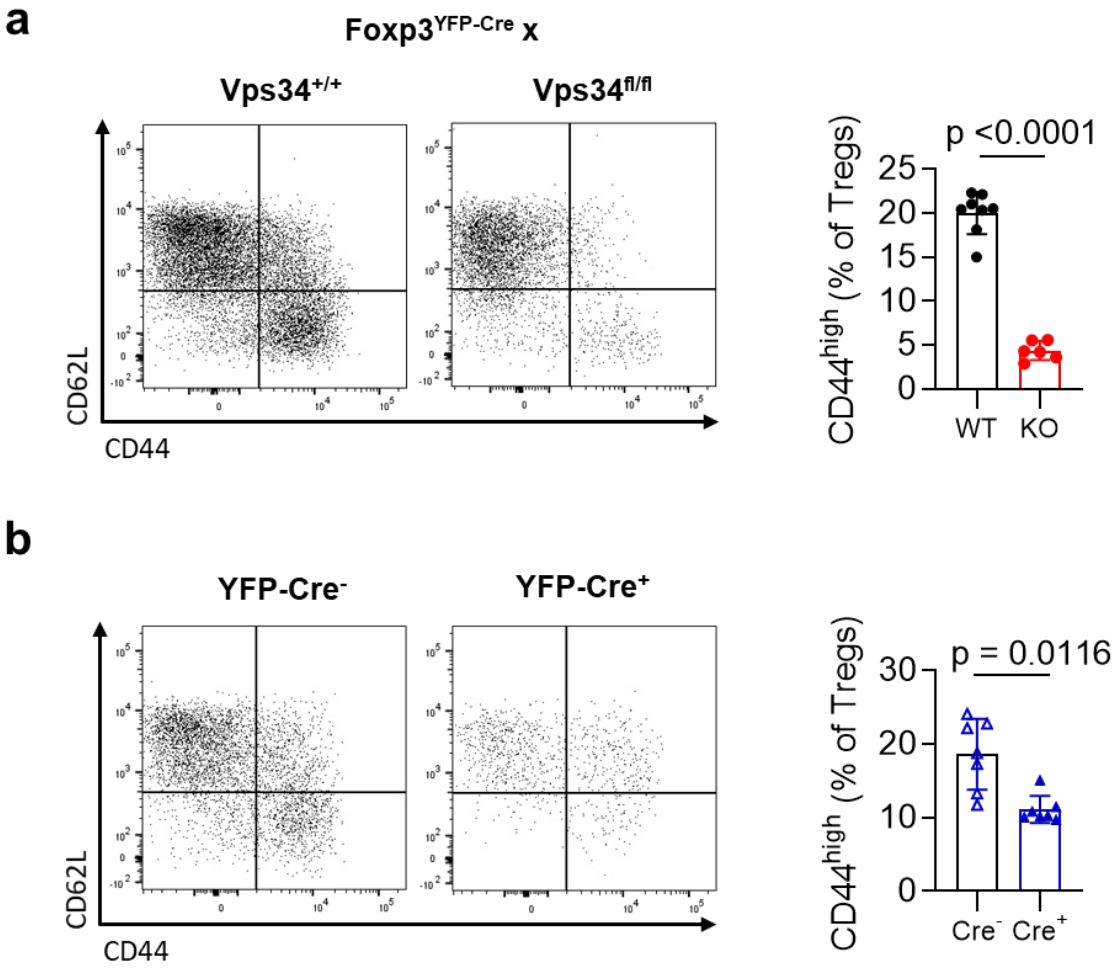

Figure 3.6.1: VPS34-deficient Treg cells have a reduced expression of the activation marker CD44.
a) Representative flow cytometry plot for CD44 and CD62L expression (left) and bar graph representing levels of CD44-expression (right) on splenic Treg cells of *FoxP3*$^{YFP\text{-}Cre}$ *Pik3c3*$^{fl/fl}$ mice (KO) and the respective wild-type control mice (WT).
b) Representative flow cytometry plot for CD44 and CD62L expression (left) and bar graph representing levels of CD44-expression (right) on splenic VPS34-deficient (Cre^{+}) and VPS34-sufficient (Cre^{-}) Treg cells from F*oxP3*$^{YFP\text{-}Cre/WT}$ *Pik3c3*$^{fl/fl}$ mosaic mice. *FoxP3*$^{YFP\text{-}Cre}$ *Pik3c3*$^{fl/fl}$ mice and the respective control mice were between 4 and 5.5 weeks of age. *FoxP3*$^{YFP\text{-}Cre/WT}$ *Pik3c3*$^{fl/fl}$ mosaic mice and the respective control mice were between 8 and 12 weeks of age. n = 6 mice per group. Statistical significance was determined using an unpaired two-tailed Student's t-test (a and b) or paired two-tailed Student's t-test (c). Results are pooled from four independent experiments.

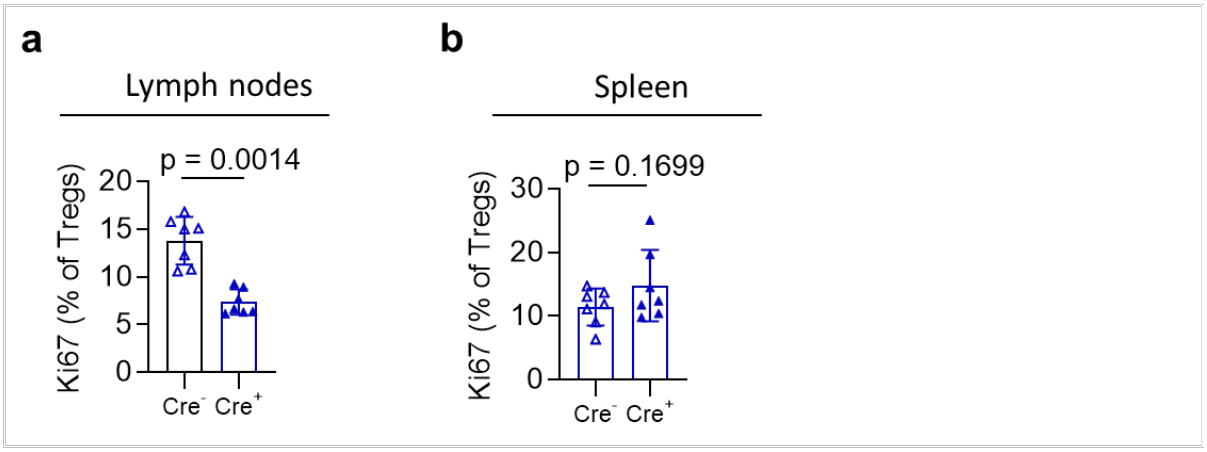

Figure 3.6.2: VPS34-deficient Treg cells from the lymph nodes proliferate less.
Percentage of Ki67^{+} VPS34-deficient (Cre^{+}) and VPS34-sufficient (Cre^{-}) Treg cells in the lymph nodes (pooled from inguinal, brachial, and axiliary) (**a**) and spleen (**b**) from from F*oxP3*$^{YFP\text{-}Cre/WT}$ *Pik3c3*$^{fl/fl}$ mosaic mice. Mice were between 8 and 12 weeks of age. n = 6 mice per group. Statistical significance was determined using a paired two-tailed Student's t-test. Results are representative of two independent experiments.

3.2.7 VPS34-deletion does not interfere with IL-2 consumption nor CD80-transendocytosis

The ongoing lympho-proliferative disease in *FoxP3*$^{YFP\text{-}Cre}$ *Pik3c3*$^{fl/fl}$ mice, along with the low expression levels of the activation markers CD44, CD69, and LAG3 on the cell surface of VPS34-deficient Treg cells from mosaic *FoxP3*$^{YFP\text{-}Cre/WT}$ *Pik3c3*$^{fl/fl}$ mice suggested that the loss of VPS34-kinase activity impairs the maturation of Treg cells in effector cells, thereby compromising the suppression of conventional T cells.

However, Elisabeth demonstrated that VPS34-deficient Treg cells from *FoxP3*$^{YFP\text{-}Cre}$ *Pik3c3*$^{fl/fl}$ mice were similarly competent at suppressing the proliferation of Tcons *in vitro (data not shown*), and even in a superior manner compared to wild-type Treg cells at the ratio 1:1, 1:2, and 1:4. Meanwhile, IL-2 concentration was reduced in a stepwise manner with increasing Treg:Tcon ratio but did not differ between co-cultures with Treg cells from *FoxP3*$^{YFP\text{-}Cre}$ *Pik3c3*$^{fl/fl}$ and wild-type mice (*data not shown*). These results demonstrate that Treg cells are able to develop without VPS34 and maintain functions associated with wild-type Treg cells *in vitro*, yet fail to prevent lethal autoimmune disease *in vivo*. We therefore hypothesised that another suppressive mechanism than the suppression of Tcon proliferation is critical for immune homeostasis.

Treg cells employ diverse mechanisms of suppression to ensure peripheral tolerance, including the production of immunomodulatory cytokines, the expression of inhibitory receptors, the consumption of cytokines and direct cytotoxic killing through granzymes and perforin. Elisabeth therefore assessed whether the suppressive functions of Treg cells were abrogated by the loss of VPS34-kinase activity. Her results indicated that loss of VPS34-kinase activity does not affect the consumption and downstream signalling of IL-2 (*data not shown*).

Next, the capacity of VPS34-deficient Treg cells to indirectly suppress the activation of naïve $CD4^+$ T cells by capturing the co-stimulatory molecules CD80/CD86 from the cell surface of DCs through the CTLA-4 receptor expressed on Treg cells was evaluated. The ability of Treg cells to rip off and endocytose CD80/CD86 from the cell surface of DCs was shown in an *in vitro* assay using *ex vivo* isolated Treg cells and CD80-GFP expressing *Chinese hamster ovary* (CHO) cells and is referred to as transendocytosis [42], [275]. When CTLA-4 expressed on the cell surface of Treg cells binds to these molecules, the CTLA-4 – CD80 /CTLA-4 – CD86 complexes are rapidly internalized by clathrin-mediated endocytosis and degraded through the lysosomal pathway [276]. Based on the altered expression of CTLA-4 and CD80 on Treg

cells and DCs, respectively, from *FoxP3*$^{YFP\text{-}Cre}$ *Pik3c3*$^{fl/fl}$ mice, we hypothesized that VPS34-deletion impairs the transendocytosis of CD80 in CTLA-4 – expressing Treg cells.

To test that, Treg cells were co-cultured with *Chinese Hamster Ovary* (CHO) cells expressing a C-terminally tagged CD80-GFP (CD80-GFP) protein (**Fig. 3.7 a**). Using flow cytometry, we observed a transfer of CD80-GFP into Treg cells (*data not shown*). Strikingly, Treg cells from *FoxP3*$^{YFP\text{-}Cre}$ *Pik3c3*$^{fl/fl}$ mice acquired more CD80 than Treg cells from *FoxP3*$^{YFP\text{-}Cre}$ *Pik3c3*^{WT} control mice (*data not shown*). Following transendocytosis, the internalized cargo is degraded through the endo-lysosomal pathway, a system relying on PI3P for the recruitment of several endosomal sorting machineries, such as retromer and ESCRT (16). Therefore, I considered whether the delivery of the endosomal cargo to the lysosomes for degradation is impaired, despite intact initial internalisation. To test this hypothesis, I developed a 'pulse-chase' assay. To ensure similar uptakes of CD80 and to delimit the effect of VPS34-deficiency to the degradation step, I used wild-type Treg cells for the initial co-culture with CHO cells (pulse) (**Fig. 3.7 a**). Treg cells were then separated from CHO cells by *fluorescence-activated cell sorting* (FACS) (gated on GFP^+ $CD25^+$ $CD4^+$ cells) and treated with VPS34 IN1, a selective inhibitor of VPS34 [277]. The percentage of GFP-positive Treg cells was assessed by flow cytometry at 0h, 24h, and 48h and taken as a measure for the presence of CD80 (**Fig. 3.7 b**). In the presence of pharmacological inhibitor VPS34-IN1, the degradation of the internalised CD80 was delayed (**Fig. 3.7 c**). Together, these results suggest that VPS34-inhibition results in alterations in endolysosomal dynamics, possibly resulting in knock-on effects on Treg cells and reduce their overall capacity for suppression.

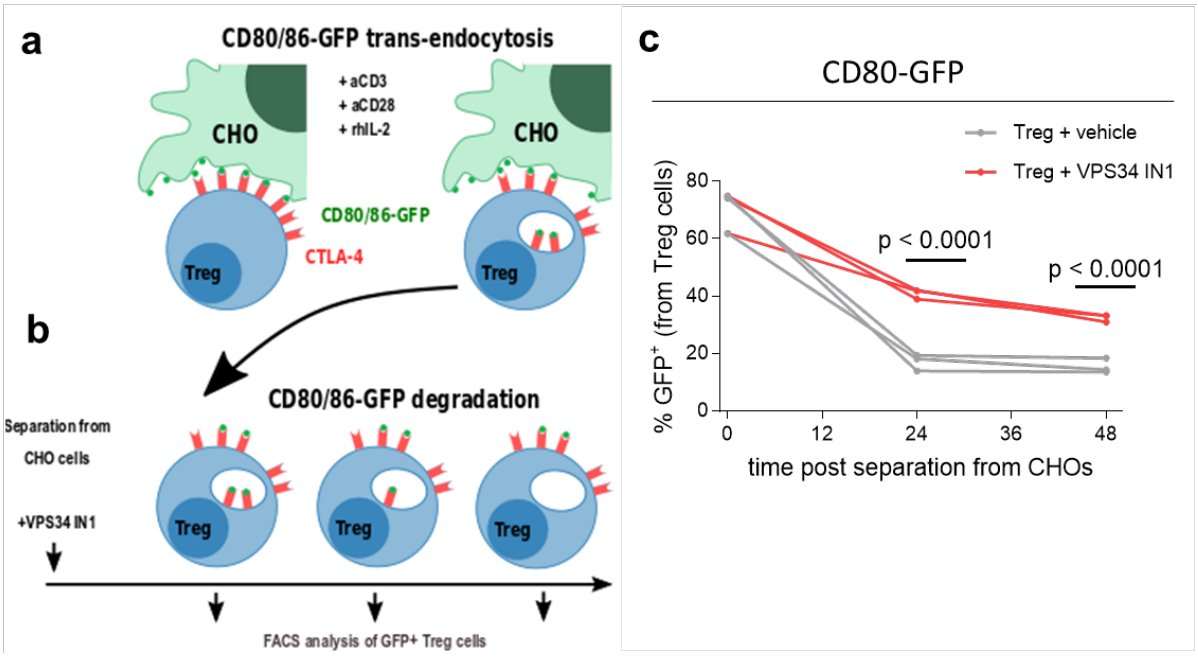

Figure 3.7: VPS34 inhibition impairs the degradation, but not the trans-endocytosis, of CD80-GFP *in vitro*.

a) Schematic representation of the trans-endocytosis assay: $CD4^+$ cells from the lymph nodes of *FoxP3*$^{YFP\text{-}Cre}$ *Pik3c3*$^{fl/fl}$ mice by magnetic cell sorting (MACS) and co-cultured for 24 hours with in a 10:1 ratio with Chinese Hamster Ovary (CHO) cells expressing CD80-GFP on their surface. Treg cells should internalize and accumulate CD80-GFP. *Modified from Elisabeth Slack*.

b) Schematic of the pulse-chase assay: trans-endocytosis as shown in **a**) and after 24h co-culture, Treg cells were separated from the rest of the cells by fluorescence-activated cell sorting (FACS) and cultured presence of VPS34 IN1, a selective Vps34 inhibitor for up to 48 hours.

c) The percentage of the GFP signal was assessed by flow cytometry directly after separation from the CHO cells (0h), and then 24 and 48 hours after separation. n = 4 biological replicates. Results are pooled from two independent experiments. Statistical significance was determined using an unpaired two-tailed Student's *t*-test for each time point.

3.3 Discussion

3.3.1 Inactivation of VPS34 has interfered with a fundamental suppressive mechanism essential for Treg cell functions

When Elisabeth started to investigate the role of VPS34 in Treg cells, only two studies had investigated the contribution of VPS34 in T cell homeostasis [227], [257], but none has concentrated on the role of VPS34 in Treg cells. During her PhD thesis, Elisabeth established that Treg cells critically rely on VPS34.

McLeod et *al*. assessed the role of VPS34 in $CD4^+$ and $CD8^+$ T cells using the Lck-Cre recombinase system [227]. Doing so, they observed a defect in IL-7Rα trafficking and therefore impaired naïve T cell survival. Willinger and Flavell described a similar phenotype using a CD4-Cre recombinase system, but showed that impaired IL-7Rα trafficking in VPS34-deficient T cells was due to the lymphopenic environment rather than a direct effect of VPS34-deletion [257]. They observed that loss of VPS34 results in impaired mitochondrial homeostasis and thus reduced T cell survival. Neither studies reported any gross phenotype associated with T cell-specific deletion of VPS34. It was therefore a surprise to Elisabeth that Treg cell-specific deletion of VPS34 resulted in such a fatal inflammatory and lymphoproliferative disease, strikingly resembling the *Scurfy* phenotype. However, unlike the *Scurfy* mouse, the onset of the disease was delayed: while *Scurfy* mice become sick at around 14 days after birth and succumb to their phenotype around 24 days after birth [278], *FoxP3*$^{YFP\text{-}Cre}$ *Pik3c3*$^{fl/fl}$ mice started to develop abnormalities at around 21 days of age, and reached on average 35 days before they had to be sacrificed. Secondly, Treg cells were present in mice with VPS34-deficient Treg cells while *Scurfy* mice completely lack functional Treg cells.

The absence or presence of Treg cells could reflect the point at which cells become affected by the lack of *FoxP3* or VPS34. Since *FoxP3* is necessary [278], [279] and sufficient [21] to generate Treg cells, a frame shift mutation in this gene impairs the formation of Treg cells in the *Scurfy* mouse. In *FoxP3*$^{YFP\text{-}Cre}$ *Pik3c3*$^{fl/fl}$ mice, VPS34 is only deleted once *FoxP3* is expressed. *FoxP3*-expression occurs three days after birth and Treg cells should therefore develop normally in the thymus of *FoxP3*$^{YFP\text{-}Cre}$ *Pik3c3*$^{fl/fl}$ mice. Furthermore, VPS34 has a long half-life [227], so that Treg cells could easily contain functional VPS34 for some time after *FoxP3* induction and Cre-recombinase expression. This resulting lag phase between Treg cells

development, the induction of *FoxP3,* and the actual functional defect due to the lack of VPS34-kinase activity could explain the delayed onset of the fatal phenotype.

The development of the fatal immune-proliferative disease in the presence of Treg cells established that inactivation of VPS34 interferes with a fundamental suppressive mechanism essential for Treg cells rather than their survival. A few genetic manipulations of Treg cells or their key molecules recapitulate the *Scurfy* phenotype. Obviously, the deletion of *FoxP3* and the selective ablation of Treg cells are virtually identical to the firstly described *Scurfy* mouse [21], [280]. Other deletions have generated similar phenotypes. Among those, Treg cell-specific deletion of the transcription factor Foxo1 causes a similar disease to the *Scurfy* mouse, and Treg cell numbers are greatly reduced [281]. Foxo1 regulates around 300 target genes that are distinct from the *FoxP3*-regulated gene repertoire [281] and suppresses detrimental IFN-γ transcription in Treg cells. However, deletion of Foxo1 does not affect any mechanisms relating to Treg cell functions and the observed phenotype is solely based on a lack of Treg cells [21], [280] or wider-ranging effects on their transcriptional programme [281]. In contrast, *FoxP3*$^{YFP\text{-}Cre}$ *Pik3c3*$^{fl/fl}$ mice do not lack Treg cells, and as a kinase whose role has been, so far, ascribed to autophagy and endocytosis, we speculated that VPS34 is unlikely to control Treg cell transcriptional programmes.

CTLA-4 is a critical negative regulator of T cell activation and its deletion is sufficient to cause fatal disease [46]. Hence, mice with Treg cell-specific deletion of CTLA-4 develop lymphadenopathy and splenomegaly from seven weeks of age onwards, and ultimately die from severe myocarditis [48]. In CTLA-4 deficient mice, Treg cells are unable to downregulate CD80 and CD86 from dendritic cells, resulting in the uninterrupted co-stimulation of naïve T cells [48]. This was of particular interest in the context of *FoxP3*$^{YFP\text{-}Cre}$ *Pik3c3*$^{fl/fl}$ mice since CD80 and CD86 expression is increased on the surface of dendritic cells despite increased expression of CTLA-4 on VPS34-deficient Treg cells. This raised the hypothesis that VPS34-deficient Treg cells have a defect in CD80 transendocytosis, that is the ripping off and the internalization of the CD80 molecules by CTLA-4. However, Elisabeth observed that the transendocytosis of CD80 by VPS34-deficient Treg cells was elevated compared to VPS34-sufficient Treg cells. The enhanced uptake likely reflects higher levels of CTLA-4 on the surface of VPS34-deficient Treg cells. This increase is most likely due to the activated immune phenotype of these mice, since VPS34-deficient Treg cells from *FoxP3*$^{YFP\text{-}Cre/WT}$ *Pik3c3*$^{fl/fl}$ mosaic mice display normal levels of CTLA-4.

3.3.2 Impaired function of VPS34-deficient Treg cells may relate to impaired endolysosomal trafficking

Autophagy is a highly conserved degradation process that is critical to maintain cellular homeostasis, is critical to establish Treg cell-mediated immune tolerance, and supports lineage stability and survival fitness [152]. Autophagy is increased after the initial activation of T cells, presumably as a mechanism to degrade the increasing cytoplasmic content that is generated as the T cells become more metabolically active [282].

Kabat et *al*. showed that autophagy is essential for Treg cell homeostasis and control of effector T cell responses in the gut by depleting Atg16l1 in Treg cells (Atg16l1$^{\Delta Foxp3}$ mice) [224]. Atg16l1 is an essential part of the autophagy complex with Atg5 and Atg12 that facilitates the elongation of the initial isolation membrane, resulting in the engulfment of the cargo and formation of the autophagosome. Atg16l1$^{\Delta Foxp3}$ mice appeared normal in early life, but developed a severe inflammatory disease characterized by progressive weight loss, splenomegaly, lymphadenopathy and leukocyte infiltration in multiple organs at around 5 months [224].

We therefore considered whether defective autophagy may be the reason of the fatal lymphoproliferative disease observed in *FoxP3*$^{YFP\text{-}Cre}$ *Pik3c3*$^{fl/fl}$ mice. In order to specifically disable autophagy in Treg cells, we deleted Atg7, a protein essential for the induction of autophagy [268]. These mice were initially healthy and survived for up to a year ($t_{1/2}$ = 269 days). Hence, defective autophagy may contribute to, but is not the primary cause of the profound autoimmunity observed upon inactivation of VPS34 in Treg cells. Furthermore, these results strongly imply that inactivation of VPS34 has interfered with a fundamental suppressive mechanism essential for Treg cell function which we suspect is related to the role of VPS34 in endocytosis rather than autophagy.

PI3P is localised to early endosomes where it is required for the recruitment of PX- or FYVE- domain – containing proteins, as found in several endosomal sorting machineries, such as retromer and ESCRT [283]. Inhibition of VPS34, and subsequent loss of PI3P, prevents the recruitment of Armus, a Rab7 GAP, and results in the hyperactivation of Rab7, enlarged endosomes, and altered endosomal dynamics [239]. Therefore, I considered whether the delivery of the endosomal cargo to lysosomes for degradation is impaired, despite intact initial internalisation. Indeed, in the presence of VPS34-IN1, a pharmacological inhibitor of

VPS34, the degradation of the internalised CD80 was delayed. A block in the degradation of endocytosed material could have knock-on effects on Treg cells and reduce their overall capacity for suppression, either because the total number of ligands endocytosed per Treg cell may be reduced or because Treg cells become congested and stop functioning altogether.

3.3.3 VPS34 is either required for Treg cell differentiation into a CD44^{high} phenotype or CD44^{high} Treg cells depend on VPS34 for their survival

TCR signalling is essential for the maintenance and function of Treg cells [284]. The lack of Treg cells with a more mature phenotype may therefore reflect an inability of VPS34-deficient Treg cells to respond to TCR-dependent cues that promote their maturation and hence the development of a fully suppressive phenotype *in vivo*.

Phenotypic analyses of Treg cells in *FoxP3*$^{YFP\text{-}Cre}$ x *Pik3c3*$^{fl/fl}$ mice revealed that a smaller proportion expressed high levels of CD44, a marker of activated or memory T cells. However, VPS34-deficient Treg cells were able to suppress CD4^{+} CD25^{-} Tcon *in vitro*. These results demonstrate that Treg cells maintain suppressive functions *in vitro*, yet fail to acquire a mature phenotype and to prevent lethal autoimmune disease.

Analysis of mosaic mice showed that the VPS34-deficient Treg cells were at a competitive disadvantage compared to VPS34-sufficient Treg cells. Furthermore, the proportion of Treg cells expressing CD44 was lower among VPS34-deficient Treg cells from mosaic mice, suggesting that VPS34 is intrinsically required for Treg cells to differentiate into a more mature phenotype or alternatively, that mature Treg cells depend on VPS34 for their survival. Future work will aim to provide an answer to this open question.

3.4 Chapter summary

I consolidated the data produced by Elisabeth and further worked on understanding the role of VPS34 in Treg cells. I have established that while VPS34-deficiency does not affect CD80 transendocytosis, it is required for the degradation of the endocytosed cargo. At which point the blockage occurs remains to be determined and is the content of future work that I am currently undertaking.

While autophagy might be defective in VPS34-deficient Treg cells, I have shown that mitophagy is indeed impaired in VPS34-deficient Treg cells. The implications of this observation will be further investigated and put into context in ***Chapter 4***.

Based on the observations that VPS34-defiicent Treg cells have a competitive disadvantage and express less of the activation marker CD44, I have started to investigate whether VPS34 is required for the maturation of Treg cells using a tumour model. Together, future work will provide further insight into suppressive function of Treg cells affected by VPS34-kinase loss.

Chapter 4

Discovery of novel mechanisms of regulatory T cell suppression

4.1 Introduction

Results presented in the previous chapter suggest that while VPS34 is redundant for Treg cell development and survival, it is critical for Treg cell suppression and maintenance of immune homeostasis. Which Treg cell suppression mechanism(s) is/are affected needs to be determined. Although the lysosomal degradation of the endocytosed cargo appears to be impaired, VPS34-deficient Treg cells are still able to deplete costimulatory ligands and cytokines and yet lack one or more hitherto unrecognised mechanisms of suppression.

The abundance of newly-synthesised proteins is regulated by post-transcriptional mechanisms. It is therefore important to determine the relative amount of any given protein in a cell in addition to determining individual mRNA expression levels. This is especially pertinent for VPS34, which is primarily thought to affect trafficking of subcellular vesicles and their associated proteins. A block at any stage in these processes should alter the steady-state levels of proteins involved in steps before and after the block had occurred. Therefore, with the aim to discover such novel suppressive functions of Treg cells, I determined how VPS34-deficiency affects the Treg cell proteome.

Because *FoxP3*$^{\text{YFP-Cre}}$ *Pik3c3*$^{\text{fl/fl}}$ mice develop such a profound inflammatory disease, we could not be certain whether any observed Treg cell phenotype is due to VPS34 specifically or whether alterations are secondary to the inflammatory milieu. Therefore, the studies performed and described in this chapter are conducted using female *FoxP3*$^{\text{YFP-Cre/WT}}$ *Pik3c3*$^{\text{fl/fl}}$ mosaic mice in which VPS34 was lacking in only about half of the Treg cells.

4.2 Results

4.2.1 Ablation of VPS34 kinase activity destabilizes VPS34 complex II

To gain insight into the molecular mechanisms underlying the defects in VPS34-deficient Treg cells, I used quantitative label-free high-resolution *mass spectrometry* (MS) to compare the proteome of VPS34-deficient and VPS34-sufficient Treg cells (in collaboration with Prof. Doreen Cantrell, Dr. Laura Spinelli and Dr. Christina Rollings from the University of Dundee, School of Life Sciences). To exclude potentially secondary effects caused by systemic inflammation, I performed the analysis on YFP$^+$ VPS34-deficient Treg cells from phenotypically normal mosaic *FoxP3*$^{YFP\text{-}Cre/WT}$ *Pik3c3*$^{fl/fl}$ female mice and used YFP$^+$ VPS34-sufficient Treg cells from *FoxP3*$^{YFP\text{-}Cre/WT}$ *Pik3c3*$^{WT/WT}$ mice as a control. Proteins from three different biological replicates were analysed. Identified peptides were matched to a single protein or multiple proteins, termed protein groups, using MaxQuant software [285]. This approach led to the identification of more than 6400 protein groups per biological replicate (*see: https://drive.google.com/open?id=1Cvc7qbHMBNE6pF-ZypL3GzAJhxxDhihZ*). Copy numbers for proteins from three biological replicates showed strong Pearson correlation coefficients (r^2=0.9899 – 0.9948), with very few outliers indicating robustness and reproducibility of this MS-based peptide quantitation method (**Fig. 4.1.1 a**).

The percentage of histone content from the total protein content was slightly but significantly reduced for VPS34-deficient compared to VPS34-sufficient Treg cells (**Fig. 4.1.1 b**). Assuming that the histone content is consistent in a same population, a relative reduction in the histone content indicates that the amount of the remaining non-histone proteins is elevated, suggesting an increase in the cell size. Indeed, the protein content was significantly increased in VPS34-deficient Treg cells compared to wild-type Treg cells (**Fig. 4.1.1 c**); however, this was not reflected by flow cytometry analysis of forward (FSC-A) and side scatter (SSC-A) (**Fig. 4.1.1 d**).

In total, 6498 proteins with a minimum of two unique peptides were identified in both VPS34-deficient and –sufficient Treg cells (**Fig. 4.1.2 a** and **b,** respectively). There was >99% overlap in the proteins identified among the three biological replicates of each condition (**Fig. 4.1.2 c**).

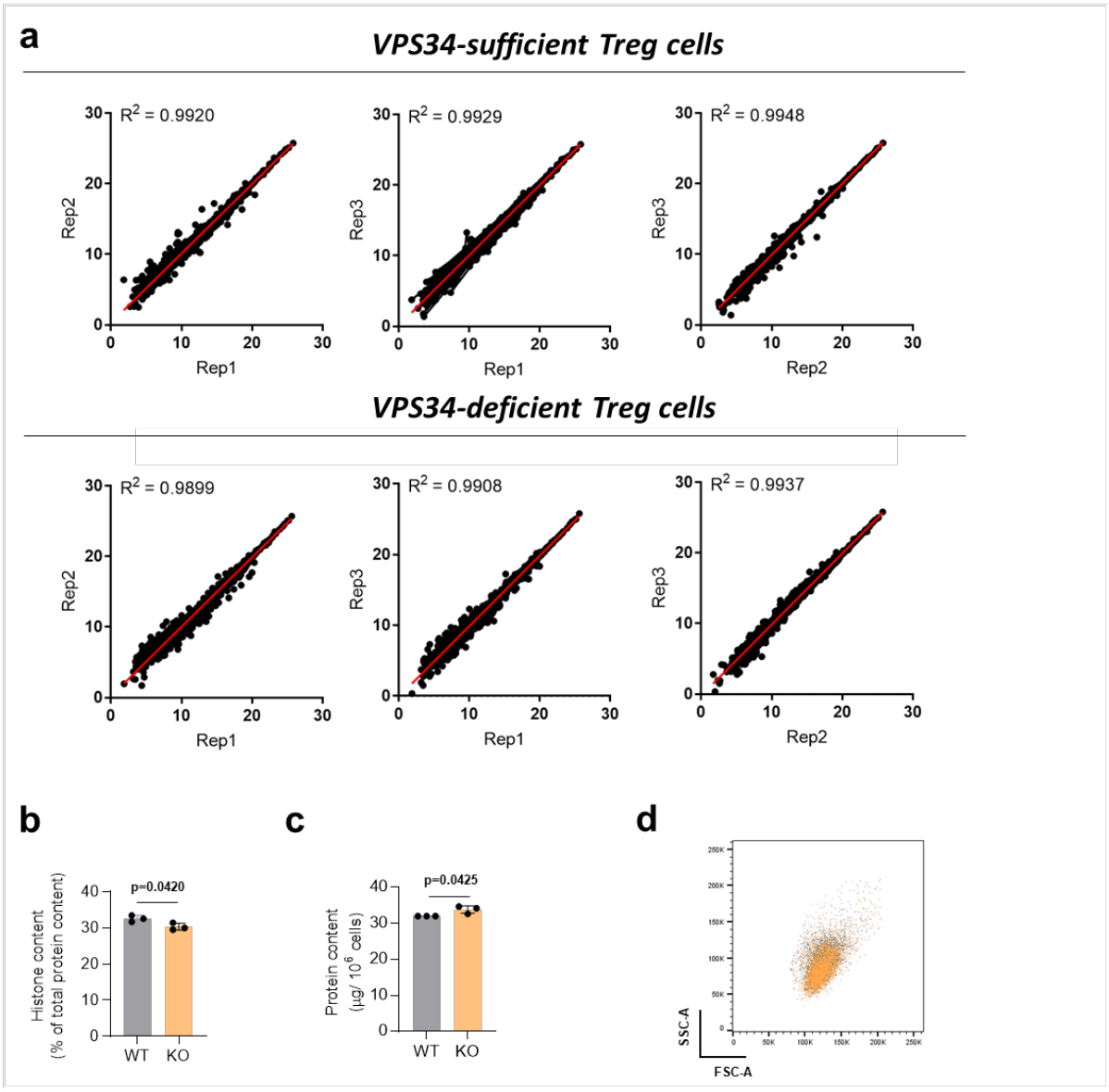

Figure 4.1.1: Proteomic profiling of VPS34-deficient Treg cells.

a) Scatter plots of estimated protein copy numbers using the proteomic ruler approach show high reproducibility of protein intensities and ~98% of identified proteins are detected in all three biological replicates for VPS34-sufficent and VPS34-deficient Treg cells. R^2 = coefficient of determination.

b) Total histone content as the percentage of total protein content of VPS34-sufficent (WT) and VPS34-deficient (KO) Treg cells.

c) Total protein content of VPS34-sufficent (WT) and VPS34-deficient (KO) Treg cells.

d) Flow cytometry plot of forward and side scatter VPS34-sufficent (WT, grey) and VPS34-deficient (KO, orange) Treg cells.

n = 3 biologically independent samples for each of the Treg cell populations. Statistical significance was determined using an unpaired two-tailed Student's t-test. Histogram bars represent means ± S.D.

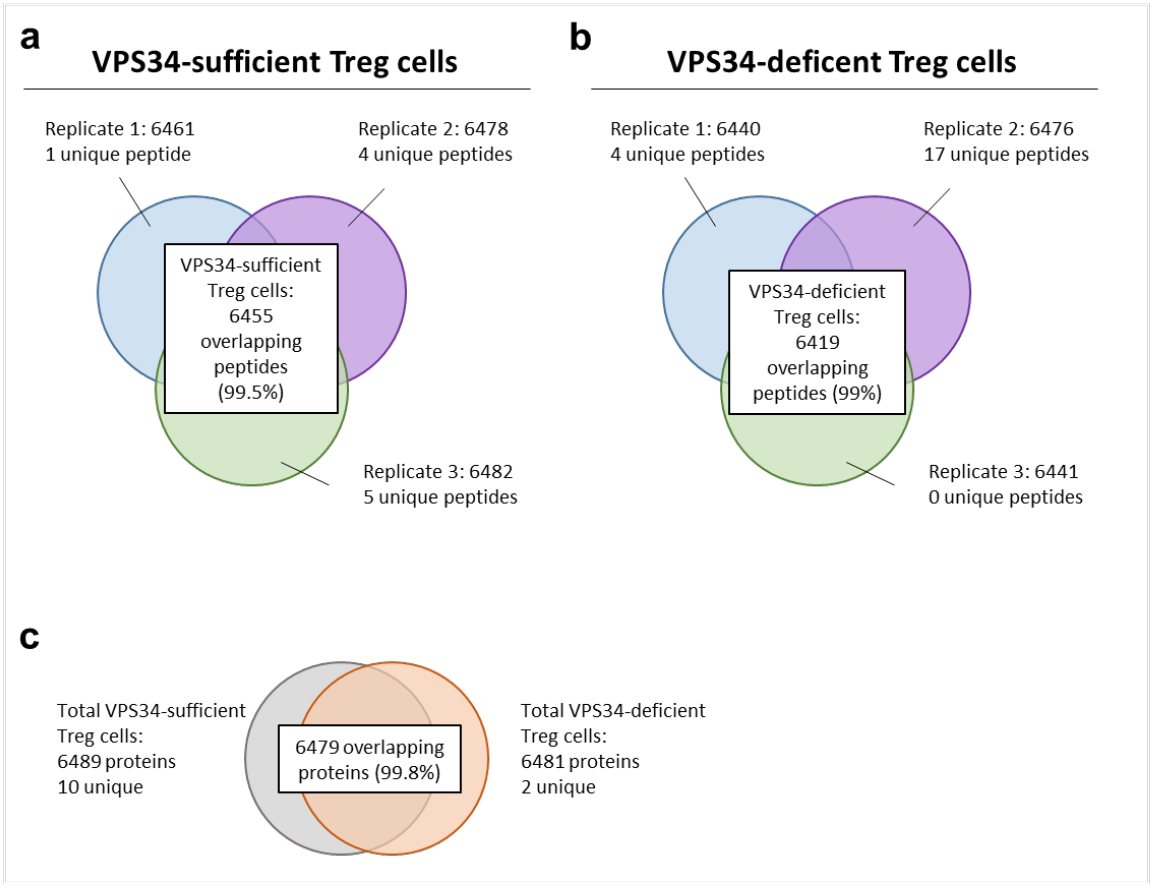

Figure 4.1.2: Commonality of proteins identified in the proteomic analysis.
The Venn diagram shows the commonality of proteins identified in the proteomic analysis among the three biological replicates for VPS34-sufficent and VPS34-deficient Treg cells (**a** and **b**), and commonality between total VPS34-sufficient and VPS34-deficient Treg cells (**c**). $n = 3$ biologically independent samples for each of the Treg cell populations.

I carried out statistical analyses to classify proteins specifically up- or down-regulated in VPS34-deficient Treg cells compared to VPS34-sufficient Treg cells. A two-sided paired t-test was performed on the three biological replicates and the proteins presenting a p-value under or equal to 0.05 and a minimum 2-fold change between VPS34-deficient and VPS34-sufficient Treg cells were considered significative. According to these criteria, I identified a total of 140 differentially expressed proteins, 122 more abundant and 18 less abundant in VPS34-deficient Treg cells compared to VPS34-sufficient Treg cells (**Fig. 4.1.3 a**).

Among proteins down-regulated in VPS34-deficient Treg cells, VPS34 protein level was reduced by half (**Fig. 4.1.3 b**), suggesting that the internal deletion of 25 amino acids in the kinase domain not only inhibits kinase activity but also affects the stability of the VPS34 protein. The copy numbers of VPS15, Beclin-1 and UVRAG, three binding partner of VPS34 complex II (endocytosis complex), were also decreased by half in VPS34-deficient Treg cells

compared to VPS34-sufficient Treg cells (**Fig. 4.1.3 b**). Atg14L was not detectable in this data set for both VPS34-deficient and VPS34-sufficient Treg cells. Taken together, these results suggest that VPS34 is necessary for the stability of the endocytosis complex, and loss of VPS34-kinase activity results in the reduction by half of VPS34, along with its binding partners VPS15, Beclin-1 and UVRAG.

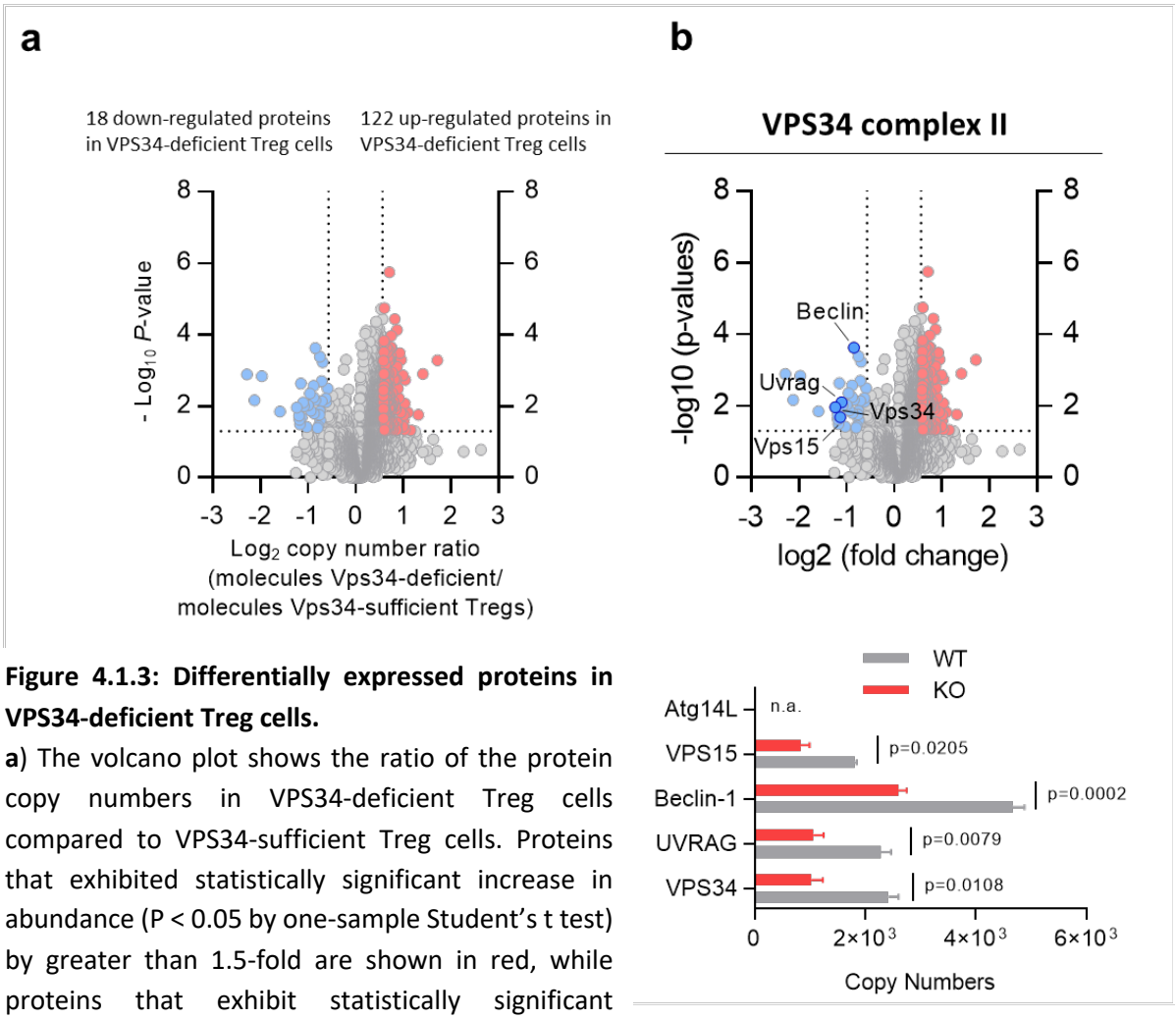

Figure 4.1.3: Differentially expressed proteins in VPS34-deficient Treg cells.

a) The volcano plot shows the ratio of the protein copy numbers in VPS34-deficient Treg cells compared to VPS34-sufficient Treg cells. Proteins that exhibited statistically significant increase in abundance ($P < 0.05$ by one-sample Student's t test) by greater than 1.5-fold are shown in red, while proteins that exhibit statistically significant reduction in abundance are shown in blue (the cut-off is indicated by the horizontal dashed line). A twofold decrease in protein abundance is indicated by the vertical dashed line.

b) Volcano plots of the VPS34-dependent proteome in Treg cells: ratio of the protein abundance (copy number) in VPS34-deficient compared to VPS34-sufficent Treg cells was plotted against P value (as determined by one-sample Student's t test). Proteins with ratios that were statistically significantly regulated ($P < 0.05$) by >1.5-fold are shown in blue, with binding partners of the VPS34 complex II highlighted. Bar graphs show estimated copy numbers calculated using the proteomic data for Atg14L, VPS15, Beclin-1, UVRAG, and VPS34. Individual data points from the three biological replicates performed for the proteomic analysis are shown, with the bar showing the means ± S.D. *p* values were calculated by two-tailed, one-sample Student's *t* test.

4.2.2 Various protein classes are affected by VPS34-deletion in Treg cells

To understand the dominant consequences of VPS34-deletion on the Treg cell proteome, I first focused on proteins that were most increased and decreased in VPS34-deficient Treg cells (i.e. outliers). The rationale behind this approach was that a striking difference in the abundance of a specific protein might reveal of strong dependency of this protein and related pathways to VPS34 kinase activity.

In total, ten proteins were considered as 'outliers', among which three were highly upregulated (**Fig. 4.2 a**) while seven downregulated (**Fig. 4.2 b**). **Tables 4.2.1** and **4.2.2** summarize the function of each protein. Apart of Beclin-1, none of the down- or upregulated proteins mapped to a common pathway or biological process, nor was I able to attribute any of the given proteins to a process involved in known Treg cell suppression mechanisms or T cell function, nor were any of them PI3P binders.

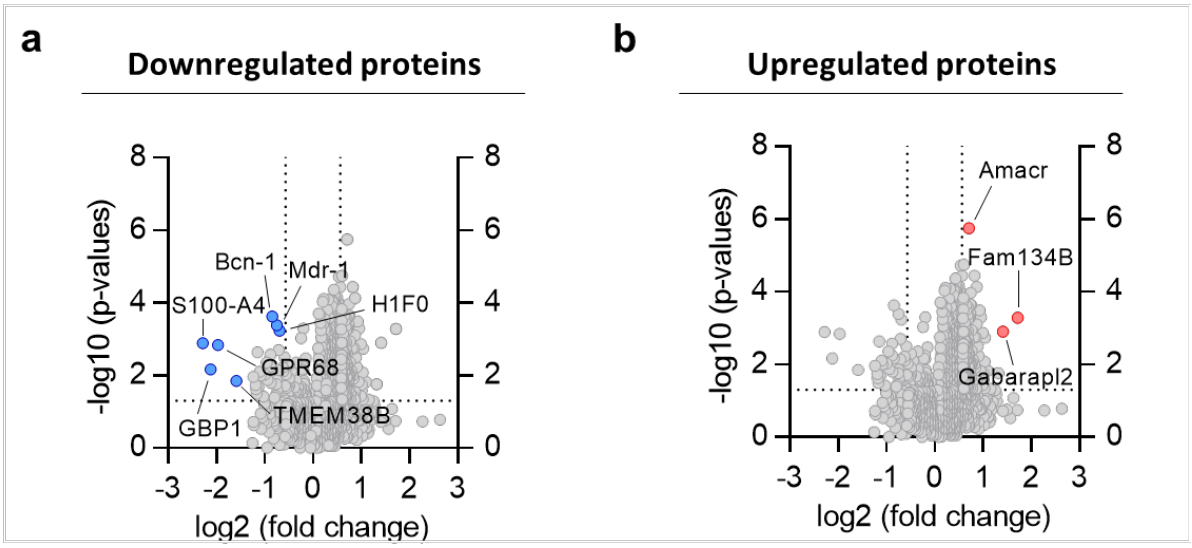

Figure 4.2: Volcano plots of strongly differentially expressed proteins in VPS34-deficient Treg cells. Volcano plots of the VPS34-dependent proteome in Treg cells: ratio of the protein abundance (copy number) in VPS34-deficient compared to VPS34-sufficent Treg cells was plotted against P value (as determined by one-sample Student's t test). Strongly downregulated proteins with ratios that were statistically significantly downregulated ($p < 0.05$) by >1.5-fold are highlighted in blue (**a**) while strongly upregulated proteins are shown in red (**b**). $n = 3$ biologically independent samples for each of the Treg cell populations.

Table 4.2.1: List of downregulated 'outliers' in VPS34-deficient Treg cells.

Downregulated proteins	
H1F0 (Histone H1.0)	The H1F0 histones are found in cells that are in terminal stages of differentiation or that have low rates of cell division.
Mdr-1 (Multidrug resistance protein 1A)	The membrane-associated protein encoded by this gene is a member of the superfamily of ATP-binding cassette (ABC) transporters. This protein is a member of the MDR/TAP subfamily. Members of the MDR/TAP subfamily are involved in multidrug resistance. The protein encoded by this gene is an ATP-dependent drug efflux pump for xenobiotic compounds with broad substrate specificity. It is responsible for decreased drug accumulation in multidrug-resistant cells and often mediates the development of resistance to anticancer drugs. This protein also functions as a transporter in the blood-brain barrier. Mutations in this gene are associated with colchicine resistance and Inflammatory bowel disease. Alternative splicing and the use of alternative promoters results in multiple transcript variants.
TMEM-38 (Trimeric intracellular cation channel type B)	Monovalent cation channel required for maintenance of rapid intracellular calcium release. May act as a potassium counter-ion channel that functions in synchronization with calcium release from intracellular stores. Probably requires binding to PIP2. Located in ER.
GPR68 (Ovarian cancer G-protein coupled receptor 1)	Metastasis suppressor gene for prostate cancer. OGR1's constitutive activity via G alpha(i) contributes to its inhibitory effect on cell migration in vitro.
GBP-1 (Interferon-induced guanylate-binding protein 1)	Interferon-induced guanylate-binding protein 1 is a protein that in humans is encoded by the GBP1 gene. It belongs to the dynamin superfamily of large GTPases.
S100-A1 (Protein S100;Protein S100-A4)	The protein encoded by this gene is a member of the S100 family of proteins containing 2 EF-hand calcium-binding motifs. S100 proteins are localized in the cytoplasm and/or nucleus of a wide range of cells, and involved in the regulation of a number of cellular processes such as cell cycle progression and differentiation. S100 genes include at least 13 members which are located as a cluster on chromosome 1q21. This protein may function in motility, invasion, and tubulin polymerization. Chromosomal rearrangements and altered expression of this gene have been implicated in tumor metastasis. Multiple alternatively spliced variants, encoding the same protein, have been identified.
Beclin-1	Plays a central role in autophagy. Acts as core subunit of different PI3K complex forms that mediate formation of phosphatidylinositol 3-phosphate and are believed to play a role in multiple membrane trafficking pathways: PI3KC3-C1 is involved in initiation of autophagosomes and PI3KC3-C2 in maturation of autophagosomes and endocytosis. Involved in regulation of degradative endocytic trafficking and required for the abcission step in cytokinesis, probably in the context of PI3KC3-C2. Essential for the formation of PI3KC3-C2 but not PI3KC3-C1 PI3K complex forms. Involved in endocytosis including endosome formation in neuronal cells.

Table 4.2.2: List of upregulated 'outliers' in VPS34-deficient Treg cells.

Upregulated proteins

Protein FAM134B	The protein encoded by this gene is a cis-Golgi transmembrane protein that may be necessary for the long-term survival of nociceptive and autonomic ganglion neurons. It interacts with ATG8 family modifier proteins MAP1LC3A, MAP1LC3B, GABARAP, GABARAPL1 and GABARAPL2 and LC3 The protein encoded by FAM134B is a reticulophagy receptor that regulates turnover of the endoplasmic reticulum (ER) by selective phagocytosis. Absence or non-functional expression of FAM134B protein impairs ER-turnover and thereby is involved in the pathogenesis of some human diseases. FAM134B inhibition contributes to impair proteostasis in the ER due to the accumulation of misfolded or aggregated proteins, which in turn leads to compromised neuronal survival and progressive neuronal degenerative diseases. FAM134B overexpression results in ER fragmentation and lysosomal degradation. Endogenous and overexpressed FAM134B co-localized with CLIMP-63 and SEC61B, marker proteins of sheet-like cisternal ER and to a lesser extent with RTN4-positive tubular.
GABARAPL2 (Gamma-aminobutyric acid receptor-associated protein-like 2)	Ubiquitin-like modifier involved in intra-Golgi traffic. Modulates intra-Golgi transport through coupling between NSF activity and SNAREs activation. It first stimulates the ATPase activity of NSF which in turn stimulates the association with GOSR1. Involved in autophagy. Plays a role in mitophagy which contributes to regulate mitochondrial quantity and quality by eliminating the mitochondria to a basal level to fulfill cellular energy requirements and preventing excess ROS production. Whereas LC3s are involved in elongation of the phagophore membrane, the GABARAP/GATE-16 subfamily is essential for a later stage in autophagosome maturation. Part of LAPosome. Involved in (protein) transport, intra-Golgi vesicle-mediated transport, mitophagy, autophagosome assembly.
AMARC (Alpha-methylacyl-CoA racemase)	Catalytic activity:(2S)-2-methylacyl-CoA = (2R)-2-methylacyl-CoA., function: Racemization of 2-methyl-branched fatty acid CoA esters. Responsible for the conversion of pristanoyl-CoA and C27-bile acyl-CoAs to their (S)-stereoisomers., Pathway: - Lipid metabolism; - bile acid biosynthesis. Belongs to the caiB/baiF CoA-transferase family.

Downregulated 'outlier' proteins were H1F0 (Histone H1.0), Mdr-1 (Multidrug resistance protein 1A), TMEM-38 (Trimeric intracellular cation channel type B), GPR68 (Ovarian cancer G-protein coupled receptor 1), GBP-1 (Interferon-induced guanylate-binding protein 1), S100-A1 (Protein S100), and Beclin-1 (**Table 4.2.1**).

Downregulation of S100-A1, which is involved in the regulation of a number of cellular processes such as cell cycle progression and differentiation, could support the observation made in ***Chapter 3*** **(Fig. 3.5.1)** that VPS34-deficient Treg cells have a block in cell maturation, thus do not differentiate into effector cells with suppressive functions. Furthermore, downregulation of histone H1F0, found in cells that are in terminal stages of differentiation

or that have low rates of cell division [286], rather suggests that VPS34-deficient Treg cells are in a state of high proliferation, and not yet in a state of final differentiation.

Upregulated 'outlier' proteins were protein FAM134B, Gabarapl2 (Gamma-aminobutyric acid receptor-associated protein-like 2), and AMARC (Alpha-methylacyl-CoA racemase).

It has been suggested that protein FAM134B overexpression results in ER fragmentation and lysosomal degradation. Gabarapl2 is involved in autophagosome maturation and mitophagy, and regulates mitochondrial quantity and quality by eliminating mitochondria to a basal level. Upregulation of Gabarapl2 would therefore be predicted to lead to less mitochondria and more autophagy, contrary to the results described in ***Chapter 3*** (**Fig. 3.2.1**).

4.2.3 Known pathways and biological functions of Treg cells are not affected by VPS34-deletion

VPS34 has been attributed to two main functions, depending on the proteins it complexes with. In metazoans, VPS34 has been found to play a critical role in endocytosis, autophagy, and mTOR activation [287]. I therefore quantified the effect of VPS34-deletion on the content of proteins involved in processed known to be dependent on VPS34, pathways relating to autophagy, endocytosis, and trafficking as well as proteins required for Treg cell development, survival and fitness.

Regarding Treg cell or broader T cell identity, protein content of FoxP3, CD25 (IL2-Rα), CD4, and CD45 was unchanged changed (**Fig. 4.3.1 a**). In contrast to the results from the phenotyping performed in ***Chapter 3*** (**Fig. 3.6.1 c, Fig. 3.5.1 b** and **Fig. 3.6.2**), protein levels of CD44, CD69, and Ki67 (*Mki67*) were similar between VPS34-deficient and –sufficient Treg cells (**Fig. 4.3.1 b**). Only CTLA-4 and ICOS levels matched previous observations, i.e. were unchanged in VPS34-deficient Treg cells compared to VPS34-sufficient Treg cells (**Fig. 3.4.1 b** and **Fig. 3.4.2 d**).

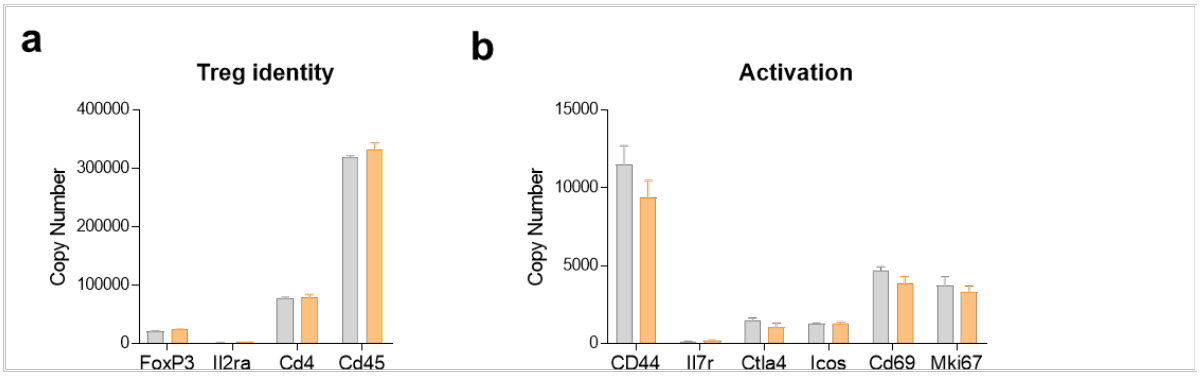

Figure 4.3.1: Estimated copy numbers of proteins involved in Treg cell identity and cell activation. **a**) Bar graphs show estimated copy numbers calculated using the proteomic data for FoxP3, IL2Rα, CD4, and CD45. **b**) Bar graphs show estimated copy numbers calculated using the proteomic data for CD44, IL7-R, CTLA-4, ICOS, CD69, and Ki67 (*Mki67*). Individual data points from the three biological replicates performed for the proteomic analysis are shown, with the bar showing the means ± S.D. *p* values were calculated by two-tailed, one-sample Student's *t* test.

Next, I assessed protein levels of different Foxo and Stat transcription factors, components of the TCR, tyrosine kinases and phosphatases (involved in T cell receptor (TCR) and IL-2 receptor signalling), as well as IL-2 receptor and associates tyrosine kinases and found no differences between VPS34-deficient and – sufficient Treg cells (**Fig. 4.3.2 a – d**).

Since VPS34 has been linked to mTORC1, I analysed whether VPS34-deficiency would affect mTOR signalling and downstream signalling. I found no differences in protein levels (**Fig. 4.3.3 a – c**). Similarly, proteins involved in glycolysis as well as nutrient transporters and nutrient receptors were unchanged (**Fig. 4.3.4 a – c**, respectively).

Next, I assessed autophagy genes, autophagy-related and – interacting proteins (**Fig. 4.3.5 a – c** and **Fig. 4.3.6**). The only differentially expressed protein was Atg2A, which was significantly upregulated (ratio WT/KO = 1.989889802, p = 0.0014) in VPS34-deficient Treg cells. Atg2A binds to WIPI (WD-repeat protein interacting with phosphoinositides). WIPI plays an important role in recognising and decoding the PI3P signal at the nascent autophagosome, hence Atg2A contributes in regulating the size of nascent auto-phagosomes [288].

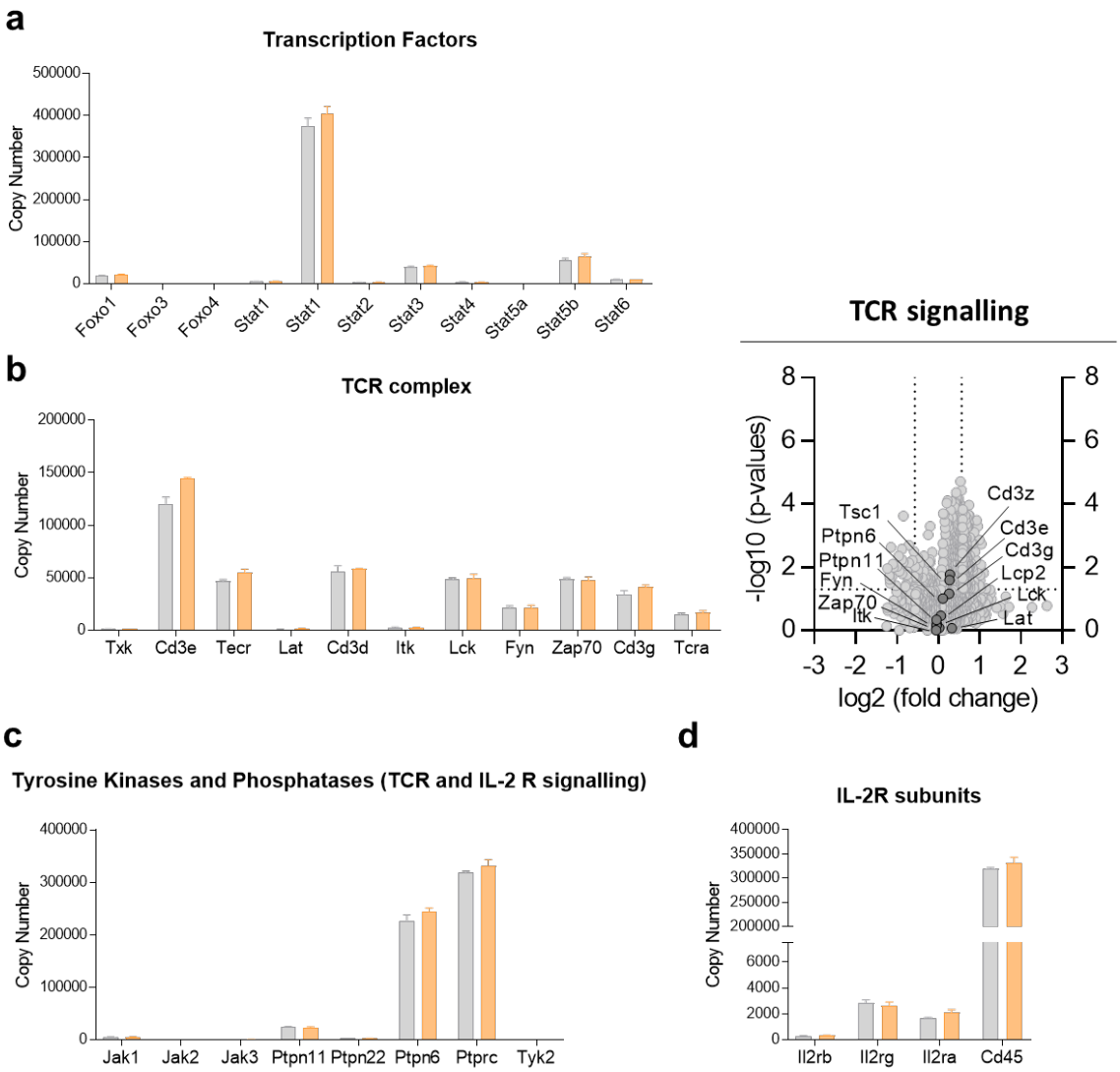

Figure 4.3.2: Estimated copy numbers of Foxo and Stat transcription factors, proteins of the TRC complex, tyrosine kinases and phosphatases, and IL-2R subunits.

a) Bar graphs show estimated copy numbers calculated using the proteomic data for Foxo and Stat transcription factors.

b) Bar graphs show estimated copy numbers calculated using the proteomic data for proteins of the T cell receptor (TCR) complex. Volcano plots of the VPS34-dependent proteome in Treg cells: ratio of the protein abundance (copy number) in VPS34-deficient compared to VPS34-sufficent Treg cells was plotted against P value (as determined by one-sample Student's t test). Proteins of the TRC complex are highlighted.

(**c - d**) Bar graphs show estimated copy numbers calculated using the proteomic data for tyrosine kinases and phosphatases (**c**) and IL-2R subunits (**d**). Individual data points from the three biological replicates performed for the proteomic analysis are shown, with the bar showing the means ± S.D. *p* values were calculated by two-tailed, one-sample Student's *t* test.

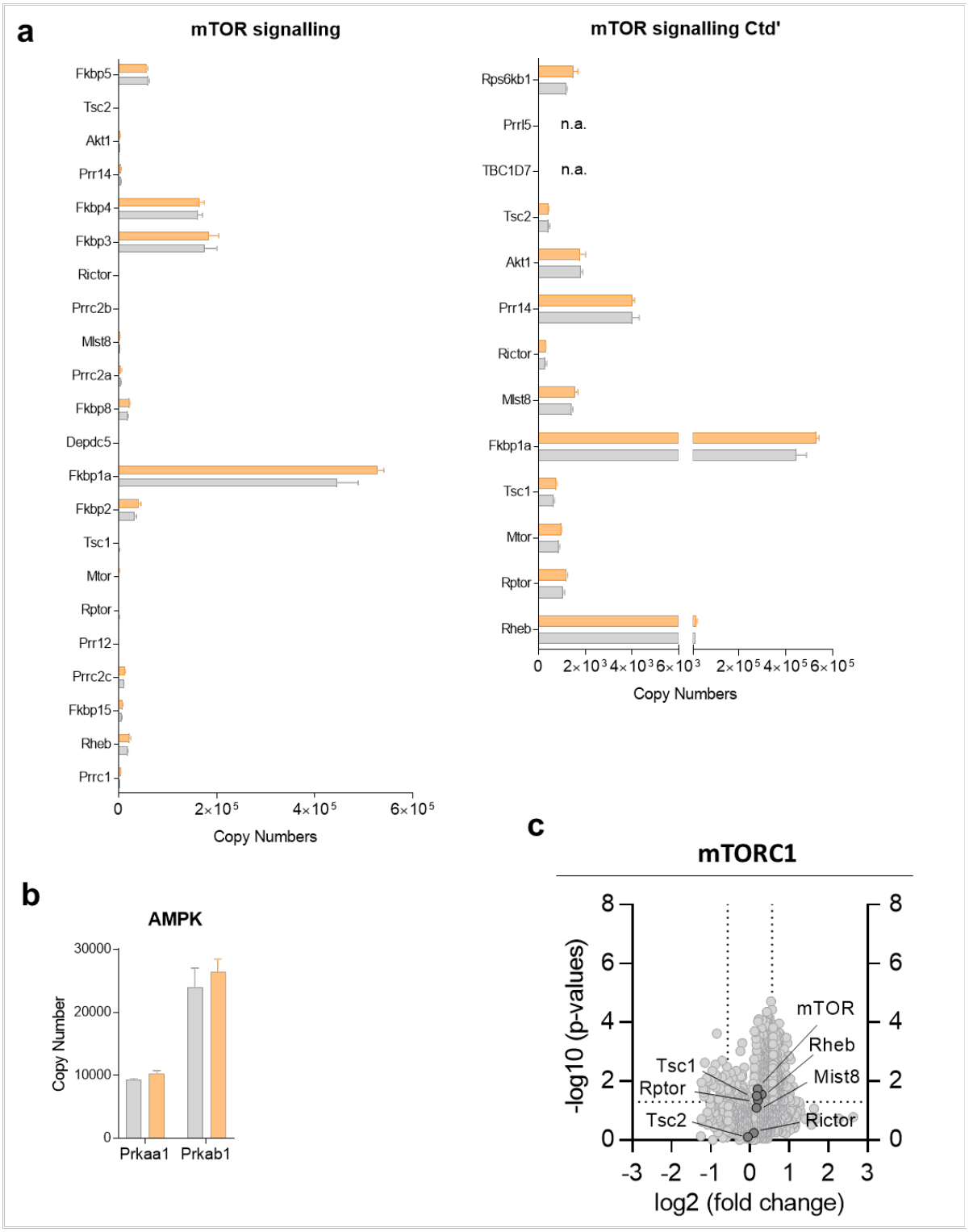

Figure 4.3.3: Estimated copy numbers of proteins involved in mTOR signalling and AMPK, tyrosine kinases and phosphatases, and IL-2R subunits.

a) Bar graphs show estimated copy numbers calculated using the proteomic data for of proteins involved in mTOR signalling.

b) Bar graphs show estimated copy numbers calculated using the proteomic data for AMPK (*Prkaa 1 and Prkab1*).

c) Volcano plots of the VPS34-dependent proteome in Treg cells: ratio of the protein abundance (copy number) in VPS34-deficient compared to VPS34-sufficent Treg cells was plotted against P value (as determined by one-sample Student's t test). Proteins of mTORC1 complex are highlighted. Individual data points from the three biological replicates performed for the proteomic analysis are shown, with the bar showing the means ± S.D. *p* values were calculated by two-tailed, one-sample Student's *t* test.

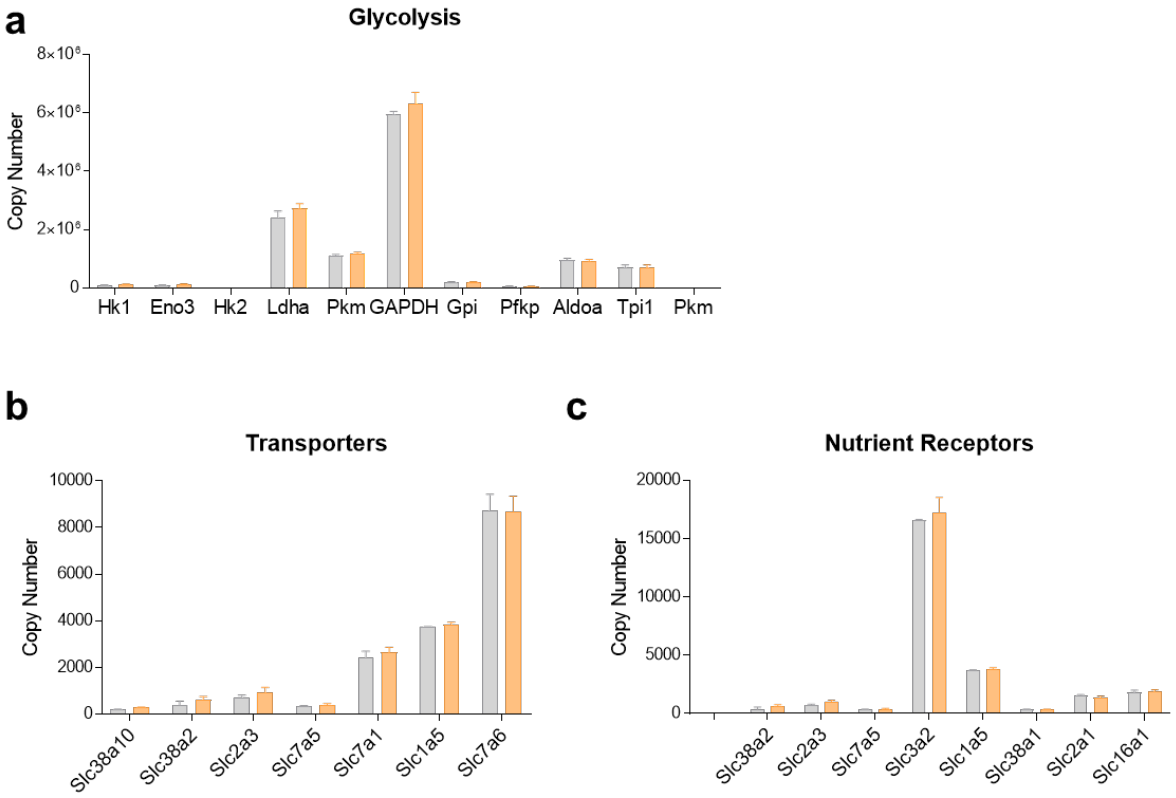

Figure 4.3.4: Estimated copy numbers of proteins involved in glycolysis, nutrient transporters and nutrient receptors.

a - c) Bar graphs show estimated copy numbers calculated using the proteomic data for of proteins involved in glycolysis (**a**), nutrient transporters (**b**), and nutrient transporters (**c**). Individual data points from the three biological replicates performed for the proteomic analysis are shown, with the bar showing the means ± S.D. *p* values were calculated by two-tailed, one-sample Student's *t* test.

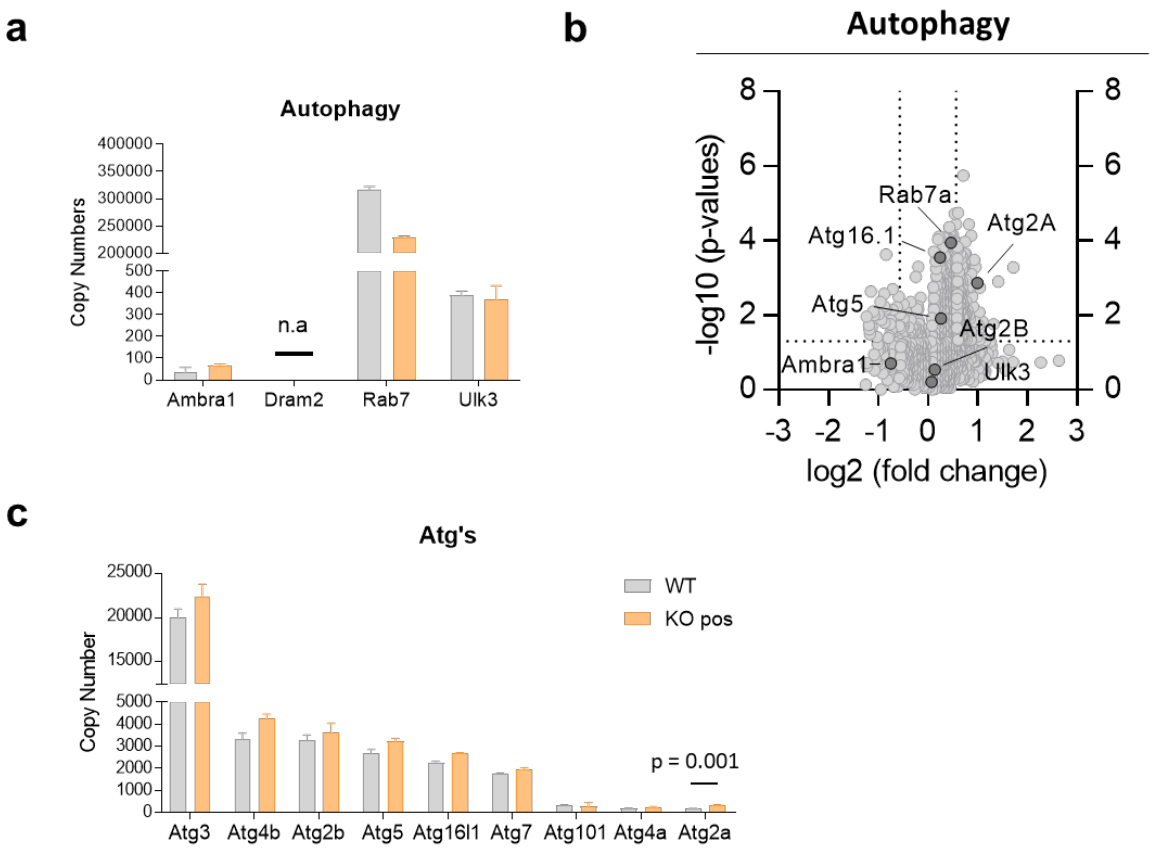

Figure 4.3.5: Estimated copy numbers of proteins involved in autophagy and autophagy-related proteins.

a) Bar graphs show estimated copy numbers calculated using the proteomic data for proteins involved in autophagy.

b) Volcano plots of the VPS34-dependent proteome in Treg cells: ratio of the protein abundance (copy number) in VPS34-deficient compared to VPS34-sufficent Treg cells was plotted against P value (as determined by one-sample Student's t test). Proteins involved in autophagy are highlighted.

c) Bar graphs show estimated copy numbers calculated using the proteomic data for autophagy-related proteins (Atg's). Individual data points from the three biological replicates performed for the proteomic analysis are shown, with the bar showing the means ± S.D. *p* values were calculated by two-tailed, one-sample Student's *t* test.

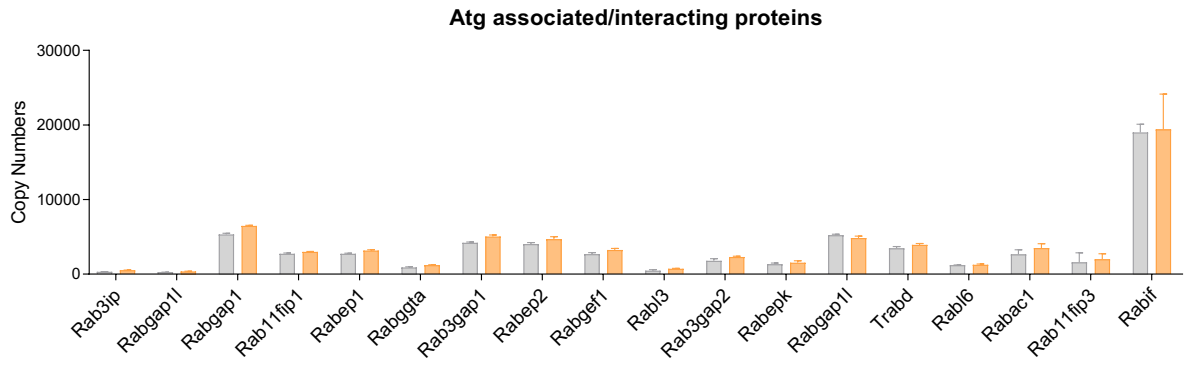

Figure 4.3.6: Estimated copy numbers of Atg-related and interacting proteins involved.
Bar graphs show estimated copy numbers calculated using the proteomic data for Atg-related and integrating Individual data points from the three biological replicates performed for the proteomic analysis are shown, with the bar showing the means ± S.D. *p* values were calculated by two-tailed, one-sample Student's *t* test.

Within the Rab proteins, members of the Ras-related small GTPases family, Rab1a, Rab2a, Rab2b, and Rab18 were significantly upregulated (**Fig. 4.3.7 a**). **Table 4.3** summarizes the function of each differentially expressed Rab protein in this data set. In regards to proteins associated with vesicle and membrane trafficking (Syntaxins, Vamps and LAMPs), none of these were differentially expressed in VPS34-sufficient Treg cells (**Fig. 4.3.7 b – d**). Similarly, vacuolar protein sorting (Vps)-associated proteins and lysosomal components were expressed as levels similar to VPS34-sufficient Treg cells (**Fig. 4.3.8 a – d**), apart of VPS34 as already mentioned in ***Chapter 4.2.1***.

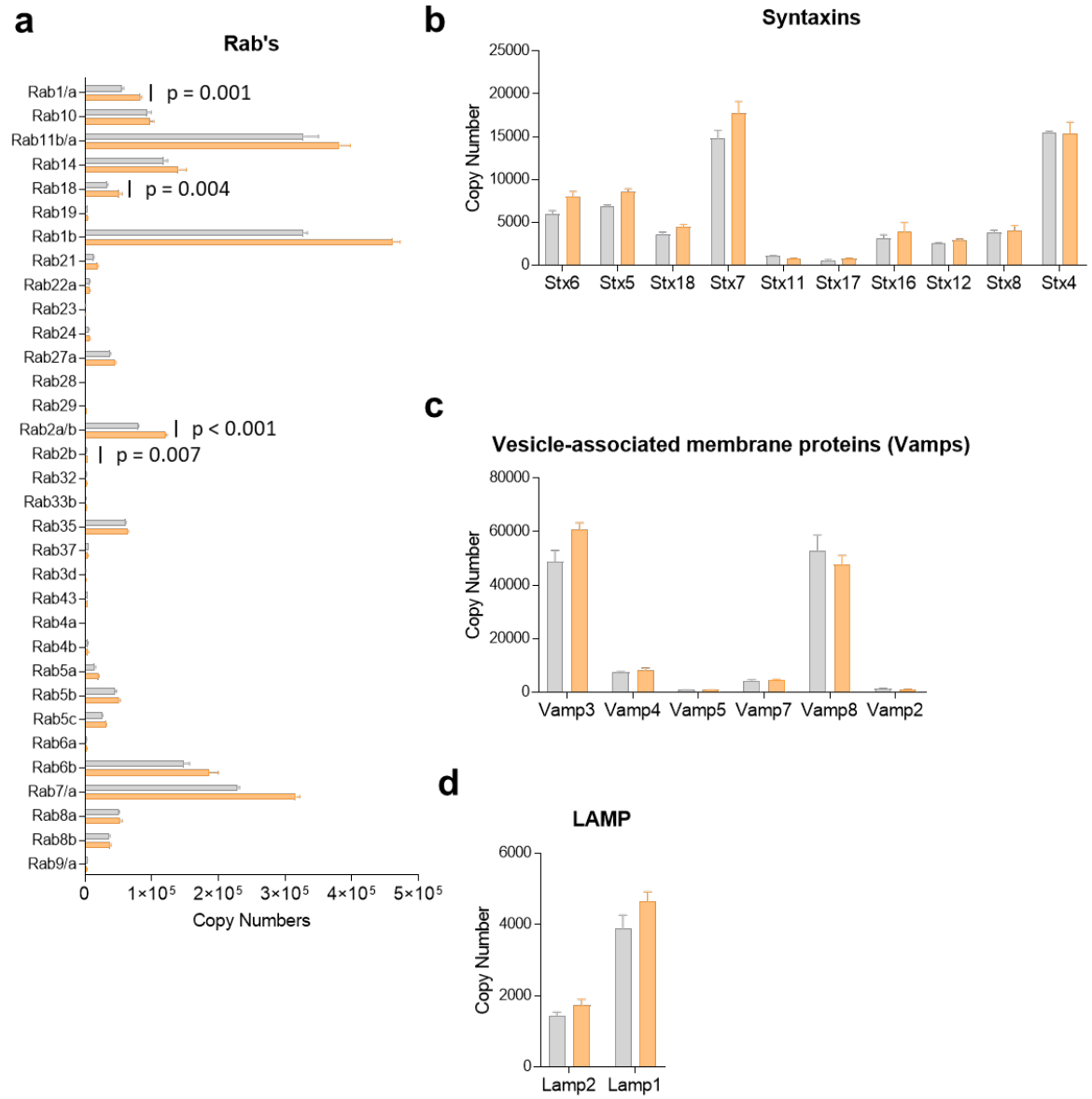

Figure 4.3.7: Estimated copy numbers of Rab proteins, syntaxins, VAMPs and LAMPs.

a - d) Bar graphs show estimated copy numbers calculated using the proteomic data for Rab proteins (**a**), syntaxins (**b**), vesicle-associated membrane proteins (VAMPs) (**d**), and lysosome-associated membrane glycoprotein (LAMPs) (**d**). Individual data points from the three biological replicates performed for the proteomic analysis are shown, with the bar showing the means ± S.D. *p* values were calculated by two-tailed, one-sample Student's *t* test.

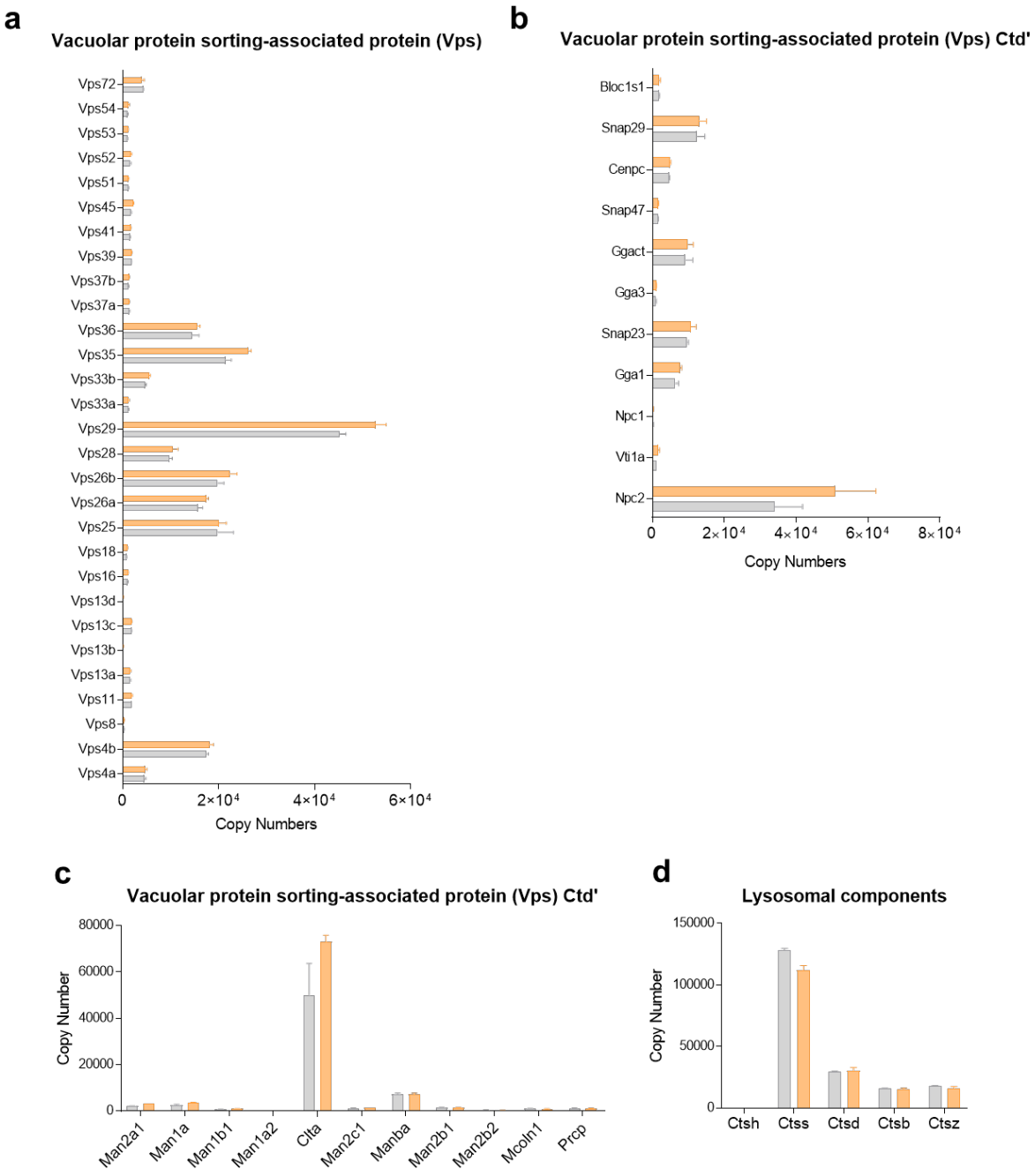

Figure 4.3.8: Estimated copy numbers of vacuolar protein sorting-associated proteins and lysosomal components.

Bar graphs show estimated copy numbers calculated using the proteomic data for vacuolar protein sorting-associated proteins (**a - c**) and lysosomal components (**d**). Individual data points from the three biological replicates performed for the proteomic analysis are shown, with the bar showing the means ± S.D. *p* values were calculated by two-tailed, one-sample Student's *t* test.

Table 4.3: Function of Rab-proteins differentially expressed in VPS34-deficient Treg cells.

Protein	***Description***
Rab1a	This protein controls vesicle traffic from the endoplasmic reticulum to the Golgi apparatus. Diseases associated with RAB1A include Hypotrichosis 3 and Rectum Adenocarcinoma. Among its related pathways are Vesicle-mediated transport and Transport to the Golgi and subsequent modification. An important paralog of this gene is *RAB1B*.
Rab2a	This protein is a resident of pre-Golgi intermediates, and is required for protein transport from the endoplasmic reticulum (ER) to the Golgi complex. Diseases associated with Rab2a include Sezary's Disease and Warburg Micro Syndrome 4. Among its related pathways are AMP-activated Protein Kinase (AMPK) signalling and cell cycle (mitosis). An important paralog of this gene is *RAB2B*.
Rab2b	Among its related pathways are Sertoli-Sertoli Cell Junction Dynamics and RAB geranylgeranylation. An important paralog of this gene is *RAB2A*.
Rab18	This protein may have a role in eye and brain development. Diseases associated with RAB18 include Warburg Micro Syndrome 3 and Warburg Micro Syndrome 1. Among its related pathways are Vesicle-mediated transport and Innate Immune System. An important paralog of this gene is *RAB2A.*

Next, I used DAVID functional annotation clustering [289] to assess whether differentially expressed proteins map to common pathways. This could shed light on the process(es) altered in mice VPS34-deficient Treg cells leading to the overt lymphoproliferative phenotype, as well as identify possible blockage in these pathways that would alter the steady-state levels of proteins involved in steps before and after the block occurred. To this end, I ran DAVID clustering analysis using the combined list of differentially expressed proteins (i.e. combining both up- and downregulated proteins) and observed that these proteins mapped to five different pathways (**Fig. 4.3.9 – Fig. 4.3.11**). Two pathways, namely 'TLR9 cascade' and 'Signal transduction: RHO GTPases Activate NADPH Oxidases' involved only downregulated proteins (**Fig. 4.3.9 a** and **b**, respectively). Only three proteins, i.e. *early endosome antigen 1* (EEA1), VPS15 and VPS34 mapped to 'TLR9 cascade' (**Fig. 4.3.9 a)**. In the 'Signal transduction: RHO GTPases Activate NADPH Oxidases' pathway, three proteins were downregulated, i.e. *cytochrome b-245, beta polypeptide* (Cybb), as well as VPS15 and VPS34 (**Fig. 4.3.9 b**).

Two other pathways mapped only proteins that were upregulated in VPS34-deficient Treg cells: 'Golgi Stack Pericentriolar Reorganization' and 'O-linked glycolysation' (**Fig. 4.3.10 a** and **b**, respectively). Proteins those expression was upregulated and that mapped to 'Golgi Stack Pericentriolar Reorganization' pathway were Rab1A, Rab2A and *Golgi reassembly stacking protein 2* (GORASP2) (**Fig. 4.3.10 a**). GORASP2, also known as GRASP55, may play a role in the stacking of Golgi cisternae and Golgi ribbon formation, as well as Golgi fragmentation during apoptosis or mitosis. Furthermore, it also plays a role in the intracellular transport of transforming growth factor alpha and may function as a molecular chaperone. GORASP2/GRASP55 and Rab2A are part of a larger complex located on medial-Golgi that is essential for normal protein transport and Golgi structure [290]. GORASP1, also referred to as GRASP65, is important for the organization of cis-Golgi cisternae [290]. The GTP form of Rab1 interacts with GRASP65 the vesicle tethering factor p115 and the cis-Golgi matrix protein GM130, and together regulate the transport from the *endoplasmatic reticulum* (ER) to the Golgi apparatus.

Five proteins were significantly upregulated in the 'O-glycolysation' pathway: *Galnt7*, *Galnt12*, *Galnt1*, *C1galt1c1,* and *C1galt1* (**Fig. 4.3.10 b**).

The *N-acetylgalactosaminyltransferase 7* (Galnt7) is a type II transmembrane protein and a member of the GalNAc-transferase family. It controls the initiation step of mucin-type O-linked protein glycosylation and the transfer of N-acetylgalactosamine to serine and threonine amino acid residues [291]. An important paralog is Galnt1.

The polypeptide *N-acetylgalactosaminyltransferase 1* (Galnt1) is a member of the UDP-N-acetyl-α-D-galactosamine:polypeptide N-acetylgalactosaminyltransferase (GalNAc-T) family of enzymes and catalyses the initial reaction in O-linked oligosaccharide biosynthesis, i.e. the transfer of an N-acetyl-D-galactosamine residue to a serine or threonine residue on the protein receptor [292].

Galnt12 encodes a member of a family of UDP-GalNAc:polypeptide N-acetylgalactosaminyltransferases, which catalyse the transfer of N-acetylgalactosamine (GalNAc) from UDP-GalNAc to a serine or threonine residue on a polypeptide acceptor in the initial step of O-linked protein glycosylation [293]. It induces the initial reaction in O-linked oligosaccharide biosynthesis, i.e. the transfer of an N-acetyl-D-galactosamine residue to a serine or threonine residue on the protein receptor [293].

C1galt1c1 is a type II transmembrane protein that is similar to the core 1 β1,3-galactosyltransferase 1, which catalyses the synthesis of the core-1 structure, also known as Thomsen-Friedenreich antigen, on O-linked glycans. This gene product lacks the galactosyltransferase activity itself, but instead acts as a molecular chaperone required for the folding, stability and full activity of the core 1 β1,3-galactosyltransferase 1 [294]. It is probably a molecular chaperone required for the generation of 1 O-glycan Gal-β1-3GalNAc-α1-Ser/Thr (T antigen), which is a precursor for many extended O-glycans in glycoproteins, and probably assists the folding/stability of core 1 β-3-galactosyltransferase (C1galt1) [295]. C1galt1 (Core 1 Synthase, Glycoprotein-N-Acetylgalactosamine 3-Beta-Galactosyltransferase 1) generates the common core 1 O-glycan structure, Gal-β-1-3GalNAc-R, by the transfer of Gal from UDP-Gal to GalNAc-α-1-R, which is a precursor for many extended O-glycans in glycoproteins expressed on cell surface and secreted glycoproteins [296].

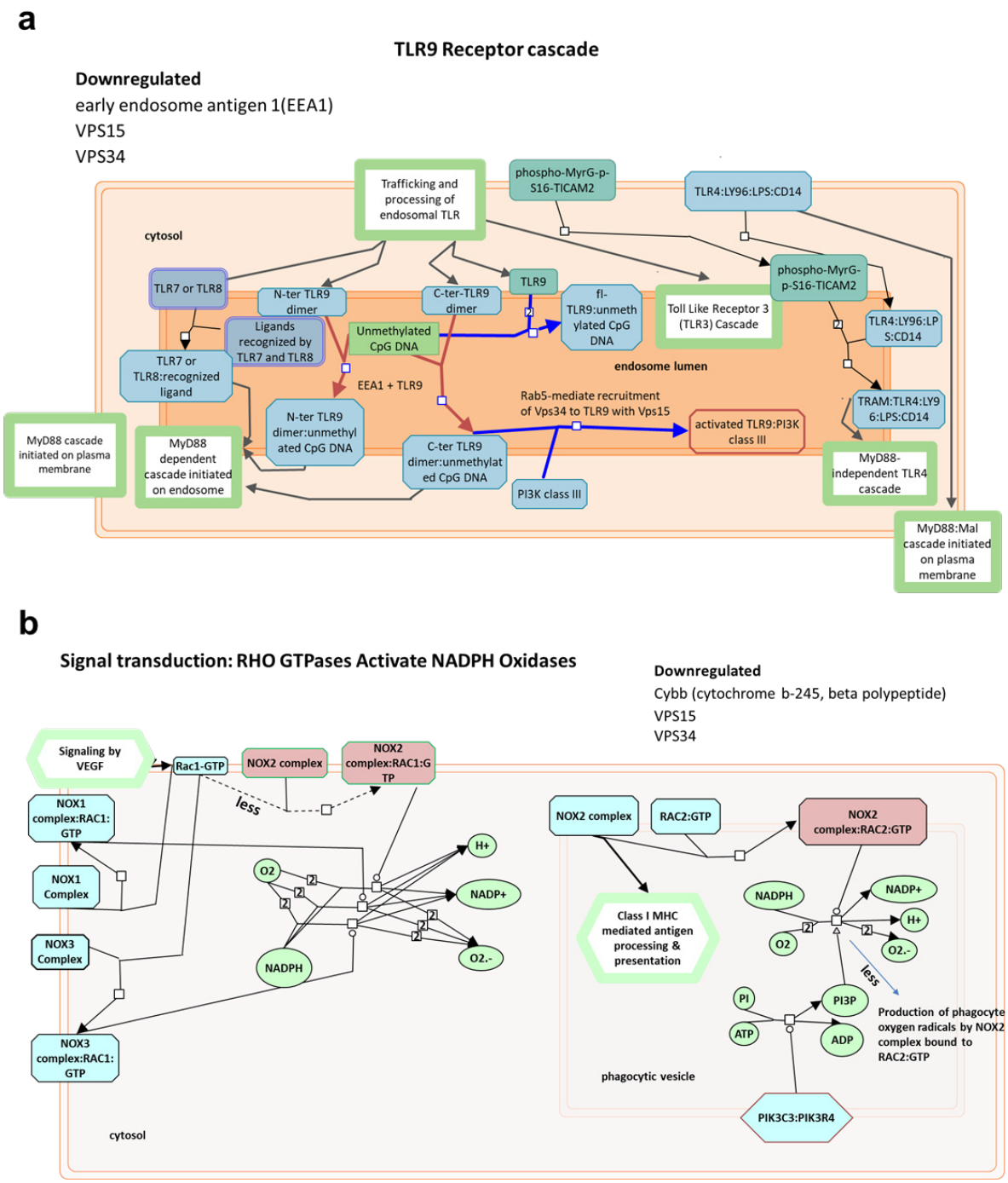

Figure 4.3.9: Pathway analysis of proteins downregulated in VPS34-deficient Treg cells.
DAVID functional clustering analysis using the combined list of differentially expressed proteins identified in the proteomic profiling analysis was performed to assess to which pathway(s) the differentially expressed proteins in VPS34-deficient Treg cells mapped to. The pathways involving only downregulated proteins are shown here. *Scheme based on https://reactome.org/content/detail/R-MMU-168898 and https://reactome.org/content/detail/R-HSA-5668599.*

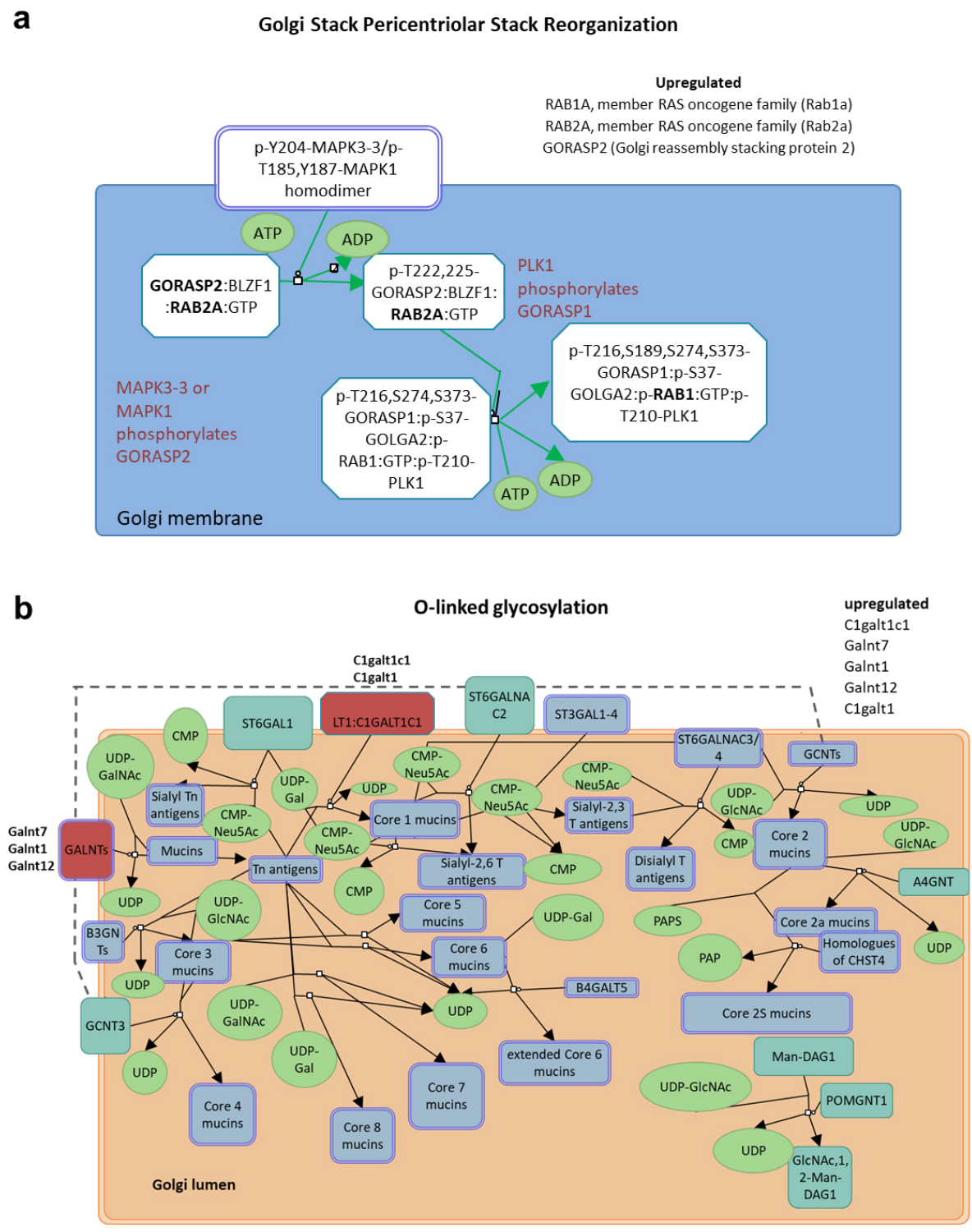

Figure 4.3.10: Pathway analysis of proteins upregulated in VPS34-deficient Treg cells.
DAVID functional clustering analysis using the combined list of differentially expressed proteins identified in the proteomic profiling analysis was performed to assess to which pathway(s) the differentially expressed proteins in VPS34-deficient Treg cells mapped to. The pathways involving only upregulated proteins are shown here. *Scheme based on https://reactome.org/content/detail/R-HSA-162658 and https://reactome.org/content/detail/R-HSA-5173105.*

'Macroautophagy' was the only pathway that includes both up- and downregulated proteins (**Fig. 4.3.11**). Downregulated proteins comprised the VPS34 complex 2 (UVRAG, Beclin-1, VPS34, and VPS15). Meanwhile, only one protein, *gamma-aminobutyric acid (GABA) A receptor-associated protein-like 2* (Gabarapl2), was upregulated in this pathway. Gabarapl2 was identified as an 'outlier' and its function has been described in ***Chapter 4.2.2***.

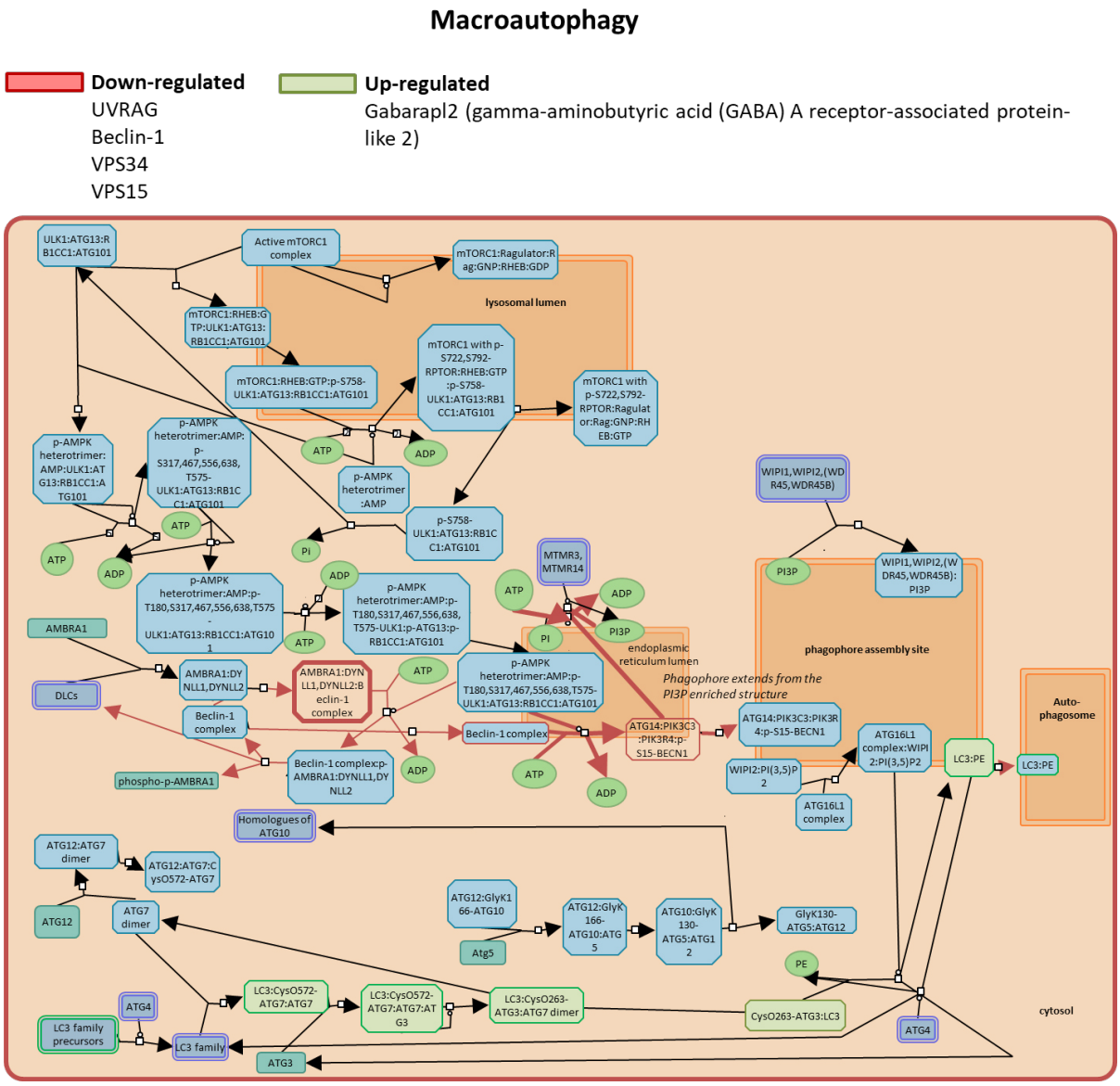

Figure 4.3.11: Pathway analysis of proteins up- and downregulated in VPS34-deficient Treg cells. DAVID functional clustering analysis using the combined list of differentially expressed proteins identified in the proteomic profiling analysis was performed to assess to which pathway(s) the differentially expressed proteins in VPS34-deficient Treg cells mapped to. 'Macroautophagy' was the only pathway involving both up- and downregulated proteins and is shown here. *Scheme based on https://reactome.org/content/detail/R-MMU-1632852.*

In conclusion, analysis of expression levels of proteins involved in pathways known to be dependent on VPS34, relating to autophagy, endocytosis, and trafficking as well as proteins required for Treg cell development, survival and fitness did not provide obvious insights into pathways or processes being affected by loss of VPS34 kinase activity in Treg cells. From the few differentially expressed proteins mentioned above, it is hard to deduce the effects of the loss of VPS34-kinase activity and the ensuing effects on Treg cells at a protein level. Furthermore, I could not map more than a few proteins (apart of the known complex binding partners of VPS34) to a common pathway, and only 'macroautophagy' involved both up- and downregulated proteins. From this analysis, the primary reason for the observed phenotype of *FoxP3*$^{YFP\text{-}Cre}$ *Pik3c3*$^{fl/fl}$ mice remains elusive.

4.2.4 Loss of VPS34 kinase activity increases metabolic potential in Treg cells

Using DAVID functional annotation clustering to identify biologically relevant groups of proteins with altered expression, I observed that downregulated proteins are involved in biological processes relating to 'Regulation of cytokinesis', 'Receptor catabolic process', 'Macroautophagy', 'Cellular response to glucose starvation', 'Late endosome to vacuole transport', 'Autophagy', 'Intestinal absorption', 'Endocytosis', 'Cytokinesis', 'Lysosome reorganization', 'Positive regulation of autophagy', 'Autophagosome assembly', and 'Negative regulation of neuron projection development' (**Fig. 4.4.1 a**). None of these biological processes entailed more than four differentially expressed proteins, and VPS34 and VPS15 were always among the proteins listed. *Kyoto Encyclopedia of Genes and Genomes* (KEGG) pathway analysis of downregulated proteins revealed two pathways – 'Regulation of autophagy' and 'Phagosome', each with only three differentially regulated proteins, which were namely VPS34, VPS15 and UVRAG (**Fig. 4.4.1 b**).

I noted that the loss of *VPS34 kinase activity* led to the up-regulation of proteins involved in *biological processes* (BP) relating to oxidation-reduction processes (**Fig. 4.4.2 a**). Up-regulated proteins related to *cellular components* (CC) involved mitochondrial functions, specifically mitochondrial inner membrane, mitochondrion, respiratory chain, mitochondrial respiratory chain complex I, mitochondrial intermembrane space, and membrane (**Fig. 4.4.2 a**). Proteins upregulated in VPS34-deficient Treg cells relating to *molecular function* (MF) included cytochrome c-oxidase activity (**Fig. 4.4.2 a**).

a

GO Term analysis of downregulated proteins

GO Term Biological Processes	Count	p-value
Regulation of cytokinesis	4	4.08E-06
Receptor catabolic process	3	1.11E-04
Macroautophagy	3	4.58E-04
Cellular response to glucose starvation	3	7.18E-04
Late endosome to vacuole transport	2	5.30E-03
Autophagy	3	1.51E-02
Intestinal absorption	2	2.36E-02
Endocytosis	3	2.38E-02
Cytokinesis	2	4.80E-02
Lysosome organization	2	5.05E-02
Positive regulation of autophagy	2	5.31E-02
Autophagosome assembly	2	5.68E-02
Negative regulation of neuron projection development	2	8.16E-02

b

KEGG pathway analysis of downregulated proteins

KEGG Pathway	Count	p-value
Regulation of autophagy	3	1.1e-3
Phagosome	3	3.7e-2

Figure 4.4.1: GO Term and KEGG pathway analyses of downregulated proteins.
a) *Gene Ontology* (GO) Term analysis of biological processes involving proteins downregulated in VPS34-deficient Treg cells identified in the proteomic profiling analysis.
b) *Kyoto Encyclopedia of Genes and Genomes* (KEGG) pathway analysis of biological processes involving proteins downregulated in VPS34-deficient Treg cells identified in the proteomic profiling analysis.

These data suggested that VPS34-deficiency leads to the upregulation of proteins involved in mitochondrial function and energy metabolism. Specifically, I identified increased levels of proteins involved in metabolic pathways (**Fig. *4.4.2 b***), and *oxidative phosphorylation* (OXPHOS) (**Fig. 4.4.2 b** ***and c***) with subunits of the electron transport chain complexes I, III and IV, namely *Uqcrb*, *Cox6b1*, *Cox7a2l*, *Cox5a*, *Ndufs5*, and *Ndufv3* (**Fig. 4.4.2 b**), being the most affected.

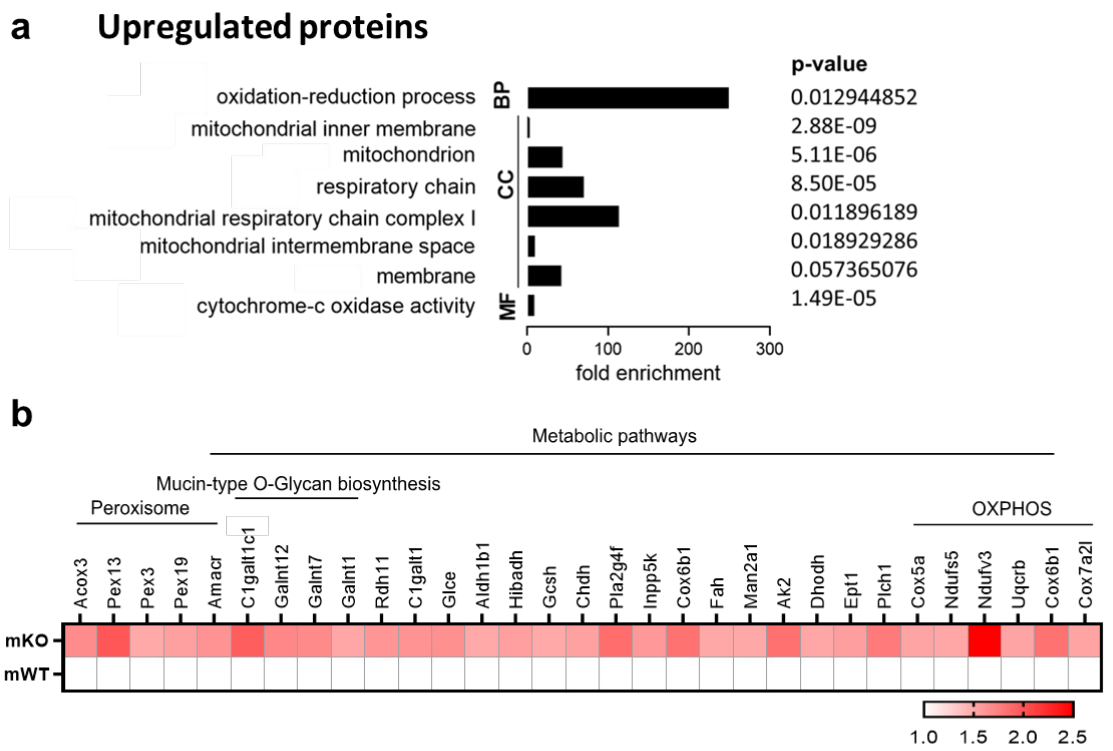

Figure 4.4.2: Pathway analyses of upregulated proteins.

a) Analysis of biological processes (PB), cellular components (CC), molecular function (MF) involving proteins upregulated in VPS34-deficient Treg cells identified in the proteomic profiling analysis.

b) Heat map presenting proteins upregulated in VPS34-deficient Treg cells identified in the proteomic profiling analysis.

To assess if alterations in mitochondrial protein levels translated into augmented mitochondrial respiration/activity, I assessed ATP levels. ATP is an indicator of metabolically active cells, and the number of viable cells can be assessed based on the amount of ATP available. Indeed, pharmacological inhibition of VPS34-kinase activity resulted in an increased ATP production (**Fig. 4.4.3 a**). These findings led to the hypothesis that the loss of VPS34 kinase activity induces a state of metabolic dysregulation in Treg cells. I therefore assessed whether differences in protein levels identified by proteomic profiling in VPS34-deficient Treg cells were accompanied by biologically relevant differences in energy levels. To quantify

mitochondrial respiration in VPS34-deficient Treg cells, I measured the mitochondrial *oxygen consumption rate* (OCR) and *extracellular acidification rate* (ECAR) using the Seahorse extracellular flux Energy Phenotype assay and found that VPS34-deficient Treg cells displayed increased OCR and ECAR (**Fig. 4.4.3 b**), leading to an increase metabolic potential (**Fig. 4.4.3 c**). An elevated OCR is indicative of increased mitochondrial respiration, while ECAR serves as an indicator of whether glucose is also catabolized through mitochondrial respiration. These results are in line with increased mitochondrial mass (**Fig. 3.2.1 c**) and numbers (**Fig. 3.2.1 d**). Collectively, these data indicate an increase in the metabolic activity of VPS34-deficient Treg cells.

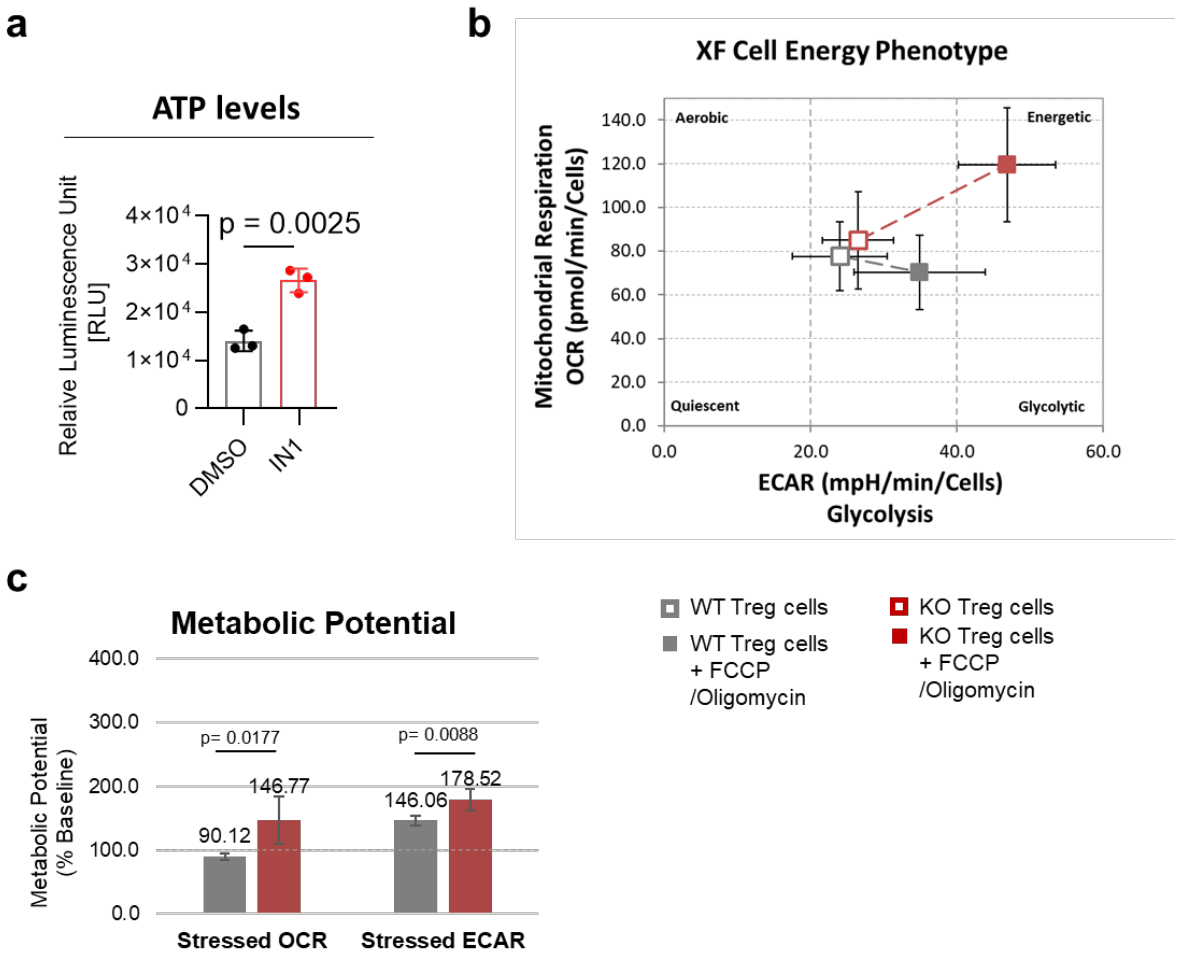

Figure 4.4.3: Metabolic rate is increased in VPS34-deficient Treg cells.

a) ATP levels of Treg cells treated with the pharmacological inhibitor VPS34-IN1 or the vehicle control DMSO. Individual data points from the three biological replicates, with the bar showing the means ± S.D. *p* values were calculated by two-tailed, one-sample Student's *t* test. Results are representative of three independent experiments.

b and **c**) Oxygen consumption rate (OCR) and extracellular acidification rate (ECAR) of VPS34-deficient Treg cells at before and after addition of 0.5uM FCCP and 10µM oligomycin following the Seahorse XF

Cell Energy Phenotype Test Assay protocol. **c**) Bar showing the means ± S.D. of the metabolic potential. *p* values were calculated by two-tailed, one-sample Student's *t* test. Results are representative of two independent experiments.

4.3 Discussion

Recent advances in proteomics allow for the unprecedented quantification of the total proteome such that one can determine the copy number of more than 8000 proteins from one million or fewer primary T cells [297]. The known role of VPS34 in trafficking of subcellular vesicles (and their associated proteins), rather than regulating transcriptional activities, supported the rationale to determine the proteome rather than individual mRNA expression levels. I have therefore analysed the protein content of VPS34-deficient Treg cells and compared it to VSP34-sufficient Treg cells. I generated a list of differentially expressed proteins as well as assessed whether the level of proteins involved in pathways and cellular processes relating to autophagy, endocytosis, and trafficking or required for Treg cell development, survival and fitness are affected by the loss of VPS34 kinase activity.

4.3.1 Analysis of differentially expressed proteins in VPS34-deficient Treg cells

Analysis of the data set led to a list of 140 differentially expressed proteins – among which 122 were more abundant and 18 less abundant in VPS34-deficient Treg cells. Loss of VPS34-kinase activity led to a reduction by half of VPS34 as well as of binding partners of VPS34 complex II (namely VPS15, UVRAG, and Beclin-1). This suggested that kinase-dead VPS34 protein is not stable, and reduced amounts of VPS34 induces a reduction of the other VPS34 complex binding partners. This might represent a disadvantage as we cannot ascertain the observed phenotype solely to VPS34-kinase activity. We aimed to circumvent the complete loss of VPS34 protein by inducing a truncation rather than a deletion of the VPS34 protein through the excision of exon 21 of *Pik3c3,* rather than exon 4 as used by Willinger and Flavell [228]. In our mouse model, the loxP sites are flanking a region of 75 nucleotides, leading to an in-frame mutation that is predicted to produce a truncated VPS34 protein. Indeed, we have confirmed that such a truncated protein can be expressed in cells and is kinase dead (**Fig. 3.1 d**).

Among the differentially expressed proteins, I first focused on proteins the most affected by loss of VPS34-kinase activity – i.e. ‘outliers’. Among those, Beclin-1 was highly downregulated, in line with the notion that Beclin-1 stability requires the presence of VPS34 [298]. Strikingly, none of these ‘outliers’ mapped to a common pathway nor were PI3P-

binders. Next, I focused on pathways and known biological functions of Treg cells as well as proteins required for Treg cell development, survival and fitness. Using this approach, I could only partially confirm results obtained from flow cytometric analyses (described in ***Chapter 3***). In contrast to results from phenotyping analyses performed in ***Chapter 3***, protein levels of CD44, CD69 and Ki67 (*Mki67*) were similar between VPS34-deficient and –sufficient Treg cells. Only CTLA-4 and ICOS levels matched previous observations, i.e. were unchanged.

One class of proteins was overrepresented in the list of differentially expressed proteins in Treg cells lacking VPS34-kinase activity. Members of the Ras-related small GTPases family, Rab1a, Rab2b, and Rab18 were significantly upregulated. Rab proteins are small molecular weight guanosine triphosphatases (GTPases) that contain four highly conserved domains involved in GTP binding and hydrolysis and cycle between inactive GDP-bound and active GTP-bound form [299]. These proteins are membrane-bound proteins, involved in vesicular fusion and regulate membrane trafficking in organelles and transport vesicle [300]. This is in line with the hypothesis presented in ***Chapter 3***, suggesting that loss of VPS34-kinase activity is affecting endolysosomal trafficking. As proposed in ***Chapter 3.4***, I will follow up on this observation.

Two RASP proteins, namely GRASP55 and GRASP65 [301]–[303] were significantly upregulated in VPS34-deficient Treg cells. The balance between membrane trafficking to and from the Golgi apparatus is critical for the maintenance of normal secretion and Golgi functions. In this context, Golgi matrix proteins, together with Rab GTPases, are perfectly positioned to control both Golgi structure and membrane traffic. Sort et *al*. observed that GRASP55- and GRASP65-golgin complexes interact with multiple Rab GTPases and upregulation of these proteins in VPS34-deficient Treg cells might promote the stacking of Golgi cisternae [302]. The implications of this observations will have to be studied further.

Four of the downregulated proteins related to cytokinesis. Recent findings have suggested that PI3P is required for the recruitment and the assembly of the ESCRT-III complex during cytokinesis [248]. PI3P recruits several effector proteins to the endosome, such as FYVE-CENT [249]. In turn, FYVE-CENT recruits other effector proteins, such as Beclin-1, VPS15, and UVRAG, that I found to be downregulated in VPS34-deficient Treg cells. These results suggest that VPS34-deficient Treg cells do not progress through the cell cycle – specifically mitosis. This hypothesis is supported by the decrease in the protein S100.A1 and the histone H1F0 (results presented in ***Chapter 4.2.2***), and further reinforced by the lack of mature Treg

cells (presented in ***Chapter 3.2.5***) and decreased proliferation potential (presented in ***Chapter 3.2.6***). S100-A1 is involved, amongst other processes, in cell cycle progression and differentiation. Histone H1F0 accumulates in cells that are in a terminal stage of differentiation or have a low rate of cell divisions [286]. Together, data obtained from flow cytometric analyses (***Chapter 3***) and proteomic profiling data (***Chapter 4***) suggest that loss of VPS34-kinase activity in Treg cells impairs cell cycle progression, which has an impact on proliferation potential and cellular maturation.

4.3.2 Metabolic potential is increased in VPS34-deficient Treg cells

Using DAVID functional annotation clustering, I observed that loss of VPS34-kinase activity in Treg cells leads to the upregulation of proteins involved in biological processes relating to mitochondrial functions and energy metabolism, suggesting that VPS34-deficient Treg cells display an increased metabolic state. I confirmed this hypothesis by measuring the mitochondrial respiration rate by Seahorse. These observations seemed contra-intuitive to the lack of activated Treg cells in mosaic *FoxP3*$^{YFP\text{-}Cre/WT}$ *Pik3c3*$^{fl/fl}$ mice, as determined by the expression of the activation markers CD44 and CD69. Possibly, loss of VPS34-kinase activity induces a state of higher metabolic activity, which in turn leads to faster exhaustion of VPS34-deficient Treg cells, and a reduced level of maturation. It is increasingly accepted that metabolism can shape immune cell development, trafficking, and functions [127]. In this context, mTORC1 has a critical role in bridging environmental cues to cell homeostasis and suppressive functions of Treg cells [131], [132], [137]–[139]. Hence, Treg cell-specific deletion of mTORC1 results in the spontaneous activation of effector T cells leading to the development of inflammation in barrier tissues [141]. By contrast, *Toll-like receptor* (TLR) signals enhance Treg cell proliferation through mTORC1 signalling pathway, *glucose transporter 1* (Glut1) upregulation, and glycolysis. However, these signals decrease the suppressive ability of Treg cells [142]. It is likely that TLR signal results in high levels of pro-inflammatory cytokines that decrease Treg cells functions even when mTORC1 expression is maintained in Treg cells [136]. However, I could not find evidence from the proteomic profiling data that mTORC1, associated proteins and downstream signalling were affected by the loss of VPS34-kinase activity in Treg cells. I rather found an increase in proteins associated

with metabolic pathways, and downstream analyses confirmed that VPS34-deficient Treg cells are metabolically more active.

It has been proposed that Treg cells need to reduce transiently their metabolic rate to enter the cell cycle and proliferate [131]. This would imply that because of their increased metabolic rate, VPS34-deficient Treg cells cannot progress through the cell cycle and hence proliferate. Should indeed VPS34 also regulate the maturation of Treg cells, the combined effect of VPS34-kinase loss would lead to a smaller Treg cell population which is less mature, and suppressive.

4.4 Chapter summary

In this chapter, I investigated the effect of the loss of VPS34-kinase activity on the proteome of Treg cells. More proteins were upregulated than downregulated in VPS34-deficient Treg cells. VPS34 as well as its complex II binding partners Beclin-1, UVRAG, and VPS15 were downregulated by half. Most upregulated proteins were involved in metabolic pathways, and indeed, VPS34-deficient Treg cells were metabolically more active, as assessed by SeaHorse assay and increased ATP-levels. Future work will aim at further investigating how VPS34-kinase activity links to kinase-associated signalling networks in Treg cells and how these in turn control metabolic fitness and potentially the generation of metabolites or other soluble factors involved in Treg cell-mediated suppression.

Chapter 5

The role of VPS34 in activated $CD8^+$ T cells

5.1 Introduction

To study the role of VPS34 in activated CD8$^+$ T cells, I used a mouse model in which the Cre-recombinase is expressed under the Granzyme B promoter, and exon 21 of *Pik3c3* is only excised in activated CD8$^+$ T cells while the full length VPS34 protein is present in naïve CD8$^+$ T cells. To activate naïve CD8$^+$ T cells, I used three different approaches:

First, I bulk-activated total splenocytes *in vitro* with αCD3/CD28 for 48h followed by expansion in the presence of *human recombinant IL-2* (hrIL-2). This approach allows to routinely generate large amounts of activated CD8$^+$ T cells, that can be used for flow cytometric and biochemical analyses.

The second and the third approach were used to activate CD8$^+$ T cells *in vivo*. In the first instance, I infected mice with the Gram-positive intracellular bacterium *Listeria monocytogenes* known to elicit a robust CD8$^+$ T cell response. Genetic modification of *Listeria monocytogenes* (*Lm*) to secrete foreign chicken antigen ovalbumin (OVA) allows to track the responding CD8$^+$ T cells using recombinant MHC tetramer molecules.

Lm induces a CD8$^+$ T cell response which peaks between eight to nine days after infection. The effector CD8$^+$ T cell pool can be divided into MPECs, which develop into memory T cells, and SLECs, which kill infected cells through the release of cytotoxic granules, and eventually die by apoptosis during the contraction phase. Memory T cells are maintained and remain ready to respond faster and stronger to re-infection.

Thirdly, I inoculated mice with the murine melanoma cell line B78ChOVA-mCherry. I used this model as tumours are fast growing (tumours reach the humane endpoint of 300m^3 at around 18 days post inoculation), express OVA, allowing me to use recombinant MHC tetramer molecules to detect antigen-specific T cells, and can be tracked using the mCherry reporter. This model allowed me to assess the proportions, phenotype, and effector functions of antigen-specific CD8$^+$ T cells infiltrating the tumour mass. Similar to the *Listeria* infection model, I aimed to assess whether the inactivation of the kinase activity of VPS34 may affect the development or effector functions of effector and/ or memory T cells.

5.2 Results

5.2.1 Specific deletion of VPS34-kinase activity in activated CD8⁺ T cells

To investigate the role of VPS34 in activated CD8⁺ T cells, I used a system to ablated VPS34 in effector CD8⁺ T cells by crossing mice containing loxP sites flanking exon 21 of *Pik3c3* (*Pik3c3*$^{fl/fl}$) to mice carrying the transgenes encoding the Cre recombinase and a ROSA26-loxP-STOP cassette followed by the transgene for enhanced YFP (eYFP) driven by the *granzyme B* promoter (*GzmB*$^{YFP\text{-}Cre}$ mice) to generate *GzmB*$^{YFP\text{-}Cre}$ *Pik3c3*$^{fl/fl}$ mice (the targeting strategy is summarized in **Fig. 5.1**). I refer to these mice as *GzmB*$^{YFP\text{-}Cre}$ *Pik3c3*$^{fl/fl}$ or KO mice, heterozygous mice as *GzmB*$^{YFP\text{-}Cre}$ *Pik3c3*$^{fl/wt}$ or HET mice and wild-type littermate controls as *GzmB*$^{YFP\text{-}Cre}$ *Pik3c3*^{wt} or WT mice. This targeting strategy allows to breed reporter mice in which naïve CD8⁺ T cells develop normally because exon 21 of *Pik3c3* is deleted only after the activation of CD8⁺ T cells. In this system, deletion of the exon 21 of *Pik3c3* occurs specifically upon the expression of *GzmB*, which is expressed in activated CD8⁺ T cells, and these cells become YFP⁺. I will refer at this genetic deletion as *Pik3c3*$^{\Delta 21}$.

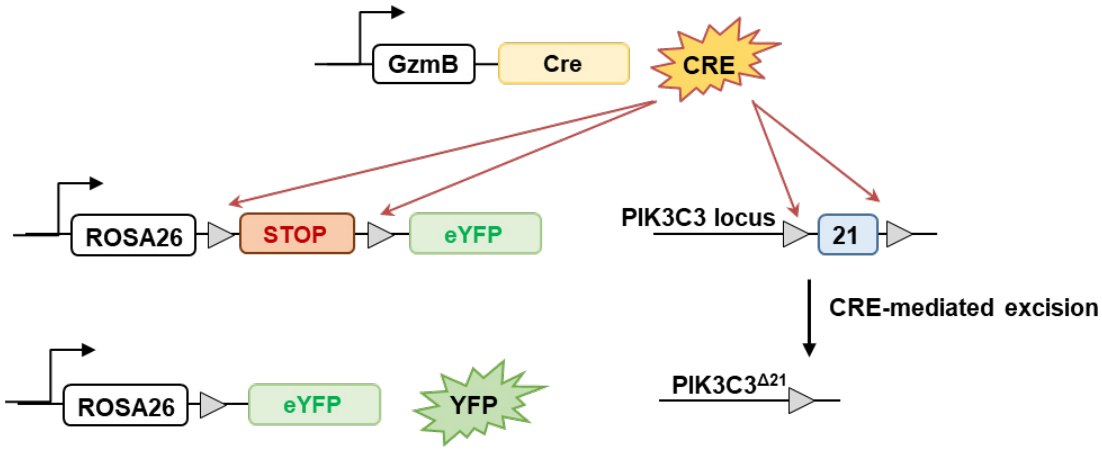

Figure 5.1: Generation of VPS34-kinase dead activated CD8⁺ T cell.
Targeting strategy to generate activated CD8⁺ T cell with cell-specific VPS34-kinase dead mice: exon 21 (located in the kinase domain) of the *Pik3c3* gene encoding VPS34 was flanked with LoxP sites. The enframed region is 75 nucleotides long, and Cre-mediated excision does not change the open reading frame, thereby giving rise to a truncated VSP34 protein that is 25 amino acids shorter than the wild-type version. For activated CD8⁺ T cell-specific deletion, *Pik3c3*$^{fl/fl}$ mice were crossed with a transgenic mice strain carrying the transgenes encoding the Cre recombinase and a ROSA26-loxP-STOP cassette followed by the transgene for enhanced YFP (eYFP) driven by the *granzyme B* promoter (*GzmB*$^{YFP\text{-}Cre}$ mice) to generate *GzmB*$^{YFP\text{-}Cre}$ *Pik3c3*$^{fl/fl}$ mice.

5.2.2 Immuno-phenotyping of unchallenged GzmB$^{Cre\text{-}YFP}$ Pik3c3$^{fl/fl}$ *mice*

In a first instance, I assessed the percentage of lymphocytes including CD4$^+$ and CD8$^+$ T cells, regulatory T cells (Treg cells), and B cells as well as the activation status of CD8$^+$ T cells in the spleen, lymph nodes (axillary, brachial, cervical, and inguinal), and thymus of unchallenged mice by flow cytometry (**Fig. 5.2.1 a – d**, **Fig. 5.2.2 a – d**, and **Fig. 5.2.3 a – c**, respectively). I did not observe any differences between knock-out *GzmB*$^{YFP\text{-}Cre}$ *Pik3c3*$^{fl/fl}$ mice, heterozygous *GzmB*$^{YFP\text{-}Cre}$ *Pik3c3*$^{fl/wt}$ mice, and wild-type *GzmB*$^{YFP\text{-}Cre}$ *Pik3c3*^{wt} littermate controls for any of the analysed cell populations. Of note, eYFP$^+$ cells constituted around 5% of the NK cell population as well as the above mentioned cell populations (**Fig. 5.2.4**). In addition to CD8$^+$ T cells, NK cells also express *Granzyme B*, explaining the presence of YFP$^+$ NK cells.

In summary, these data show that in unchallenged mice, CD8$^+$ T cells have a minimal expression of the Cre-recombinase and that VPS34 kinase activity is therefore virtually untouched in CD8$^+$ T cells from naïve mice.

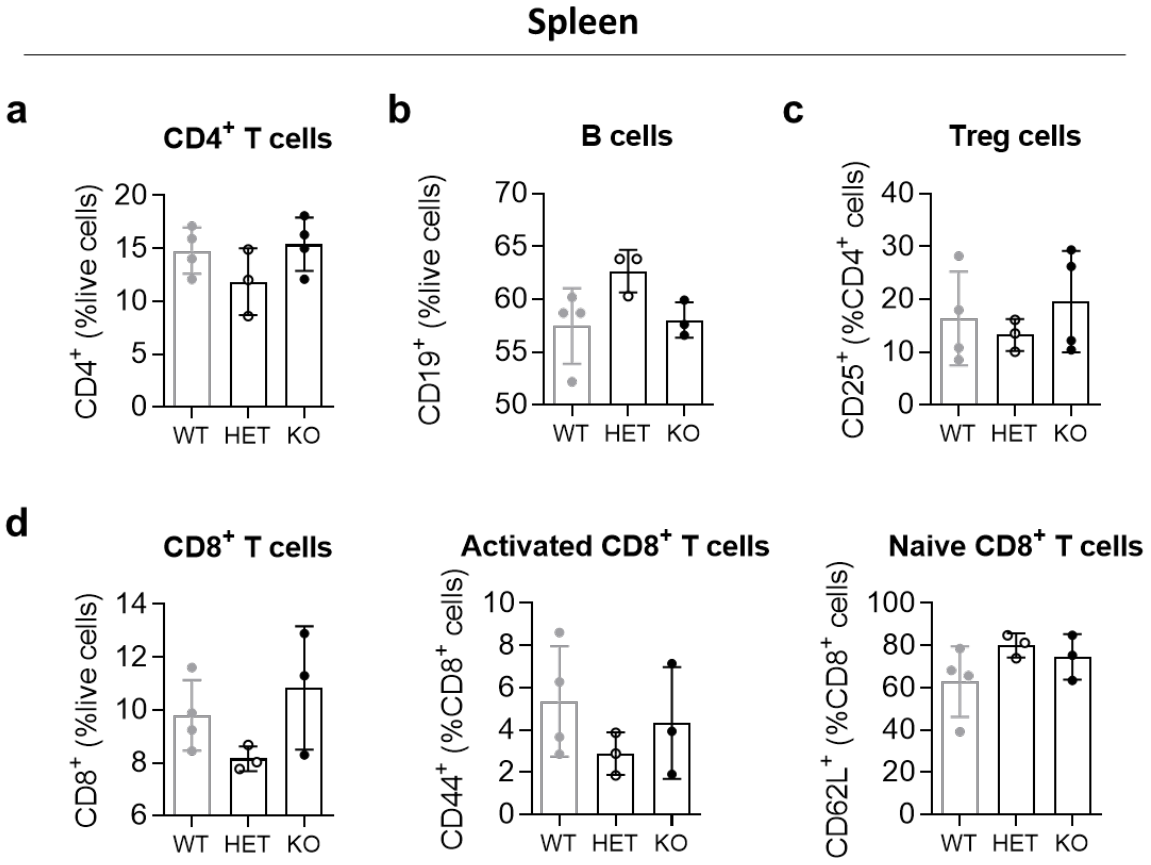

Figure 5.2.1: Immuno-phenotyping of splenocytes of unchallenged *GzmB*$^{Cre\text{-}YFP}$ *Pik3c3*$^{fl/fl}$ mice.
a – d) The percentage of CD4⁺ T cells (**a**), B cells (**b**), Treg cells (**c**), CD8⁺ T cells as well as the percentage of activated and naïve CD8⁺ T cells (**d**) in the spleen of *GzmB*$^{Cre\text{-}YFP}$ *Pik3c3*$^{fl/fl}$ and *GzmB*$^{Cre\text{-}YFP}$ *Pik3c3*$^{fl/+}$ and littermate controls (*GzmB*-Cre^{-} mice) was analysed by flow cytometry. n = 3 – 6 mice. Results are representative of two independent experiments. Statistical significance was determined using a one-way ANOVA followed by a Tukey's post-hoc test.

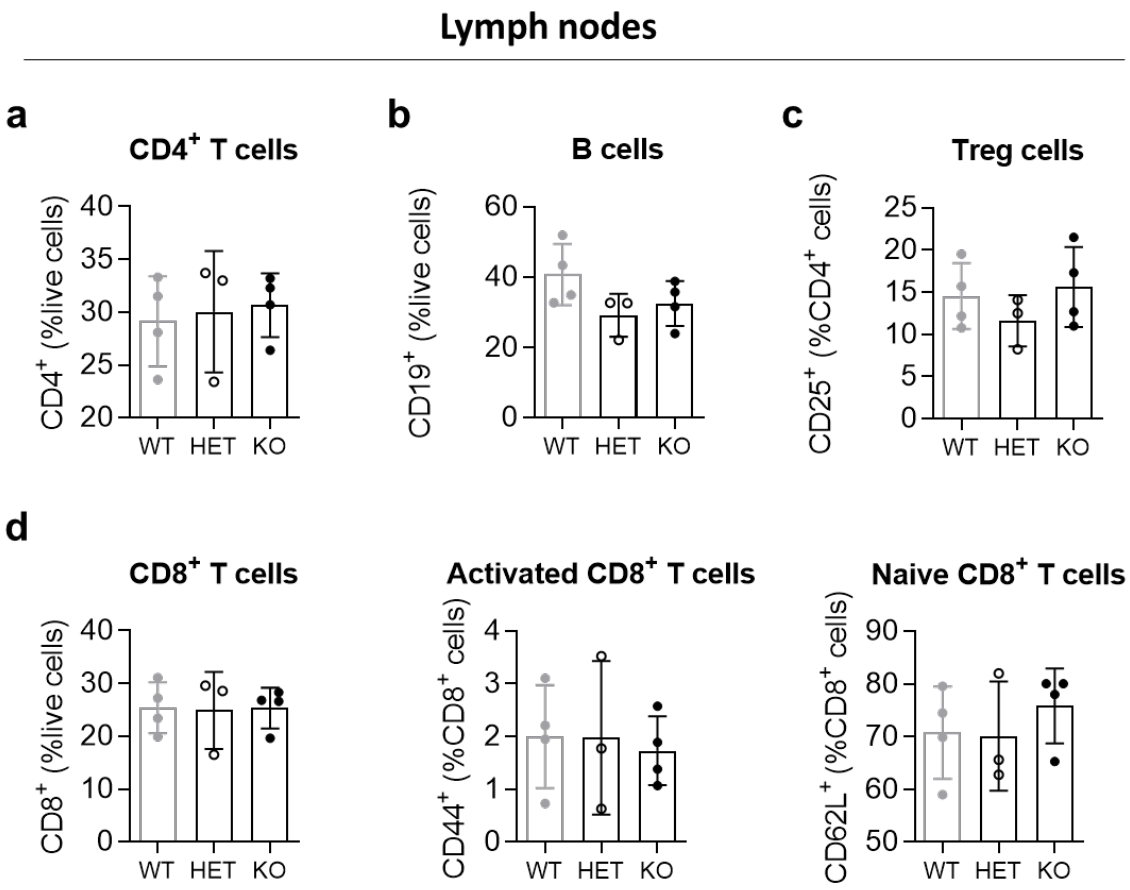

Figure 5.2.2: Immuno-phenotyping of lymphocytes in the lymph nodes of unchallenged *GzmB*$^{Cre\text{-}YFP}$ x *Pik3c3*$^{fl/fl}$ mice.

a – d) The percentage of CD4⁺ T cells (**a**), B cells (**b**), Treg cells (**c**), CD8⁺ T cells as well as the percentage of activated and naïve CD8⁺ T cells (**d**) in the lymph nodes (pooled from axiliary, brachial, cervical and inguinal) of *GzmB*$^{Cre\text{-}YFP}$ *Pik3c3*$^{fl/fl}$ and *GzmB*$^{Cre\text{-}YFP}$ *Pik3c3*$^{fl/+}$ and littermate controls (*GzmB*-Cre^{-} mice) was analysed by flow cytometry. n = 3 – 6 mice. Results are representative of two independent experiments. Statistical significance was determined using a one-way ANOVA followed by a Tukey's post-hoc test.

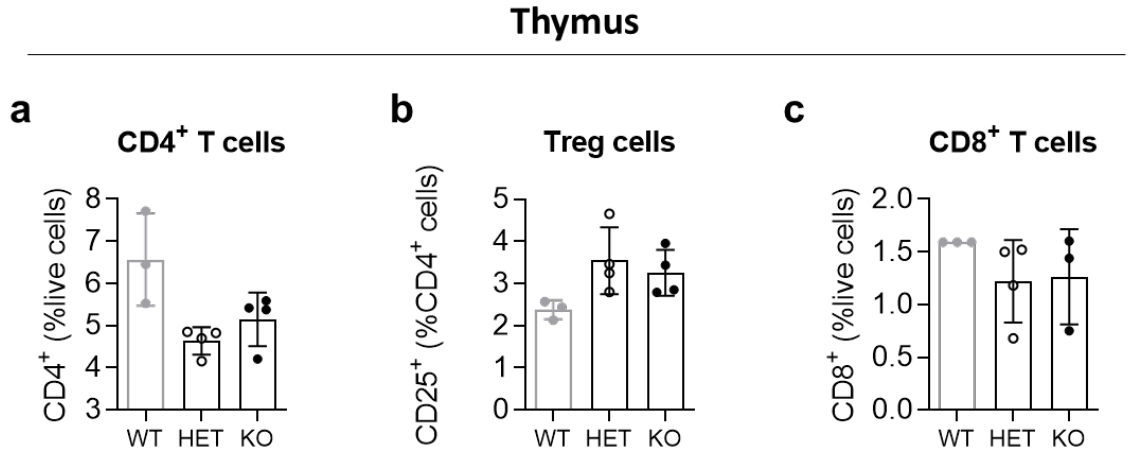

Figure 5.2.3: Immuno-phenotyping of lymphocytes in the thymus of unchallenged *GzmB*$^{Cre\text{-}YFP}$ x *Pik3c3*$^{fl/fl}$ mice.

a – c) The percentage of CD4⁺ T cells (**a**), Treg cells (**c**), and CD8⁺ T cells (**c**) in the thymus of *GzmB*$^{Cre\text{-}YFP}$ *Pik3c3*$^{fl/fl}$ and *GzmB*$^{Cre\text{-}YFP}$ *Pik3c3*$^{fl/+}$ and littermate controls (*GzmB*-Cre^{-} mice) was analysed by flow cytometry. n = 3 – 6 mice. Results are representative of two independent experiments. Statistical significance was determined using a one-way ANOVA followed by a Tukey's post-hoc test.

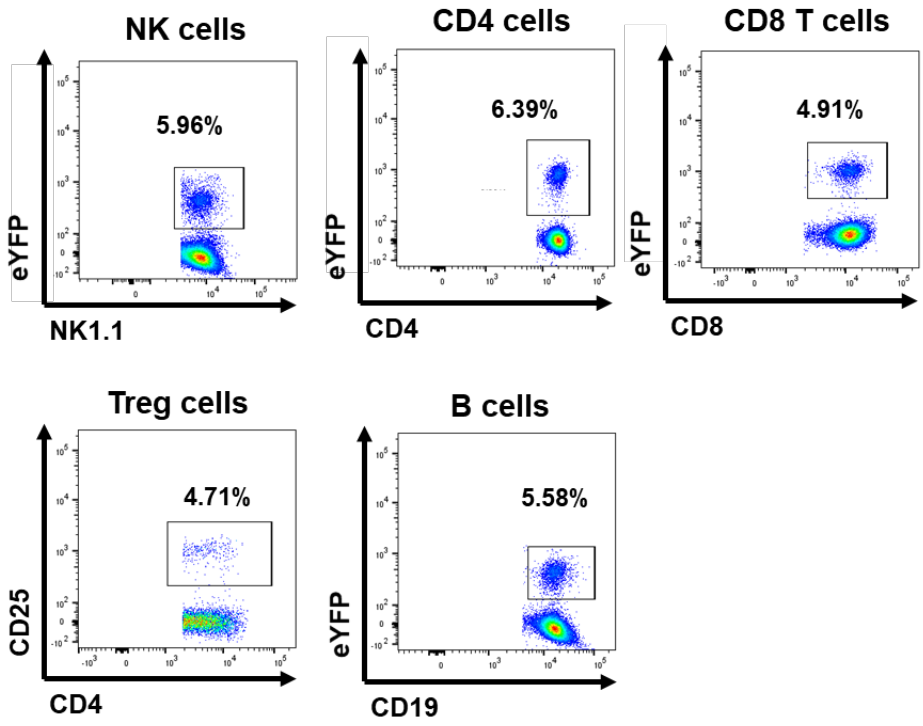

Figure 5.2.4: Diverse immune cell types express eYFP in unchallenged *GzmB*$^{eYFP\text{-}Cre}$ x *Pik3c3*$^{fl/fl}$ mice. Representative FACS plot for the expression of eYFP in CD4⁺ and CD8⁺ T cells, Treg cells, B cells and NK cells of an unchallenged *GzmB*$^{eYFP\text{-}Cre}$ *Pik3c3*$^{fl/fl}$ mouse.

5.2.3 In vitro analyses of Pik3c3$^{\Delta 21}$ *CD8$^+$ T cells*

To assess the role of VPS34 in activated CD8$^+$ T cells, I induced Cre-mediated deletion of exon 21 of the *Pik3c3* gene *in vitro* by bulk-activating total splenocytes with α-CD3/CD28 for 24h followed by expansion in the presence of human recombinant IL-2 (hrIL-2) for five days. On day 7 after stimulation, the extent of *Pik3c3*$^{\Delta 21}$ deletion was reflected by the abundance of VPS34 protein in bulk-activated CD8$^+$ T cells: VPS34 protein was reduced by half in the CD44^{hi} CD8$^+$ T cell population from *GzmB*$^{YFP\text{-}Cre}$ *Pik3c3*$^{fl/fl}$ mice (**Fig. 5.3.1 a**). Similarly, protein levels of VPS15 were also decreased by half in activated CD8$^+$ T cells from GzmB$^{YFP\text{-}Cre}$ *Pik3c3*$^{fl/fl}$ mice compared to heterozygous *GzmB*$^{YFP\text{-}Cre}$ *Pik3c3*$^{fl/wt}$ mice and wild-type control mice (**Fig. 5.3.1 b**). Strikingly, levels of Atg14L was increase by factor 2 in CD8$^+$ T cells from GzmB$^{YFP\text{-}Cre}$ *Pik3c3*$^{fl/fl}$ mice compared to heterozygous and wild-type CD8$^+$ T cells (**Fig. 5.3.1 c**).

Seven days after activation, the proportion of CD44$^+$ from CD8$^+$ T cells was similar across the three genotypes (*GzmB*$^{YFP\text{-}Cre}$ *Pik3c3*$^{fl/fl}$ (KO), heterozygous *GzmB*$^{YFP\text{-}Cre}$ *Pik3c3*$^{fl/wt}$ (HET), and wild-type littermate control *GzmB*$^{YFP\text{-}Cre}$ *Pik3c3*^{wt} mice (WT)) (**Fig. 5.3.2 a**). Against my expectation, the percentage of YFP$^+$ cells among activated CD8$^+$ T cells was only around 15%, while I would have assumed that nearly all activated CD8$^+$ T cells would express *GzmB* and therefore the Cre-recombinase, eventually leading to the excision of exon 21 of *Pik3c3* and the expression of the reporter transgene eYFP. Of note, when comparing the proportion of YFP$^+$ cells among CD44$^+$ CD8$^+$ T cells, I did not observe any differences between heterozygous (HET) and *Pik3c3*$^{\Delta 21}$ CD8$^+$ T cells (KO) (**Fig. 5.3.2 b**). Similarly, the percentage of activated cells expressing CD103 or PD-1 among CD44$^+$ CD8$^+$ T cells (**Fig. 5.3.2 c**) or YFP$^+$ CD44$^+$ CD8$^+$ T cells (**Fig. 5.3.2 d**) did not differ between KO, HET and WT CD8$^+$ T cells.

Next, I assessed the expression of the transcription factors T-bet and Eomes. T-bet is required for the differentiation of CD8$^+$ T cells into functioning cytokine secreting SLECs [304] while Eomes is key for the function of CD8$^+$ T cells. There was a trend towards increase T-bet level, and reduced Eomes/T-bet double positive cells in activated CD8$^+$ T cells lacking VPS34, but this was not significant (**Fig. 5.3.3 a**). Interestingly, the level of IFN-γ was greatly increased in VPS34-deficient CD44$^+$ CD8$^+$ T cells (**Fig. 5.3.3 b**). These data suggest that while the absence of VPS34 kinase activity does not affect the differentiation of CD8$^+$ T cells into activated CTLs, it might affect the effector functions, as suggested by changes in IFN-γ levels.

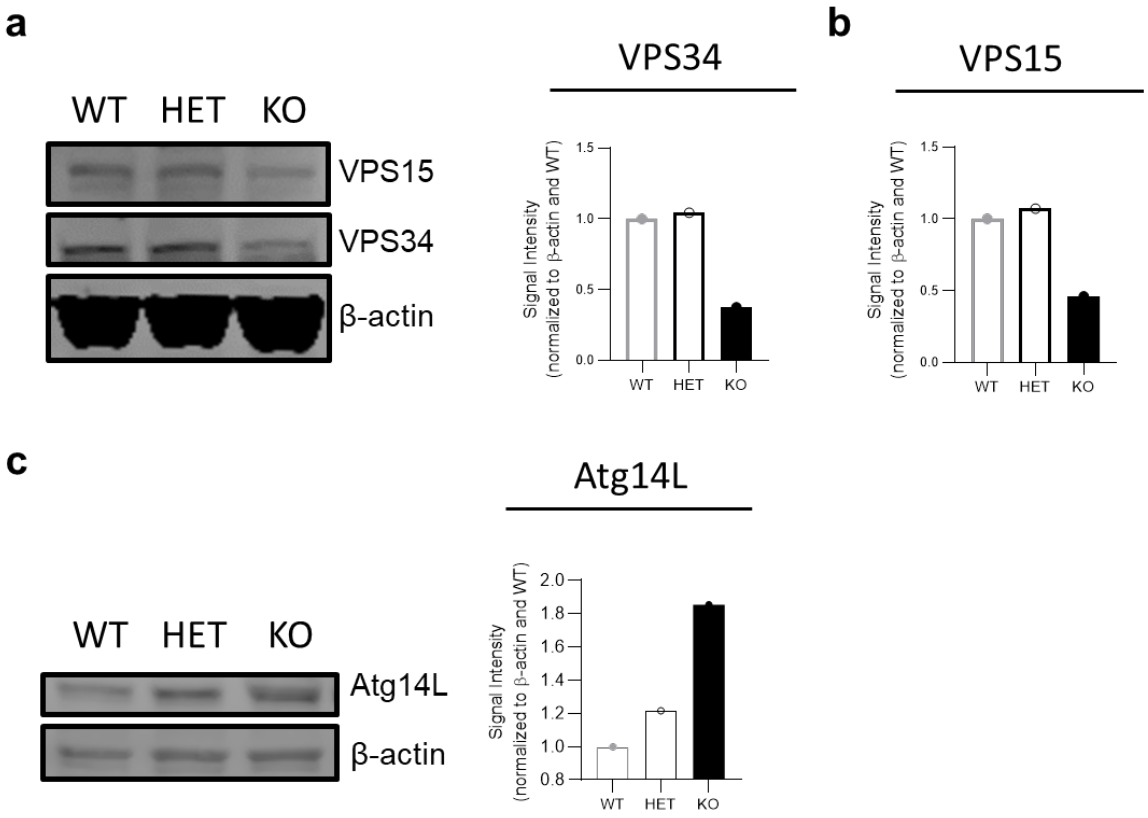

Figure 5.3.1: Loss of VPS34-kinase activity affects the stability of its binding partners.
Western blot analysis of the protein content of VPS34 (**a**), VPS15 (**a** and **b**) and Atg14L (**c**) from CD8⁺ T cells bulk-activated with αCD3 and αCD28 for 48h and further expanded in human recombinant IL-2 for five days. Results are representative of two independent experiments.

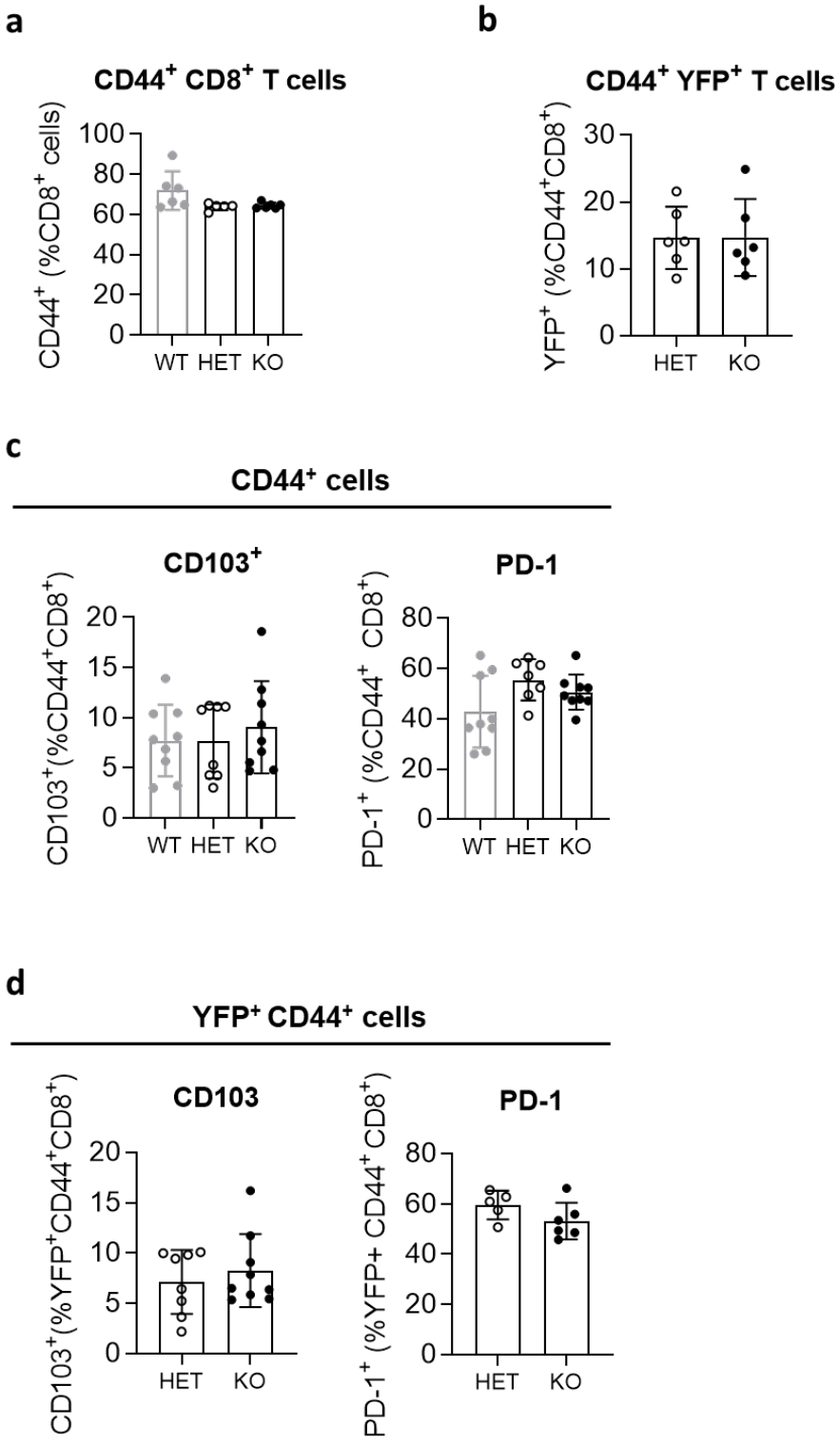

Figure 5.3.2: *In vitro* activated VPS34-deficient CD8⁺ T cells display normal levels of CD44, CD103 and PD-1.

(**a – b**) Percentage of CD44⁺ cells (**a**) and CD44⁺ YFP⁺ cells (**b**) from CD8⁺ T cells bulk-activated with αCD3 and αCD28 for 48h and further expanded in human recombinant IL-2 for five days.

(**c – d**) Percentage of CD103⁺ CD44⁺ cells and PD-1⁺ CD44⁺ cells (**c**) and CD103⁺ YFP⁺ CD44⁺ cells and PD-1⁺ YFP⁺ CD44⁺ cells (**d**) from CD8⁺ T cells bulk-activated with αCD3 and αCD28 for 48h and further

expanded in human recombinant IL-2 for five days. Statistical significance was determined using a one-way ANOVA followed by a Tukey's post-hoc test. n = 6 – 9 biological replicates per group. Results are pooled from three independent experiments.

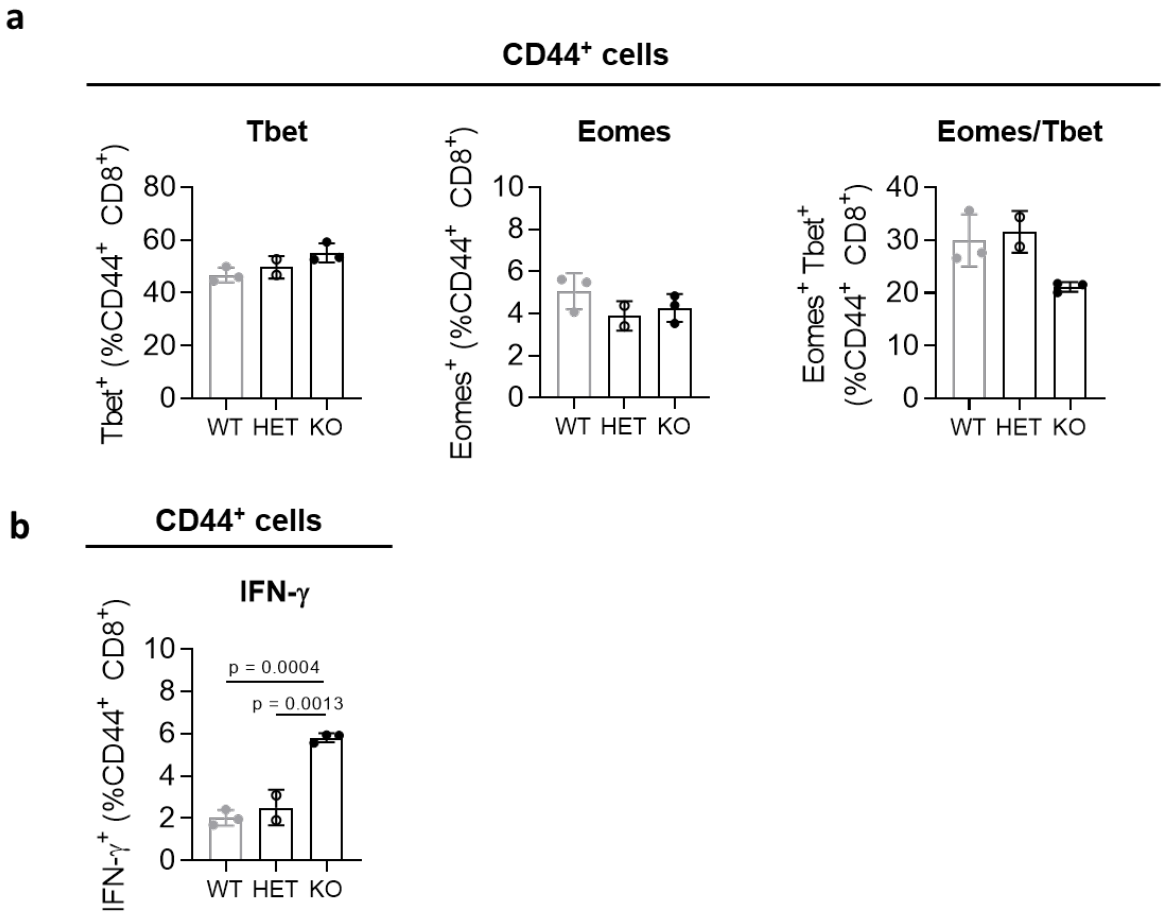

Figure 5.3.3: *In vitro* activated VPS34-deficient CD8⁺ T cells display normal levels of T-bet and Eomes, but have an increase in IFN-γ production.

(**a**) Percentage of Tbet⁺, Eomes⁺, or Tbet⁺ Eomes⁺ CD44⁺ cells from CD8⁺ T cells bulk-activated with αCD3 and αCD28 for 48h and further expanded in human recombinant IL-2 for five days.

(**b**) Percentage of IFN-γ⁺ CD44⁺ cells from CD8⁺ T cells bulk-activated with αCD3 and αCD28 for 48h and further expanded in human recombinant IL-2 for five days. Statistical significance was determined using a one-way ANOVA followed by a Tukey's post-hoc test. n = 3 biological replicates per group. Results are representative from three independent experiments.

5.2.4 In vitro activated Pik3c3$^{\Delta 21}$ *CD8$^+$ T cells do not show increased cell death but a decrease in cell division*

During the naïve-to-effector-to-memory – differentiation stages, CD8$^+$ T cells proliferate and differentiate into distinct CD8$^+$ T cell subsets. As VPS34 is an evolutionary conserved protein and essential for autophagy and endocytosis, two processes key for proliferative and differentiating cells, I investigated whether the inactivation of the kinase activity of VPS34 may affect the proliferation and/or the survival of activated CD8$^+$ T cells.

First, I considered whether the loss of VPS34 might increase the proportion of cells that undergo apoptosis. Activated CD8$^+$ T cells were generated by bulk-activating splenocytes with αCD3/CD28 for 48h and subsequent expansion in rhIL-2 for five days. On days seven after *in vitro* activation, the proportions of early apoptotic cells determined as Annexin V-single positive cells was significantly decreased in *Pik3c3$^{\Delta 21}$* and heterozygous *Pik3c3$^{\Delta 21}$* CD44$^+$ CD8$^+$ T cells compared to wild-type CD8$^+$ T cells (**Fig. 5.4.1 a**, left graph). The proportion of late apoptotic cells, determined as positive for Annexin V and the live dead dye, was slightly, but not significantly increased for both heterozygous and *Pik3c3$^{\Delta 21}$* CD44$^+$ CD8$^+$ T cells compared to wild-type CD8$^+$ T cells (**Fig. 5.4.1 a**, right graph). When assessing YFP$^+$ CD44$^+$ CD8$^+$ T cells from heterozygous and *Pik3c3$^{\Delta 21}$*mice, I could not detect any differences in the proportions of early apoptotic or late apoptotic cells (**Fig. 5.4.1 b**).

Secondly, I considered whether the loss of VPS34 might affect the proportion of cells undergoing cell division. Seven days after *in vitro* activation with αCD3/CD28 and subsequent expansion in rhIL-2, I measured the incorporation of the nucleotide analogue *bromo-2'-deoxyuridine* (BrdU) in activated CD8$^+$ T cells to investigate their ability to proceed through the cell cycle, and Ki67-levels to determine cell proliferation capacity.

I did not observe any differences between activated CD44$^+$ CD8$^+$ T cells and YFP$^+$ CD44$^+$ CD8$^+$ T cells from wild-type, heterozygous and *Pik3c3$^{\Delta 21}$* CD8$^+$ T cells in terms of proliferation, as assessed by the proliferation marker Ki67 (**Fig. 5.4.2 a** and **b**, respectively). Ki67 antigen is expressed in all phases of the cell cycle except G0 and provides an estimate of the fraction of dividing cells [305].

In regards to cell cycle analysis, proportions of *Pik3c3$^{\Delta 21}$* CD8$^+$ T cells were found to be reduced in the G2/M phase, while increased proportions of *Pik3c3$^{\Delta 21}$* CD8$^+$ T cells were

incorporating BrdU, reflecting the S phase (**Fig. 5.4.2 c**). Since this experiment was done only once, I need to perform further repeats to confirm these observations.

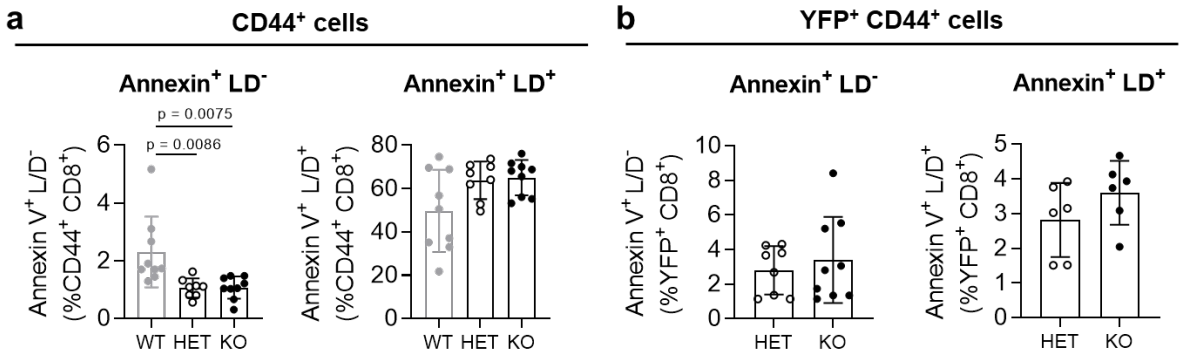

Figure 5.4.1: Granzyme B and LAMP1 are reduced in GzmB$^{Pik3c3\Delta21}$ mice during the primary but not the secondary response.

Graphical representation of Annexin V⁺ Viability Dye⁻ (left) and Annexin V⁺ Viability Dye⁺ (right) of CD44⁺ cells (**a**) and YFP⁺ CD44⁺ cells (**b**) from CD8⁺ T cells bulk-activated with αCD3 and αCD28 for 48h and further expanded in human recombinant IL-2 for five days. Results are representative of two independent experiments. *n* = 9 per group. Statistical significance was determined using a one-way ANOVA followed by a Tukey's post-hoc test (a) or a two-tailed Student's *t*-test (b). Results are pooled from two independent experiments.

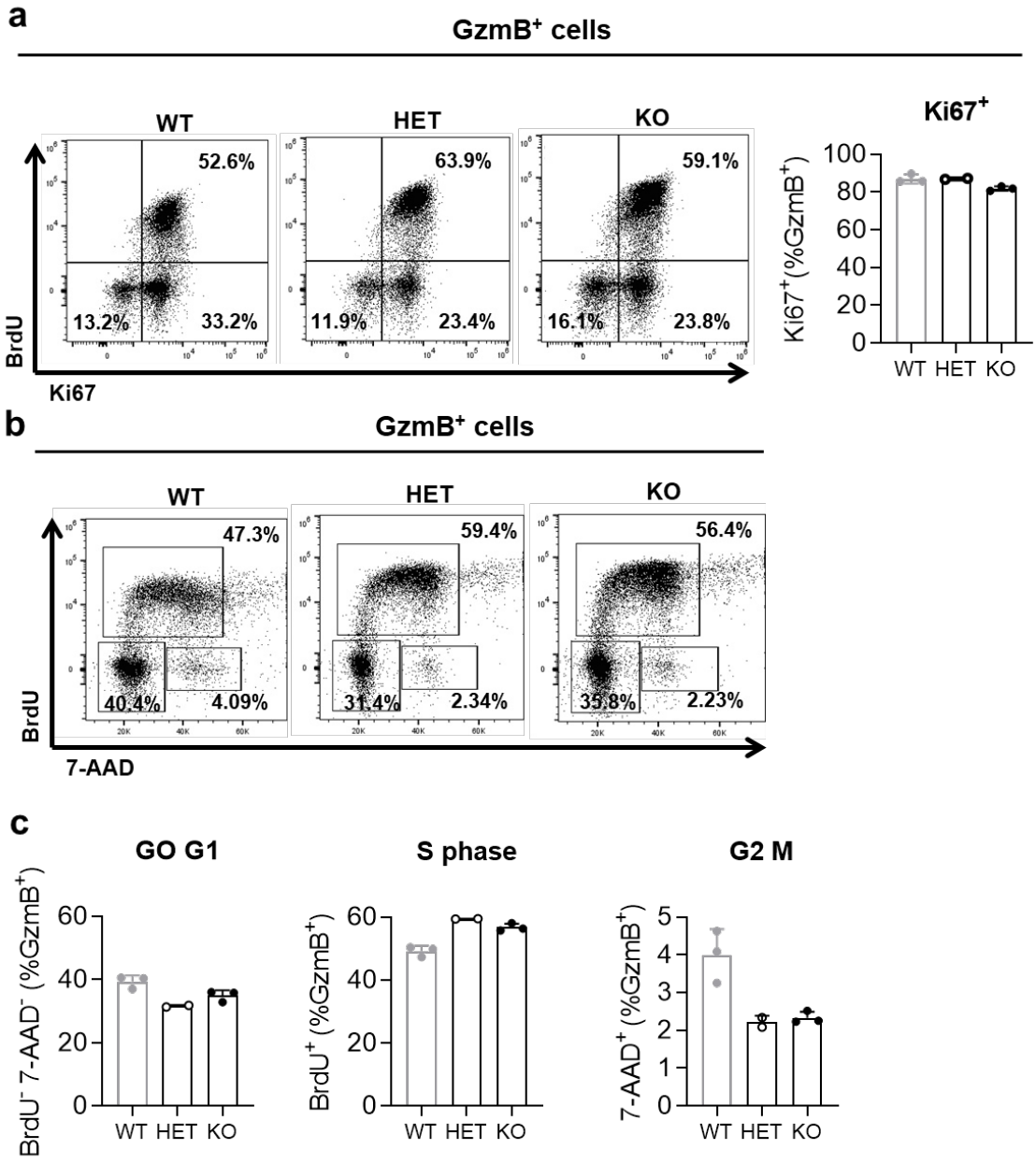

Figure 5.4.2: VPS34-deficiency impairs the cell cycle of *in vitro* activated CD8⁺ T cells.

(**a**) Representative flow cytometry plots and graphical representation of the percentage of the proliferation marker Ki67 and the nucleotide analog bromo-2'-deoxyuridine (BrdU) in CD44⁺ cells from CD8⁺ T cells bulk-activated with αCD3 and αCD28 for 48h and further expanded in human recombinant IL-2 for five days.

(b – c) Representative flow cytometry plots and graphical representation of the percentage of the nucleotide analog bromo-2'-deoxyuridine (BrdU) and 7-AAD in CD44⁺ cells from CD8⁺ T cells bulk-activated with αCD3 and αCD28 for 48h and further expanded in human recombinant IL-2 for five days. n = 2 – 3. Results are from one experiment.

5.2.5 Antigen-specific CD8⁺ T cells are reduced in VPS34-deficient cells during the primary and the secondary response to L. monocytogenes infection

To assess the role of VPS34 in activated CD8⁺ T cells *in vivo*, I infected mice with a transgenic strain of *L. monocytogenes* that expresses chicken OVA and detected OVA-specific CD8⁺ T cells using MHC class I H-2b tetramers loaded with OVA257–264 (SIINFEKL) peptide. The kinetics of the CD8⁺ T cell response to *Listeria* is shown in **Fig. 5.5.1**. Naïve CD8⁺ T cell are activated in response to *Listeria* infection, proliferate rapidly and reach the peak of expansion and effector functions at around 8-9 days during the primary response. Subsequently, most of the CD8⁺ T cells die by apoptosis, and a pool of memory cells remains. Upon re-infection, memory CD8⁺ T cells are activated and generate a larger secondary response that peaks 5 days after re-infection.

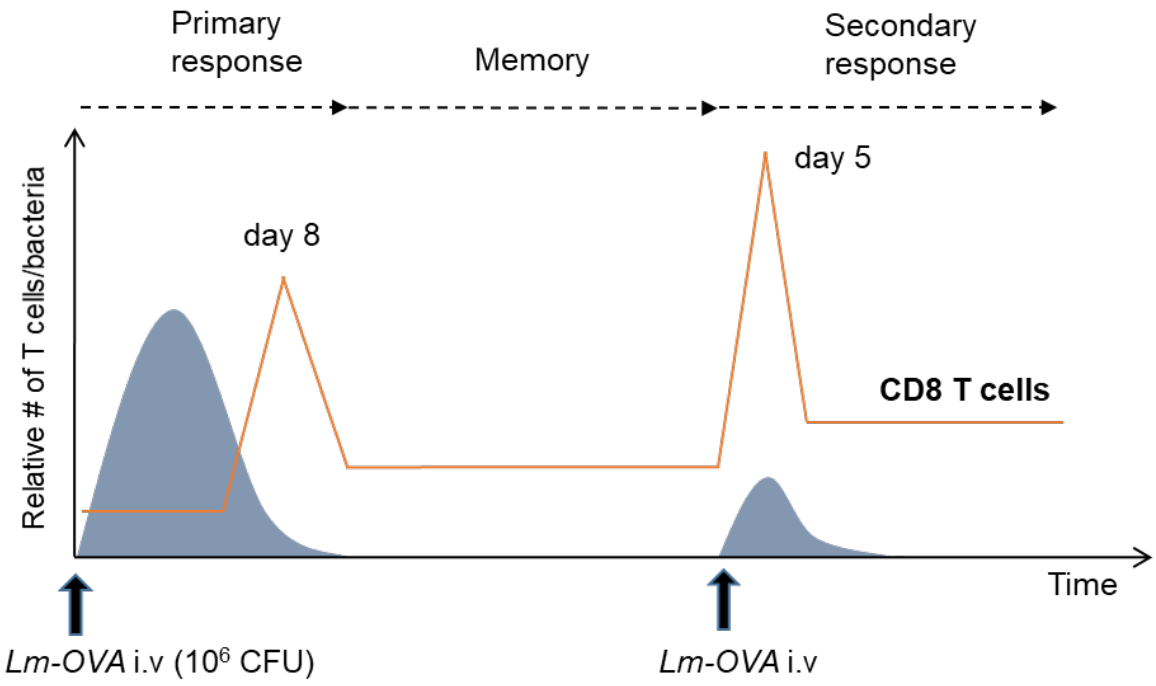

Figure 5.5.1: Kinetics of the CD8⁺ T cell response following intravenous infection with *Listeria*. Following infection with *Listeria,* the bacterial load in the spleen and liver increases until the peak at around two to three days post infection (blue line). At the same this time, antigen-specific CD8⁺ T cells become activated and proliferate, reaching a peak response at eight days post infection (orange line). A pool of antigen-specific CD8⁺ memory T cells remains and will generate a faster and larger immune response that peaks around five days in the case of reinfection, leading to a faster and better control of the bacterial load during the secondary infection. *Modified from Verity Pearce.*

The proportions of CD8⁺ T cells in the blood that stained positive with the tetramer (Tet⁺ CD8⁺) were reduced in *GzmB*$^{YFP\text{-}Cre}$ *Pik3c3*$^{fl/fl}$ mice (**Fig. 5.4.2 a**). This reduction in the proportion of Tet⁺ CD8⁺ T cells was apparent both at the peak of the response (7 days after the first challenge) as well as five days after subsequent re-challenge (**Fig. 5.4.2 b – d**).

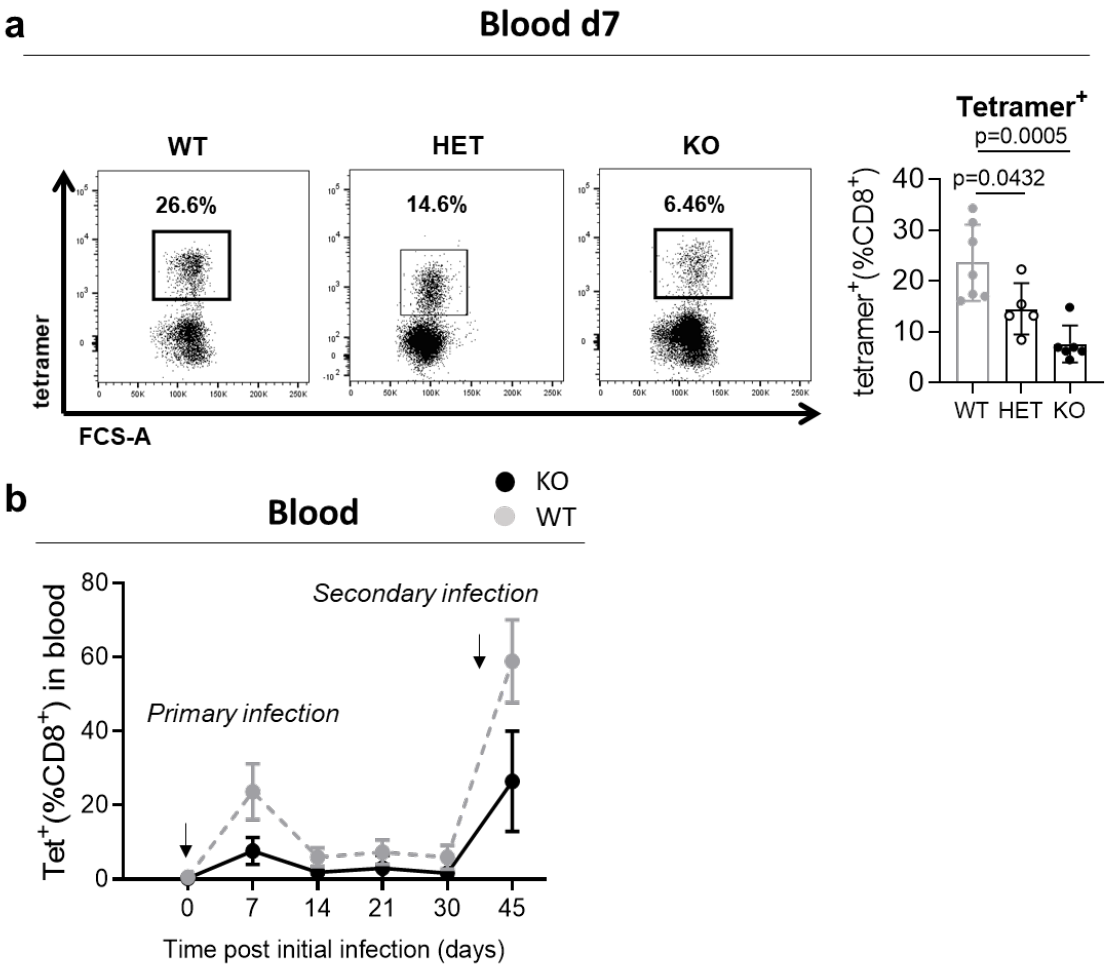

Figure 5.5.2: Defective primary and secondary immune response in *GzmB*$^{YFP\text{-}Cre}$ *Pik3c3*$^{fl/fl}$ mice.
GzmB$^{YFP\text{-}Cre}$ *Pik3c3*^{wt} (WT), *GzmB*$^{YFP\text{-}Cre}$ *Pik3c3*$^{fl/wt}$ (HET), and *GzmB*$^{YFP\text{-}Cre}$ *Pik3c3*$^{fl/fl}$ mice (KO) were infected with Lm-OVA on days 0 with 5x10^6 CFU Lm-OVA. Representative flow cytometry plots and graph show the percentage of tetramer⁺ (antigen-specific) CD8⁺ T cells in blood samples on day 7 (**a**) and on day 14, 21, 30 and five days after re-infection (**b**); *n* = 5 – 7 per group. Results are representative of two independent experiments. *n* = 9 per group. Statistical significance was determined using a one-way ANOVA followed by a Tukey's post-hoc test. Results are representative from two independent experiments.

To address whether the reduced proportion of antigen-specific CD8⁺ T cells in the blood reflected their altered distribution, I enumerated Tet⁺ CD8⁺ T cells in the spleen and lymph nodes. In *GzmB*$^{YFP\text{-}Cre}$ *Pik3c3*$^{fl/fl}$ mice, the proportions of Tet⁺ CD8⁺ T cells were significantly reduced at the peak of the primary response (7 days post infection) in the spleen but not in the lymph nodes (**Fig. 5.5.3 a** and **b**, respectively). During the secondary response (5 days after re-challenge), Tet⁺ CD8⁺ T cell numbers were significantly reduced in the spleen and in the lymph nodes (**Fig. 5.5.4 a** and **b**, respectively). These data indicate that in *GzmB*$^{YFP\text{-}Cre}$ *Pik3c3*$^{fl/fl}$ mice, VPS34 deletion leads to a reduced magnitude of antigen-specific CD8⁺ T cells upon acute challenge with *Lm*-OVA.

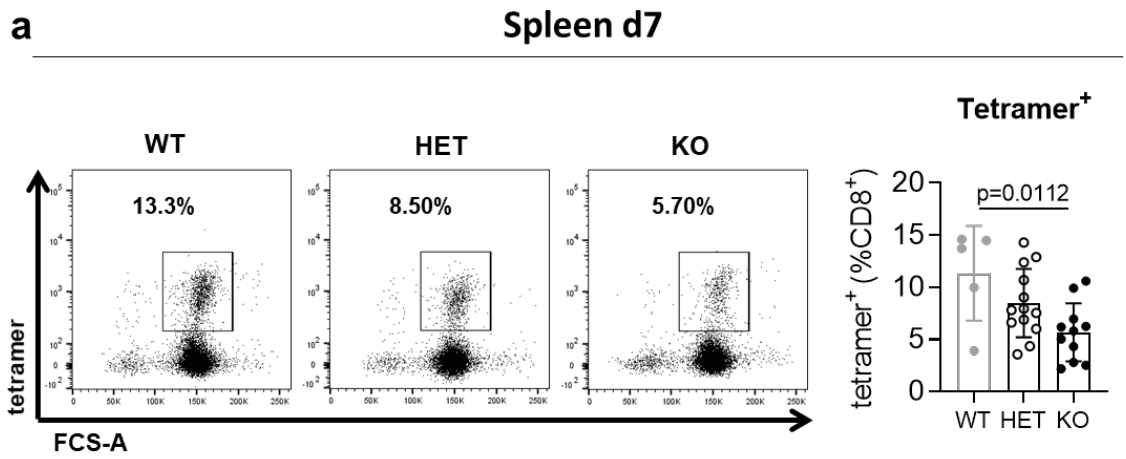

Figure 5.5.3: Defective primary immune response in the spleen of *GzmB*$^{Pik3c3\Delta21}$ mice.

Representative flow cytometry plots and bar graph showing the percentage of tetramer⁺ CD8⁺ T cells recovered for the spleen (**a**) and the lymph node (**b**) 7 days after primary infection of *GzmB*$^{YFP\text{-}Cre}$ *Pik3c3*^{wt} (WT), *GzmB*$^{YFP\text{-}Cre}$ *Pik3c3*$^{fl/wt}$ (HET), and *GzmB*$^{YFP\text{-}Cre}$ *Pik3c3*$^{fl/fl}$ mice (KO) with 5x10^6 CFU Lm-OVA; *n* = 5 – 7 per group. Results are representative of two independent experiments. *n* = 9 per group. Statistical significance was determined using a one-way ANOVA followed by a Tukey's post-hoc test. Results are pooled from two independent experiments.

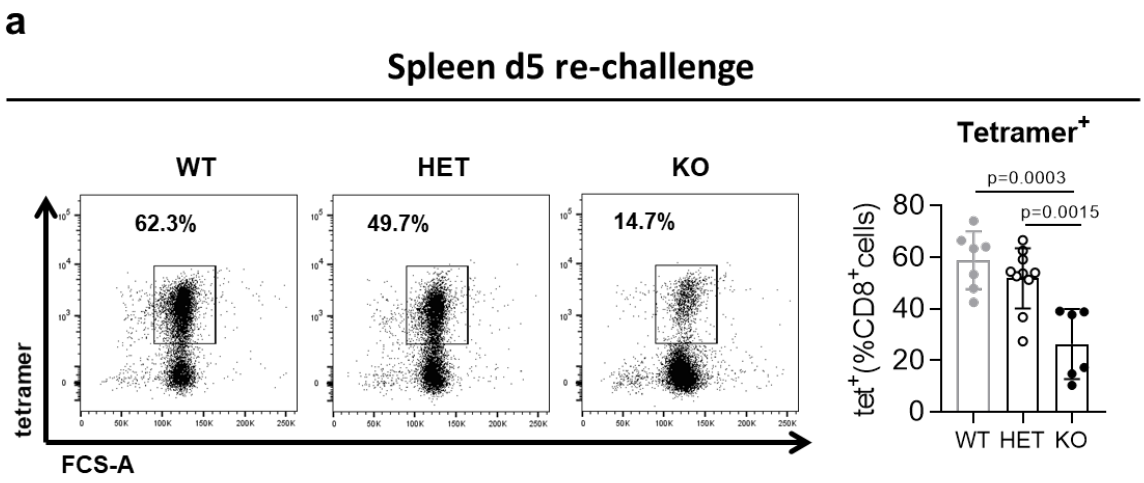

Figure 5.5.4: Defective secondary immune response in the spleen and the lymph nodes of GzmB$^{Pik3c3\Delta21}$ mice.

Representative flow cytometry plots and bar graph showing the percentage of tetramer⁺ CD8⁺ T cells recovered for the spleen (**a**) and the lymph node (**b**) five days after secondary infection of *GzmB*$^{YFP\text{-}Cre}$ *Pik3c3*^{wt} (WT), *GzmB*$^{YFP\text{-}Cre}$ *Pik3c3*$^{fl/wt}$ (HET), and *GzmB*$^{YFP\text{-}Cre}$ *Pik3c3*$^{fl/fl}$ mice (KO) with 5x10^6 CFU Lm-OVA; *n* = 6 – 7 per group. Results are representative of two independent experiments. *n* = 9 per group. Statistical significance was determined using a one-way ANOVA followed by a Tukey's post-hoc test. Results are pooled from two independent experiments.

5.2.6 VPS34 activity within CD8⁺ T cell populations impairs bacterial clearance by innate immunity

The reduced primary and recall T cell response in *GzmB*$^{YFP\text{-}Cre}$ *Pik3c3*$^{fl/fl}$ mice could be the consequence of impaired signalling within CD8⁺ T cells or due to factors extrinsic to the responding T cells, such as differences in bacterial load, antigen presentation, or cytokine production by macrophages and dendritic cells and/or paracrine help from other responding or bystander T cell populations. To assess whether *GzmB*-driven deletion of VPS34 is affecting the innate immune response, I infected wild-type and *GzmB*$^{YFP\text{-}Cre}$ *Pik3c3*$^{fl/fl}$ mice with a virulent strain (still expressing the ActA protein) of Lm-OVA ($5x10^4$ CFUs) and measured CFUs in the liver and the spleen 48h after infection.

I found the counts to be significantly increased in the spleen but not in the liver of *GzmB*$^{YFP\text{-}Cre}$ *Pik3c3*$^{fl/fl}$ mice (**Fig. 5.6 a** and **b**, respectively). Because *Listeria* clearance happens before *Listeria*-specific CD8⁺ T cells can be detected, these findings suggest that bacterial clearance by the innate immune system is slightly impaired by VPS34 deletion. Since NK cells also express *Granzyme B*, VPS34 is also being deleted in these cells, thereby possibly affecting the ability of these cells to clear infected cells.

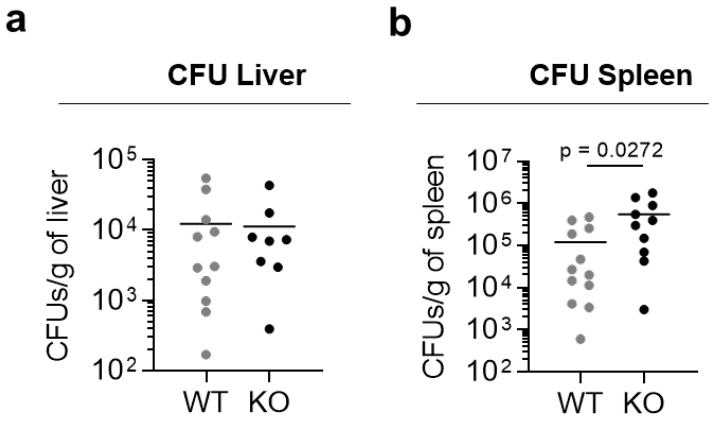

Figure 5.6: Reduced bacteria clearance in *GzmB*$^{YFP\text{-}Cre}$ *Pik3c3*$^{fl/fl}$ mice.
GzmB$^{YFP\text{-}Cre}$ *Pik3c3*^{wt} (WT) and *GzmB*$^{YFP\text{-}Cre}$ *Pik3c3*$^{fl/fl}$ mice (KO) were infected with a virulent *Listeria* strain ($5x10^4$ CFUs). Colony forming units (CFUs) recovered from the liver (a) and the spleen (b) were enumerated 48h after infection. *n* = 8 – 11 per group. Statistical significance was determined using a one-way ANOVA. Results are pooled from two independent experiments.

5.2.7 Short-lived effector cells from the spleen are affected by VPS34-deletion in GzmB$^{YFP\text{-}Cre}$ Pik3c3$^{fl/fl}$ *mice*

During the primary immune response, responding CD8$^+$ T cells can be classified as *short-lived effector cells* (SLECs) or as *memory precursor effector cells* (MPECs) based on the differential expression of KLRG1 and CD127 (41). SLECs (KLRG1^{high}, CD127^{low}) are responsible for the immediate clearance of bacteria and most die following resolution of the infection. Some of the MPECs (KLRG1^{low}, CD127^{high}), in contrast, form long-lived memory T cells. At the peak of the primary infection, the numbers of SLECs and MPECS in the blood and the lymph nodes were similar in WT, heterozygous *GzmB*$^{YFP\text{-}Cre}$ *Pik3c3*$^{fl/wt}$ and *GzmB*$^{YFP\text{-}Cre}$ *Pik3c3*$^{fl/fl}$ mice 7 days following infection (**Fig. 5.7.1 a** and **b**, respectively). In the spleen, the percentage of SLECs was slightly but insignificantly decreased while the percentage of MPECs was unchanged in *GzmB*$^{YFP\text{-}Cre}$ *Pik3c3*$^{fl/fl}$ mice (**Fig. 5.7.1 c - e**, respectively). During the secondary response, the proportions of SPECs and MPECs were unchanged in the spleen and lymph nodes for wild-type, heterozygous *GzmB*$^{YFP\text{-}Cre}$ *Pik3c3*$^{fl/wt}$ and *GzmB*$^{YFP\text{-}Cre}$ *Pik3c3*$^{fl/fl}$ mice (**Fig. 5.7.2 a – e**, respectively).

T cell activation leads to the expression of activation markers such as CD44 and the downregulation of CD62L, which facilitates the trafficking of T cells to the lymph nodes. Consistent with normal proportions of SLECs, *Pik3c3*$^{\Delta 21}$ Tet$^+$ CD8$^+$ T cells in the lymph nodes expressed similar levels of CD44 compared to wild type CD8$^+$ T cells 7 days post infection and 5 days after re-challenge (**Fig. 5.7.2 f and g,** respectively).

Together, these results suggest that inhibition of VPS34 in activated CD8$^+$ T cells preferentially impairs the generation of antigen-specific cells without having a strong impact on the generation of memory T cells.

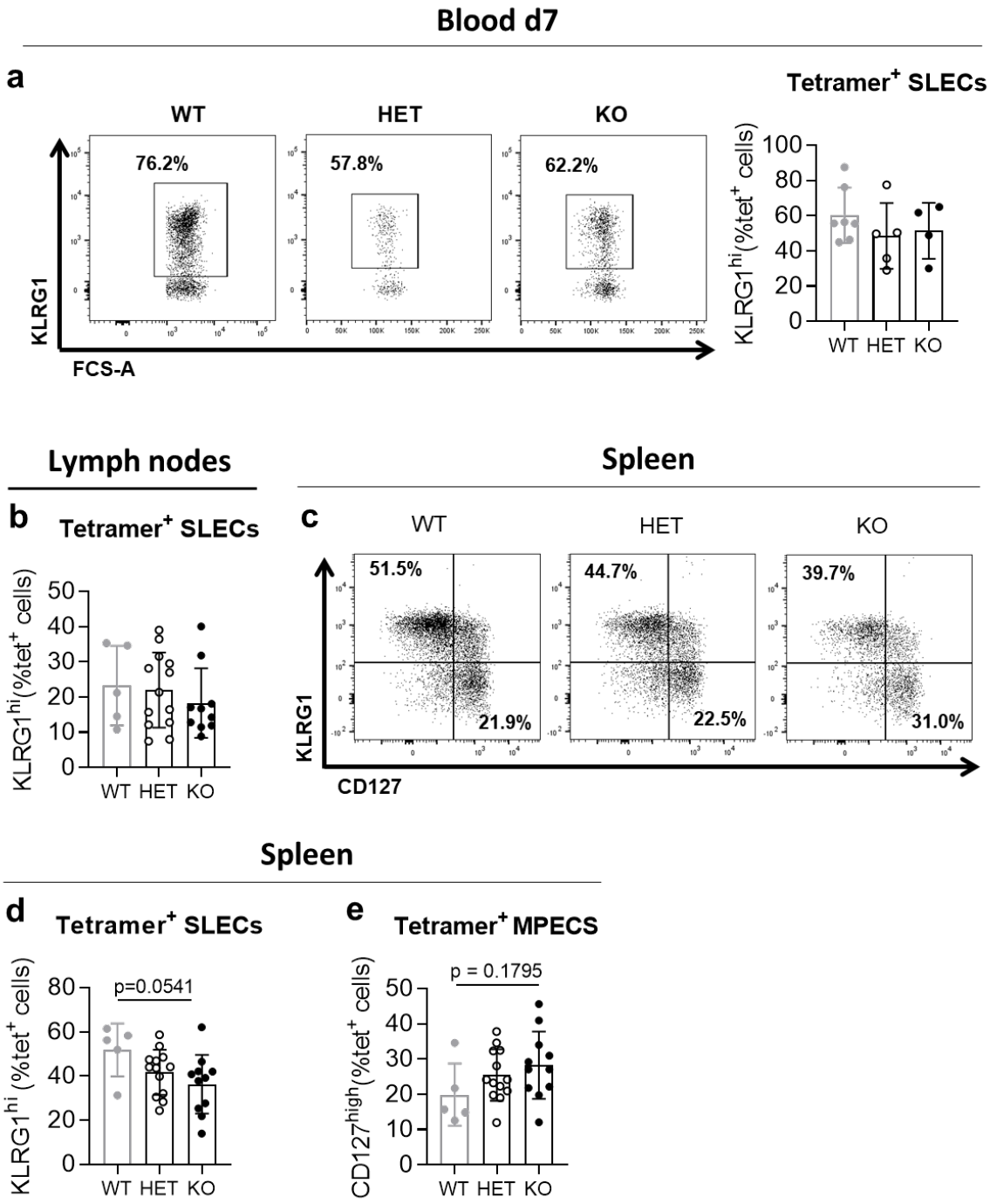

Figure 5.7.1: Intact formation of memory T cells in GzmB$^{Pik3c3\Delta21}$ mice during the primary response.
(**a**) Representative flow cytometry plots and graphical representation showing KLRG1 expression on tetramer⁺ CD8⁺ T cells isolated from the blood of *GzmB*$^{YFP\text{-}Cre}$ *Pik3c3*^{wt} (WT), *GzmB*$^{YFP\text{-}Cre}$ *Pik3c3*$^{fl/wt}$ (HET), and *GzmB*$^{YFP\text{-}Cre}$ *Pik3c3*$^{fl/fl}$ mice (KO) 7 days after the primary infection with Lm-OVA.
(**b**) Graphical representation of CD127^{low} KLRG1^{high} SLECs in the lymph node 7 days after infection.
(**c**) Representative flow cytometry plots and graphical representation showing CD127 and KLRG1 expression on tetramer⁺ CD8⁺ T cells isolated from the spleem of *GzmB*$^{YFP\text{-}Cre}$ *Pik3c3*^{wt} (WT), *GzmB*$^{YFP\text{-}Cre}$ *Pik3c3*$^{fl/wt}$ (HET), and *GzmB*$^{YFP\text{-}Cre}$ *Pik3c3*$^{fl/fl}$ mice (KO) 7 days after the primary infection with Lm-OVA. *n* = 5 – 13 per group. Results are representative of two independent experiments. Statistical

significance was determined using a one-way ANOVA followed by a Tukey's post-hoc test. Results are pooled from two independent experiments.

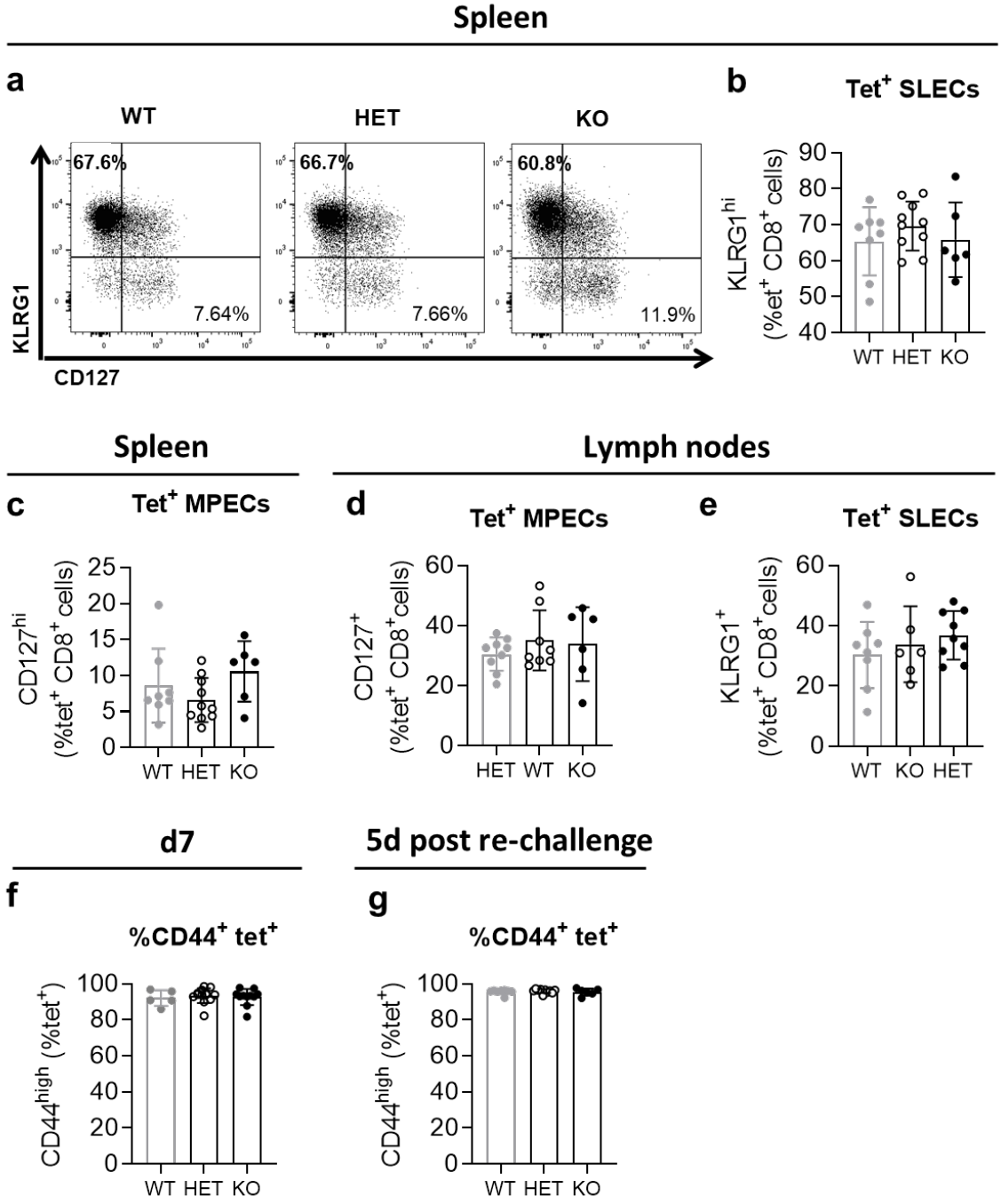

Figure 5.7.2: Intact formation of memory T cells in GzmB$^{Pik3c3\Delta21}$ mice during the secondary response.
(**a**) Representative flow cytometry plots and graphical representation showing CD127 and KLRG1 expression on tetramer⁺ CD8⁺ T cells isolated from the spleen of *GzmB*$^{YFP\text{-}Cre}$ *Pik3c3*^{wt} (WT), *GzmB*$^{YFP\text{-}Cre}$ *Pik3c3*$^{fl/wt}$ (HET), and *GzmB*$^{YFP\text{-}Cre}$ *Pik3c3*$^{fl/fl}$ mice (KO) 5 days after re-infection with Lm-OVA.
(**b – c**) Graphical representation of CD127^{low} KLRG1^{high} SLECs (**b**) and CD127^{high} KLRG1^{low} MPECs in the spleen 5 days after re-infection (**c**).

(**d – e**) Graphical representation of CD127^{high} KLRG1^{low} MPECs (**d**) and CD127^{low} KLRG1^{high} SLECs in the lymph nodes 5 days after re-infection (**e**).
(**f – g**) Graphical representation of CD44^{high} tetramer+ CD8+ T cells in the spleen eight days after the primary infection (**f**) and 5 days after re-infection (**g**).
n = 5 – 13 per group. Results are representative of two independent experiments. *n* = 9 per group. Statistical significance was determined using a one-way ANOVA followed by a Tukey's post-hoc test.

5.2.8 Pik3c3$^{\Delta 21}$ *CD8$^+$ T cells responding to* Listeria *infection express reduced amounts of cytokines, LAMP-1, and GzmB*

An important function of CD8$^+$ T cells is the ability to produce the antiviral cytokines *interferon-γ* (IFN-γ) and *tumour-necrosis factor-α* (TNF-α). *Ex vivo* stimulation of splenocytes at the peak of the primary immune response, i.e. 7 days after infection, and 5 days after re-infection, using OVA-peptides indicated a reduced ability of *Pik3c3$^{\Delta 21}$* CD8$^+$ T cells to produce these cytokines (**Fig. 5.8.1 a – c,** and **Fig. 5.8.2 a – c, respectively)**. Interestingly, the production of Granzyme B was significantly reduced at the peak of the primary immune response (7 days after the first challenge), but unchanged in *Pik3c3$^{\Delta 21}$* CD8$^+$ T cells after subsequent challenge (5 days after re-infection) (**Fig. 5.8.3 a** and **b,** respectively).

Based on the role of VPS34 in endocytosis and vesicle trafficking, I investigated the cell surface expression of LAMP-1, a marker of vesicle release. After *ex vivo* stimulation of splenocytes, the level of LAMP-1 (CD107a) was reduced by half in *Pik3c3$^{\Delta 21}$* CD8$^+$ T cells at the peak of the primary infection, whereas only slightly reduced after re-challenge (**Fig. 5.8.3 c** and **d**, respectively). Of note, results about CD107a expression after re-challenge would require an increase in the group size in order to make a definite conclusion.

Together, these results suggest that VPS34-kinase activity is critical for effector functions of activated CD8$^+$ T cells during both the primary and the secondary immune response. Levels of cytokine production and cell surface CD107a expression were reduced, suggesting that the lack of VPS34 kinase activity impairs the production of effector cytokines and the formation/release of vesicles possibly containing these effector cytokines.

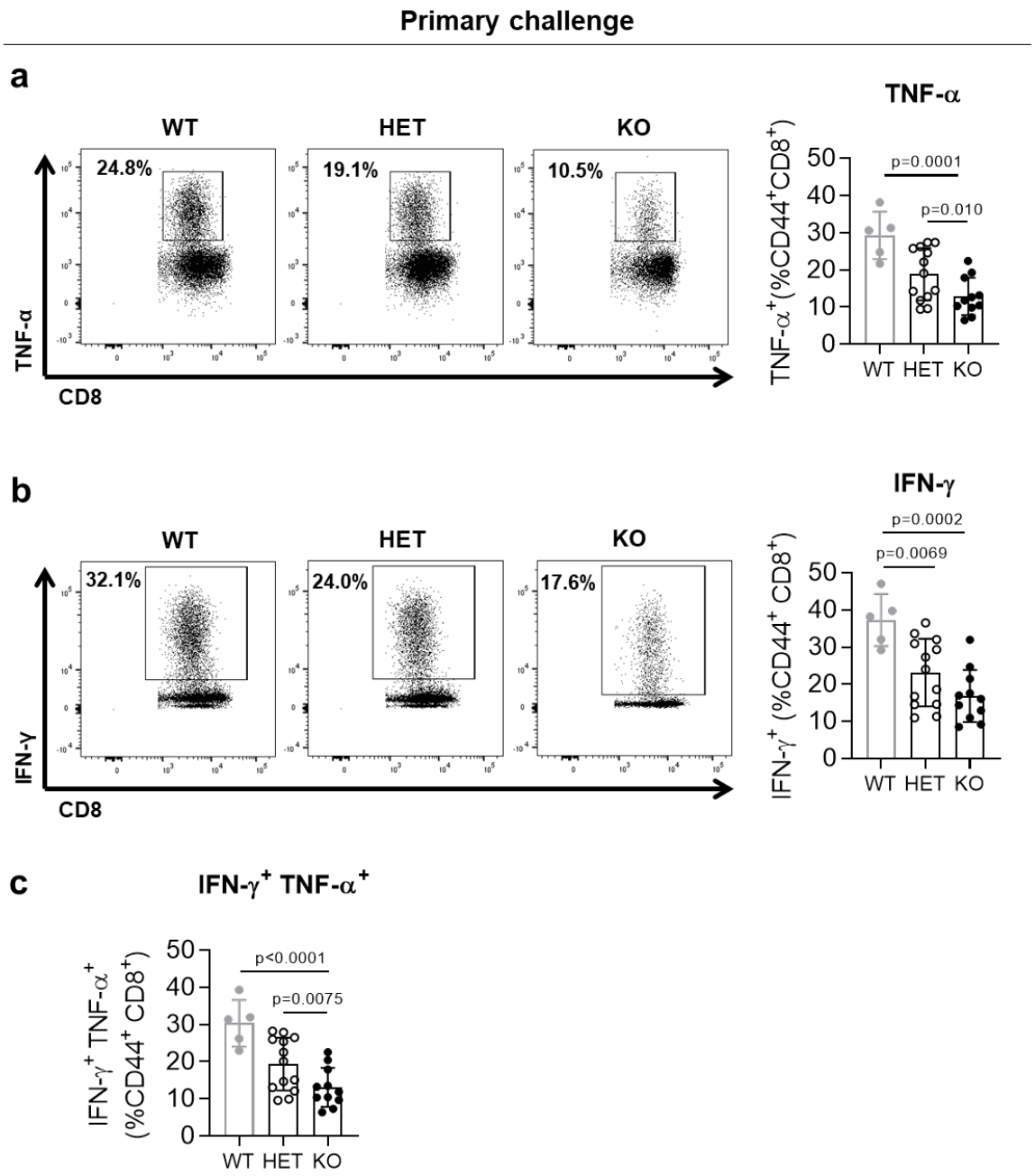

Figure 5.8.1: Cytokine production is reduced in *GzmB*$^{YFP\text{-}Cre}$ *Pik3c3*$^{fl/fl}$ mice during the primary immune response.

(**a – c**) Representative flow cytometry plots and graphical representation showing TFN-α (**a**), IFN-γ (**b**) and double positive TFN-α IFN-γ (**c**) CD44⁺ CD8⁺ T cells isolated from the spleen of *GzmB*$^{YFP\text{-}Cre}$ *Pik3c3*^{wt} (WT), *GzmB*$^{YFP\text{-}Cre}$ *Pik3c3*$^{fl/wt}$ (HET), and *GzmB*$^{YFP\text{-}Cre}$ *Pik3c3*$^{fl/fl}$ mice (KO) 8 days after infection with Lm-OVA. *n* = 5 – 13 per group. Results are representative of two independent experiments. *n* = 9 per group. Statistical significance was determined using a one-way ANOVA followed by a Tukey's post-hoc test. Results are pooled from two independent experiments.

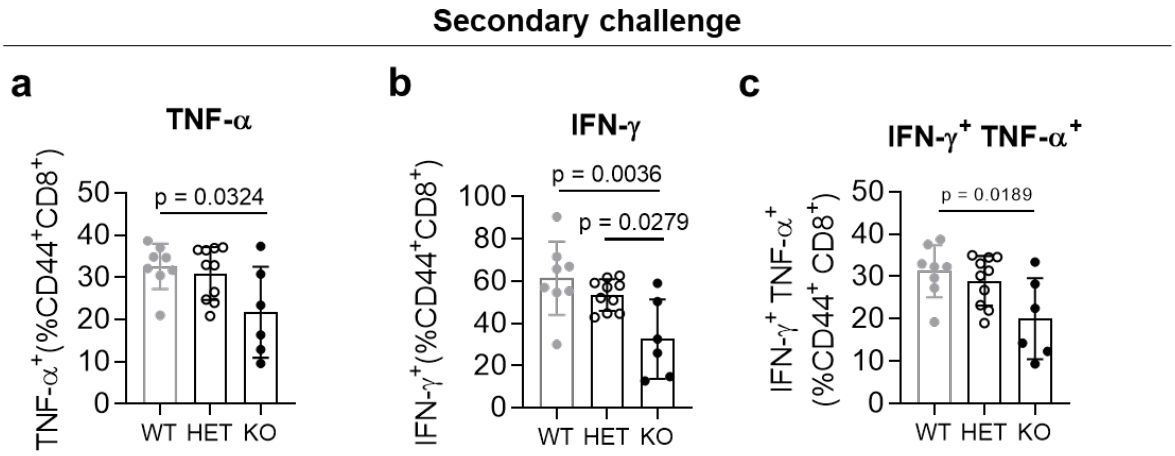

Figure 5.8.2: Cytokine production is reduced in *GzmB*$^{YFP\text{-}Cre}$ *Pik3c3*$^{fl/fl}$ mice during the secondary response.

(**a – c**) Representative flow cytometry plots and graphical representation showing TFN-α (**a**), IFN-γ (**b**) and double positive TFN-α IFN-γ (**c**) CD44⁺ CD8⁺ T cells isolated from the spleen of *GzmB*$^{YFP\text{-}Cre}$ *Pik3c3*^{wt} (WT), *GzmB*$^{YFP\text{-}Cre}$ *Pik3c3*$^{fl/wt}$ (HET), and *GzmB*$^{YFP\text{-}Cre}$ *Pik3c3*$^{fl/fl}$ mice (KO) 5 days after re-infection with Lm-OVA. *n* = 7 – 10 per group. Results are representative of two independent experiments. *n* = 9 per group. Statistical significance was determined using a one-way ANOVA followed by a Tukey's post-hoc test. Results are pooled from two independent experiments.

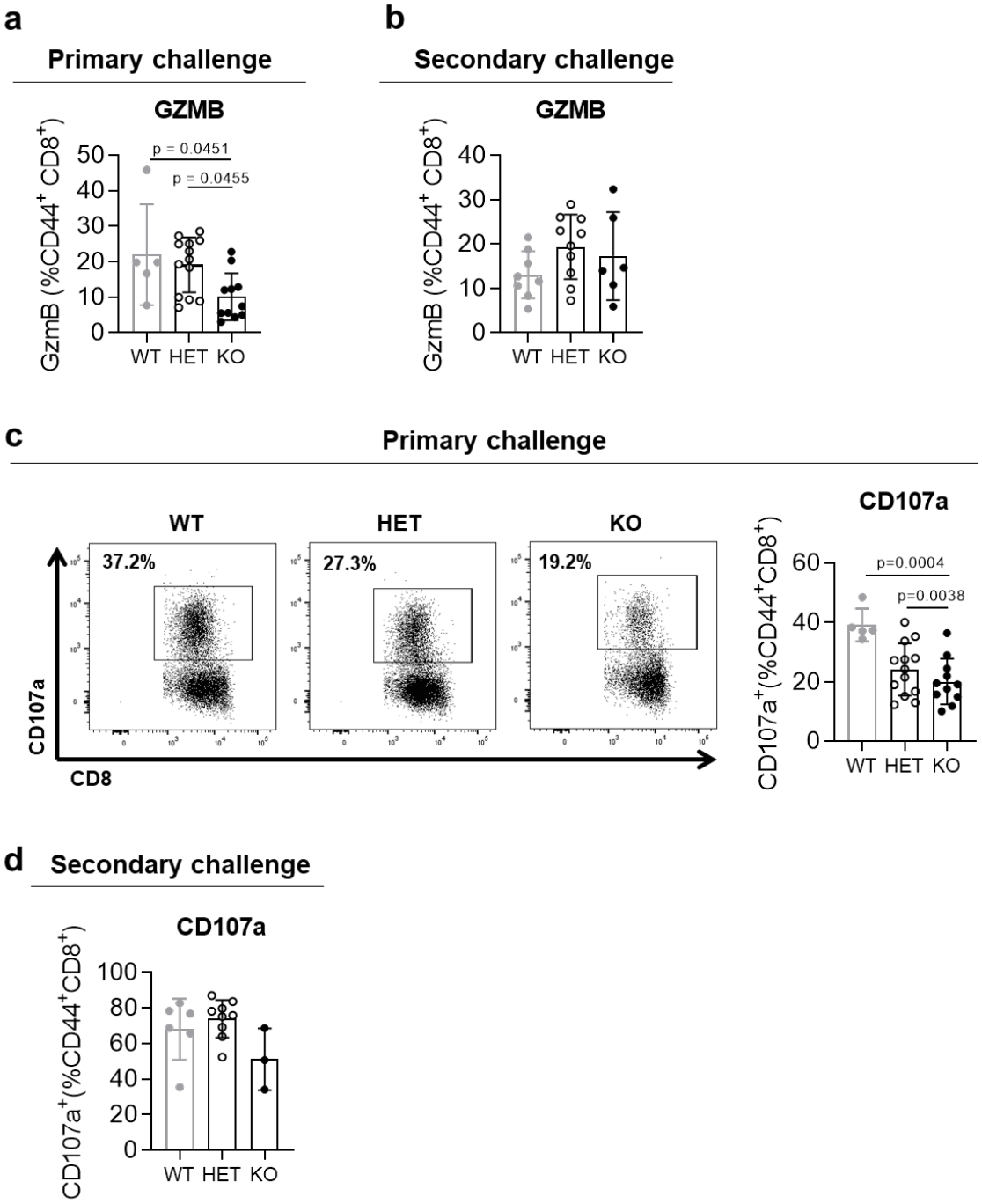

Figure 5.8.3: Granzyme B and LAMP1 are reduced in *GzmB*$^{YFP\text{-}Cre}$ *Pik3c3*$^{fl/fl}$ mice during the primary but not the secondary response.

(**a – b**) Graphical representation of Granzyme B production in CD44⁺ CD8⁺ T cells isolated from the spleen of *GzmB*$^{YFP\text{-}Cre}$ *Pik3c3*^{wt} (WT), *GzmB*$^{YFP\text{-}Cre}$ *Pik3c3*$^{fl/wt}$ (HET), and *GzmB*$^{YFP\text{-}Cre}$ *Pik3c3*$^{fl/fl}$ mice (KO) 7 days after the primary infection (**a**) and 5 days after re-infection (**b**) with Lm-OVA.

(**c – d**) Representative flow cytometry plots and graphical representation of LAMP1 (CD107a) expression on CD44⁺ CD8⁺ T cells isolated from the spleen of *GzmB*$^{YFP\text{-}Cre}$ *Pik3c3*^{wt} (WT), *GzmB*$^{YFP\text{-}Cre}$ *Pik3c3*$^{fl/wt}$ (HET), and *GzmB*$^{YFP\text{-}Cre}$ *Pik3c3*$^{fl/fl}$ mice (KO) 7 days after the primary infection (**c**) and 5 days after re-infection (**d**) with Lm-OVA. Representative flow cytometry plots and n = 5 – 13 per group. Results are representative of two independent experiments. n = 9 per group. Statistical significance

was determined using a one-way ANOVA followed by a Tukey's post-hoc. Results are pooled from two independent experiments.

5.2.9 Mice with Pik3c3$^{\Delta 21}$ *CD8$^+$ T cells have increased tumour growth*

The immune system responds to intracellular bacterial pathogens (such as *Listeria monocytogenes*) and cancer in a similar way. Antigen-specific CD8$^+$ T cells recognize antigens presented in the context of MHC class I and eliminate malignant cells (expressing neo-antigens) or infected cells (expressing pathogen antigens) by direct cytotoxicity.

The reduced proportions of tetramer-positive CD8$^+$ T cells in infection studies with *Listeria*, along with the reduced proportions of cells undergoing mitosis prone me to further explore the effect of VPS34-deficiency using another model, i.e. I inoculated mice subcutaneously with the murine melanoma cell line B78ChOVA-mCherry. B78ChOVA-mCherry is derived from the amelanotic clone B16.F10, but has been genetically engineered to express the mCherry reporter and OVA.

I injected *GzmB*$^{YFP\text{-}Cre}$ *Pik3c3*$^{fl/fl}$, heterozygous *GzmB*$^{YFP\text{-}Cre}$ *Pik3c3*$^{fl/wt}$ and wild-type control mice sub. cut. in the right flank with 1.5 x 10^5 B78ChOVA-mCherry tumour cells and measured the tumour growth until day 28 post-inoculation or when human endpoint was reached. Only half of the mice developed tumours and I am currently working on the optimization of the cell culturing and inoculation protocol. From the mice that developed tumours, I observed rapid tumour growth from day 14 onwards and by day 28, two *GzmB*$^{YFP\text{-}Cre}$ *Pik3c3*$^{fl/fl}$ mice had developed tumours four times bigger than the only wild-type mouse that had developed a tumour. From the three heterozygous *GzmB*$^{YFP\text{-}Cre}$ *Pik3c3*$^{fl/wt}$ mice that had developed tumours, two displayed a tumour growth curve similar to the wild-type mouse, while the third followed the growth curve of tumours from knock-out *GzmB*$^{YFP\text{-}Cre}$ *Pik3c3*$^{fl/fl}$ mice (**Fig. 5.9.1 a**).

Because only half of the mice developed tumours, I injected a second cohort of *GzmB*$^{YFP\text{-}Cre}$ *Pik3c3*$^{fl/fl}$, *GzmB*$^{YFP\text{-}Cre}$ *Pik3c3*$^{fl/w}$ and wild-type mice, this time with 5 x 10^5 B78ChOVA-mCherry tumour cells. Nine from eleven mice developed tumours. The weights of the tumours harvested at the end of the second experiment on day 13 were variable among the different genotypes, but there was a trend towards bigger tumours in *GzmB*$^{YFP\text{-}Cre}$

Pik3c3$^{fl/fl}$ mice compared to wild-type control mice (**Fig. 5.9.1 b**). Of note, the tumour volume deduced from the measurements of the tumours with a calliper (calculated as mm^3 = ½(a*b*(a+b)/2, where a was the length and b the width) correlated with the actual mass of the tumours (tumours where weighted after harvesting) (**Fig. 5.9.1 c**), validating our method to determine tumour size.

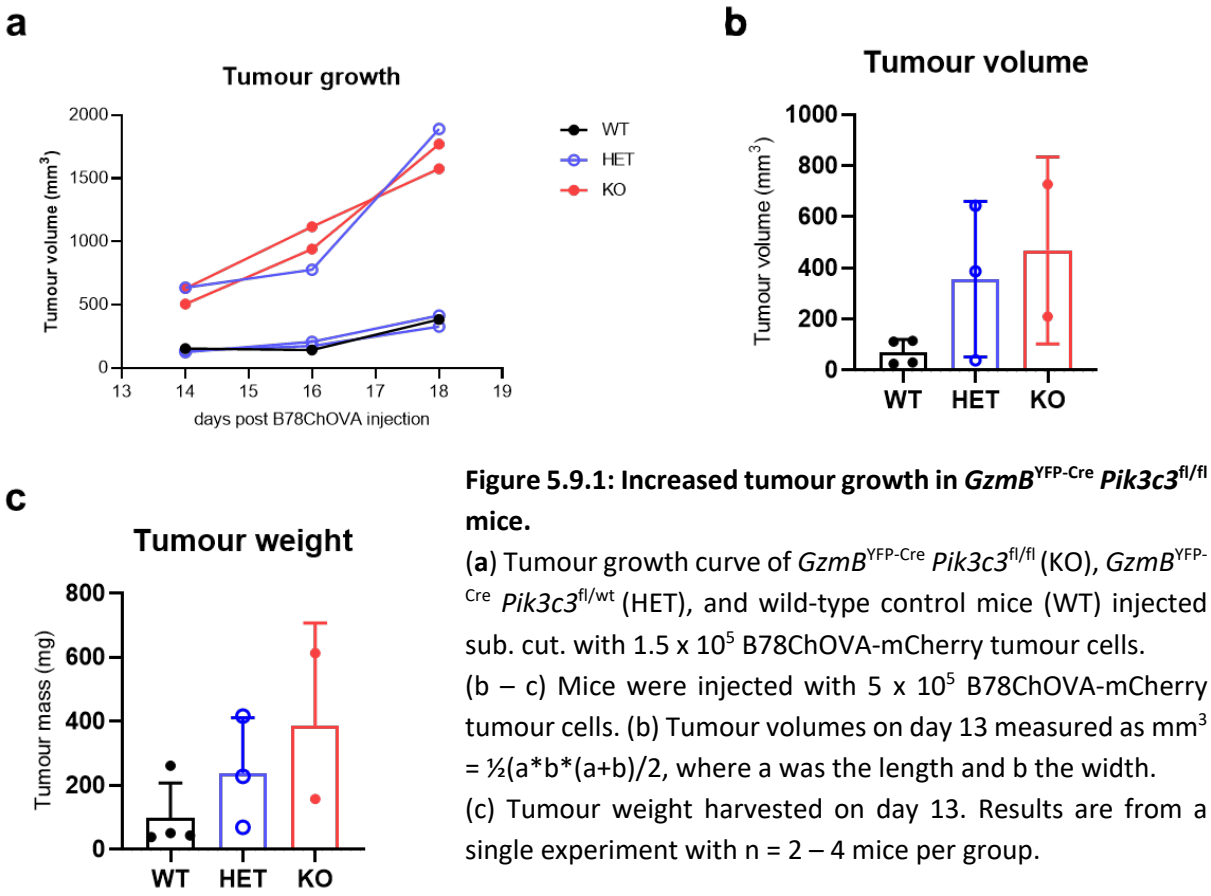

Figure 5.9.1: Increased tumour growth in *GzmB*$^{YFP\text{-}Cre}$ *Pik3c3*$^{fl/fl}$ mice.
(**a**) Tumour growth curve of *GzmB*$^{YFP\text{-}Cre}$ *Pik3c3*$^{fl/fl}$ (KO), *GzmB*$^{YFP\text{-}Cre}$ *Pik3c3*$^{fl/wt}$ (HET), and wild-type control mice (WT) injected sub. cut. with 1.5 x 10^5 B78ChOVA-mCherry tumour cells.
(b – c) Mice were injected with 5 x 10^5 B78ChOVA-mCherry tumour cells. (b) Tumour volumes on day 13 measured as mm^3 = ½(a*b*(a+b)/2, where a was the length and b the width.
(c) Tumour weight harvested on day 13. Results are from a single experiment with n = 2 – 4 mice per group.

I performed a simple functional analysis of the infiltrating CD8⁺ T cell, assaying for the expression of antigen-specific CD8⁺ T cells (**Fig. 5.9.2 a**), YFP⁺ cells amongst CD8⁺ cells (**Fig. 5.9.2 b**), TNF-α production (**Fig. 5.9.2 c**), and PD-1 expression (**Fig. 5.9.2 d**). None of the analysed markers were significantly different in *Pik3c3*$^{\Delta 21}$ compared to wild-type CD8⁺ T cells, solely a trend towards decrease expression of PD-1 was detectable for *Pik3c3*$^{\Delta 21}$ CD8⁺ T cells. I also analysed the expression of other markers and cytokines, such as CD184 (CXCR-4), IFN-γ, CD103, CD127, KLRG1, and the transcription factors T-bet and Eomes, but did not obtain any results for those markers due to technical issues.

I used Annexin V to assess apoptosis. *Pik3c3*$^{\Delta 21}$ CD8⁺ T cells displayed a trend towards increase Annexin V staining (**Fig. 5.9.2 e**), however the percentage of cells staining for both

Annexin V and the viability dye was similar between *Pik3c3*$^{\Delta 21}$ and wild-type CD8⁺ T cells (**Fig. 5.9.2 f**). These results are obtained from one single experiment and while the experiment has to be repeated to examine a greater number of mice, these initial results lend support to the conclusions drawn from *Listeria* infection studies, i.e. that loss of VPS34-kinase activity in CD8⁺ T cells affects the effector phase of CD8⁺ T cells, leading to less antigen-specific CD8⁺ T cells with reduced effector functions (in *Listeria* infection studies) or reduced tumour control (in B78ChOVA-mCherry tumour studies).

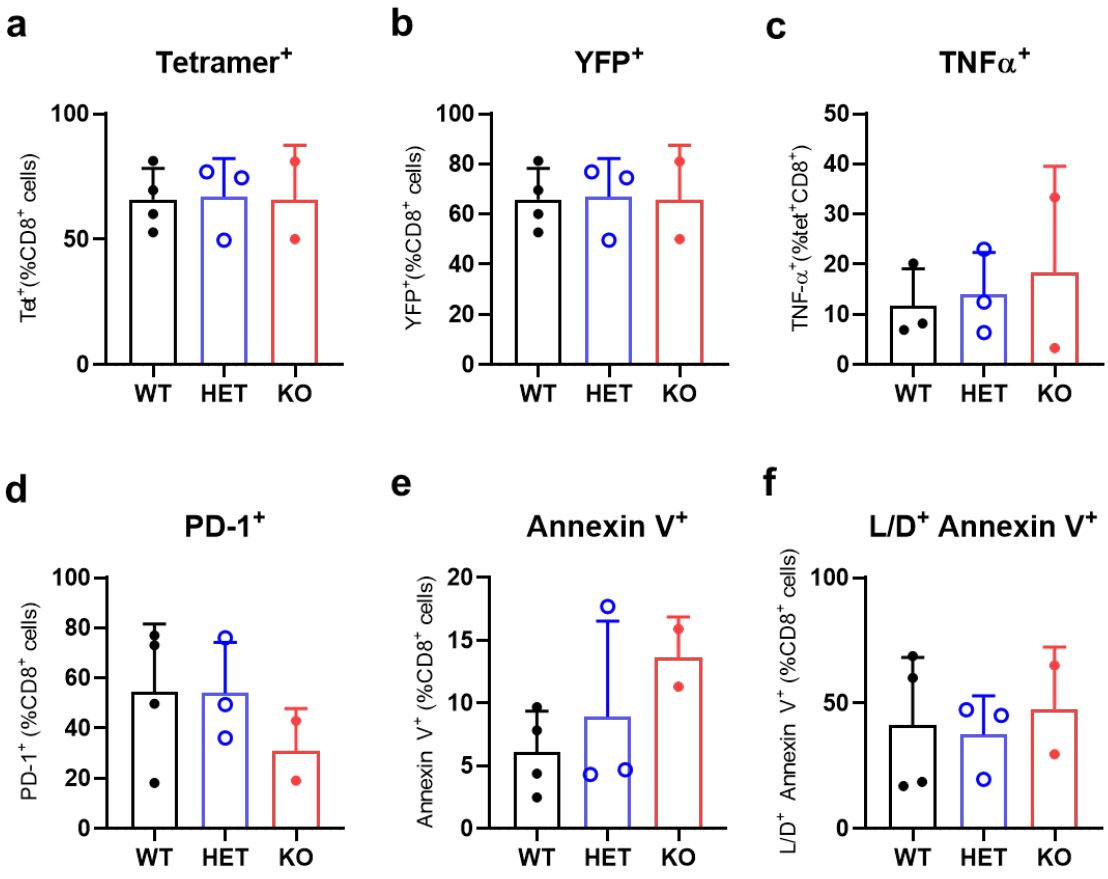

Figure 5.9.2: Flow cytometric analysis of B78ChOVA-mCherry – infiltrating lymphocytes.
Mice were injected with 5 x 10^5 B78ChOVA-mCherry tumour cells and tumours harvested on day 13. Flow cytometric analyses of antigen-specific CD8⁺ T cells (a), YFP⁺ CD8⁺ T cells (b), TNF-α production after restimulation with PdbU/Ionomycin for 5.5h (c), PD-1+ CD8+ T cells (d), and of the apoptosis marker Annexin V and the viability dye (L/D) (e-f). Results are from a single experiment with n = 2 – 4 mice per group.

5.3 Discussion

So far, the role of VPS34 has been investigated in CD4$^+$ T cells by Willinger and Flavell, Mcleod et *al*., and Parekh et *al*. [227], [228], [254] and in Treg cells by Elisabeth, Priya, and me. However, its role in activated CD8$^+$ T cells has so far not been, to my knowledge, a matter of investigation. Here, I describe for the first time the effects of VPS34-kinase activity loss on CD8$^+$ T cell functions and memory formation.

The importance of intact autophagy for CD8$^+$ T cells has been previously demonstrated using a mouse model lacking the gene encoding for either the autophagy-related molecules Atg7 or Atg5 specifically in CD8$^+$ T cells [219], [223]. While *Atg7* or *Atg5*-deletion had little effects on the proliferation and effector functions, these cells displayed a survival defect and a compromised memory formation [219]. In light of the involvement of VPS34 in endocytosis and autophagy, it is of great interest to investigate whether VPS34-deletion in antigen-specific CD8$^+$ T cells results in a similar phenotype. For this mean, I used the same Granzyme B-Cre system as used by Xu et *al*. [219], in which naïve CD8$^+$ T cells develop normally and VPS34 is deleted only after CD8$^+$ T cell activation.

In line with my expectations, naïve CD8$^+$ T cells developed normally and the phenotype of unchallenged GzmB$^{Cre\text{-}eYFP}$ *Pik3c3*$^{fl/fl}$ mice was similar to wild-type mice; the proportion of key immune cell populations and the activation status of CD8$^+$ T cells in Cre-positive mice were comparable to Cre-negative mice.

5.3.1 Unchallenged GzmB$^{YFP\text{-}Cre}$ Pik3c3$^{fl/fl}$ *mice are phenotypically similar to wild-type mice*

Unchallenged GzmB$^{YFP\text{-}Cre}$ Pik3c3$^{fl/fl}$ *mice* developed normally and had normal ratio of CD4$^+$ T cells, CD8$^+$ T cells, B cells, and NK cells. The Cre-recombinase being expressed under the *Granzyme B* promoter, VPS34-kinase activity is abrogated only in cells expressing Granzyme B, hence activated CD8$^+$ T cells and NK cells. Flow cytometric analyses of naïve *GzmB*$^{YFP\text{-}Cre}$ *Pik3c3*$^{fl/fl}$ mice showed that indeed, 95% of CD8$^+$ T cells were YFP$^-$. Surprisingly, only 5% of NK cells were positive for YFP, while I assumed that GzmB is constitutively expressed in those cells. It is known that certain fixation/permeabilisation methods used for the staining of intracellular markers affects YFP fluorescence, possibly explaining the low proportion of YFP$^+$

NK cells. Immune phenotyping of naïve *GzmB*$^{YFP\text{-}Cre}$ *Pik3c3*$^{fl/fl}$ mice will have to be repeated while leaving out fixation/permeabilisation of the cells.

Other than CD8$^+$ T cells, CD4$^+$ T cells and B cells had a minimal expression of YFP. This suggests that the Cre-recombinase is active in those cells, either because these cells transiently express the Cre-recombinase during early development (referred to as 'ectopic' expression [306]) or because indeed a small subset of CD4$^+$ T cells [307] and B cells [308] express Granzyme B. However, since the percentage of YFP$^+$ cells was relatively low (5%), hence the percentage of Cre$^+$ cells, I concluded that VPS34-kinase activity is preserved in the majority of lymphocytes in unchallenged mice.

5.3.2 In vitro activated Pik3c3$^{\Delta 21}$ *CD8$^+$ T are similar to wild-type CD8$^+$ T cells*

I supplemented results from *in vivo* studies with *in vitro* assays using bulk-activated CD8$^+$ T cells to gather mechanistic information regarding cell cycle assay, proliferation potential and cell death. *In vitro* stimulation with αCD3 and αCD28 for 48h followed by expansion in recombinant human IL-2 up to five more days is a frequently used method to activate T cells *in vitro* allowing to harvest large numbers of the desired cell population.

In vitro bulk-activated CD8$^+$ T cells from *GzmB*$^{YFP\text{-}Cre}$ *Pik3c3*$^{fl/fl}$ mice were phenotypically similar to CD8$^+$ T cells from wild-type mice in regards to the activation marker CD44, CD103 and PD-1 as well as the expression of the transcription factors T-bet, Eomes and Granzyme B. The only difference was an increase in the production of the cytokine IFN-γ. This might stay in contrast to the unchanged expression of T-bet, as it has been previously observed that T-bet regulates IFN-γ to some extent [80]. However, I have to acknowledge that the *in vitro* conditions might not have been robust enough to ensure efficient deletion of VPS34 in most of the CD8$^+$ T cells. This issue will have to be addressed in future experimental settings.

5.3.3 Loss of VPS34-kinase activity leads to reduced antigen-specific CD8$^+$ T cells with impaired effector functions

Listeria infection is a mouse model widely used to study both the innate and the adaptive immune system. Since *Listeria* replicates within cells and move from cell to cell without being

exposed to antibodies, the cell-mediated immunity is key for the clearance of the bacteria [309]. Fifteen minutes following intravenous injection of *Listeria* into a mouse, 60% can be found within the liver while 40% are found in the spleen [310]–[312]. The bacterial load increases in those organs until it reaches a peak at 2 to 3 days post infection. In the spleen, the detection and the uptake of the bacteria is taking place in the marginal zone by $CD8^+$ *dendritic cells* (DCs) [313], [314]. One to two days after infection with *Listeria*, T cell activation is initiated by the presentation of processed bacterial peptides. Although the innate immunity is ultimately required for the clearance of the infection, the adaptive immune response is necessary to avoid chronic infection (or to achieve sterile immunity) [315]. While $CD4^+$ T cells control the infection through the release of IFN-γ, $CD8^+$ T cells are the main contributors to long-term protective immunity to *Listeria monocytogenes*; hence *Listeria* is a suitable model to study $CD8^+$ T cell responses.

In this study, I aimed to assess the role of VPS34 at distinct stages of the $CD8^+$ T cell response: at the peak of expansion (day 8 after infection, when effector $CD8^+$ T cells stop to proliferate); during the contraction phase (day 14 and 21 after infection); and the memory phase (day 30 after infection).

Upon infection with *Lm*-OVA, $CD8^+$ T cells from $GzmB^{Cre\text{-}YFP}$ $Pik3c3^{fl/fl}$ mice showed a reduced capacity to respond to the infection. At the peak of the immune response, the percentage of antigen-specific $CD8^+$ T cells was reduced. Meanwhile, the proportions *of short-lived effector cells* (SLECs) and *memory precursor effector cells* (MPECs) were comparable between VPS34-deficient and -sufficient $CD8^+$ T cells.

Memory $CD8^+$ T cells provide protection against re-infection with the same pathogen and contribute to the long-term control of chronic infection, such as during infection with herpes viruses or hepatitis viruses [114]. Memory cells allow the organism to respond to re-infection by mounting an immune response which is faster and higher than the primary immune response. Memory formation involves cellular and metabolic reprogramming and is dependent of catabolic processes that mediate the reduction in cell size and cell numbers. In accordance with that, autophagy is crucial for memory formation [219]. To investigate whether CTLs are also dependent on VPS34 kinase activity for memory formation, I re-infected $GzmB^{Cre\text{-}YFP}$ $Pik3c3^{fl/fl}$ mice with *Lm*-OVA thirty days after the primary infection.

In line with the reduced level of antigen-specific CD8$^+$ T cells during the primary infection, the percentage of antigen-specific CTLs during the secondary response was similarly decreased in the spleen. The unchanged proportions of MPECs and SLECs during the primary response suggested that the pool of memory cells is unaffected by VPS34-deletion and that reduced levels of OVA-specific CD8$^+$ T cells during the secondary immune response was due to impaired survival or proliferation of effector cells rather than a defective memory formation. However, these observations were against the expectation that, since VPS34 is involved in autophagy, VPS34-deficiency would lead to an impaired CD8$^+$ T cell memory formation, as depicted for *Atg7*$^{-/-}$ or *Atg5*$^{-/-}$ CD8$^+$ T cells.

Although the percentage of SLECs was unchanged during the primary and the secondary immune responses, the production of effector molecules was significantly decreased in VPS34-deficient CTLs. The proportions of activated *Pik3c3*$^{\Delta 21}$ CD8$^+$ T cells producing IFN-γ and TNF-α was reduced in response to $OVA_{257-264}$ peptide re-stimulation *in vitro*, both seven days after the primary infection and five days after re-challenge. This suggested that loss of VPS34-kinase activity influences the effector functions of CD8$^+$ T cells. The proportion of Granzyme B-producing *Pik3c3*$^{\Delta 21}$ CD8$^+$ T cells was also reduced, further supporting the idea that VPS34-deficient CD8$^+$ T cells have an impaired effector molecule production. Furthermore, the level of LAMP-1 (CD107a) was also reduced in those cells, suggesting either a defect in vesicle trafficking or a primary reduced production of cytokines, leading to a reduced numbers of vesicles to be released.

An effect on vesicle trafficking would be in line with what is already know about the function of VPS34 [316]. Reduced levels of Lamp-1 affects the movement of lytic granules, i.e. leads to the retention of transport vesicles with lytic granules outside the lysosomal compartments in trans-Golgi network–derived transport vesicles, and results in reduced levels of perforin, but not granzyme B, in lytic granules [317]. Similarly, inhibition of the Lamp-1 binding partner *adaptor protein 1* (AP-1) sorting complex also leads to the retention of perforin in the transport vesicles. Disrupted motility and levels of perforin in lytic granules would lead to the inability to deliver Granzyme B to the target cells and therefore impairs cytotoxicity.

Furthermore, VPS34 is possibly involved in the trafficking and recycling of cell-surface receptors required for the sensing of proliferation and/or activation clues. For example, the activation of CD8$^+$ T cells depends, besides signal 1 and signal 2, on stimulation with

inflammatory cytokines including IL-12 and type I IFNs. IL-12 signalling is critical for the accumulation of antigen-specific CD8$^+$ T cells in the context of *Lm*-infection [318], [319]. Failure to sense IL-12 due to defective trafficking of IL-12 receptor to the cell surface would therefore lead to impaired CTL activation. This hypothesis could be tested by staining the IL-12Rβ2 subunit for flow cytometry and assess phosphorylation of STAT4 to test intact IL-12 signalling.

Finally, mitophagy is essential for T cell development and homeostasis [320] and data obtained from FoxP3$^{YFP\text{-}Cre}$ *Pik3c3*$^{fl/fl}$ mice suggest that loss of VPS34-kinase activity increases mitochondrial load and functions in Treg cells. During activation and differentiation of naïve cells to effector cells, CTLs undergo drastic metabolic changes relying on anabolic processes. Loss of VPS34-kinase activity might increase the number of mitochondria, which might generate high levels of energy and ROS, or alternatively, lead to the accumulation of defective mitochondria as there are not being cleared by mitophagy. In the phase of CD8$^+$ T cells and concomitant metabolic reprogramming, T cells might rely even more on appropriate energy levels and the removal of toxins and mal-functioning organelles, and failure to do so could ensue in impaired survival and/or reduced effector functions.

5.3.4 Reduced proportions of antigen-specific CD8$^+$ T cells in mice infected with **Listeria** *is probably due to a defect in cell division following antigenic stimulation*

To stimulate CD8$^+$ T cells *in vivo*, I infected mice with *Listeria* and evaluated the proportions of CD8$^+$ T cells and their phenotype in the blood, spleen and lymph nodes of *GzmB*$^{YFP\text{-}Cre}$ *Pik3c3*$^{fl/fl}$ mice. *GzmB*$^{YFP\text{-}Cre}$ *Pik3c3*$^{fl/fl}$ mice have reduced proportions of antigen-specific CD8$^+$ T cells in the blood and the spleen seven days after infection. The level of antigen-specific CD8$^+$ T cells was also reduced in the blood and the spleen five days after re-challenge of *GzmB*$^{YFP\text{-}Cre}$ *Pik3c3*$^{fl/fl}$ mice compared to wild-type mice, nevertheless, *GzmB*$^{YFP\text{-}Cre}$ *Pik3c3*$^{fl/fl}$ mice did show evidence of memory formation, as the secondary response achieved a greater peak magnitude than during the primary response.

Memory cell precursors can be identified in the effector CD8$^+$ T cell response to *Listeria* using the surface markers CD127 and KLRG1. CD127 is the alpha chain of the IL-7 receptor, and signalling through the IL7R is required for T cell survival [321]. KLRG1 is currently the best-described SLEC marker although it is recognised that it does not play a significant

role in their formation [76]. Within the pool of antigen-specific CD8$^+$ T cells in *GzmB*$^{YFP\text{-}Cre}$ *Pik3c3*$^{fl/fl}$ mice responding to *Listeria,* the proportions of CD127^{high} KLRG1^{low} MPECs and CD127^{low} KLRG1^{high} SLECs was unchanged. These results suggested that loss of VPS34 kinase activity impairs the generation or the survival rather than the activation or the memory formation of antigen-specific CD8$^+$ T cells.

Results form *in vitro* studies suggested that VPS34 is not required for the survival of activated CD8$^+$ T cells. Meanwhile, cell cycle analysis suggested that the reduced number of Tet$^+$ CD8$^+$ *Pik3c3*$^{\Delta 21}$ T cells found in mice infected with *Listeria* likely reflects the inability to undergo mitosis, i.e. an inability to undergo cell division following antigenic stimulation *in vivo*, thereby leading to a reduced number of cells going back to the G1 phase. These hypothesis is in line with the suggested role of VPS34 in cytokinesis and the results obtained for VPS34-deficient Treg cells (presented in ***Chapter 3*** and ***Chapter 4***), suggesting that loss of VPS34-kinase activity impairs cell cycle progression due to increased metabolic rate hence impaired cell proliferation. It would now be of interest to confirm a cell cycle defect in CD8$^+$ T cells activated *in vivo* (using either the *Listeria* infection model or the tumour model) as well as perform metabolic analyses to investigate whether activated CD8$^+$ T cells are metabolically more active, similar to VPS34-deficient Treg cells.

In summary, these results suggest that while VPS34 is not required for the survival of activated CD8$^+$ T cells *in vitro*, it might interfere with the capacity of activated CD8$^+$ T cells to undergo cell division, at least *in vitro.*

5.4 Chapter summary

I used a mouse model in which the Cre-recombinase is expressed under the *Granzyme B* promoter, and exon 21 of *Pik3c3* is only excised in activated CD8$^+$ T cells while the full length VPS34 protein is present in naïve CD8$^+$ T cells. I first investigated the phenotype of immune cell populations in unchallenged GzmB$^{YFP\text{-}Cre}$ *Pik3c3*$^{fl/fl}$ mice and did not observed any differences in proportions and phenotype compared to littermate controls. Next, I chose three different approaches to activated CD8$^+$ T cells. *In vitro* activated *Pik3c3*$^{\Delta 21}$ CD8$^+$ T cells were similar to activated wild-type CD8$^+$ T cells, apart of increased production of the cytokine IFN-γ in *Pik3c3*$^{\Delta 21}$ CD8$^+$ T cells.

In vivo activated CD8$^+$ T cells using a *Lm*-OVA infection model displayed a reduced level of antigen-specific CD8$^+$ T cells, with impaired cytokine productions (IFN-γ and TNF-α) as well as reduced degranulation capacity, as assessed by Lamp-1 levels. Interestingly, both SLECs and MPECs proportions were unaffected by the loss of VPS34-kinase activity. Data gained from *in vitro* assays suggested that VPS34-deficiency affects cell cycle progression, in line with the described role of VPS34 in cytokinesis.

I used a second model to activate CD8$^+$ T cells *in vivo*. GzmB$^{YFP\text{-}Cre}$ *Pik3c3*$^{fl/fl}$ mice injected with B78ChOVA-mCherry cancer cells did not control the tumour growth as well as wild-type control mice. I will analyse in depth the phenotype of antigen-specific CD8$^+$ T cells as well as by-stander cells within the tumour as well as in the draining lymph node and extend this analysis to further lymphoid organs if needed.

Taken together, these results suggest that VPS34 is important for the formation of antigen-specific CD8$^+$ T cells, probably involved in cytokinesis, as well the trafficking and release of vesicle granules, required for effector functions.

Chapter 6

Conclusions

6.1 General discussion

6.1.1 The role of VPS34 in Treg cell maturation

The evolutionary conserved class III PI3-kinase VPS34 is critically involved in autophagy and endocytosis in yeast and similar roles have been described for some mammalian cells [186], [322]. Meanwhile, the role of VPS34 in immune cells is yet not perfectly understood. T cell-specific deletion of VPS34 in mice leads to defective T cell homeostasis [217], [227], [228], which was attributed to either impaired autophagy and organelle removal [217], [228], or compromised survival due to altered IL-7Rα trafficking dynamics [227]. Furthermore, aged CD4^{Cre} *Pik3c3*$^{fl/fl}$ mice developed intestinal inflammation and anaemia, which was due to reduced Treg cell numbers and impaired *in vitro* and *in vivo* suppressive functions [217].
The intrinsic role of VPS34 in Treg cells was investigated by Elisabeth Slack who found that Treg cell-specific deletion of VPS34 caused a *Scurfy*-phenotype despite the presence of Treg cells, suggesting that loss of VPS34 affects Treg cell suppressive functions rather than survival. However, none of the known Treg cell suppressive mechanisms were impaired by the loss of VPS34.

We hypothesised that the inflammatory environment present in *FoxP3*$^{YFP\text{-}Cre}$ *Pik3c3*$^{fl/fl}$ mice might drive compensatory mechanisms masking the effect of VPS34-deficiency in Treg cells. Indeed, the generation of mice with a 'mosaic' deletion of VPS34 in Treg cells (using the location of the *FoxP3* promoter on the X chromosome to generate heterozygous *FoxP3*$^{YFP\text{-}Cre/WT}$ female mice which were crossed to *Pik3c3*$^{fl/fl}$ mice) showed that VPS34-deficient Treg cells are not intrinsically pathological. However, VPS34-deficient Treg cells from mosaic *FoxP3*$^{YFP\text{-}Cre/WT}$ *Pik3c3*$^{fl/fl}$ mice had a competitive disadvantage compared to VPS34-sufficient Treg cells. Furthermore, the proportion of Treg cells expressing CD44 was lower among VPS34-deficient Treg cells from mosaic mice, similar to what we had observed when VPS34 was knocked out in all Treg cells, suggesting that VPS34 is intrinsically required for Treg cells to differentiate into a more mature phenotype or alternatively, that mature Treg cells depend on VPS34 for their survival ***(Chapter 3)***. Furthermore, lack of systemic inflammation in mosaic *FoxP3*$^{YFP\text{-}Cre/WT}$ *Pik3c3*$^{fl/fl}$ mice provided us with a suitable tool to assess the cell intrinsic effects of VPS34-deficiency in Treg cells.

Consistent with previous reports, I observed that the frequency of YFP^{+} Treg cells in mosaic *FoxP3*$^{YFP\text{-}Cre/WT}$ *Pik3c3*$^{fl/fl}$ mice was less than 50% of total Treg cells, as would be

expected given random X chromosome inactivation. This hypomorphic effect of *FoxP3*^{Cre} alleles on Treg cells in a competitive context (i.e. in chimeric/mosaic mice) has been previously described [323], [324]. In our experiments, we controlled for these Cre-mediated effects by using both control and experimental mice expressing the same *FoxP3*$^{YFP\text{-}Cre/WT}$ genotype.

Treg cells can be divided into *resting Treg* (rTreg) cells and *activated Treg* (aTreg) cells based on the expression of T cell activation markers (such as CD44, KLRG1, and CD69) and homing molecules, e.g. CD62L [325]. rTreg cells are predominantly found in secondary lymphoid organs, whereas aTreg cells are enriched in peripheral tissues [326]. Signals from the *T cell receptor* (TCR) play a critical role in Treg cell differentiation and survival [327]. Indeed, TCR signalling is required for the differentiation of rTreg cells into aTreg cells, and conditional ablation of TCR components following Treg cell lineage commitment results in loss of aTreg cells and the inability of the residual population of rTreg cells to limit inflammation [284], [328].

Treg cells are maintained over time, suggesting a mechanism to limit TCR-driven activation programs among rTreg cells. Since loss of VPS34-kinase activity reduced the proportions of aTreg cells, this implies that VPS34 might be involved in TCR-driven activation programs in Treg cells. The relationship between VPS34 and the activation of Treg cells is an attractive subject of investigation, not at least offering additional targets for the therapeutic suppression of Treg cells in cancer, with the potential to avoid deleterious effects on effector cells. This hypothesis will be subject to investigations (discussed in ***Chapter 6*** – '***Ongoing work***').

6.1.2 VPS34-deletion induces a state of heightened metabolic activity in Treg cells

In an attempt to determine which Treg cell suppression mechanisms are affected by the loss of VPS34, I performed proteomic profiling and while the results could not provide a definite clue about the mechanism(s) leading to the observed phenotype in mice with VPS34-deficient Treg cells, they suggested that loss of VPS34-kinase activity induces a state of heightened metabolic activity (***Chapter 4***).

A number of recent reports have shown that the numbers of Treg cells and their phenotypical plasticity are regulated by metabolic processes [329]. Treg cells are known to have a ''metabolic edge'' for survival through their bias toward mitochondrial respiration, and

mitochondrial metabolism supports both their immunosuppressive functions as well as survival in lactate-rich environments [330].

Reports investigating the relationship between Treg cell fitness, suppressive functions, and metabolic activity, show that mice developed a fatal inflammatory disorder similar to the one observed in *FoxP3*$^{Cre\text{-}YFP}$ *Pik3c3*$^{fl/fl}$ mice when impairing mitochondrial function and cellular metabolism, rather than increasing metabolic activity [331]–[334]. For example, Treg cell-specific deletion of Uqcrsf1 (encoding RISP) or Uqcrq (encoding QPC) in mice led to a lymphoproliferative pathology, with enlarged lymph nodes and spleen, increased lymphocytic cell infiltration in multiple organs and increased proportions of activated $CD4^+$ and $CD8^+$ T cells in lymph nodes and spleen [335]. These mice died by weeks 4 of age, similar to *Scurfy* mice and *FoxP3*$^{Cre\text{-}YFP}$ *Pik3c3*$^{fl/fl}$ mice. Like *FoxP3*$^{Cre\text{-}YFP}$ *Pik3c3*$^{fl/fl}$ mice, RISP-KO and QPC-KO mice had normal Treg cell numbers. However, their metabolic flux was drastically shifted away from mitochondria and cytoplasmic glycolysis.

A recent study reports that FoxP3 reprograms T cell metabolism by suppressing Myc and glycolysis and enhancing *oxidative phosphorylation* (OXPHOS), suggesting a close collaboration between FoxP3 and mitochondrial respiratory complexes to ensure functioning Treg cells. In *FoxP3*$^{Cre\text{-}YFP}$ *Pik3c3*$^{fl/fl}$ mice and *FoxP3*$^{Cre\text{-}YFP/WT}$ *Pik3c3*$^{fl/fl}$ mosaic mice, expression of FoxP3 was unchanged (*data not shown*), suggesting that VPS34 influences metabolic reprogramming towards OXPHOS at another level.

Rapamycin was routinely used to elucidate how mTOR inhibition modulates Treg cell functions. Rapamycin induces *de novo* expression of FoxP3 in naïve T cells *in vitro* [336], and promotes the expansion of $CD4^+$ $CD25^+$ T cells which then display enhanced suppressive functions. However, rapamycin treatment ablates some, but not all, of mTORC1 function – e.g., rapamycin treatment can suppress S6 phosphorylation, while 4E-BP1 phosphorylation remains largely intact [337], [338].

mTORC1 activity is essential for the metabolic programming of Treg cells and their functional fitness [132]. mTORC1 activity is associated with an increase in Treg cell suppressive ability, and mice with Treg cell-specific deletion of Raptor, the fundamental component of mTORC1 [339], developed a *Scurfy*-like inflammatory disease [132]. Treg cell numbers, activation and suppressive capacity appeared normal in these mice, but this was due to a compensatory response to the ongoing inflammation. Using bone marrow

chimaeras, it was shown that mTORC1 is essential for Treg cell suppressive functions and proliferation.

The same study revealed that genes involved in cholesterol biosynthesis were strikingly downregulated in mTORC1-deficient Treg cells and, accordingly, mTORC1-deficient Treg cells failed to synthesise lipids from glucose following TCR stimulation. Moreover, inhibiting lipid synthesis by blocking the rate-limiting enzyme HMGCR (3-hydroxy-3-methyl-glutaryl-CoA reductase) abrogated Treg cell suppressive abilities, proliferation and the ability to upregulate effector molecules. This state was overcome by the addition of mevalonate, the direct downstream metabolite of HMGCR. Therefore, mTORC1 critically regulates Treg cell fitness by promoting lipogenesis, demonstrating the importance of mTORC1 to mediate metabolic programming and suppressive functions of Treg cells.

In order to meet metabolic demands during the ongoing immune response, T cells must regulate nutrient uptake, including amino acids. Activation of T cells via antigens or IL-2 promotes the uptake of large neutral amino-acids via the induction of system L transporters [340]. System L transporters are heterodimers, comprising CD98 and Slc7a5, Slc7a6, Slc7a7 or Slc7a8 [341]–[344]. Slc7a5 is the most highly induced transporter following TCR stimulation, and T cell-specific deletion of Slc7a5 results in abnormal immune responses [340]. Slc7a5-deficient T cells showed impaired phosphorylation of S6 following activation, demonstrating that mTORC1 is not activated in the absence of this key amino-acid transporter. Furthermore, inhibition of system L transporters and deprivation of amino-acids reduced mTORC1 in effector T cells, which was overcome by the provision of leucine. Therefore, mTORC1 is critically regulated by amino acid uptake in T cells.

The mechanism by which amino acids control mTORC1 in T cells is still under investigation. It is proposed to occur at the lysosome, involving amino acid-dependent activation of the Ragulator complex [340]. The Ragulator complex comprises five proteins (p18, p14, and MP1, HBXIP and C7orf59), which tether the heterodimeric Rag GTPases to the lysosome, facilitating the recruitment of mTORC1 to the lysosome and its activation by Rheb [345].

Nutrient-induced activation of S6 and 4E-BP, downstream of mTORC1, requires VPS34 [346], [347]. Conventionally, mTOR function is regulated via class I PI 3-kinases, but overexpression of VPS34 in cell lines increases the activation of the mTORC1 target S6K1, thereby increasing the levels of *phosphorylated S6* (pS6) [347]. On the other hand, inhibition

of VPS34 blocks S6K1 induction [347]. VPS34-kinase activity and PI3P levels are reduced under conditions of amino acid or glucose starvation [346], [347], and knock-down of VPS34 prevents amino acid-induced activation of S6K1 [348]. Therefore, a role for VPS34 upstream of mTORC1 in amino acid-mediated activation has been proposed [346], [347], and it is possible that VPS34 integrates amino acid availability with mTORC1 activation to promote Treg cell fitness. The striking resemblance of *FoxP3*$^{YFP\text{-}Cre}$ *Pik3c3*$^{fl/fl}$ mice to those with Treg cell-specific deletion of mTORC1 [132] strongly supports this hypothesis. Both strains of mice develop a *Scurfy*-like inflammatory disease despite the present of Treg cells, Treg cells of both genotype suppress effectively *in vitro*, and both mTORC1- and VPS34-deficient Treg cells are at a competitive disadvantage in bone marrow chimera or mosaic mice, respectively. However, a link between mTORC1 and VPS34 did not become apparent from investigations using proteomic profiling. It would be of great interest to focus on the phosphorylation status of mTORC1 target proteins, such as phospho-S6 and phospho-4E-BP1, in VPS34-deficient Treg cells as a measure of mTORC1 activity.

Based on published studies and the knowledge I have gained from my studies, I hypothesise that under stimulating conditions (TCR-activating, stress, etc), autophagy is upregulated in VPS34-sufficient Treg cells, leading to the sequestration of mitochondria, and a reduction of glycolysis. Stimulation of VPS34- and PI3P-dependent pathways negatively regulates mTOCR1, repressing c-Myc expression and favouring the expression of protein supporting quality control mitochondria, energetic balance, and proteome remodelling required for Treg cell maintenance and homeostasis (**Fig. 6.1 a**). Under activating conditions, VPS34-deletion in Treg cells (**Fig. 6.1 b**), on the other side, leads to a defect in TCR signalling, with altered cell proliferation and survival. The reduced turn-over of specific proteins, due to a (mild) defect in autophagy, is also detrimental for the proliferation and the survival of Treg cells. VPS34-deletion might also lead to the dysregulation of programs of cell senescence and activation programs of cell exhaustion. Lack of VPS34 leads to an increased activation of mTORC1 signalling, which drives c-Myc expression, leading to an aberrant increase in glycolysis. Together with the accumulation of mitochondria, this drives ATP production, leading to a dysregulated T cell metabolism, and an abnormal energetic balance.

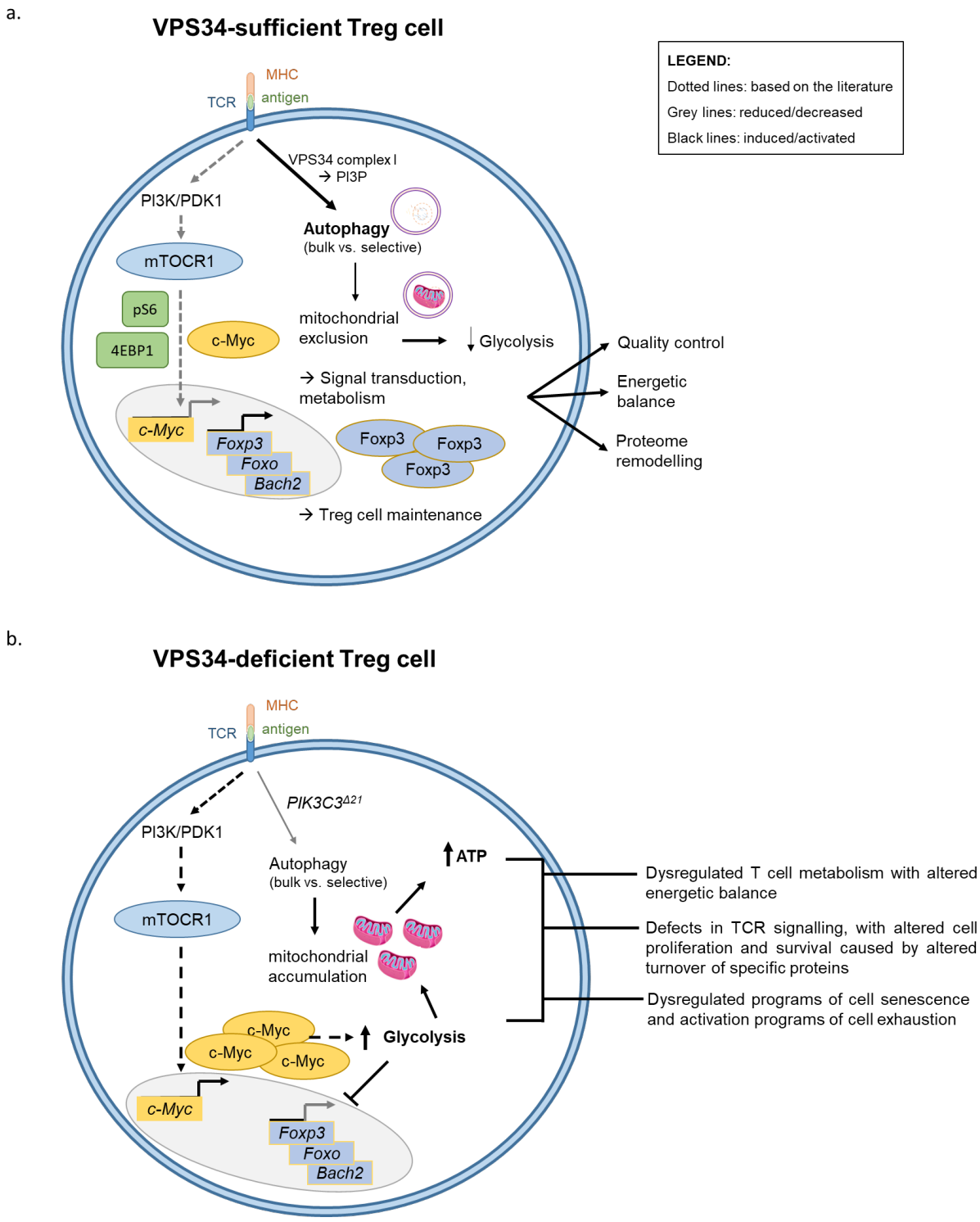

Figure 6.1: Proposed model of the role of VPS34 in Treg cells.

a) VPS34 is required for maintaining Treg cell homeostasis by coupling multiple pathways to ensure mitochondrial quality control, energetic balance, and proteome remodelling.

b) In stimulating conditions, lack of VPS34 in Treg cells leads to the dysregulation of Treg cell metabolism, defect in TCR signalling, and dysregulated programs of cell senescence and activation programs of cell exhaustion.

6.1.3 The role of VPS34 in activated CD8⁺ T cells

During the course of an infection, CD8⁺ T cells initially expand and differentiate to effector T cells. Upon successful clearance of the pathogen, the majority of short-lived effector T cells die and the remaining cells differentiate into a population of *memory T cells* (Tmem) that provides long lasting immunity. Cytokines, surface molecules, and signalling components involved in T cell memory formation have been extensively studied. However, the molecular pathways supporting cell fate decisions are poorly understood.

Several studies have described a role for autophagy in CD8⁺ T cell memory formation, while the effector phase seems unaffected by impaired autophagy. Hence, mice lacking the autophagy gene *Atg7* or *Atg5* in T cells failed to establish CD8⁺ T cell memory to influenza and MCMV infection [219], [223]. While *Atg7*$^{-/-}$ T cells responded normally during the early stages of a pathogenic challenge, the compartment of memory CD8⁺ T cells was severely reduced in response to influenza and *murine cytomegalovirus* (MCMV). Antigen-specific *Atg7*$^{-/-}$ CD8⁺ T cells displayed increased cell death at the time of memory formation, compromised mitochondrial health, and increased expression of the glucose receptor GLUT1, a marker for glycolysis.

The pool of memory T cells is controlled by PI3K/Akt and AMPK signalling as well as mTOR inhibition [349]–[351], all of which also control autophagy [352]. The maintenance of memory CD8⁺ T cells relies on autophagy to eliminate damaged mitochondria and ROS and to facilitate the switch from glycolysis to mitochondrial respiration important for the survival of memory CD8⁺ T cells [223]. In the context of metabolic switching, studies have shown the involvement of TRAF6 (TNFR-associated factor 6) in the regulation of CD8⁺ Tmem development by modulating fatty acid metabolism and thereby increasing mitochondrial respiration [353], [354]. TRAF6 is an E3 ubiquitin ligase and stabilizes essential proteins in the autophagy pathway such as ULK1 [355] and Beclin-1 [356].

Since VPS34 complex I (comprising VPS34, VPS15, Beclin-1, and Atg14) and the production of PI3P at the isolation membrane is required for autophagy induction, it was striking to observe that deletion of VPS34 in activated CD8⁺ T cells did not result in a phenotype similar to the one observed by Xu et *al*. in mice with deletion of *Atg*7 or *Atg*5 in activated CD8⁺ T cells (using the same GzmB-Cre system) [219]. Rather, GzmB$^{YFP\text{-}Cre}$ *Pik3c3*$^{fl/fl}$ mice infected with an attenuated Lm-OVA strain displayed reduced proportions of antigen-

specific CD8⁺ T cells with reduced effector functions at the peak of expansion (both during the primary and the secondary challenge), while memory formation seemed intact. Loss of VPS34-kinase activity led to reduced levels of TNF-α and IFN-γ, as well as reduced proportions of the degranulation marker LAMP-1. Overall, however, the percentage of shortly-activated effector cells and memory precursor cells were unchanged (***Chapter 5***). Results from *in vitro* data suggested that while the proliferation of activated CD8⁺ T cells was not affected, the transition into the mitotic phase was impaired by VPS34-deficiency.

Figure 6.2 summarizes the findings and depicts a proposed model for the effect of VPS34-deficiency in activated CD8⁺ T cells.

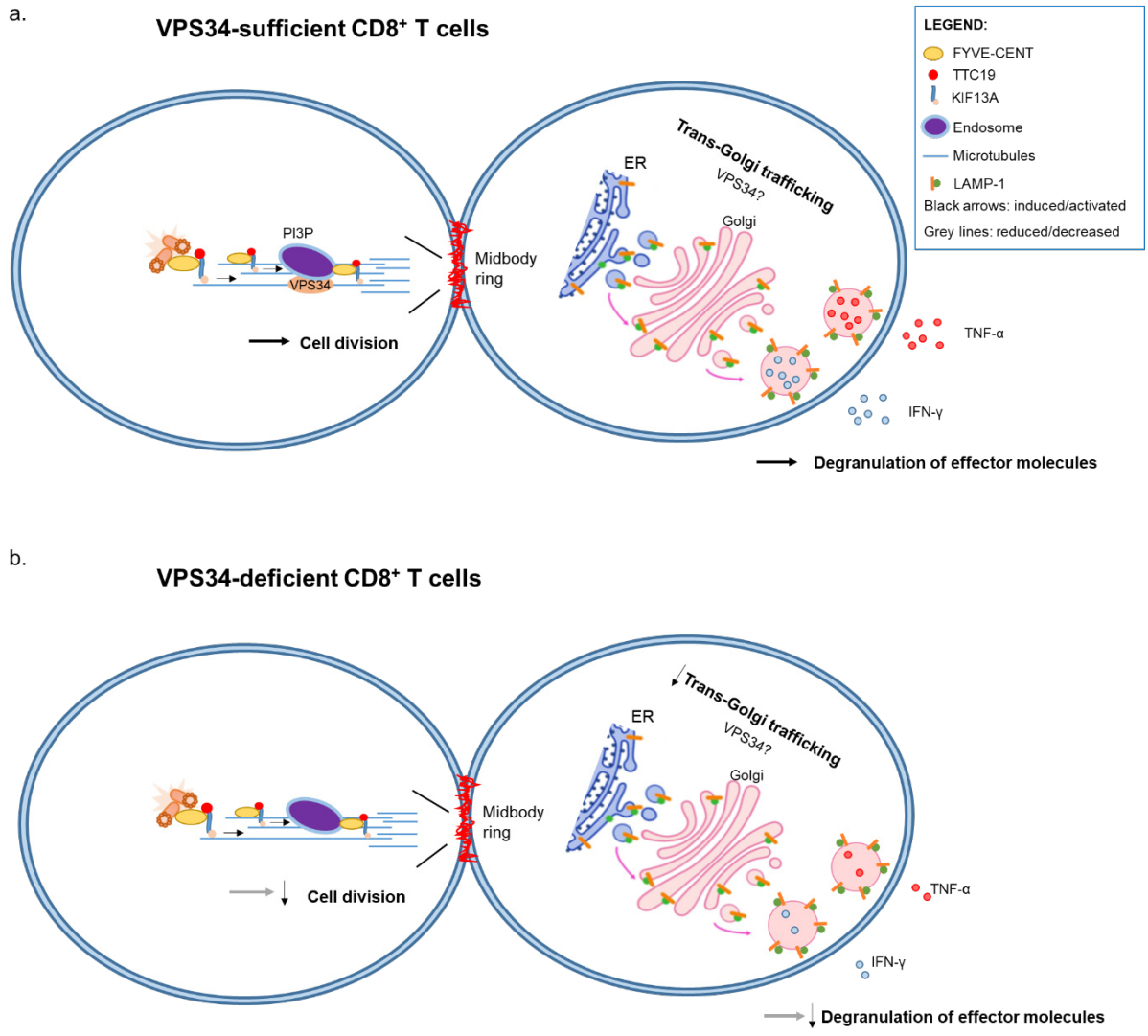

Figure 6.2: Proposed model of the role of VPS34 in activated CD8⁺ T cells.
a) Cell division, trans-Golgi trafficking and degranulation of effector molecules (TNF-α and IFN-γ) in VPS34-sufficient, activated CD8⁺ T cells.
b) Proposed effect VPS34-deletion on cell division, trans-Golgi trafficking, and degranulation of effector molecules (TNF-α and IFN-γ) in activated CD8⁺ T cells.

6.2 Ongoing work

6.2.1 Investigating whether VPS34 is required for Treg cell maturation

In order to explore the role of VPS34 during the recruitment, the expansion and the activation of Treg cells *in vivo*, I will use two different experimental strategies to analyse the numbers and phenotype of Treg cells responding to an antigenic stimulus *in vivo*. Currently, I am implanting female *FoxP3*$^{Cre/WT}$ *Pik3c3*$^{fl/fl}$ mosaic mice subcutaneously with the murine melanoma cell line B78ChOVA-mCherry. B78ChOVA-mCherry is derived from the amelanotic clone B16.F10, but has been genetically engineered to express the mCherry reporter and OVA (obtained as a generous gift from Prof. Matthew F. Krummel (UCSF)). Treg cells infiltrate the tumour and become activated by cognate antigens expressed by the cancer cells. Alternatively, the presence of TGF-β within the tumour might increase the conversion of naive CD4$^+$ T cells into *induced Treg cells* (iTreg cells). Since the tumour cells express OVA, I can use recombinant MHC tetramer molecules to detect antigen-specific T cells. Eighteen days after inoculation, I will isolate tumours, draining and resting lymph nodes, and spleens, and compared the number and phenotype of VPS34-sufficient and VPS34-deficient Treg cells within these tissues.

In the future, I will also analyse antigen-specific Treg cells that have undergone clonal expansion in response to infection with *Listeria* using antigen-specific MHC-II tetramers. Using this model system, I will be able to address whether the TCR can drive clonal expansion of Treg cells in the absence of VPS34.

I want to use both models to assess whether the expression of CD44 and additional differentiation markers on antigen-challenged Treg cells depend on VPS34. Furthermore, a competitive disadvantage will be become evident by determining changes in the ratio between VPS34-deficient (YFP$^+$) and VPS34-sufficient (YFP$^-$) Treg cells.

Future work will involve the fluorescence-activating cell sorting of naïve and tumour-infiltrating VPS34-deficient and -sufficient Treg cells and profile their mRNA by next generation sequencing. The analysis of mRNA expression levels will not only reveal potential changes in gene-expression due to VPS34-deficiency, but will also allow to track gene expression patterns associated with changes in Treg cell maturation and differentiation as described recently [357].

It remains possible that the inactivation of VPS34 has an impact on the thymic development of Treg cells that would subsequently affect mature Treg cells in the periphery. In order to specifically test the function of VPS34 on fully developed Treg cells, we plan to cross *Pik3c3*$^{fl/fl}$ mice with a *FoxP3*$^{ERT2\text{-}Cre}$ and a Rosa26^{tdRFP} reporter mouse line. This new cross will enable us to determine if acute elimination of VPS34 in Treg cells following the administration of tamoxifen in adult mice also leads to lethal lymphoproliferation and autoimmunity. It may also provide a window of opportunity to challenge mice with homozygous deletion of *Pik3c3 in vivo,* should they survive for a few weeks following tamoxifen administration. The RFP reporter will allow us to distinguish iTreg cells from tTreg cells if tamoxifen is administered before tumour implantation, since iTreg cells derived from Tcon will not be marked by RFP expression whereas all Treg cells present at the time of tamoxifen administration will be positive for RFP.

These different approaches will demonstrate whether VPS34 plays a role in antigen-dependent activation of Treg cells *in vivo,* help identifying transcriptional profiles associated with Treg cell-activation and differentiation and how those are affected by the loss of VPS34.

6.2.2 VPS34-deficiency affects signalling pathways regulating Treg cell metabolism

To further explore the involvement of VPS34 in maintaining metabolic and functional fitness of Treg cells, I focused on genes involved in cellular metabolism and energy homeostasis. The evolutionary conserved regulator of cellular metabolism *Liver-Kinase B1* (LKB1, encoded by the *Stk11* gene) was down-regulated by half ($p = 0.05724$) (*data not shown*). There is evidence from studies using Drosophila that inactivation of endosomal VPS34 and lack of PI3P at endosomal membranes leads to the delocalization and the increased activity of LKB1 [358]. In mammals, LKB1 is one of the two kinases that activate AMPK by phosphorylation of threonine 172 (T172) within the activation loop. LKB1 phosphorylates and activates AMPK at the late endosome, which in turn negatively regulates mTORC1. The activity of LKB1 is regulated by WDFY2, a protein that is recruited to the endosome through the interaction between its FYVE domain and PI3P [358]. Therefore, interrupting endosomal maturation through the loss of VPS34 and PI3P might lead to a reduction in the recruitment of WDFY2, thereby increasing LKB1 signalling and resulting in higher p-AMPK/AMPK ratio. Furthermore, unbound LKB1 might be more prone to degradation, providing a possible explanation for the

reduced level of LKB1 in VPS34-deficient Treg cells. AMPK is a central mediator of cellular energy homeostasis and its activation of AMPK leads to selective regulation of a subset of genes involved in metabolism, autophagy and lysosomal function. I therefore aim to monitor the phosphorylation status of AMPK1 in VPS34-deficient Treg cells.

6.2.3 Analysis of the phosphoproteomic of Treg cells

Using proteomic profiling, I can only determine the total protein amount, but cannot draw any conclusions on the location of a given protein. Therefore, should the total protein content remain the same, it is impossible to determine whether VPS34-deficiency leads to a blockage in the transport of the given protein. This limitation might lead to incorrect conclusions about which pathways or cellular processes rely on VPS34-kinase activity and will have to be taken into account and addressed when designing further experiments.

Since results from the proteomic profiling could not provide me with a definite clue about the mechanism leading to the observed phenotype in mice with VPS34-deficient Treg cells, the next step will be to analyse the phosphoproteome of VPS34-deficient Treg cells. Phosphorylation of proteins is an extensively employed mode of signal transduction, frequently involving cascades of phosphorylation events among kinases [359]. In the past decade, technological advances have made quantitative phosphoproteomics a method of choice for studying protein phosphorylation in an unbiased manner [360]. This methodology has been applied to characterize the system-wide regulation of phosphorylation in many different settings and processes, thereby providing valuable information about crucial regulatory events [361]. Hence, in order to characterize the impact of VPS34-deficiency on the early and late temporal dynamics of the phosphoproteome, I aim to assess global changes in phosphorylation after short-term (15 min) and long-term (4h) stimulation of VPS34-deficient Treg cell before and after activation with anti-CD3, anti-CD28, and IL-2. We have already established collaborations with Pedro Cutillas (University College London) and Doreen Cantrell (University of Dundee), with whom we aim to carry out this analysis. Considering the reduced percentage of activated Treg cells (based on the expression levels of CD44, CD69, KLRG1, and LAG3 as shown in ***Chapter 3***), it is worth considering further the activation status on VPS34-deficient Treg cells after activation, since the differential expression of

(phospho)proteins involved in the pathway(s) responsible for the fatal phenotype observed in *FoxP3*^{Cre} *Pik3c3*$^{fl/fl}$ mice might only be detectable upon activation of Treg cells.

6.2.4 Knock-down of PI3P-binding proteins with CRISPR/Cas9 gene editing

In collaboration with Kristopher Johansen (another PhD student in Klaus Okkenhaug's laboratory), I will evaluate the role of different VPS34 effector proteins in Treg cells using CRISPR/Cas9 gene editing. Treg cells do not grow vigorously in culture, but it is possible to induce iTreg cells from naive CD4$^+$ T cell precursors in the presence of IL-2 and TGF-β *in vitro*, during which genes can be knocked out by CRISPR/Cas9 using retroviral transduction of Treg cells isolated from Cas9 transgenic mice [362]. We have generated a list of all (potential) PI3P-binding proteins, proteins with PX domains, FYVE domains as well as other proteins containing BAR domains, A/ENTH domains, C2 domains, and PDZ domains, resulting in a list of 757 genes. We used Benchling (Benchling [Biology Software] (2019)) to design guide RNAs (gRNAs) (3 guides per target gene, leading to a total of 3028 gRNAs).

We routinely achieve up to 80% knockout efficiency in primary CD8$^+$ T cells and anticipate that we can adopt this technology for Treg cells. As an alternative approach, genes of candidate proteins will be knocked out in bone marrow cells *in vitro*, using another recently described protocol [363], and used to reconstitute Treg cell-deficient hosts, allowing to evaluate whether the lack of the candidate protein is recapitulating the observed phenotype of *FoxP3*$^{YFP\text{-}Cre}$ *Pik3c3*^{flox} mice and its effect on Treg cell function. Eventually, should we find evidence for the role of a particular protein being responsible for VPS34-dependent Treg cell suppression, we will generate or acquire mice with the corresponding floxed gene and use *FoxP3*$^{YFP\text{-}Cre}$ mice or inducible *FoxP3*$^{Cre\text{-}ERT2}$ mice to test its function *in vivo.*

6.2.5 Investigating the cell cycle progression of antigen-specific CD8$^+$ T cells in vivo

In order to investigate the role of VPS34 during the activation and effector function of antigen-specific CD8$^+$ T cells *in vivo*, I will use different experimental strategies to analyse the numbers and phenotype of antigen-specific CD8$^+$ T cells responding to an antigenic stimulus *in vivo*.

Currently, I am implanting GzmB$^{YFP\text{-}Cre}$ *Pik3c3*$^{fl/fl}$ mice subcutaneously with the murine melanoma cell line B78ChOVA-mCherry. I observed that the tumour growth is less well controlled in GzmB$^{YFP\text{-}Cre}$ *Pik3c3*$^{fl/fl}$ mice, but the mouse group size was not sufficient to provide definite results about the phenotype of infiltrating immune cells.

In the realm of the tumour experiments, I am still facing some technical issues, such as the divergent efficacy of the mice to form tumours upon inoculation. I am currently optimizing the culturing method of the cancer cells. Furthermore, I aim to move towards a tumour cell line that does not express a fluorescent tag, as this will facilitate the design of the panels for flow cytometry and the ensuing analysis of the data. I am considering the MC-38 cell line, derived from the C57BL6 murine colon adenocarcinoma, as a suitable choice for my purpose.

Once these technical issues have been solved, I will inoculate GzmB$^{YFP\text{-}Cre}$ *Pik3c3*$^{fl/fl}$ mice with cancer cells and analyse tumour-infiltrating CD8$^+$ T cells as well as antigen-specific CD8$^+$ T cells within the tumour mass and migrating to the draining lymph node. I will perform cell cycle analysis by injecting mice with BrdU two to four hours before sacrificing them and analyse CD8$^+$ T cells in the tumour, draining lymph nodes and spleen by flow cytometry. This approach will allow to assess whether *in vivo*-activated *Pik3c3*$^{\Delta 21}$ CD8$^+$ T cells also display a defect in cell cycle progression, and if so, in which stage. I will also assess the proliferation capacity of antigen-specific CD8$^+$ T cells using the proliferation marker Ki67, and enumerate the proportion of cells undergoing apoptosis using Annexin V staining. Obtained results aim to provide a better understanding of why antigen-specific CD8$^+$ T cells are reduced in GzmB$^{YFP\text{-}Cre}$ *Pik3c3*$^{fl/fl}$ mice, and the reason for their reduced effector functions.

6.2.6 Determine whether endosomal vesicular trafficking is required for the function of activated CD8$^+$ T cells

Based on the observations from *FoxP3*$^{YFP\text{-}Cre}$ x *Pik3c3*$^{fl/fl}$ mice (presented in ***Chapter 3.2.8***) and the reduced levels of CD107a (results presented in ***Chapter 5.2.7***), I aim to assess whether endosomal dynamics are affected by the loss of VPS34-kinase activity in CD8$^+$ T cells and to which extend intact endosomal vesicular trafficking is required in the context of activated CD8$^+$ T cells. As cytokine production and release is key to effector functions of CD8$^+$ T cells,

and I observed that both the production of IFN-γ and TNF-α, as well as levels of LAMP-1 (CD107a) on the surface of splenocytes seven days after the primary infections was reduced in activated *Pik3c3*$^{\Delta 21}$ CD8^{+} T cells, it lies close to assume a defect in vesicular trafficking. To the end, I will at first bulk-activate splenocytes with αCD3 and αCD28 for 48 hours followed by a five day-expansion phase in hrIL-2 and assess endosomal dynamics by flow cytometry and fluorescence microscopy using markers for early endosomes (EEA1 or APPL1), late endosomes (Rab7), and lysosomes (LAMP-1).

6.3 Conclusions

In conclusion, this work revealed a fundamental and novel role for the class III PI 3-kinase VPS34 in the maintenance of Treg cell suppressive mechanisms, and has drawn a link between VPS34 and Treg cell metabolism. Also, it reinforced the complexity of VPS34 signalling in mammalian cells, and thus the need to further define the upstream and downstream pathways involved. These results in turn could profoundly affect our understanding of how immunological tolerance is maintained by Treg cells.

In addition, the data presented in this thesis demonstrated that VPS34 is important for activated $CD8^+$ T cells. Based on the requirement of VPS34 for the induction of autophagy and the described role of autophagy for memory formation of $CD8^+$ T cells, I had hypothesised that loss of VPS34 would recapitulate the phenotype of mice with autophagy-deficient $CD8^+$ T cells. Rather, VPS34 resulted in decreased proportions of antigen-specific $CD8^+$ T cells and reduced effector functions, i.e. cytokine production and degranulation, while memory formation was intact. Therefore, it would be of great interest to delineate the molecular process(es) required for the formation of effector $CD8^+$ T cells that depend on VPS34, and understand better why VPS34-deletion does not affect memory formation, despite its role in autophagy. Therefore, future experiments will aim at delineating the role of VPS34 in the formation of effector cells rather than memory cells.

Chapter 7

References

[1] Janeway Jr, Charles A. "How the immune system protects the host from infection." *Microbes and infection* 3.13 (2001): 1167-1171.

[2] Medzhitov, Ruslan, and Charles A. Janeway. "Decoding the patterns of self and nonself by the innate immune system." *Science* 296.5566 (2002): 298-300.

[3] Iwasaki, Akiko, and Ruslan Medzhitov. "Regulation of adaptive immunity by the innate immune system." *science* 327.5963 (2010): 291-295.

[4] Ramsdell, Fred, and B. J. Fowlkes. "Clonal deletion versus clonal anergy: the role of the thymus in inducing self tolerance." *Science* 248.4961 (1990): 1342-1348.

[5] Sohn, Sue J., Jennifer Thompson, and Astar Winoto. "Apoptosis during negative selection of autoreactive thymocytes." *Current opinion in immunology* 19.5 (2007): 510-515.

[6] Griesemer, Adam D., Eric C. Sorenson, and Mark A. Hardy. "The role of the thymus in tolerance." *Transplantation* 90.5 (2010): 465.

[7] Klein, Ludger, et al. "Positive and negative selection of the T cell repertoire: what thymocytes see (and don't see)." *Nature Reviews Immunology* 14.6 (2014): 377-391.

[8] Lenschow, Deborah J., Theresa L. Walunas, and Jeffrey A. Bluestone. "CD28/B7 system of T cell costimulation." *Annual review of immunology* 14.1 (1996): 233-258.

[9] Asano, Masanao, et al. "Autoimmune disease as a consequence of developmental abnormality of a T cell subpopulation." *The Journal of experimental medicine* 184.2 (1996): 387-396.

[10] Sakaguchi, S., Toshitada Takahashi, and Y. Nishizuka. "Study on cellular events in post-thymectomy autoimmune oophoritis in mice. II. Requirement of Lyt-1 cells in normal female mice for the prevention of oophoritis." *The Journal of experimental medicine* 156.6 (1982): 1577-1586.

[11] Nishizuka, Yasuaki, and Teruyo Sakakura. "Thymus and reproduction: sex-linked dysgenesia of the gonad after neonatal thymectomy in mice." *Science* 166.3906 (1969): 753-755.

[12] Nishizuka, Yasuaki, and Teruyo Sakakura. "Thymus and reproduction: sex-linked dysgenesia of the gonad after neonatal thymectomy in mice." *Science* 166.3906 (1969): 753-755.

[13] Vignali, Dario AA, Lauren W. Collison, and Creg J. Workman. "How regulatory T cells work." *Nature Reviews Immunology* 8.7 (2008): 523-532.

[14] Sakaguchi, Shimon, et al. "Regulatory T cells and immune tolerance." *Cell* 133.5 (2008): 775-787.

[15] Wong, Jamie, et al. "Adaptation of TCR repertoires to self-peptides in regulatory and nonregulatory CD4+ T cells." *The Journal of Immunology* 178.11 (2007): 7032-7041.

[16] Pacholczyk, Rafal, et al. "Nonself-antigens are the cognate specificities of Foxp3+ regulatory T cells." *Immunity* 27.3 (2007): 493-504.

[17] Pacholczyk, Rafal, and Joanna Kern. "The T-cell receptor repertoire of regulatory T cells." *Immunology* 125.4 (2008): 450-458.

[18] Chen, W. "Conversion of peripheral CD4+. Conversion of peripheral CD4+CD25-naive T cells to CD4+CD25+ regulatory T cells by TGF-beta induction of transcription factor Foxp3." *J. Exp. Med* 198 (2003): 1875-1886.

[19] Weiss, Jonathan M., et al. "Neuropilin 1 is expressed on thymus-derived natural regulatory T cells, but not mucosa-generated induced Foxp3+ T reg cells." *Journal of Experimental Medicine* 209.10 (2012): 1723-1742.

[20] Yadav, Mahesh, et al. "Neuropilin-1 distinguishes natural and inducible regulatory T cells among regulatory T cell subsets in vivo." *Journal of Experimental Medicine* 209.10 (2012): 1713-1722.

[21] Fontenot, Jason D., Marc A. Gavin, and Alexander Y. Rudensky. "Foxp3 programs the development and function of CD4+ CD25+ regulatory T cells." *Nature immunology* 4.4 (2003): 330-336.

[22] Khattri, Roli, et al. "An essential role for Scurfin in CD4+ CD25+ T regulatory cells." *Nature immunology* 4.4 (2003): 337-342.

[23] Brunkow, Mary E., et al. "Disruption of a new forkhead/winged-helix protein, scurfin, results in the fatal lymphoproliferative disorder of the scurfy mouse." *Nature genetics* 27.1 (2001): 68-73.

[24] Wildin, Robert S., et al. "X-linked neonatal diabetes mellitus, enteropathy and endocrinopathy syndrome is the human equivalent of mouse scurfy." *Nature genetics* 27.1 (2001): 18-20.

[25] Bennett, Craig L., et al. "The immune dysregulation, polyendocrinopathy, enteropathy, X-linked syndrome (IPEX) is caused by mutations of FOXP3." *Nature genetics* 27.1 (2001): 20-21.

[26] Josefowicz, Steven Z., Li-Fan Lu, and Alexander Y. Rudensky. "Regulatory T cells:

mechanisms of differentiation and function." *Annual review of immunology* 30 (2012): 531-564.

[27] Zheng, Ye, et al. "Genome-wide analysis of Foxp3 target genes in developing and mature regulatory T cells." *Nature* 445.7130 (2007): 936-940.

[28] Marson, Alexander, et al. "Foxp3 occupancy and regulation of key target genes during T-cell stimulation." *Nature* 445.7130 (2007): 931-935.

[29] Li, Bin, et al. "FOXP3 interactions with histone acetyltransferase and class II histone deacetylases are required for repression." *Proceedings of the National Academy of Sciences* 104.11 (2007): 4571-4576.

[30] Patel, Jagruti H., et al. "The c-MYC oncoprotein is a substrate of the acetyltransferases hGCN5/PCAF and TIP60." *Molecular and cellular biology* 24.24 (2004): 10826-10834.

[31] Wu, Yongqing, et al. "FOXP3 controls regulatory T cell function through cooperation with NFAT." *Cell* 126.2 (2006): 375-387.

[32] Kohlhaas, Susan, et al. "Cutting edge: the Foxp3 target miR-155 contributes to the development of regulatory T cells." *The Journal of Immunology* 182.5 (2009): 2578-2582.

[33] Lu, Li-Fan, et al. "Foxp3-dependent microRNA155 confers competitive fitness to regulatory T cells by targeting SOCS1 protein." *Immunity* 30.1 (2009): 80-91.

[34] Lu, Li-Fan, et al. "Function of miR-146a in controlling Treg cell-mediated regulation of Th1 responses." *Cell* 142.6 (2010): 914-929.

[35] Liston, Adrian, et al. "Dicer-dependent microRNA pathway safeguards regulatory T cell function." *The Journal of experimental medicine* 205.9 (2008): 1993-2004.

[36] Chong, Mark MW, et al. "The RNAseIII enzyme Drosha is critical in T cells for preventing lethal inflammatory disease." *The Journal of experimental medicine* 205.9 (2008): 2005-2017.

[37] Zhou, Xuyu, et al. "Selective miRNA disruption in T reg cells leads to uncontrolled autoimmunity." *The Journal of experimental medicine* 205.9 (2008): 1983-1991.

[38] Williams, Luke M., and Alexander Y. Rudensky. "Maintenance of the Foxp3-dependent developmental program in mature regulatory T cells requires continued expression of Foxp3." *Nature immunology* 8.3 (2007): 277-284.

[39] Sakaguchi, Shimon, et al. "Regulatory T cells: how do they suppress immune responses?." *International immunology* 21.10 (2009): 1105-1111.

[40] Russell, John H., and Timothy J. Ley. "Lymphocyte-mediated cytotoxicity." *Annual review of immunology* 20.1 (2002): 323-370.

[41] Sansom, David M., and Lucy SK Walker. "The role of CD28 and cytotoxic T-lymphocyte antigen-4 (CTLA-4) in regulatory T-cell biology." *Immunological reviews* 212.1 (2006): 131-148.

[42] Qureshi, Omar S., et al. "Trans-endocytosis of CD80 and CD86: a molecular basis for the cell-extrinsic function of CTLA-4." *Science* 332.6029 (2011): 600-603.

[43] Grohmann, Ursula, et al. "CTLA-4–Ig regulates tryptophan catabolism in vivo." *Nature immunology* 3.11 (2002): 1097-1101.

[44] Munn, David H., et al. "Potential regulatory function of human dendritic cells expressing indoleamine 2, 3-dioxygenase." *Science* 297.5588 (2002): 1867-1870.

[45] Harden, Jamie L., and Nejat K. Egilmez. "Indoleamine 2, 3-dioxygenase and dendritic cell tolerogenicity." *Immunological investigations* 41.6-7 (2012): 738-764.

[46] Waterhouse, Paul, et al. "Lymphoproliferative disorders with early lethality in mice deficient in Ctla-4." *Science* 270.5238 (1995): 985-988.

[47] Tivol, Elizabeth A., et al. "Loss of CTLA-4 leads to massive lymphoproliferation and fatal multiorgan tissue destruction, revealing a critical negative regulatory role of CTLA-4." *Immunity* 3.5 (1995): 541-547.

[48] Wing, Kajsa, et al. "CTLA-4 control over Foxp3+ regulatory T cell function." *Science* 322.5899 (2008): 271-275.

[49] Oderup, Cecilia, et al. "Cytotoxic T lymphocyte antigen-4-dependent down-modulation of costimulatory molecules on dendritic cells in CD4+ CD25+ regulatory T-cell-mediated suppression." *Immunology* 118.2 (2006): 240-249.

[50] Liang, Bitao, et al. "Regulatory T cells inhibit dendritic cells by lymphocyte activation gene-3 engagement of MHC class II." *The Journal of Immunology* 180.9 (2008): 5916-5926.

[51] Fontenot, Jason D., et al. "A function for interleukin 2 in Foxp3-expressing regulatory T cells." *Nature immunology* 6.11 (2005): 1142-1151.

[52] Grassart, Alexandre, et al. "Clathrin-independent endocytosis used by the IL-2 receptor is regulated by Rac1, Pak1 and Pak2." *EMBO reports* 9.4 (2008): 356-362.

[53] Pandiyan, Pushpa, et al. "CD4+ CD25+ Foxp3+ regulatory T cells induce cytokine deprivation–mediated apoptosis of effector CD4+ T cells." *Nature immunology* 8.12

(2007): 1353-1362.

[54] Bopp, Tobias, et al. "Cyclic adenosine monophosphate is a key component of regulatory T cell–mediated suppression." *The Journal of experimental medicine* 204.6 (2007): 1303-1310.

[55] Deaglio, Silvia, et al. "Adenosine generation catalyzed by CD39 and CD73 expressed on regulatory T cells mediates immune suppression." *Journal of Experimental Medicine* 204.6 (2007): 1257-1265.

[56] Zarek, Paul E., et al. "A2A receptor signaling promotes peripheral tolerance by inducing T-cell anergy and the generation of adaptive regulatory T cells." *Blood* 111.1 (2008): 251-259.

[57] Parish, Ian A., and Susan M. Kaech. "Diversity in CD8+ T cell differentiation." *Current opinion in immunology* 21.3 (2009): 291-297.

[58] Dunn, Gavin P., Lloyd J. Old, and Robert D. Schreiber. "The three Es of cancer immunoediting." *Annu. Rev. Immunol.* 22 (2004): 329-360.

[59] Berke, G. "The binding and lysis of target cells by cytotoxic lymphocytes: molecular and cellular aspects." *Annual review of immunology* 12.1 (1994): 735-773.

[60] Gunn, Michael D., et al. "A chemokine expressed in lymphoid high endothelial venules promotes the adhesion and chemotaxis of naive T lymphocytes." *Proceedings of the National Academy of Sciences* 95.1 (1998): 258-263.

[61] Campbell, James J., et al. "Chemokines and the arrest of lymphocytes rolling under flow conditions." *Science* 279.5349 (1998): 381-384.

[62] Campbell, James J., et al. "6-C-kine (SLC), a lymphocyte adhesion-triggering chemokine expressed by high endothelium, is an agonist for the MIP-3β receptor CCR7." *The Journal of cell biology* 141.4 (1998): 1053-1059.

[63] Dunn, Gavin P., et al. "A critical function for type I interferons in cancer immunoediting." *Nature immunology* 6.7 (2005): 722-729.

[64] Mescher, Matthew F., et al. "Signals required for programming effector and memory development by CD8+ T cells." *Immunological reviews* 211.1 (2006): 81-92.

[65] Thompson, Lucas J., et al. "Innate inflammatory signals induced by various pathogens differentially dictate the IFN-I dependence of CD8 T cells for clonal expansion and memory formation." *The Journal of Immunology* 177.3 (2006): 1746-1754.

[66] Xiao, Zhengguo, et al. "Programming for CD8 T cell memory development requires IL-

12 or type I IFN." *The Journal of Immunology* 182.5 (2009): 2786-2794.

[67] Mercado, Roberto, et al. "Early programming of T cell populations responding to bacterial infection." *The Journal of Immunology* 165.12 (2000): 6833-6839.

[68] Nolz, Jeffrey C., Gabriel R. Starbeck-Miller, and John T. Harty. "Naive, effector and memory CD8 T-cell trafficking: parallels and distinctions." *Immunotherapy* 3.10 (2011): 1223-1233.

[69] DeGrendele, Heather C., et al. "CD44 and its ligand hyaluronate mediate rolling under physiologic flow: a novel lymphocyte-endothelial cell primary adhesion pathway." *The Journal of experimental medicine* 183.3 (1996): 1119-1130.

[70] Siegelman, Mark H., Diana Stanescu, and Pila Estess. "The CD44-initiated pathway of T-cell extravasation uses VLA-4 but not LFA-1 for firm adhesion." *The Journal of clinical investigation* 105.5 (2000): 683-691.

[71] Kaech, Susan M., et al. "Selective expression of the interleukin 7 receptor identifies effector CD8 T cells that give rise to long-lived memory cells." *Nature immunology* 4.12 (2003): 1191-1198.

[72] Huster, Katharina M., et al. "Selective expression of IL-7 receptor on memory T cells identifies early CD40L-dependent generation of distinct CD8+ memory T cell subsets." *Proceedings of the National Academy of Sciences* 101.15 (2004): 5610-5615.

[73] Schluns, Kimberly S., et al. "Interleukin-7 mediates the homeostasis of naive and memory CD8 T cells in vivo." *Nature immunology* 1.5 (2000): 426-432.

[74] Voehringer, David, et al. "Viral infections induce abundant numbers of senescent CD8 T cells." *The Journal of Immunology* 167.9 (2001): 4838-4843.

[75] Joshi, Nikhil S., et al. "Inflammation directs memory precursor and short-lived effector CD8+ T cell fates via the graded expression of T-bet transcription factor." *Immunity* 27.2 (2007): 281-295.

[76] Joshi, Nikhil S., et al. "Inflammation directs memory precursor and short-lived effector CD8+ T cell fates via the graded expression of T-bet transcription factor." *Immunity* 27.2 (2007): 281-295.

[77] Reading, James L., et al. "The function and dysfunction of memory CD 8+ T cells in tumor immunity." *Immunological reviews* 283.1 (2018): 194-212.

[78] Intlekofer, Andrew M., et al. "Effector and memory CD8+ T cell fate coupled by T-bet and eomesodermin." *Nature immunology* 6.12 (2005): 1236-1244.

[79] Hu, Joyce K., et al. "Expression of chemokine receptor CXCR3 on T cells affects the balance between effector and memory CD8 T-cell generation." *Proceedings of the National Academy of Sciences* 108.21 (2011): E118-E127.

[80] Szabo, Susanne J., et al. "Distinct effects of T-bet in TH1 lineage commitment and IFN-γ production in CD4 and CD8 T cells." *Science* 295.5553 (2002): 338-342.

[81] Dunn, Gavin P., et al. "Cancer immunoediting: from immunosurveillance to tumor escape." *Nature immunology* 3.11 (2002): 991-998.

[82] Karupiah, Gunasegaran, et al. "Inhibition of viral replication by interferon-gamma-induced nitric oxide synthase." *Science* 261.5127 (1993): 1445-1448.

[83] Shtrichman, Ronit, and Charles E. Samuel. "The role of gamma interferon in antimicrobial immunity." *Current opinion in microbiology* 4.3 (2001): 251-259.

[84] Zhou, Fang. "Molecular mechanisms of IFN-γ to up-regulate MHC class I antigen processing and presentation." *International reviews of immunology* 28.3-4 (2009): 239-260.

[85] Su, Xiaodi, et al. "Interferon-γ regulates cellular metabolism and mRNA translation to potentiate macrophage activation." *Nature immunology* 16.8 (2015): 838-849.

[86] Curtsinger, Julie M., et al. "Autocrine IFN-γ promotes naive CD8 T cell differentiation and synergizes with IFN-α to stimulate strong function." *The Journal of Immunology* 189.2 (2012): 659-668.

[87] Sercan, Özen, et al. "IFN-γ receptor signaling regulates memory CD8+ T cell differentiation." *The Journal of Immunology* 184.6 (2010): 2855-2862.

[88] Heath, William R., et al. "Cross-presentation, dendritic cell subsets, and the generation of immunity to cellular antigens." *Immunological reviews* 199.1 (2004): 9-26.

[89] Jenkins, Mark K., and Ronald H. Schwartz. "Antigen presentation by chemically modified splenocytes induces antigen-specific T cell unresponsiveness in vitro and in vivo." *The Journal of experimental medicine* 165.2 (1987): 302-319.

[90] Schwartz, Ronald H. "T cell anergy." *Annual review of immunology* 21.1 (2003): 305-334.

[91] Stinchcombe, Jane C., and Gillian M. Griffiths. "Secretory mechanisms in cell-mediated cytotoxicity." *Annu. Rev. Cell Dev. Biol.* 23 (2007): 495-517.

[92] Dustin, Michael L., et al. "A novel adaptor protein orchestrates receptor patterning and cytoskeletal polarity in T-cell contacts." *Cell* 94.5 (1998): 667-677.

[93] Monks, Colin RF, et al. "Three-dimensional segregation of supramolecular activation clusters in T cells." *Nature* 395.6697 (1998): 82-86.

[94] Grakoui, Arash, et al. "The immunological synapse: a molecular machine controlling T cell activation." *Science* 285.5425 (1999): 221-227.

[95] Nagata, Shigekazu, and Pierre Golstein. "The Fas death factor." *Science* 267.5203 (1995): 1449-1456.

[96] Catalfamo, Marta, and Pierre A. Henkart. "Perforin and the granule exocytosis cytotoxicity pathway." *Current opinion in immunology* 15.5 (2003): 522-527.

[97] Lieberman, Judy. "The ABCs of granule-mediated cytotoxicity: new weapons in the arsenal." *Nature Reviews Immunology* 3.5 (2003): 361-370.

[98] Bolitho, Paul, et al. "Apoptosis induced by the lymphocyte effector molecule perforin." *Current opinion in immunology* 19.3 (2007): 339-347.

[99] Brinkley, B. R. "Microtubule organizing centers." *Annual review of cell biology* 1.1 (1985): 145-172.

[100] Jenkins, Misty R., et al. "The strength of T cell receptor signal controls the polarization of cytotoxic machinery to the immunological synapse." *Immunity* 31.4 (2009): 621-631.

[101] Kägi, David, et al. "Cytotoxicity mediated by T cells and natural killer cells is greatly impaired in perforin-deficient mice." *Nature* 369.6475 (1994): 31-37.

[102] Trapani, Joseph A. "Dual mechanisms of apoptosis induction by cytotoxic lymphocytes." *International review of cytology*. Vol. 182. Academic Press, 1998. 111-192.

[103] Kaiserman, Dion, et al. "The major human and mouse granzymes are structurally and functionally divergent." *The Journal of cell biology* 175.4 (2006): 619-630.

[104] Wolf, Beni B., et al. "Caspase-3 is the primary activator of apoptotic DNA fragmentation via DNA fragmentation factor-45/inhibitor of caspase-activated DNase inactivation." *Journal of Biological Chemistry* 274.43 (1999): 30651-30656.

[105] Larsen, Brian D., et al. "Caspase 3/caspase-activated DNase promote cell differentiation by inducing DNA strand breaks." *Proceedings of the National Academy of Sciences* 107.9 (2010): 4230-4235.

[106] Sarin, Apurva, et al. "Target cell lysis by CTL granule exocytosis is independent of ICE/Ced-3 family proteases." *Immunity* 6.2 (1997): 209-215.

[107] Sarin, Apurva, Elias K. Haddad, and Pierre A. Henkart. "Caspase dependence of target

cell damage induced by cytotoxic lymphocytes." *The Journal of Immunology* 161.6 (1998): 2810-2816.

[108] Bonzon, Christine, et al. "Caspase-2–induced apoptosis requires bid cleavage: a physiological role for bid in heat shock–induced death." *Molecular biology of the cell* 17.5 (2006): 2150-2157.

[109] Chowdhury, Dipanjan, and Judy Lieberman. "Death by a thousand cuts: granzyme pathways of programmed cell death." *Annu. Rev. Immunol.* 26 (2008): 389-420.

[110] Pinkoski, Michael J., et al. "Entry and trafficking of granzyme B in target cells during granzyme B-perforin–mediated apoptosis." *Blood, The Journal of the American Society of Hematology* 92.3 (1998): 1044-1054.

[111] Reinhardt, R. Lee, et al. "Visualizing the generation of memory CD4 T cells in the whole body." *Nature* 410.6824 (2001): 101-105.

[112] Whitmire, Jason K., Boreth Eam, and J. Lindsay Whitton. "Tentative T cells: memory cells are quick to respond, but slow to divide." *PLoS Pathog* 4.4 (2008): e1000041.

[113] Veiga-Fernandes, Henrique, et al. "Response of naive and memory CD8+ T cells to antigen stimulation in vivo." *Nature immunology* 1.1 (2000): 47-53.

[114] Chandok, Meena R., and Donna L. Farber. "Signaling control of memory T cell generation and function." *Seminars in immunology*. Vol. 16. No. 5. Academic Press, 2004.

[115] Hildeman, David A., et al. "Activated T cell death in vivo mediated by proapoptotic bcl-2 family member bim." *Immunity* 16.6 (2002): 759-767.

[116] Wojciechowski, Sara, et al. "Bim mediates apoptosis of CD127lo effector T cells and limits T cell memory." *European journal of immunology* 36.7 (2006): 1694-1706.

[117] Wojciechowski, Sara, et al. "Bim/Bcl-2 balance is critical for maintaining naive and memory T cell homeostasis." *The Journal of experimental medicine* 204.7 (2007): 1665-1675.

[118] Schluns, Kimberly S., et al. "Cutting edge: requirement for IL-15 in the generation of primary and memory antigen-specific CD8 T cells." *The Journal of Immunology* 168.10 (2002): 4827-4831.

[119] Schluns, Kimberly S., and Leo Lefrançois. "Cytokine control of memory T-cell development and survival." *Nature Reviews Immunology* 3.4 (2003): 269-279.

[120] Klonowski, Kimberly D., et al. "Cutting edge: IL-7-independent regulation of IL-7

receptor α expression and memory CD8 T cell development." *The Journal of Immunology* 177.7 (2006): 4247-4251.

[121] Becker, Todd C., et al. "Interleukin 15 is required for proliferative renewal of virus-specific memory CD8 T cells." *The Journal of experimental medicine* 195.12 (2002): 1541-1548.

[122] Sallusto, Federica, Jens Geginat, and Antonio Lanzavecchia. "Central memory and effector memory T cell subsets: function, generation, and maintenance." *Annu. Rev. Immunol.* 22 (2004): 745-763.

[123] Williams, Matthew A., and Michael J. Bevan. "Effector and memory CTL differentiation." *Annu. Rev. Immunol.* 25 (2007): 171-192.

[124] Wherry, E. John, et al. "Lineage relationship and protective immunity of memory CD8 T cell subsets." *Nature immunology* 4.3 (2003): 225-234.

[125] Sallusto, Federica, et al. "Two subsets of memory T lymphocytes with distinct homing potentials and effector functions." *Nature* 401.6754 (1999): 708-712.

[126] Masopust, David, et al. "Preferential localization of effector memory cells in nonlymphoid tissue." *Science* 291.5512 (2001): 2413-2417.

[127] Wing, Kajsa, and Shimon Sakaguchi. "Regulatory T cells exert checks and balances on self tolerance and autoimmunity." *Nature immunology* 11.1 (2010): 7-13.

[128] Luo, Chong T., and Ming O. Li. "Transcriptional control of regulatory T cell development and function." *Trends in immunology* 34.11 (2013): 531-539.

[129] Painter, Michio W., et al. "Transcriptomes of the B and T lineages compared by multiplatform microarray profiling." *The Journal of Immunology* 186.5 (2011): 3047-3057.

[130] Galgani, Mario, et al. "Role of metabolism in the immunobiology of regulatory T cells." *The Journal of Immunology* 197.7 (2016): 2567-2575.

[131] Procaccini, Claudio, et al. "An oscillatory switch in mTOR kinase activity sets regulatory T cell responsiveness." *Immunity* 33.6 (2010): 929-941.

[132] Zeng, Hu, et al. "mTORC1 couples immune signals and metabolic programming to establish T reg-cell function." *Nature* 499.7459 (2013): 485-490.

[133] Vukmanovic-Stejic, Milica, et al. "The kinetics of CD4+ Foxp3+ T cell accumulation during a human cutaneous antigen-specific memory response in vivo." *The Journal of clinical investigation* 118.11 (2008): 3639-3650.

[134] Delgoffe, Greg M., et al. "The mTOR kinase differentially regulates effector and regulatory T cell lineage commitment." *Immunity* 30.6 (2009): 832-844.

[135] Berod, Luciana, et al. "De novo fatty acid synthesis controls the fate between regulatory T and T helper 17 cells." *Nature medicine* 20.11 (2014): 1327-1333.

[136] Chen, Ye, et al. "Cellular metabolic regulation in the differentiation and function of regulatory T cells." *Cells* 8.2 (2019): 188.

[137] Powell, Jonathan D., and Greg M. Delgoffe. "The mammalian target of rapamycin: linking T cell differentiation, function, and metabolism." *Immunity* 33.3 (2010): 301-311.

[138] Zheng, Yan, et al. "A role for mammalian target of rapamycin in regulating T cell activation versus anergy." *The Journal of Immunology* 178.4 (2007): 2163-2170.

[139] Kang, Johnthomas, et al. "De novo induction of antigen-specific CD4+ CD25+ Foxp3+ regulatory T cells in vivo following systemic antigen administration accompanied by blockade of mTOR." *Journal of leukocyte biology* 83.5 (2008): 1230-1239.

[140] Wang, Beatrice T., et al. "The mammalian target of rapamycin regulates cholesterol biosynthetic gene expression and exhibits a rapamycin-resistant transcriptional profile." *Proceedings of the National Academy of Sciences* 108.37 (2011): 15201-15206.

[141] Whibley, Natasha, Andrea Tucci, and Fiona Powrie. "Regulatory T cell adaptation in the intestine and skin." *Nature immunology* 20.4 (2019): 386-396.

[142] Gerriets, Valerie A., et al. "Foxp3 and Toll-like receptor signaling balance T reg cell anabolic metabolism for suppression." *Nature immunology* 17.12 (2016): 1459-1466.

[143] Procaccini, Claudio, et al. "The proteomic landscape of human ex vivo regulatory and conventional T cells reveals specific metabolic requirements." *Immunity* 44.2 (2016): 406-421.

[144] Michalek, Ryan D., et al. "Cutting edge: distinct glycolytic and lipid oxidative metabolic programs are essential for effector and regulatory CD4+ T cell subsets." *The Journal of Immunology* 186.6 (2011): 3299-3303.

[145] Wang, Ruoning, et al. "The transcription factor Myc controls metabolic reprogramming upon T lymphocyte activation." *Immunity* 35.6 (2011): 871-882.

[146] Gerriets, Valerie A., et al. "Metabolic programming and PDHK1 control CD4+ T cell subsets and inflammation." *The Journal of clinical investigation* 125.1 (2015): 194-207.

[147] Thorens, Bernard, and Mike Mueckler. "Glucose transporters in the 21st

Century." *American Journal of Physiology-Endocrinology and Metabolism* 298.2 (2010): E141-E145.

[148] Porstmann, Thomas, et al. "SREBP activity is regulated by mTORC1 and contributes to Akt-dependent cell growth." *Cell metabolism* 8.3 (2008): 224-236.

[149] De Rosa, Veronica, et al. "A key role of leptin in the control of regulatory T cell proliferation." *Immunity* 26.2 (2007): 241-255.

[150] Huynh, Alexandria, et al. "Control of PI (3) kinase in T reg cells maintains homeostasis and lineage stability." *Nature immunology* 16.2 (2015): 188-196.

[151] Shrestha, Sharad, et al. "T reg cells require the phosphatase PTEN to restrain TH 1 and T FH cell responses." *Nature immunology* 16.2 (2015): 178-187.

[152] Wei, Jun, et al. "Autophagy enforces functional integrity of regulatory T cells by coupling environmental cues and metabolic homeostasis." *Nature immunology* 17.3 (2016): 277-285.

[153] Engelman, Jeffrey A., Ji Luo, and Lewis C. Cantley. "The evolution of phosphatidylinositol 3-kinases as regulators of growth and metabolism." *Nature Reviews Genetics* 7.8 (2006): 606-619.

[154] Vanhaesebroeck, Bart, et al. "The emerging mechanisms of isoform-specific PI3K signalling." *Nature reviews Molecular cell biology* 11.5 (2010): 329-341.

[155] Engelman, Jeffrey A. "Targeting PI3K signalling in cancer: opportunities, challenges and limitations." *Nature Reviews Cancer* 9.8 (2009): 550-562.

[156] Okkenhaug, Klaus. "Signaling by the phosphoinositide 3-kinase family in immune cells." *Annual review of immunology* 31 (2013).

[157] Schu, Peter V., et al. "Phosphatidylinositol 3-kinase encoded by yeast VPS34 gene essential for protein sorting." *Science* 260.5104 (1993): 88-91.

[158] Simonsen, Anne, et al. "The role of phosphoinositides in membrane transport." *Current opinion in cell biology* 13.4 (2001): 485-492.

[159] Backer, Jonathan M. "The regulation and function of Class III PI3Ks: novel roles for Vps34." *Biochemical Journal* 410.1 (2008): 1-17.

[160] Lemmon, Mark A. "Membrane recognition by phospholipid-binding domains." *Nature reviews Molecular cell biology* 9.2 (2008): 99-111.

[161] Birkeland, H. C. G., and H. Stenmark. "Protein targeting to endosomes and phagosomes via FYVE and PX domains." *Phosphoinositides in Subcellular Targeting and Enzyme*

Activation. Springer, Berlin, Heidelberg, 2004. 89-115.

[162] Lemmon, Mark A. "Phosphoinositide recognition domains." *Traffic* 4.4 (2003): 201-213.

[163] Stack, Jeffrey H., et al. "A membrane-associated complex containing the Vps15 protein kinase and the Vps34 PI 3-kinase is essential for protein sorting to the yeast lysosome-like vacuole." *The EMBO journal* 12.5 (1993): 2195-2204.

[164] Ktistakis, Nicholas T., et al. "How phosphoinositide 3-phosphate controls growth downstream of amino acids and autophagy downstream of amino acid withdrawal." (2012): 37-43.

[165] Pattingre, Sophie, et al. "Bcl-2 antiapoptotic proteins inhibit Beclin 1-dependent autophagy." *Cell* 122.6 (2005): 927-939.

[166] Fimia, Gian Maria, et al. "Ambra1 regulates autophagy and development of the nervous system." *Nature* 447.7148 (2007): 1121-1125.

[167] Matsunaga, Kohichi, et al. "Two Beclin 1-binding proteins, Atg14L and Rubicon, reciprocally regulate autophagy at different stages." *Nature cell biology* 11.4 (2009): 385-396.

[168] Zhong, Yun, et al. "Distinct regulation of autophagic activity by Atg14L and Rubicon associated with Beclin 1–phosphatidylinositol-3-kinase complex." *Nature cell biology* 11.4 (2009): 468-476.

[169] Kaushik, Susmita, and Ana Maria Cuervo. "The coming of age of chaperone-mediated autophagy." *Nature Reviews Molecular Cell Biology* 19.6 (2018): 365-381.

[170] Mizushima, Noboru. "Autophagy: process and function." *Genes & development* 21.22 (2007): 2861-2873.

[171] Jia, Wei, and You-Wen He. "Temporal regulation of intracellular organelle homeostasis in T lymphocytes by autophagy." *The Journal of Immunology* 186.9 (2011): 5313-5322.

[172] Geng, Jiefei, and Daniel J. Klionsky. "The Atg8 and Atg12 ubiquitin-like conjugation systems in macroautophagy." *EMBO reports* 9.9 (2008): 859-864.

[173] Ichimura, Yoshinobu, et al. "A ubiquitin-like system mediates protein lipidation." *Nature* 408.6811 (2000): 488-492.

[174] Burman, Chloe, and Nicholas T. Ktistakis. "Autophagosome formation in mammalian cells." *Seminars in immunopathology*. Vol. 32. No. 4. Springer-Verlag, 2010.

[175] Vergne, Isabelle, et al. "Control of autophagy initiation by phosphoinositide 3-

phosphatase Jumpy." *The EMBO journal* 28.15 (2009): 2244-2258.

[176] Taguchi-Atarashi, Naoko, et al. "Modulation of local PtdIns3P levels by the PI phosphatase MTMR3 regulates constitutive autophagy." *Traffic* 11.4 (2010): 468-478.

[177] Ktistakis, Nicholas T., and Sharon A. Tooze. "Digesting the expanding mechanisms of autophagy." *Trends in cell biology* 26.8 (2016): 624-635.

[178] Axe, Elizabeth L., et al. "Autophagosome formation from membrane compartments enriched in phosphatidylinositol 3-phosphate and dynamically connected to the endoplasmic reticulum." *The Journal of cell biology* 182.4 (2008): 685-701.

[179] Cebollero, Eduardo, et al. "Phosphatidylinositol-3-phosphate clearance plays a key role in autophagosome completion." *Current Biology* 22.17 (2012): 1545-1553.

[180] Ikonomov, Ognian C., et al. "Class III PI 3-kinase is the main source of PtdIns3P substrate and membrane recruitment signal for PIKfyve constitutive function in podocyte endomembrane homeostasis." *Biochimica et Biophysica Acta (BBA)-Molecular Cell Research* 1853.5 (2015): 1240-1250.

[181] Viaud, Julien, et al. "Phosphatidylinositol 5-phosphate: a nuclear stress lipid and a tuner of membranes and cytoskeleton dynamics." *BioEssays* 36.3 (2014): 260-272.

[182] Vicinanza, Mariella, et al. "PI (5) P regulates autophagosome biogenesis." *Molecular cell* 57.2 (2015): 219-234.

[183] De Tito, Stefano, et al. "The golgi as an assembly line to the autophagosome." *Trends in Biochemical Sciences* (2020).

[184] Zhou, Xiang, Jun Takatoh, and Fan Wang. "The mammalian class 3 PI3K (PIK3C3) is required for early embryogenesis and cell proliferation." *PloS one* 6.1 (2011): e16358.

[185] Jaber, Nadia, et al. "Class III PI3K Vps34 plays an essential role in autophagy and in heart and liver function." *Proceedings of the National Academy of Sciences* 109.6 (2012): 2003-2008.

[186] Zhou, Xiang, et al. "Deletion of PIK3C3/Vps34 in sensory neurons causes rapid neurodegeneration by disrupting the endosomal but not the autophagic pathway." *Proceedings of the National Academy of Sciences* 107.20 (2010): 9424-9429.

[187] Dikic, Ivan, and Zvulun Elazar. "Mechanism and medical implications of mammalian autophagy." *Nature reviews Molecular cell biology* 19.6 (2018): 349-364.

[188] Hosokawa, Nao, et al. "Nutrient-dependent mTORC1 association with the ULK1–Atg13–FIP200 complex required for autophagy." *Molecular biology of the cell* 20.7

(2009): 1981-1991.

[189] Walker, Simon A., and Nicholas T. Ktistakis. "Autophagosome biogenesis machinery." *Journal of molecular biology* (2019).

[190] Shaw, Reuben J., et al. "The LKB1 tumor suppressor negatively regulates mTOR signaling." *Cancer cell* 6.1 (2004): 91-99.

[191] Gwinn, Dana M., et al. "AMPK phosphorylation of raptor mediates a metabolic checkpoint." *Molecular cell* 30.2 (2008): 214-226.

[192] Kim, Joungmok, et al. "AMPK and mTOR regulate autophagy through direct phosphorylation of Ulk1." *Nature cell biology* 13.2 (2011): 132-141.

[193] Egan, Dan, et al. "The autophagy initiating kinase ULK1 is regulated via opposing phosphorylation by AMPK and mTOR." *Autophagy* 7.6 (2011): 643-644.

[194] Russell, Ryan C., et al. "ULK1 induces autophagy by phosphorylating Beclin-1 and activating VPS34 lipid kinase." *Nature cell biology* 15.7 (2013): 741-750.

[195] Park, Ji-Man, et al. "ULK1 phosphorylates Ser30 of BECN1 in association with ATG14 to stimulate autophagy induction." *Autophagy* 14.4 (2018): 584-597.

[196] Park, Ji-Man, et al. "The ULK1 complex mediates MTORC1 signaling to the autophagy initiation machinery via binding and phosphorylating ATG14." *Autophagy* 12.3 (2016): 547-564.

[197] Kim, Byeong-Won, et al. "The C-terminal region of ATG101 bridges ULK1 and PtdIns3K complex in autophagy initiation." *Autophagy* 14.12 (2018): 2104-2116.

[198] Dunlop, Elaine A., et al. "ULK1 inhibits mTORC1 signaling, promotes multisite Raptor phosphorylation and hinders substrate binding." *Autophagy* 7.7 (2011): 737-747.

[199] Orsi, A., et al. "Dynamic and transient interactions of Atg9 with autophagosomes, but not membrane integration, are required for autophagy." *Molecular biology of the cell* 23.10 (2012): 1860-1873.

[200] Dooley, Hannah C., et al. "WIPI2 links LC3 conjugation with PI3P, autophagosome formation, and pathogen clearance by recruiting Atg12–5-16L1." *Molecular cell* 55.2 (2014): 238-252.

[201] Mercer, Thomas J., Andrea Gubas, and Sharon A. Tooze. "A molecular perspective of mammalian autophagosome biogenesis." *Journal of biological chemistry* 293.15 (2018): 5386-5395.

[202] Mizushima, Noboru. "The ATG conjugation systems in autophagy." *Current Opinion in*

Cell Biology 63 (2020): 1-10.

[203] Lane, Jon D., and Hitoshi Nakatogawa. "Two ubiquitin-like conjugation systems that mediate membrane formation during autophagy." *Essays in biochemistry* 55 (2013): 39-50.

[204] Johansen, Terje, and Trond Lamark. "Selective autophagy: ATG8 family proteins, LIR motifs and cargo receptors." *Journal of molecular biology* 432.1 (2020): 80-103.

[205] Bilanges, Benoit, York Posor, and Bart Vanhaesebroeck. "PI3K isoforms in cell signalling and vesicle trafficking." *Nature Reviews Molecular Cell Biology* 20.9 (2019): 515-534.

[206] Hurley, James H., and Lindsey N. Young. "Mechanisms of autophagy initiation." *Annual review of biochemistry* 86 (2017): 225-244.

[207] Sridhar, Sunandini, et al. "The lipid kinase PI4KIIIβ preserves lysosomal identity." *The EMBO journal* 32.3 (2013): 324-339.

[208] Rong, Yueguang, et al. "Clathrin and phosphatidylinositol-4, 5-bisphosphate regulate autophagic lysosome reformation." *Nature cell biology* 14.9 (2012): 924-934.

[209] Yu, Li, et al. "Termination of autophagy and reformation of lysosomes regulated by mTOR." *Nature* 465.7300 (2010): 942-946.

[210] Schulze, Ryan J., et al. "Lipid droplet breakdown requires dynamin 2 for vesiculation of autolysosomal tubules in hepatocytes." *Journal of Cell Biology* 203.2 (2013): 315-326.

[211] Li, Changyou, et al. "Autophagy is induced in CD4+ T cells and important for the growth factor-withdrawal cell death." *The Journal of Immunology* 177.8 (2006): 5163-5168.

[212] Pua, Heather H., et al. "A critical role for the autophagy gene Atg5 in T cell survival and proliferation." *The Journal of experimental medicine* 204.1 (2007): 25-31.

[213] Copetti, Tamara, et al. "p65/RelA modulates BECN1 transcription and autophagy." *Molecular and cellular biology* 29.10 (2009): 2594-2608.

[214] Jia, Wei, et al. "Autophagy regulates T lymphocyte proliferation through selective degradation of the cell-cycle inhibitor CDKN1B/p27Kip1." *Autophagy* 11.12 (2015): 2335-2345.

[215] Hubbard, Vanessa M., et al. "Macroautophagy regulates energy metabolism during effector T cell activation." *The Journal of Immunology* 185.12 (2010): 7349-7357.

[216] Stephenson, Linda M., et al. "Identification of Atg5-dependent transcriptional changes and increases in mitochondrial mass in Atg5-deficient T lymphocytes." *Autophagy* 5.5 (2009): 625-635.

[217] Parekh, Vrajesh V., et al. "Impaired autophagy, defective T cell homeostasis, and a wasting syndrome in mice with a T cell–specific deletion of Vps34." *The Journal of Immunology* 190.10 (2013): 5086-5101.

[218] Murera, Diane, et al. "CD4 T cell autophagy is integral to memory maintenance." *Scientific reports* 8.1 (2018): 1-13.

[219] Murera, Diane, et al. "CD4 T cell autophagy is integral to memory maintenance." *Scientific reports* 8.1 (2018): 1-13.

[220] Schlie, Katrin, et al. "Survival of effector CD8+ T cells during influenza infection is dependent on autophagy." *The Journal of Immunology* 194.9 (2015): 4277-4286.

[221] Pua, Heather H., et al. "Autophagy is essential for mitochondrial clearance in mature T lymphocytes." *The Journal of Immunology* 182.7 (2009): 4046-4055.

[222] Jia, Wei, et al. "Autophagy regulates endoplasmic reticulum homeostasis and calcium mobilization in T lymphocytes." *The Journal of Immunology* 186.3 (2011): 1564-1574.

[223] Puleston, Daniel J., et al. "Autophagy is a critical regulator of memory CD8+ T cell formation." *Elife* 3 (2014): e03706.

[224] Kabat, Agnieszka M., et al. "The autophagy gene Atg16l1 differentially regulates Treg and TH2 cells to control intestinal inflammation." *Elife* 5 (2016): e12444.

[225] Arsov, Ivica, et al. "A role for autophagic protein beclin 1 early in lymphocyte development." *The Journal of Immunology* 186.4 (2011): 2201-2209.

[226] Kovacs, J. R., et al. "Autophagy promotes T-cell survival through degradation of proteins of the cell death machinery." *Cell Death & Differentiation* 19.1 (2012): 144-152.

[227] McLeod, Ian X., et al. "The class III kinase Vps34 promotes T lymphocyte survival through regulating IL-7Rα surface expression." *The Journal of Immunology* 187.10 (2011): 5051-5061.

[228] Willinger, Tim, and Richard A. Flavell. "Canonical autophagy dependent on the class III phosphoinositide-3 kinase Vps34 is required for naive T-cell homeostasis." *Proceedings of the National Academy of Sciences* 109.22 (2012): 8670-8675.

[229] Yang, Guan, et al. "Autophagy-related protein PIK3C3/VPS34 controls T cell metabolism and function: PIK3C3/VPS34 in T cell metabolism and function." *Autophagy* (2020): 1-12.

[230] Lodish, Harvey, et al. "Molecular cell biology 4th edition." *National Center for*

Biotechnology Information, Bookshelf 9 (2000).

[231] Wallroth, Alexander, and Volker Haucke. "Phosphoinositide conversion in endocytosis and the endolysosomal system." *Journal of Biological Chemistry* 293.5 (2018): 1526-1535.

[232] Raiborg, Camilla, and Harald Stenmark. "The ESCRT machinery in endosomal sorting of ubiquitylated membrane proteins." *Nature* 458.7237 (2009): 445-452.

[233] Zerial, Marino, and Heidi McBride. "Rab proteins as membrane organizers." *Nature reviews Molecular cell biology* 2.2 (2001): 107-117.

[234] Poteryaev, Dmitry, et al. "Identification of the switch in early-to-late endosome transition." *cell* 141.3 (2010): 497-508.

[235] Fukuda, Mitsunori. "TBC proteins: GAPs for mammalian small GTPase Rab?." *Bioscience reports* 31.3 (2011): 159-168.

[236] Murray, James T., et al. "Role of Rab5 in the recruitment of hVps34/p150 to the early endosome." *Traffic* 3.6 (2002): 416-427.

[237] Christoforidis, Savvas, et al. "Phosphatidylinositol-3-OH kinases are Rab5 effectors." *Nature cell biology* 1.4 (1999): 249-252.

[238] Stein, Mary-Pat, et al. "Human VPS34 and p150 are Rab7 interacting partners." *Traffic* 4.11 (2003): 754-771.

[239] Jaber, Nadia, et al. "Vps34 regulates Rab7 and late endocytic trafficking through recruitment of the GTPase-activating protein Armus." *Journal of cell science* 129.23 (2016): 4424-4435.

[240] Hong, Zhi, et al. "PtdIns3P controls mTORC1 signaling through lysosomal positioning." *Journal of Cell Biology* 216.12 (2017): 4217-4233.

[241] Juhász, Gábor, et al. "The class III PI (3) K Vps34 promotes autophagy and endocytosis but not TOR signaling in Drosophila." *The Journal of cell biology* 181.4 (2008): 655-666.

[242] Cao, Canhong, et al. "Myotubularin lipid phosphatase binds the hVPS15/hVPS34 lipid kinase complex on endosomes." *Traffic* 8.8 (2007): 1052-1067.

[243] Vieira, Otilia V., et al. "Distinct roles of class I and class III phosphatidylinositol 3-kinases in phagosome formation and maturation." *The Journal of cell biology* 155.1 (2001): 19-26.

[244] Fratti, Rutilio A., et al. "Role of phosphatidylinositol 3-kinase and Rab5 effectors in phagosomal biogenesis and mycobacterial phagosome maturation arrest." *The Journal*

of cell biology 154.3 (2001): 631-644.

[245] Ellson, Chris, et al. "PtdIns3P binding to the PX domain of p40phox is a physiological signal in NADPH oxidase activation." *The EMBO journal* 25.19 (2006): 4468-4478.

[246] Ellson, Chris, et al. "PtdIns3P binding to the PX domain of p40phox is a physiological signal in NADPH oxidase activation." *The EMBO journal* 25.19 (2006): 4468-4478.

[247] Schiel, John A., Carly Childs, and Rytis Prekeris. "Endocytic transport and cytokinesis: from regulation of the cytoskeleton to midbody inheritance." *Trends in cell biology* 23.7 (2013): 319-327.

[248] Schuh, Amber L., and Anjon Audhya. "The ESCRT machinery: from the plasma membrane to endosomes and back again." *Critical reviews in biochemistry and molecular biology* 49.3 (2014): 242-261.

[249] Sagona, Antonia P., et al. "PtdIns (3) P controls cytokinesis through KIF13A-mediated recruitment of FYVE-CENT to the midbody." *Nature cell biology* 12.4 (2010): 362-371.

[250] Abrahamsen, Hilde, Harald Stenmark, and Harald W. Platta. "Ubiquitination and phosphorylation of Beclin 1 and its binding partners: Tuning class III phosphatidylinositol 3-kinase activity and tumor suppression." *FEBS letters* 586.11 (2012): 1584-1591.

[251] Lee, Heung Kyu, et al. "In vivo requirement for Atg5 in antigen presentation by dendritic cells." *Immunity* 32.2 (2010): 227-239.

[252] Paludan, Casper, et al. "Endogenous MHC class II processing of a viral nuclear antigen after autophagy." *Science* 307.5709 (2005): 593-596.

[253] Münz, Christian. "Antigen processing via autophagy—not only for MHC class II presentation anymore?." *Current opinion in immunology* 22.1 (2010): 89-93.

[254] Parekh, Vrajesh V., et al. "Impaired autophagy, defective T cell homeostasis, and a wasting syndrome in mice with a T cell–specific deletion of Vps34." *The Journal of Immunology* 190.10 (2013): 5086-5101.

[255] Pua, Heather H., et al. "A critical role for the autophagy gene Atg5 in T cell survival and proliferation." *The Journal of experimental medicine* 204.1 (2007): 25-31.

[256] HPua, Heather H., et al. "Autophagy is essential for mitochondrial clearance in mature T lymphocytes." *The Journal of Immunology* 182.7 (2009): 4046-4055.

[257] Willinger, Tim, and Richard A. Flavell. "Canonical autophagy dependent on the class III phosphoinositide-3 kinase Vps34 is required for naive T-cell homeostasis." *Proceedings*

of the National Academy of Sciences 109.22 (2012): 8670-8675.

[258] Waterhouse, Andrew, et al. "SWISS-MODEL: homology modelling of protein structures and complexes." *Nucleic acids research* 46.W1 (2018): W296-W303.

[259] Sarkar, Surojit, et al. "Functional and genomic profiling of effector CD8 T cell subsets with distinct memory fates." *The Journal of experimental medicine* 205.3 (2008): 625-640.

[260] Pope, Constance, et al. "Organ-specific regulation of the CD8 T cell response to Listeria monocytogenes infection." *The Journal of Immunology* 166.5 (2001): 3402-3409.

[261] Brundage, Rodney A., et al. "Expression and phosphorylation of the Listeria monocytogenes ActA protein in mammalian cells." *Proceedings of the National Academy of Sciences* 90.24 (1993): 11890-11894.

[262] Busch, Dirk H., Sujata Vijh, and Eric G. Pamer. "Animal model for infection with Listeria monocytogenes." *Current protocols in immunology* 36.1 (2000): 19-9.

[263] Engelhardt, John J., et al. "Marginating dendritic cells of the tumor microenvironment cross-present tumor antigens and stably engage tumor-specific T cells." *Cancer cell* 21.3 (2012): 402-417.

[264] Hughes, Christopher S., et al. "Single-pot, solid-phase-enhanced sample preparation for proteomics experiments." *Nature protocols* 14.1 (2019): 68-85.

[265] Wiśniewski, Jacek R., et al. "A “proteomic ruler” for protein copy number and concentration estimation without spike-in standards." *Molecular & cellular proteomics* 13.12 (2014): 3497-3506.

[266] E. C. M. Slack, “The role of phosphoinositide 3-kinases in regulatory T cell function - Submitted for the award of Doctor of Philosophy,” no. November, pp. 1–279, 2013.

[267] Bilanges, Benoit, et al. "Vps34 PI 3-kinase inactivation enhances insulin sensitivity through reprogramming of mitochondrial metabolism." *Nature communications* 8.1 (2017): 1-14.

[268] Komatsu, Masaaki, et al. "Impairment of starvation-induced and constitutive autophagy in Atg7-deficient mice." *Journal of Cell Biology* 169.3 (2005): 425-434.

[269] Okamoto, Ikuhiro, et al. "Epigenetic dynamics of imprinted X inactivation during early mouse development." *Science* 303.5658 (2004): 644-649.

[270] Redpath, Stephen A., et al. "ICOS controls Foxp3+ regulatory T-cell expansion, maintenance and IL-10 production during helminth infection." *European journal of*

immunology 43.3 (2013): 705-715.

[271] Read, Simon, et al. "CD38+ CD45RBlow CD4+ T cells: a population of T cells with immune regulatory activities in vitro." *European journal of immunology* 28.11 (1998): 3435-3447.

[272] Cibrián, Danay, and Francisco Sánchez-Madrid. "CD69: from activation marker to metabolic gatekeeper." *European journal of immunology* 47.6 (2017): 946-953.

[273] Zhang, Qianxia, et al. "LAG-3 limits regulatory T cell proliferation and function in autoimmune diabetes." *Science immunology* 2.9 (2017).

[274] Ephrem, Amal, et al. "Modulation of T reg cells/T effector function by GITR signaling is context–dependent." *European journal of immunology* 43.9 (2013): 2421-2429.

[275] Qureshi, Omar S., et al. "Trans-endocytosis of CD80 and CD86: a molecular basis for the cell-extrinsic function of CTLA-4." *Science* 332.6029 (2011): 600-603.

[276] Qureshi, Omar S., et al. "Trans-endocytosis of CD80 and CD86: a molecular basis for the cell-extrinsic function of CTLA-4." *Science* 332.6029 (2011): 600-603.

[277] Bago, Ruzica, et al. "Characterization of VPS34-IN1, a selective inhibitor of Vps34, reveals that the phosphatidylinositol 3-phosphate-binding SGK3 protein kinase is a downstream target of class III phosphoinositide 3-kinase." *Biochemical Journal* 463.3 (2014): 413-427.

[278] Godfrey, V. L., J. E. Wilkinson, and L. B. Russell. "X-linked lymphoreticular disease in the scurfy (sf) mutant mouse." *The American journal of pathology* 138.6 (1991): 1379.

[279] Gavin, Marc A., et al. "Foxp3-dependent programme of regulatory T-cell differentiation." *Nature* 445.7129 (2007): 771-775.

[280] Lahl, Katharina, et al. "Selective depletion of Foxp3+ regulatory T cells induces a scurfy-like disease." *The Journal of experimental medicine* 204.1 (2007): 57-63.

[281] Ouyang, Weiming, et al. "Novel Foxo1-dependent transcriptional programs control T reg cell function." *Nature* 491.7425 (2012): 554-559.

[282] Botbol, Yair, Ignacio Guerrero-Ros, and Fernando Macian. "Key roles of autophagy in regulating T-cell function." *European journal of immunology* 46.6 (2016): 1326-1334.

[283] Backer, Jonathan M. "The intricate regulation and complex functions of the Class III phosphoinositide 3-kinase Vps34." *Biochemical Journal* 473.15 (2016): 2251-2271.

[284] Levine, Andrew G., et al. "Continuous requirement for the TCR in regulatory T cell function." *Nature immunology* 15.11 (2014): 1070-1078.

[285] Tyanova, Stefka, Tikira Temu, and Juergen Cox. "The MaxQuant computational platform for mass spectrometry-based shotgun proteomics." *Nature protocols* 11.12 (2016): 2301.

[286] Widlak, Piotr, et al. "The histone H1 C-terminal domain binds to the apoptotic nuclease, DNA fragmentation factor (DFF40/CAD) and stimulates DNA cleavage." *Biochemistry* 44.21 (2005): 7871-7878.

[287] Burman, Chloe, and Nicholas T. Ktistakis. "Regulation of autophagy by phosphatidylinositol 3-phosphate." *FEBS letters* 584.7 (2010): 1302-1312.

[288] Bakula, Daniela, et al. "WIPI3 and WIPI4 β-propellers are scaffolds for LKB1-AMPK-TSC signalling circuits in the control of autophagy." *Nature communications* 8.1 (2017): 1-18.

[289] Sherman, Brad T., and Richard A. Lempicki. "Systematic and integrative analysis of large gene lists using DAVID bioinformatics resources." *Nature protocols* 4.1 (2009): 44.

[290] Short, Benjamin, et al. "A GRASP55-rab2 effector complex linking Golgi structure to membrane traffic." *The Journal of cell biology* 155.6 (2001): 877-884.

[291] Bennett, Eric Paul, et al. "A novel human UDP-N-acetyl-D-galactosamine: polypeptide N-acetylgalactosaminyltransferase, GalNAc-T7, with specificity for partial GalNAc-glycosylated acceptor substrates." *FEBS letters* 460.2 (1999): 226-230.

[292] White, Thayer, et al. "Purification and cDNA cloning of a human UDP-N-acetyl-α-D-galactosamine: polypeptide N-acetylgalactosaminyltransferase." *Journal of Biological Chemistry* 270.41 (1995): 24156-24165.

[293] Guo, Jian-Ming, et al. "Molecular cloning and characterization of a novel member of the UDP-GalNAc: polypeptide N-acetylgalactosaminyltransferase family, pp-GalNAc-T12." *FEBS letters* 524.1-3 (2002): 211-218.

[294] Karamatic Crew, Vanja, et al. "New mutations in C1GALT1C1 in individuals with Tn positive phenotype." *British journal of haematology* 142.4 (2008): 657-667.

[295] Ju, Tongzhong, and Richard D. Cummings. "A unique molecular chaperone Cosmc required for activity of the mammalian core 1 β3-galactosyltransferase." *Proceedings of the national academy of sciences* 99.26 (2002): 16613-16618.

[296] Li, G-S., et al. "Variants of C1GALT1 gene are associated with the genetic susceptibility to IgA nephropathy." *Kidney international* 71.5 (2007): 448-453.

[297] Hukelmann, Jens L., et al. "The cytotoxic T cell proteome and its shaping by the kinase

mTOR." *Nature immunology* 17.1 (2016): 104-112.

[298] Morris, Deanna H., et al. "Beclin 1-Vps34 complex architecture: understanding the nuts and bolts of therapeutic targets." *Frontiers in biology* 10.5 (2015): 398-426.

[299] Li, Hongyang, Xin-Qiu Yao, and Barry J. Grant. "Comparative structural dynamic analysis of GTPases." *PLoS computational biology* 14.11 (2018): e1006364.

[300] Choy, Edwin, et al. "Endomembrane trafficking of ras: the CAAX motif targets proteins to the ER and Golgi." *Cell* 98.1 (1999): 69-80.

[301] Seelig, Hans Peter, et al. "Molecular genetic analyses of a 376-kilodalton Golgi complex membrane protein (giantin)." *Molecular and cellular biology* 14.4 (1994): 2564-2576.

[302] Shorter, James, et al. "GRASP55, a second mammalian GRASP protein involved in the stacking of Golgi cisternae in a cell-free system." *The EMBO journal* 18.18 (1999): 4949-4960.

[303] Barr, Francis A., et al. "GRASP65, a protein involved in the stacking of Golgi cisternae." *Cell* 91.2 (1997): 253-262.

[304] Rao, Rajesh R., et al. "Transcription factor Foxo1 represses T-bet-mediated effector functions and promotes memory CD8+ T cell differentiation." *Immunity* 36.3 (2012): 374-387.

[305] Miller, Iain, et al. "Ki67 is a graded rather than a binary marker of proliferation versus quiescence." *Cell reports* 24.5 (2018): 1105-1112.

[306] Song, Allisa J., and Richard D. Palmiter. "Detecting and avoiding problems when using the Cre–lox system." *Trends in Genetics* 34.5 (2018): 333-340.

[307] Juno, Jennifer A., et al. "Cytotoxic CD4 T cells—Friend or foe during viral infection?." *Frontiers in immunology* 8 (2017): 19.

[308] Hagn, Magdalena, et al. "Human B cells differentiate into granzyme B-secreting cytotoxic B lymphocytes upon incomplete T-cell help." *Immunology and cell biology* 90.4 (2012): 457-467.

[309] Mackaness, G. B. "Cellular resistance to infection." *The Journal of experimental medicine* 116.3 (1962): 381-406.

[311] Conlan, J. Wayne, and Robert J. North. "Neutrophil-mediated dissolution of infected host cells as a defense strategy against a facultative intracellular bacterium." *The Journal of experimental medicine* 174.3 (1991): 741-744.

[312] Gregory, Stephen H., Athanasia J. Sagnimeni, and Edward J. Wing. "Bacteria in the

bloodstream are trapped in the liver and killed by immigrating neutrophils." *The Journal of Immunology* 157.6 (1996): 2514-2520.

[313] Neuenhahn, Michael, et al. "CD8α+ dendritic cells are required for efficient entry of Listeria monocytogenes into the spleen." *Immunity* 25.4 (2006): 619-630.

[314] Aoshi, Taiki, et al. "The cellular niche of Listeria monocytogenes infection changes rapidly in the spleen." *European journal of immunology* 39.2 (2009): 417-425.

[315] Condotta, Stephanie A., et al. "Probing CD8 T cell responses with Listeria monocytogenes infection." *Advances in immunology*. Vol. 113. Academic Press, 2012. 51-80.

[316] Ronan, Baptiste, et al. "A highly potent and selective Vps34 inhibitor alters vesicle trafficking and autophagy." *Nature chemical biology* 10.12 (2014): 1013-1019.

[317] Krzewski, Konrad, et al. "LAMP1/CD107a is required for efficient perforin delivery to lytic granules and NK-cell cytotoxicity." *Blood* 121.23 (2013): 4672-4683.

[318] Keppler, Selina J., et al. "Effector T-cell differentiation during viral and bacterial infections: Role of direct IL-12 signals for cell fate decision of CD8+ T cells." *European journal of immunology* 39.7 (2009): 1774-1783.

[319] Keppler, Selina Jessica, et al. "Signal 3 cytokines as modulators of primary immune responses during infections: the interplay of type I IFN and IL-12 in CD8 T cell responses." *PloS one* 7.7 (2012): e40865.

[320] Ebinu, Julius O., et al. "RasGRP links T-cell receptor signaling to Ras." *Blood, The Journal of the American Society of Hematology* 95.10 (2000): 3199-3203.

[321] Kaech, Susan M., et al. "Selective expression of the interleukin 7 receptor identifies effector CD8 T cells that give rise to long-lived memory cells." *Nature immunology* 4.12 (2003): 1191-1198.

[322] Jaber, Nadia, et al. "Class III PI3K Vps34 plays an essential role in autophagy and in heart and liver function." *Proceedings of the National Academy of Sciences* 109.6 (2012): 2003-2008.

[323] Franckaert, Dean, et al. "Promiscuous Foxp3-cre activity reveals a differential requirement for CD28 in Foxp3+ and Foxp3− T cells." *Immunology and cell biology* 93.4 (2015): 417-423.

[324] Rubtsov, Yuri P., et al. "Regulatory T cell-derived interleukin-10 limits inflammation at environmental interfaces." *Immunity* 28.4 (2008): 546-558.

[325] Huehn, Jochen, et al. "Developmental stage, phenotype, and migration distinguish naive-and effector/memory-like CD4+ regulatory T cells." *The Journal of experimental medicine* 199.3 (2004): 303-313.

[326] Cheng, Guoyan, et al. "IL-2 receptor signaling is essential for the development of Klrg1+ terminally differentiated T regulatory cells." *The Journal of Immunology* 189.4 (2012): 1780-1791.

[327] Li, Ming O., and Alexander Y. Rudensky. "T cell receptor signalling in the control of regulatory T cell differentiation and function." *Nature Reviews Immunology* 16.4 (2016): 220-233.

[328] Vahl, J. Christoph, et al. "Continuous T cell receptor signals maintain a functional regulatory T cell pool." *Immunity* 41.5 (2014): 722-736.

[329] Das, Mrinmoy, Fawaz Alzaid, and Jagadeesh Bayry. "Regulatory T cells under the mercy of mitochondria." *Cell metabolism* 29.2 (2019): 243-245.

[330] Angelin, Alessia, et al. "Foxp3 reprograms T cell metabolism to function in low-glucose, high-lactate environments." *Cell metabolism* 25.6 (2017): 1282-1293.

[331] He, Nanhai, et al. "Metabolic control of regulatory T cell (Treg) survival and function by Lkb1." *Proceedings of the National Academy of Sciences* 114.47 (2017): 12542-12547.

[332] Wu, Di, et al. "Lkb1 maintains T reg cell lineage identity." *Nature communications* 8.1 (2017): 1-14.

[333] Yang, Kai, et al. "Homeostatic control of metabolic and functional fitness of T reg cells by LKB1 signalling." *Nature* 548.7669 (2017): 602-606.

[334] Zeng, Hu, and Hongbo Chi. "The interplay between regulatory T cells and metabolism in immune regulation." *Oncoimmunology* 2.11 (2013): e26586.

[335] Weinberg, Samuel E., et al. "Mitochondrial complex III is essential for suppressive function of regulatory T cells." *Nature* 565.7740 (2019): 495-499.

[336] Battaglia, Manuela, Angela Stabilini, and Maria-Grazia Roncarolo. "Rapamycin selectively expands CD4+ CD25+ FoxP3+ regulatory T cells." *Blood* 105.12 (2005): 4743-4748.

[337] Chi, Hongbo. "Regulation and function of mTOR signalling in T cell fate decisions." *Nature reviews immunology* 12.5 (2012): 325-338.

[338] Choo, Andrew Y., et al. "Rapamycin differentially inhibits S6Ks and 4E-BP1 to mediate cell-type-specific repression of mRNA translation." *Proceedings of the National*

Academy of Sciences 105.45 (2008): 17414-17419.

[339] Laplante, Mathieu, and David M. Sabatini. "mTOR signaling in growth control and disease." *Cell* 149.2 (2012): 274-293.

[340] Sinclair, Linda V., et al. "Control of amino-acid transport by antigen receptors coordinates the metabolic reprogramming essential for T cell differentiation." *Nature immunology* 14.5 (2013): 500-508.

[341] Gottesdiener, K. M., et al. "Isolation and structural characterization of the human 4F2 heavy-chain gene, an inducible gene involved in T-lymphocyte activation." *Molecular and cellular biology* 8.9 (1988): 3809-3819.

[342] Lindsten, T., et al. "Regulation of 4F2 heavy-chain gene expression during normal human T-cell activation can be mediated by multiple distinct molecular mechanisms." *Molecular and cellular biology* 8.9 (1988): 3820-3826.

[343] Parmacek, Michael S., et al. "Structure, expression and regulation of the murine 4F2 heavy chain." *Nucleic acids research* 17.5 (1989): 1915-1931.

[344] Verrey, François, et al. "CATs and HATs: the SLC7 family of amino acid transporters." *Pflügers Archiv* 447.5 (2004): 532-542.

[345] Bar-Peled, Liron, et al. "Ragulator is a GEF for the rag GTPases that signal amino acid levels to mTORC1." *Cell* 150.6 (2012): 1196-1208.

[346] Nobukuni, Takahiro, et al. "Amino acids mediate mTOR/raptor signaling through activation of class 3 phosphatidylinositol 3OH-kinase." *Proceedings of the National Academy of Sciences* 102.40 (2005): 14238-14243.

[347] Byfield, Maya P., James T. Murray, and Jonathan M. Backer. "hVps34 is a nutrient-regulated lipid kinase required for activation of p70 S6 kinase." *Journal of Biological Chemistry* 280.38 (2005): 33076-33082.

[348] Zhang, Chen-Song, et al. "The lysosomal v-ATPase-Ragulator complex is a common activator for AMPK and mTORC1, acting as a switch between catabolism and anabolism." *Cell metabolism* 20.3 (2014): 526-540.

[349] Araki, Koichi, et al. "mTOR regulates memory CD8 T-cell differentiation." *Nature* 460.7251 (2009): 108-112.

[350] Kim, Eui Ho, et al. "Signal integration by Akt regulates CD8 T cell effector and memory differentiation." *The Journal of Immunology* 188.9 (2012): 4305-4314.

[351] Rolf, Julia, et al. "AMPK α1: A glucose sensor that controls CD 8 T-cell

memory." *European journal of immunology* 43.4 (2013): 889-896.

[352] Jung, Chang Hwa, et al. "mTOR regulation of autophagy." *FEBS letters* 584.7 (2010): 1287-1295.

[353] Pearce, Erika L., et al. "Enhancing CD8 T-cell memory by modulating fatty acid metabolism." *Nature* 460.7251 (2009): 103-107.

[354] van der Windt, Gerritje JW, et al. "Mitochondrial respiratory capacity is a critical regulator of CD8+ T cell memory development." *Immunity* 36.1 (2012): 68-78.

[355] Nazio, Francesca, et al. "mTOR inhibits autophagy by controlling ULK1 ubiquitylation, self-association and function through AMBRA1 and TRAF6." *Nature cell biology* 15.4 (2013): 406-416.

[356] Shi, Chong-Shan, and John H. Kehrl. "TRAF6 and A20 regulate lysine 63–linked ubiquitination of Beclin-1 to control TLR4-induced autophagy." *Science signaling* 3.123 (2010): ra42-ra42.

[357] Miragaia, Ricardo J., et al. "Single-cell transcriptomics of regulatory T cells reveals trajectories of tissue adaptation." *Immunity* 50.2 (2019): 493-504.

[358] O'Farrell, Fergal, et al. "Class III phosphatidylinositol-3-OH kinase controls epithelial integrity through endosomal LKB1 regulation." *Nature cell biology* 19.12 (2017): 1412-1423.

[359] Pawson, Tony, and John D. Scott. "Protein phosphorylation in signaling–50 years and counting." *Trends in biochemical sciences* 30.6 (2005): 286-290.

[360] Macek, Boris, Matthias Mann, and Jesper V. Olsen. "Global and site-specific quantitative phosphoproteomics: principles and applications." *Annual review of pharmacology and toxicology* 49 (2009): 199-221.

[361] Rigbolt, Kristoffer TG, and Blagoy Blagoev. "Quantitative phosphoproteomics to characterize signaling networks." *Seminars in cell & developmental biology*. Vol. 23. No. 8. Academic Press, 2012.

[362] Platt, Randall J., et al. "CRISPR-Cas9 knockin mice for genome editing and cancer modeling." *Cell* 159.2 (2014): 440-455.

[363] LaFleur, Martin W., et al. "A CRISPR-Cas9 delivery system for in vivo screening of genes in the immune system." *Nature communications* 10.1 (2019): 1-10.